JOURNAL OF POLYMER SCIENCE: PART A VOL. 1, PP. 3009–3020 (1963)

On Co^{60} Gamma Ray-Initiated Emulsion Polymerization

G. J. K. ACRES* and F. L. DALTON, *Wantage Research Laboratory (A.E.R.E.), Wantage, Berks, England*

Synopsis

A study has been made of the Co^{60} γ-ray-initiated polymerization of methyl methacrylate and styrene; conversion rates have been measured by a dilatometric method. The dependence of polymerization rate on monomer concentration and radiation intensity has been determined for each monomer. It has been shown that the emulsion polymerization of methyl methacrylate can be described by accepted theories of emulsion polymerization; in the case of styrene a dependence of intensity exponent on monomer concentration has been found. Such a dependence does not occur when conventional initiating systems are used, and cannot be explained without some modification of theory.

INTRODUCTION

It has been known for several years that the general features of emulsion polymerizations initiated by ionizing radiations do not differ from those found when conventional initiating systems are used. In the course of a precise study of the rates of polymerization of both styrene and methyl methacrylate emulsions initiated by Co^{60} γ-radiations, we have observed that departures from Smith-Ewart[1] kinetics occur. The behavior of methyl methacrylate is related to known weaknesses in the Smith-Ewart theory which have been discussed by Gerrens,[2] and is not a consequence of the use of Co^{60} γ-rays to initiate the polymerization. Styrene emulsions, on the other hand, show behavior which is entirely novel and which is related to the nature of the initiating species.

EXPERIMENTAL

Radiation Facility

One of the standard 2K irradiation cells now in use at Wantage Research Laboratory, details of which have been described previously,[3] was used for all irradiations. Dosimetry measurements were made by means of the Fricke dosimeter ($G_{Fe^{3+}} = 15.6$).

*Present address: Chemistry Department, University of Nottingham, Nottingham, England.

Materials

Methyl methacrylate and styrene (British Drug Houses Ltd.) were purified by washing with a 5% aqueous caustic soda solution followed by washings with distilled water until all traces of alkali had been removed. The monomers were dried over anhydrous sodium sulfate, distilled under reduced pressure of nitrogen and transferred to a vacuum line. They were prepolymerized to about 10% conversion by means of a 125 w. Osira ultraviolet lamp and finally redistilled *in vacuo*. The stabilizer used was a Manoxal OT (dioctyl ester of sodium sulfosuccinic acid) supplied by British Drug Houses. This material was used without further purification. A stock solution of emulsifier was prepared using Analar distilled water, and this solution was used throughout a series of experiments.

Methods

All rate measurements were made using a recording dilatometer, the course of the reaction being followed continuously. Details of this apparatus have been given previously.[4]

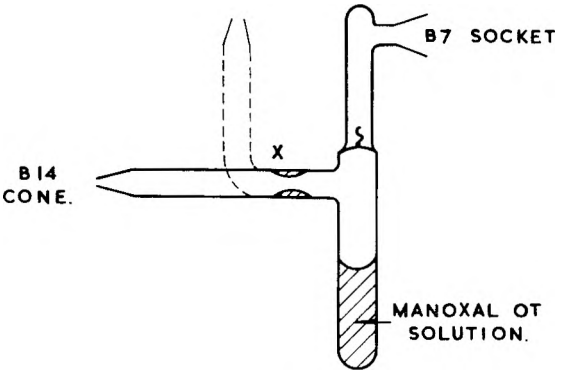

Fig. 1. Sample tube.

The sample was prepared in a break-seal tube which could be connected to the dilatometer by means of a B7 cone and socket, as shown in Figure 1. The monomer emulsion was prepared by transferring 4.5 ml. of standard Manoxal OT solution to the sample tube using a hypodermic syringe. The evacuating arm was then heated and bent into the position shown by the dotted lines (Fig. 1). The solution was outgassed on the high vacuum line by six cycles of freezing in liquid nitrogen, pumping to a pressure of less than 10^{-4} mm. of mercury, and thawing. A known volume of previously purified monomer was distilled into the sample tube, which was then sealed under vacuum at the constriction X. The still frozen sample was transferred to a water bath at 21.5°C., the temperature at which irradiation was to take place, the contents allowed to thaw, and the tube shaken. The tube was connected to the dilatometer, filled with mercury, placed in

position in a thermostat bath surrounding the source guide tube, and irradiated.

Immediately after irradiation the dilatometer was removed from the source and polymer isolated by precipitation into a twentyfold excess of methanol. The polymer was filtered off through a No. 4 glass sinter, washed with methanol, and dried in a vacuum oven at 60°C. As 100% polymerization was not always achieved, and the contraction factor of polymerization is liable to vary with monomer concentration in emulsion systems,[5] the recovered polymer was accurately weighed and this weight used to determine the maximum conversion obtained. The relationship between conversion and contraction was assumed to be linear.

RESULTS

Although samples were carefully outgassed, and purified materials were used throughout, small induction periods were always recorded in the emulsion polymerization of both styrene and methyl methacrylate. The length of the induction period varied from 1 to 8 min., depending on the radiation intensity and the concentration of monomer in the emulsion: the smallest induction period was observed at high radiation intensity and low monomer concentration. Such induction periods are characteristic of all emulsion polymerizations, whether initiated by radiation or chemically, and are not removed by the most exhaustive purification techniques which have been employed.

To study the influence of initial monomer concentration on the rate of polymerization, varying amounts of styrene were added to a solution of 5 parts emulsifier in 180 parts of water by weight; and various amounts of methyl methacrylate added to a solution of 5 parts emulsifier in 360 parts

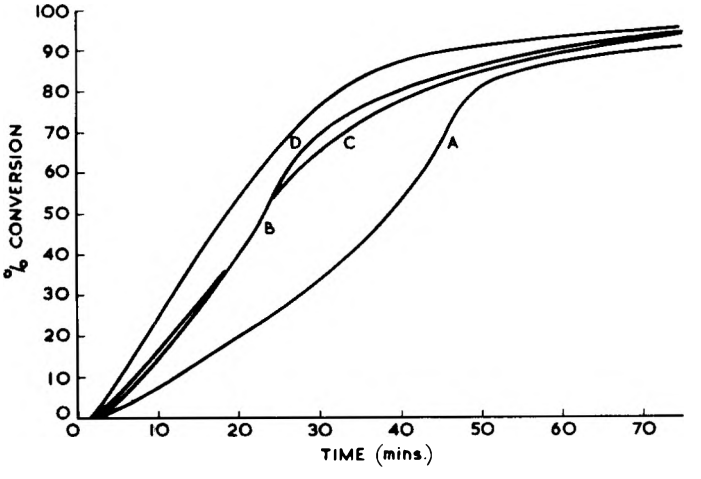

Fig. 2. Conversion vs. time curves for the Co^{60} γ-ray-initiated emulsion polymerization of methyl methacrylate at various monomer concentrations: (*A*) 5.55 moles/l.; (*B*) 2.77 moles/l.; (*C*) 2.40 moles/l.; (*D*) 1.39 moles/l.

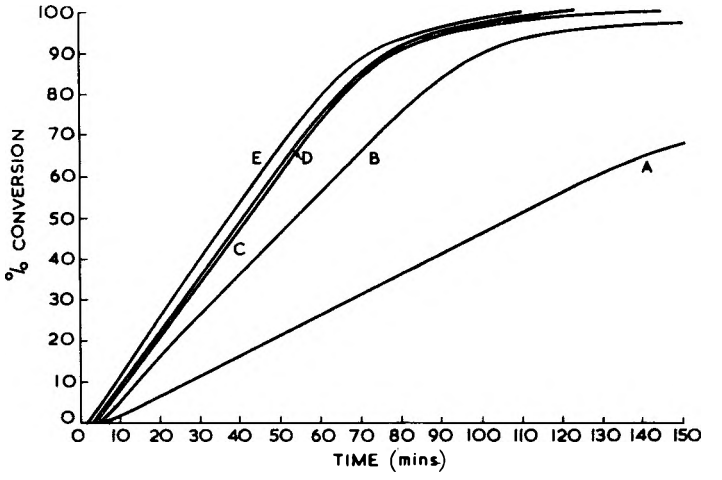

Fig. 3. Conversion vs. time curves for the Co^{60} γ-ray-initiated emulsion polymerization of styrene at various monomer concentrations: (*A*) 5.34 moles/l.; (*B*) 2.56 moles/l.; (*C*) 1.53 moles/l.; (*D*) 1.33 moles/l.; (*E*) 0.97 moles/l.

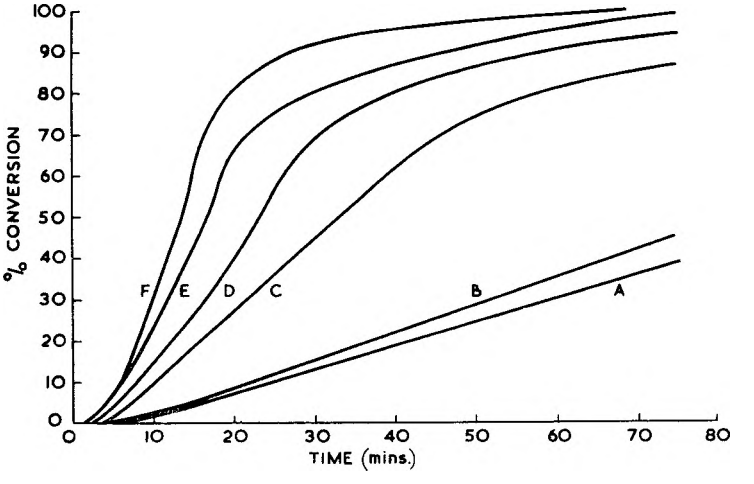

Fig. 4. Conversion vs. time curves for the Co^{60} γ-ray-initiated emulsion polymerization of methyl methacrylate at various radiation intensities; (*A*) 10^3 rads/hr.; (*B*) 1.8×10^3 rads/hr.; (*C*) 2×10^4 rads/hr.; (*D*) 4.2×10^4 rads/hr.; (*E*) 10^5 rads/hr.; (*F*) 2×10^4 rads/hr.

of water by weight. Polymerizations were carried out at 21.5°C. at a radiation intensity of 4.2×10^4 rads/hr. The conversion versus time curves for methyl methacrylate and styrene emulsions at various initial monomer concentrations are shown in Figures 2 and 3, respectively. Several rates of polymerization may be calculated from such curves, initial rate, overall rate, etc. The rate which is of most interest is that obtained above 20% conversion, when the rate of reaction is constant and independent of

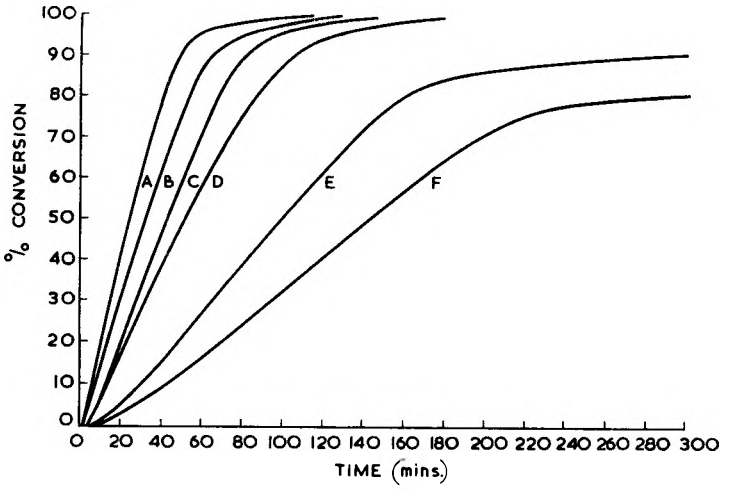

Fig. 5. Conversion vs. time curves for the Co^{60} γ-ray-initiated emulsion polymerization of styrene at various radiation intensities. (*A*) 2.5×10^5 rads/hr.; (*B*) 10^5 rads/hr.; (*C*) 4.2×10^4 rads/hr.; (*D*) 4.2×10^4 rads/hr.; (*E*) 1.8×10^3 rads/hr.; (*F*) 10^3 rads/hr.

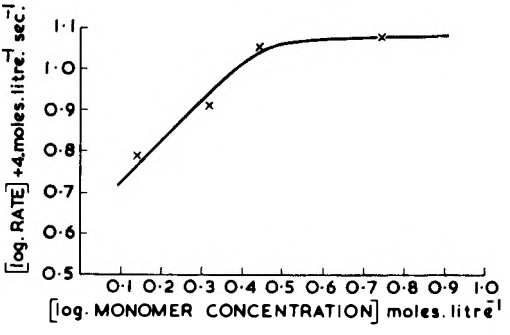

Fig. 6. Influence of monomer concentration on the rate of polymerization for a methyl methacrylate emulsion.

monomer concentration. Over this range, the rate is proportional to N, the number of particles per liter of latex. It is this rate which will be used throughout this communication. The rate remains constant until either monomer droplets disappear, when the rate decreases, or a Trommsdorff effect starts and the rate increases. Plots of log rate versus log monomer concentration are shown for methyl methacrylate and styrene emulsions in Figures 6 and 7, respectively.

The influence of radiation intensity on the rate of polymerization was studied using a styrene emulsion containing 1.525 moles of styrene/l. in a 2.78% aqueous Manoxal solution, and a methyl methacrylate emulsion containing 2.77 moles of methyl methacrylate/l. of 1.39% aqueous Manoxal solution. The temperature used was again 21.5°C. The conversion versus

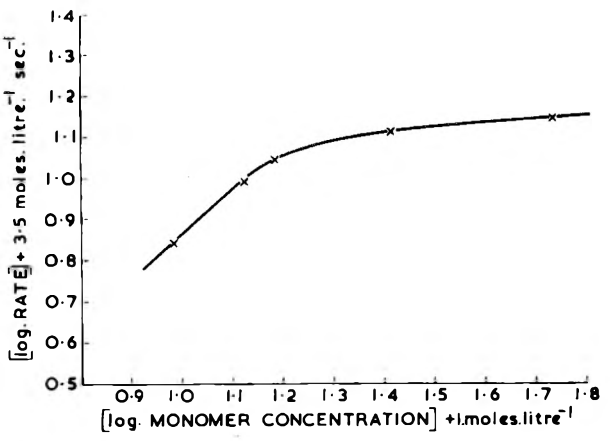

Fig. 7. Influence of monomer concentration on the rate of polymerization for a styrene emulsion.

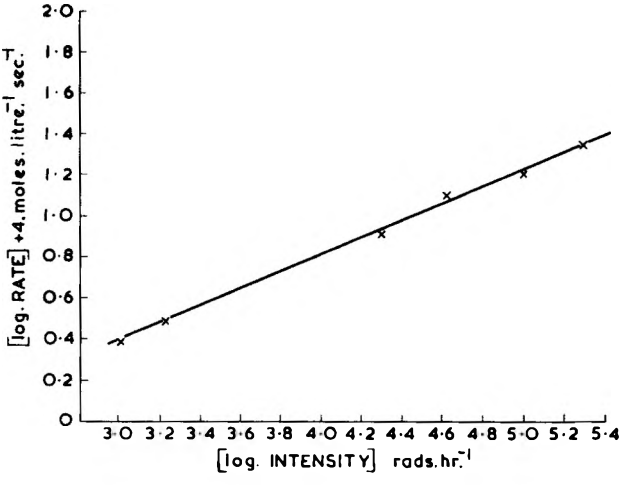

Fig. 8. Influence of radiation intensity on the rate of polymerization for a methyl methacrylate emulsion.

time curves obtained at various intensities for methyl methacrylate and styrene are shown in Figures 4 and 5. Corresponding log rate versus log intensity plots are shown in Figures 8 and 9. In view of the results obtained in the case of styrene, the dependence of rate on intensity was also studied at 5.34, 3.50, 2.50, 1.00, and 0.50 moles/l. and the logarithmic plots of rate versus intensity obtained are also shown in Figure 9.

DISCUSSION

It was shown as long ago as 1954 that the emulsion polymerization of styrene initiated by γ-irradiation is considerably faster than the correspond-

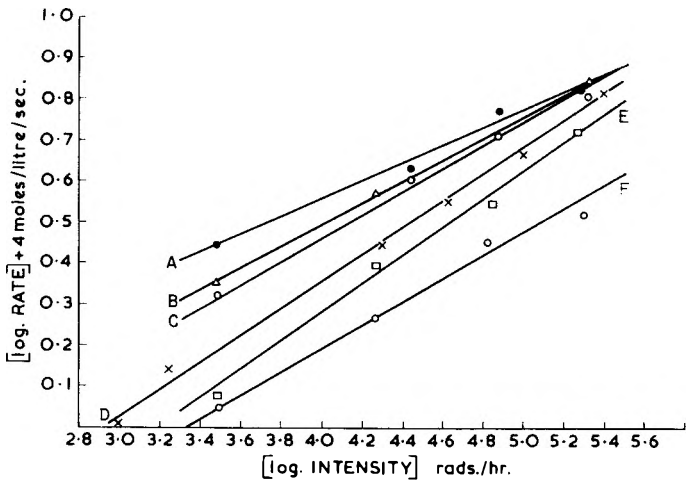

Fig. 9. Influence of radiation intensity on the rate of polymerization at various monomer concentrations for styrene emulsion: (*A*) 5.34 moles/l.; (*B*) 3.50 moles/l.; (*C*) 2.50 moles/l.; (*D*) 1.52 moles/l.; (*E*) 1.00 moles/l.; (*F*) 0.50 moles/l. Lines drawn by least squares method.

ing bulk reaction,[6] and that the molecular weight of the polymer obtained is extremely high. It was concluded that although radicals must be produced simultaneously in the oil and water phases, an emulsion polymerization initiated by γ-radiation is basically similar to a conventional emulsion system. It is therefore of interest to consider whether the kinetics developed by Smith and Ewart[1] for emulsion polymerization initiated by radicals produced only in the aqueous phase can be applied to γ-irradiation-initiated polymerizations. The systems we have studied are such that it is known that Smith-Ewart kinetics can be applied if conventional initiation is used.

The equations derived by Smith and Ewart for the rate of an emulsion polymerization at an average number of radicals per particle $\bar{n} = {}^1/_2$ are as follows:

$$-dM/dt = k_p[\mathrm{M}]N/2 \tag{1}$$

$$N = k(P/\mu)^{2/5}(a_s S')^{3/5} \tag{2}$$

where N is the number of particles per liter of latex, [M] is the concentration of monomer in the particles, $-dM/dt$ is the rate of polymerization in moles/liter/second, k_p is the rate constant for chain propagation, S' is the concentration of emulsifier, a_s is the area covered by one molecule of emulsifier, P is the rate of production of free radicals, μ is the rate of increase in volume of a single particle; hence

$$-dM/dt = k'[\mathrm{M}](P/\mu)^{2/5}(a_s S')^{3/5} \tag{3}$$

Since the rate of radical production is proportional to the radiation intensity I,

$$-dM/dt = \text{Const } [\text{M}](\text{I})^{2/6} \tag{4}$$

It would therefore be expected from Smith-Ewart kinetics that the rate of polymerization would depend on (intensity)$^{0.40}$ and be independent of monomer concentration, if sufficient monomer is added to the system to form free droplets. If less monomer than this is added the rate will be directly proportional to monomer concentration. From Figures 6 and 8 it is clear that these predictions are fulfilled in the case of methyl methacrylate but are not obeyed in the case of styrene. The only feature of the emulsion polymerization of methyl methacrylate which is not described by the Smith-Ewart theory is the occurrence of a Trommsdorff effect in some cases (Figs. 2 and 4). The occurrence of such an effect in emulsion polymerization has been explained by Gerrens.[2] If rapid chain termination does not occur after the entry of a second radical into a latex particle, eq. (1), which was deduced for $\bar{n} = {}^1/_2$, must be modified. Consider a single latex particle in which radicals enter at constant time intervals. Let t_1 be the time between the entry of the n and $(n + 1)$th radical, t_2 the time between the start of polymerization by nth and termination by the $(n + 1)$th radical. If the two radicals meet in the latex particle after a very short time, then $t_2 - t_1 = \delta t$ is negligible compared with t_1 and $\bar{n} = {}^1/_2$. If with increasing conversion the viscosity of the monomer polymer mixture in the particles increases, and/or the size of the particles increases, δt becomes greater and can no longer be neglected. In the time $2t_1$ between the entry of the nth and $(n + 2)$th radical, the latex particle contains during the time fraction $t_1/2t_1$ one radical, in the time fraction $\delta t/2t_1$ two radicals and during the rest of the time namely, $(t_1 - \delta t)2t_1$, no radicals. Then

$$\bar{n} = \frac{t_1 \times 1}{2t_1} + \frac{\delta t \times 2}{2t_1} + \frac{(t_1 - \delta t)}{2t_1} \times 0 = {}^1/_2 + \frac{\delta t}{t_1}$$

Thus, if δt is not negligible compared with t_1, $\bar{n}$ is greater than one half. This leads to an increase in the rate of polymerization, or if the effect is not very marked, to a retarded fall in the rate of polymerization. The effect will be greater, the smaller t_1 and the greater δt. It is favored if large particles appear, since this lengthens the diffusion path and increases δt. If many radicals are formed, or if the number of particles is small, t_1 is reduced by radicals entering the particles at shorter intervals.

In our experiments the effect is not observed in every case, but occurs as follows: (*1*) in an emulsion containing 2.77 moles/l. of methyl methacrylate in a 1.87% Manoxal solution, if irradiated above an intensity of 4.2×10^4 rads/hr., the effect increasing with increasing intensity; (*2*) in an emulsion containing more than 2.77 moles/l. of methyl methacrylate in a 1.87% Manoxal solution, irradiated at 4.2×10^4 rads/hr., the effect increasing with increasing initial monomer concentration.

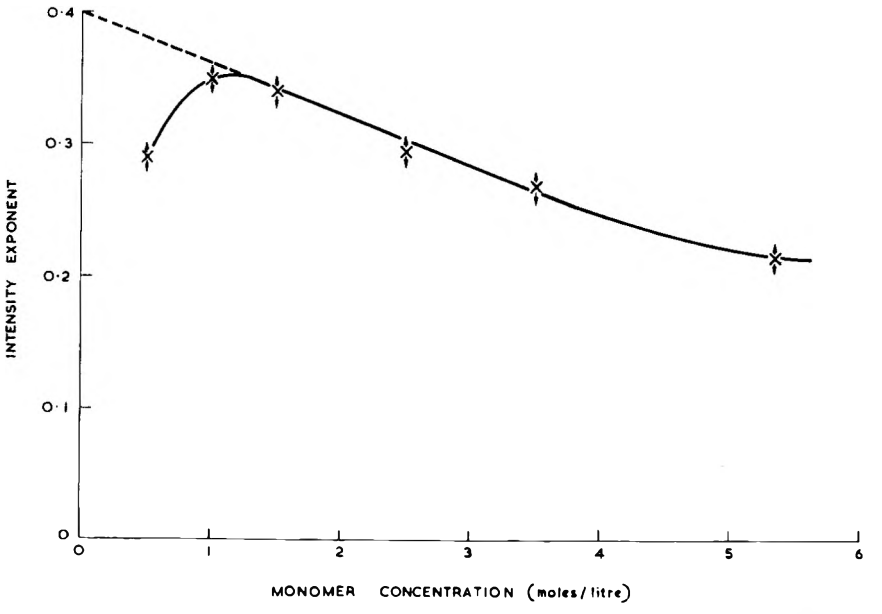

Fig 10. Variation of intensity exponent with styrene concentration.

Since the number of radicals produced in this system is proportional to the radiation intensity, t_1 is proportional to (intensity)$^{-1}$, so that the effect would be expected to increase with increasing radiation intensity as observed. The occurrence of the effect at higher monomer concentration (above 50% conversion) is presumably due to the formation of larger particles capable of containing more than one radical; i.e., δt is increased.

All the results which we have obtained using methyl methacrylate are, therefore, readily interpreted in terms of conventional theories of emulsion polymerization. Radicals produced in pairs inside the particles do not affect the kinetics because δt is negligible. In the regions where a Trommsdorff effect is observed, however, such reactions would lead to a slight enhancement of the effect.

In the case of styrene polymerization, the variation of rate with monomer concentration (Fig. 7) is roughly as predicted by the Smith-Ewart theory, although the rate does not become entirely independent of monomer concentration at higher monomer concentrations. The low value of 0.34 obtained for the intensity exponent of the reaction, however, led us to study this exponent at a range of monomer concentrations and it was found that the exponent varied with monomer concentration, as shown in Figure 10. The intensity exponent has a low value at high monomer concentrations and increases steadily until the minimum concentration at which free monomer is present is reached, after which it falls sharply. It will be noted, however, that if this effect is ignored and the results obtained above a monomer concentration of 1.1 moles/l. are extrapolated, then an intensity exponent of approximately 0.4 is obtained at zero monomer concentration.

Such behavior is entirely novel and rather difficult to account for. It was thought that energy transfer processes in the water phase, leading to a reduced yield of free radicals, might be responsible, but if the water phase (excluding micelles and particles) is considered as a two-component system of water and styrene, then the excitation energy transfer mechanisms which have been proposed for two-component systems should be applicable, although the dynamic equilibrium of the water phase with respect to styrene somewhat complicates the picture. All the energy transfer mechanisms which have been proposed for two component systems, however, lead to a rate of primary radical generation directly proportional to radiation intensity[7] and are therefore incapable of explaining the observed phenomena. An alternative explanation may be sought in the fact that radiation is the only initiating system which produces hydrogen atoms as one of the primary radicals. It may therefore be postulated that the unexpected kinetic behavior of the system is a function not of the radiation itself, but of the hydrogen atoms which are formed, since no conventional initiating species produces a hydrogen atom as a primary radical. It may be that the hydrogen atom produced in a water phase can either diffuse into a micelle and produce a particle, or react with styrene in true aqueous solution to produce a somewhat unreactive radical whose nature remains unspecified. This radical can either react with micelles and lead to particle formation or may alternatively dimerize. The formation of such a radical by a hydrogen atom within a micelle would not affect kinetics due to the relatively long time interval between successive radicals entering the particle. These ideas may be embodied in the following kinetic scheme for the initial stages of reaction:

$H_2O \xrightarrow{\sim\sim} OH + H$	$k_1 I$
$OH + M \rightarrow P$	$k_2[OH][M]$
$H + M \rightarrow P$	$k_3[H][M]$
$H + S_w \rightarrow A$	$k_4[H][S_w]$
$2A \rightarrow A - A$	$k_5[A]^2$
$A + M \rightarrow P$	$k_6[A][M]$

where I represents radiation intensity, M is the number of micelles, P is a polymer particle, S_w is a styrene molecule in true aqueous solution (not in micelles), A represents the stable radical produced by the reaction of hydrogen atoms and styrene monomer, and other symbols have their generally accepted meaning.

The Smith-Ewart theory calculates the rate of particle formation by making two extreme assumptions. Firstly, it is assumed that all the radicals formed enter the very small micelles so long as micelles are still present at all. This will give too high a particle number because radicals will certainly also enter the already formed latex particles. The second approximation assumes that the same number of radicals always enter through a given surface in unit time, whether the surface is on a small or a large par-

ticle. This gives too low a value for N because the small micelles should capture more free radicals than the large latex particles. However, Smith and Ewart have shown that the two approaches lead to a value for N differing only by a numerical factor of 1.43. Taking the first of these two assumptions we see from the above equations that the rate of particle formation is

$$dN/dt = k_2[\mathrm{M}][\mathrm{OH}] + k_3[\mathrm{M}][\mathrm{H}] + k_6[\mathrm{M}][\mathrm{A}] \tag{5}$$

and application of steady-state kinetics to the aqueous phase leads to the expression:

$$\frac{dN}{dt} = k_1\mathrm{I}\left(1 + \frac{1}{1 + \dfrac{k_4[\mathrm{S_w}]}{k_3[\mathrm{M}]}}\right) + \frac{k_6[\mathrm{M}]}{2k_5}\left\{\left(k_6^2[\mathrm{M}]^2 + \frac{4k_1k_4k_5\mathrm{I}[\mathrm{S_w}]}{k_3[\mathrm{M}] + k_4[\mathrm{S_w}]}\right)^{1/2} - k_6[\mathrm{M}]\right\} \tag{6}$$

If this value of dN/dt is substituted in the conventional Smith-Ewart equations, the overall reaction rate is found to be given by the expression:

$$-\frac{d\mathrm{S}}{dt} = k_p[\mathrm{S_p}]k'\left[k_1\mathrm{I}\left(1 + \frac{1}{1 + \dfrac{k_4[\mathrm{S_w}]}{k_3[\mathrm{M}]}}\right) + \frac{k_6[\mathrm{M}]}{2k_5}\left\{\left(k_6^2[\mathrm{M}]^2 + \frac{4k_1k_4k_5\mathrm{I}[\mathrm{S_w}]}{k_3[\mathrm{M}] + k_4[\mathrm{S_w}]}\right)^{1/2} - k_6[\mathrm{M}]\right\}\Big/\mu\right]^{2/5}(a_sS')^{2/5} \tag{7}$$

If the sharp fall of intensity exponent at low monomer concentration shown in Figure 10 is ignored, since in this region Smith-Ewart kinetics do not apply, it will be seen that extrapolation of the remainder of the curve to zero monomer concentration gives an intercept at almost exactly 0.4 as predicted by eq. (7). The equation also indicates a fall in intensity exponent with increasing $[\mathrm{S_w}]$, and if it is assumed that $[\mathrm{S_w}] = f[\mathrm{S}]$ then the observed behavior is that predicted. Since the distribution of both soap and monomer between droplets, micelles, and true aqueous solution will be governed by complex phase equilibrium curves this latter assumption is not unreasonable.

The above hypothesis is capable of explaining qualitatively the abnormalities which we have observed in the γ-ray-initiated emulsion polymerization of styrene, but further work on this system is necessary to establish the mechanism unequivocably.

References

1. Smith, W. V., and R. P. Ewart, *J. Chem. Phys.*, **16**, 592 (1948).
2. Gerrens, H., *Z. Elektrochem.*, **60**, 400 (1956).
3. Dove, D., G. S. Murray, and R. Roberts, UNESCO Intern. Conf. on Radiation in Scientific Research, Unesco/NS/RIC/19.

4. Acres, G. J. K., and F. L. Dalton, *Nature*, **184**, 335 (1959).
5. Gerrens, H., *Fortsch. Hochpolymer. Forsch.*, **1**, 234 (1959); Eng. translation A.E.R.E. 848 by R. C. Murray, see p. 21.
6. Ballantine, D. S., Brookhaven National Laboratory 294 (T50).
7. See, for example, Okamura, S., and T. Manatabe, *Mem. Fac. Eng. Kyoto University*, **21**, Pt. 3, 294 (1959).

Résumé

On a étudie la polymérisation du méthacrylate de méthyle et du styrène, initiée par les rayons-γ-d'une source de Co^{60} Pour chaque monomère, on a déterminé l'influence de la concentration en monomère et de l'intensité de la radiation sur la vitesse de polymérisation. On a démontré que la polymérisation en émulsion du méthacrylate de méthyle peut être décrite par les théories admises pour la polymérisation en émulsion. Dans le cas du styrène, on a trouvé que l'exposant de l'intensité dépend de la concentration du monomère. Une telle influence ne se produit pas dans les systémes d'initiations conventionnels et elle ne peut pas être expliquée sans une certaine modification de la théorie.

Zusammenfassung

Eine Untersuchung der ^{60}Co-γ-Strahlen-gestarteten Polymerisation von Methylmethacrylat und Styrol wurde durchgeführt; die Umsatzgeschwindigkeit wurde dilatometrisch gemessen. Die Abhängigkeit der Polymerisationsgeschwindigkeit von der Monomerkonzentration und Strahlungsintensität wurde für beide Monomere bestimmt. Es wurde gezeigt, dass die Emulsionspolymerisation von Methylmethacrylat mit der normalen Emulsionspolymerisationstheorie beschrieben werden kann; im Falle des Styrols wurde eine Abhängigkeit des Intensitätskomponenten von der Monomerkonzentration gefunden. Eine solche Abhängigkeit tritt bei Verwendung konventioneller Startersysteme nicht auf und kann ohne eine gewisse Modifizierung der Theorie nicht erklärt werden.

Received July 30, 1962

JOURNAL OF POLYMER SCIENCE: PART A VOL. 1, PP. 3021–3027 (1963)

Conductivity and Viscosity Measurements on Sodium Polyacrylates of Different Molecular Weights

A. PACKTER,* *School of Pharmacy, Chelsea College of Science, and Technology, London, England*

Synopsis

Combined conductivity and viscosity measurements have been carried out on a series of sodium polyacrylate solutions of different molecular weights with viscosities varying from 1.1 to 40 c.p. Analysis of the measurements indicates that ionic mobilities in polyelectrolyte solutions are not affected by overall solution viscosity; i.e., the Walden rule is not applicable to such solutions.

Introduction

The conductivity of polyelectrolyte solutions has been studied by several workers.[1–3] The experimental results have been explained in terms of polyion-counterion interaction and decrease in the polyion mobility with increasing association of counterion; the polyion mobility also increases with increasing ionic strength and degree of polymer coiling.

Hermans[4] and Rossi[5] have further suggested that ionic mobilities in polyelectrolyte solutions might also be affected, according to the Walden rule, by the high viscosity of polyelectrolyte solutions. This factor could be of great importance in interpreting studies on high molecular weight polyelectrolyte solutions, especially when combined conductivity and viscosity measurements are used to calculate degree of counterion-polyion interaction.[1,2]

The validity of the Walden rule was therefore checked by combined conductivity and viscosity studies on a series of solutions of sodium polyacrylates of different molecular weight and with viscosities varying from 1.1 to 40 c.p.

Analysis of the measurements indicates that ionic mobilities in polyelectrolyte solutions are *not* affected by overall solution viscosity.

Experimental

Sodium Polyacrylate Solutions

Four polyacrylic acids of different average molecular weight were prepared.[6]

* Private address: 106 Howberry Road, Canons Park, Middlesex, England.

Acrylic acid (20 ml.) and benzene (100 ml.) containing benzoyl peroxide catalyst were reacted for 4 hr. at 75°C. in a 500-ml. flask under continuous nitrogen stirring (after 30 min. previous deoxygenation). The suspended white powder was washed free of unreacted acid with benzene, then with petrol ether, filtered and dried at 40°C.

The average molecular weights, as determined viscometrically[7] were: polyacrylic acid, HA, M = 50,000; HB, 150,000; HC, 500,000; HD, 1,500,000;.

Polyacid solutions (0.1N) were titrated potentiometrically to pH 8.5 with sodium hydroxide and the sodium polyacrylate solutions diluted as required with conductivity water $K = 0.8\text{–}1.2\ 10^{-6}$ ohm^{-1} at 25°C.

All concentrations were then expressed in terms of gram equivalent monomer per liter.

Conductivity Measurements

A titration cell was used with platinized platinum dipping electrodes; the cell constant was determined using standard potassium chloride solutions. Solutions were stirred with flowing nitrogen.

Conductivity measurements were made at 25.0 ± 0.1°C. using a Pye conductance bridge (model 11700) operating at 300 cycles/sec. and fitting with a cathode-ray oscillographic detector; cell capacitance effects were balanced out by means of a variable condenser in parallel with the variable resistance. The bridge operated with an accuracy of 0.1%.

Measured volumes of sodium polyacrylate solution were run into conductivity water, the solutions allowed to reach equilibrium (at 25°C.), the stirring stopped, and the conductivity measured.

In all, 10 to 15 measurements were taken with each polymer to provide a suitable concentration range ($C = 10^{-4}N$ to $3.10^{-2}N$) for study.

Viscosity Measurements

Viscosities were measured at 25.0°C. with a suspended level dilution viscometer (Ubbelohde-type, ASTM specification D445-46T) made by Polymer Consultants Ltd. The effluent time for distilled water was 250 sec. at 25.0°C. and kinetic energy corrections were negligible. Measurements were made over the concentration range $C = 3.10^{-2}N$ to $10^{-4}N$.

Determination of Polyion Mobility

For each system studied, the polyion mobility ($\lambda_{P(0)^-}$) in dilute solution ($C = 10^{-4}N$) was calculated by Gregor's method.[2] Then at other concentrations, the polyion mobility (λ_{P^-}) was determined from the relation,[2]

$$\lambda_{P^-} = \lambda_{P(0)^-}\left[\frac{(\eta_{sp}/c)_{(0)}}{\eta_{sp}/c}\right]^{1/3}$$

where $\eta_{sp}/c = (\eta_{sp}/c)_{(0)}$ at $c = 10^{-4}N$.

$$\eta_{sp} = \frac{\eta_{\text{soln.}} - \eta_{\text{d.w.}}}{\eta_{\text{d.w.}}}$$

where d.w. indicates distilled water.

The Walden Rule Applied to Counterion Mobility

The conductivity and viscosity measurements were first analyzed on the assumption that the *polyion* mobility varied with concentration according to accepted theory,[1,2,4] but that the *counterion* mobility might be affected by overall solution viscosity.

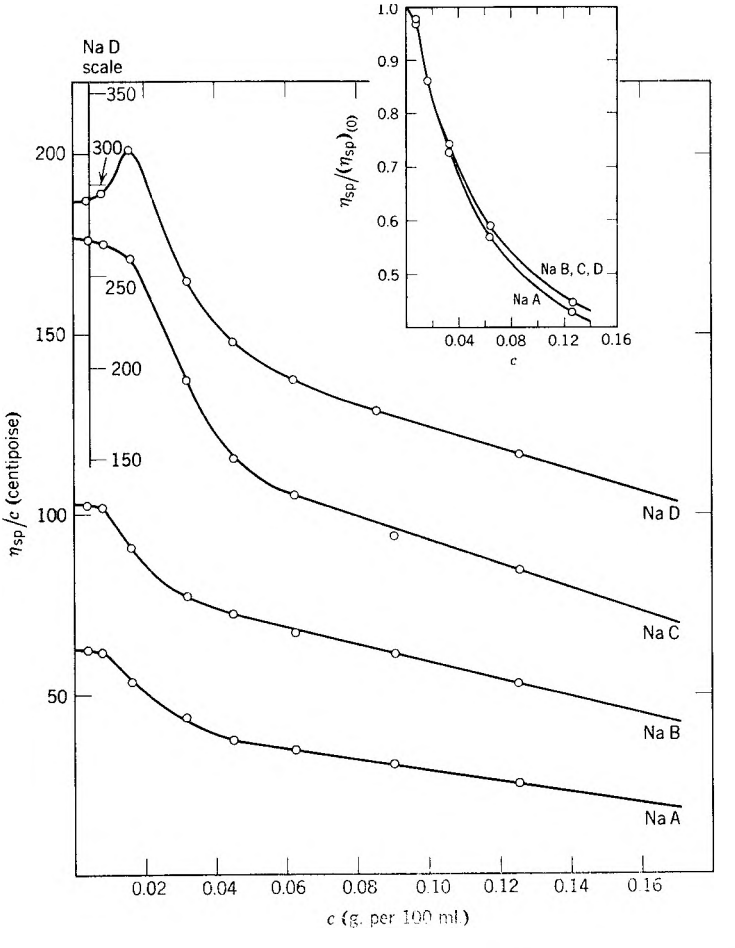

Fig. 1. Variation of specific viscosity of sodium polyacrylate solutions with concentration, 25°C.

Viscosity

Viscosity results are presented in Figure 1. The specific viscosity concentration ratio (η_{sp}/c) decreases continuously with increasing polysalt concentration (and ionic strength). At any particular polysalt concentration, η_{sp} increases with molecular weight. However, the $\eta_{sp}/\eta_{sp(0)}$ ratio at any concentration is practically independent of molecular weight (refer to Fig. 1 inset).

Polyanion Mobility

Polyanion mobility (λ_{P^-}) values, as determined by Gregor's method at $C = 10^{-3}N$ and $C = 10^{-2}N$, are presented in Table I; the results are typical for the range of concentrations studied. At any particular ionic strength, the polyion mobility is practically independent of polymer molecular weight and overall solution viscosity. The results, in fact, agree with earlier work.[4]

TABLE I

Check on Walden Rule for Counterion Mobility Only, in Sodium Polyacrylate Solutions (25.0°C.)

Polyelectrolyte soln.	$\eta_{soln.}$, c.p.	$\lambda_{d.w.Na^+}$, ohms^{-1}	$\lambda_{0Na^+corr.}$, ohms^{-1}	λ_{P^-}, ohms^{-1}	α (*i*)	α (*ii*)
			(*A*) $C = 10^{-3}N$			
Na-A	1.48	50.1	33.9	41.0	0.497	0.600
Na-B	1.81	50.1	27.7	41.0	0.499	0.642
Na-C	2.50	50.1	20.3	41.0	0.500	0.690
Na-D	2.82	50.1	17.8	41.5	0.500	0.730
			(*B*) $C = 10^{-2}N$			
Na-A	3.00	50.1	16.7	53.0	0.400	0.590
Na-B	4.32	50.1	11.6	53.0	0.401	0.625
Na-C	10.00	50.1	5.0	53.5	0.402	0.685
Na-D	32.00	50.1	1.6	54.0	0.404	0.720

Counterion Mobility and Degree of Association

The conductivity results are presented in Figure 2. The equivalent conductivity ($\Lambda = 1000K/C$) decreases rapidly from $\Lambda = \Lambda_0$ (at $C = 0$) to approximately 0.5 Λ_0 at $C = 10^{-4}N$ and then gradually decreases further to some minimum value at $C > 10^{-2}N$.

Over the polysalt concentration range investigated, there is no appreciable variation of conductivity with solution viscosity.

The degree of counterion-polyion association (α) at different polysalt concentrations was then calculated in two ways: (*1*) From Gregor et al.'s[2] relation, neglecting the Walden rule for the counterion mobility, i.e.,

$$\Lambda = \alpha(\lambda_{0Na^+(d.w.)} + \alpha\lambda_{P^-}) \quad (1)$$

TABLE II

Check on Walden Rule for Both Ions in Sodium Polyacrylate Solutions (25.0°C.)

Polyelectrolyte soln.	$C = 10^{-3}N$				$C = 10^{-2}N$			
	$\eta_{soln.}$, c.p.	$\lambda_{0Na^+(corr.)}$, ohms^{-1}	$\lambda_{P^-(corr.)}$, ohms^{-1}	α	$\eta_{soln.}$, c.p.	$\lambda_{0Na(corr.)}$, ohms^{-1}	$\lambda_{P^-(corr.)}$, ohms^{-1}	α
Na-A	1.48	33.9	27.0	0.580	3.00	16.7	13.3	0.970
Na-B	1.81	27.7	22.1	0.705	4.32	11.6	9.26	>1
Na-C	2.50	20.3	16.0	0.970	10.00	5.0	4.0	$\gg$1
Na-D	2.82	17.8	14.2	>1	32.00	1.6	1.3	$\gg$1

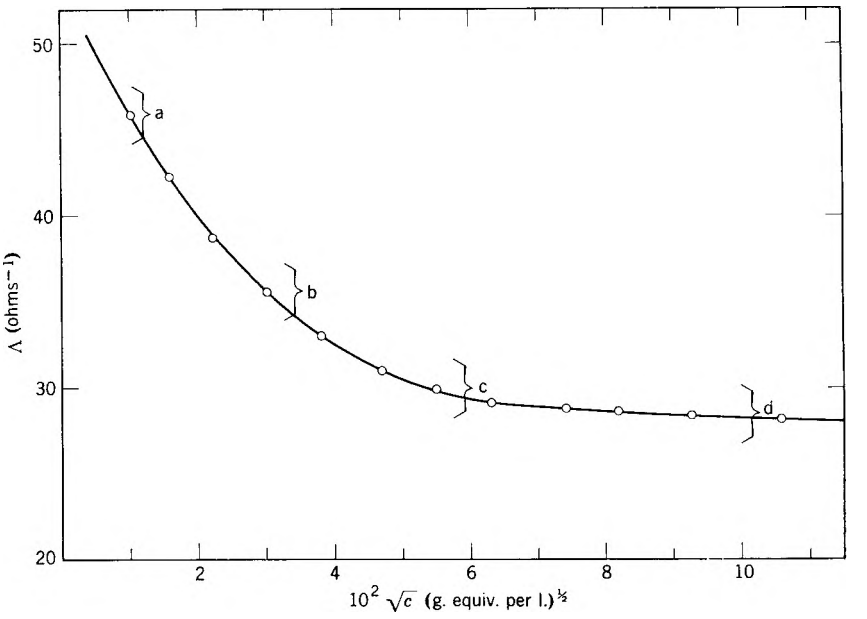

Fig. 2. Variation of conductivity of sodium polyacrylate solutions with concentration, 25°C. (*a*), η = 1.05–1.18 cp.; (*b*), η = 1.48–2.82 cp.; (*c*), η = 2.52–11.66 cp.; (*d*), η = 3.00–33.00 cp.

where

$$\lambda_{P^-} = \lambda_{P(0)^-} - \left[\frac{(\eta_{sp}/c)_{(0)}}{\eta_{sp}/c}\right]^{1/3} \tag{2}$$

(*2*) From Gregor's relation, assuming the Walden rule applies to the counterion mobility, i.e.,

$$\Lambda = \alpha(\lambda_{0Na^+(corr.)} + \alpha\lambda_{P^-}) \tag{3}$$

where

$$\lambda_{0Na^+(corr.)} = \lambda_{0Na^+(d.w.)} \times \frac{\eta_{d.w.}}{\eta_{soln.}} \tag{4}$$

and λ_{P^-} is as above.

Some typical results for $10^{-3}N$ and $10^{-2}N$ solutions are presented in Table I.

Only the α-values calculated by the first method are independent of molecular weight and agree with those obtained by techniques that are unaffected by solution viscosity.[8-10]

The Walden Rule Applied to Polyion and Counterion Mobilities

The degree of counterion-polyion association at different polysalt concentrations was then calculated on the assumption[5] that both counterion mobility (λ_{Na^+}) *and* polyion mobility (λ_{P^-}) might be affected by overall solution viscosity according to the Walden rule, i.e.,

$$\Lambda = \alpha(\lambda_{0Na^+(corr.)} + \lambda_{P^-(corr.)}) \quad (5)$$

where

$$\lambda_{0Na^+(corr.)} = \lambda_{0Na^+(d.w.)} \times \frac{\eta_{d.w.}}{\eta_{soln.}} \quad (4)$$

and

$$\lambda_{P^-(corr.)} = \lambda_{P(0)^-} \times \frac{\eta_{d.w.}}{\eta_{soln.}} \quad (6)$$

Typical results for $10^{-3}N$ and $10^{-2}N$ solutions are presented in Table II. These results are clearly incompatible with polyelectrolyte theory.[1,4,11,12]

Discussion

The conductivity measurements indicate that ionic mobilities in polyelectrolyte solutions are *not* affected by the overall solution viscosity.

Presumably, both counterions and polyions are moving in an environment of pure water and the Walden rule is not applicable to such solutions.

References

1. Oth, A., and P. Doty, *J. Phys. Chem.*, **56**, 43 (1952).
2. Gregor, H. P., D. H. Gold, and M. Frederick, *J. Polymer Sci.*, **23**, 467 (1957).
3. Bourdais, J., *J. Chim. Phys.*, **56**, 194 (1959).
4. Hermans, J. J., *Koninkl. Ned. Akad. Wetenschap. Proc.*, **B58**, 182 (1955).
5. Rossi, G., *Gazz. Chim. Ital.*, **85**, 1171 (1955).
6. Trementozzi, Q., *J. Am. Chem. Soc.*, **76**, 5273 (1956).
7. Ito, H., *Kogyo Kagaku Zasshi*, **59**, 930 (1956).
8. Chadwick, C. S., *J. Polymer Sci.*, **28**, 355 (1958).
9. Kagawa, I., *J. Polymer Sci.*, **37**, 375 (1959).
10. Crescenzi, V., V. De Rosa, and D. Maldarella, *Ric. Sci.*, **30**, 1680 (1959).
11. Wall, F. T., *J. Chem. Phys.*, **26**, 114 (1957).
12. Oosawa, F., *J. Polymer Sci.*, **23**, 421 (1957).

Résumé

Des mesures combinées de conductivité et de viscosité ont été effectuées sur une série de solutions de polyacrylate de sodium de poids moléculaires différents avec des viscosités allant de 1.1 à 4.0 centipoises. Une analyse des résultats indique que les mobilités ioniques dans les solutions de polyélectrolytes ne sont pas affectées par la viscosité globale de la solution; c'est à dire que la règle de Walden n'est pas applicable à de telles solutions.

Zusammenfassung

Kombinierte Leitfähigkeits- und Viskositätsmessungen wurden an einer Reihe von Natriumpolyacrylatlösungen mit verschiedenem Molekulargewicht im Viskositätsbereich von 1,1 bis 40 Centipose ausgeführt. Die Messergebnisse zeigen, dass die Ionenbeweglichkeit in Polyelektrolytlösungen durch die Gesamtviskosität der Lösung nicht beeinflusst wird; d.h. die Waldensche Regel ist auf solche Lösungen nicht anwendbar.

Received July 20, 1962

JOURNAL OF POLYMER SCIENCE: PART A VOL. 1, PP. 3029–3042 (1963)

Infrared Absorption Spectra of Polyacrylonitrile and Deuterated Polyacrylonitriles

HIROYUKI TADOKORO and SHUNSUKE MURAHASHI, *Department of Polymer Science, Faculty of Science, Osaka University, Nakanoshima, Kita-Ku, Osaka, Japan*, and REIZÔ YAMADERA and TEI-ICHI KAMEI, *Textile Research Institute, Tôyô Spinning Company, Ltd., Katata, Shiga, Japan*

Synopsis

Poly-α-deuteroacrylonitrile and poly-α,β,β-trideuteroacrylonitrile were synthesized. α-Deuteroacrylonitrile was prepared by the deuterium exchange reaction of acrylonitrile with D_2O in the presence of CaO. α,β,β-Trideuteroacrylonitrile was prepared by the addition reaction of C_2D_2 and DCN. The infrared spectra of polyacrylonitrile, the deuterated polyacrylonitriles, and the intermediate products of the syntheses were measured in the 4000–400 cm.$^{-1}$ region and discussed. The polarized spectra of the oriented polymer samples were also measured. The bands of PAN in the CH stretching region exhibit reasonable shifts in the spectra of the deuterated polymers, while the C≡N stretching band shows no appreciable shift. The bands in the region lower than 1400 cm.$^{-1}$ exhibit complicated behavior in deuteration. The calculation of the normal vibrations of polyacrylonitrile has been made, assuming a syndiotactic planar zigzag chain as a most simple model for calculation. The assignments of the bands are discussed.

INTRODUCTION

Only a few papers have been published on the infrared absorption spectrum of polyacrylonitrile (PAN). The assignments of the absorption bands of PAN have been studied by use of factor group analysis of the atactic planar zigzag model by Liang and Krimm.[1] The infrared absorption bands due to PAN endgroups have been reported by Yamadera.[2] Recently, a report has appeared* on the infrared spectra of PAN and poly-α-deuteroacrylonitrile (PAN-αd_1) by Liang, Pearson, and Marchessault.[3] In the present paper the syntheses and the infrared absorption spectra of PAN, deuterated PAN i.e., PAN-αd_1 and poly-α,β,β-trideuteroacrylonitrile (PAN-d_3), and of the intermediate products are reported. On the basis of these experimental data, tentative assignments of the absorption bands of PAN have been made. Furthermore, the calculation of the normal vibrations has been made for reference to the interpretation of the spectra, assuming a syndiotactic planar zigzag chain as the most simple model for calculation.

* This paper was noted only after presentation of the present work at the Annual Meeting of the Society of Polymer Science (Japan), May 27, 1961.

EXPERIMENTAL AND RESULTS

Preparation of the Samples

As has already been reported,[4,5] the α-hydrogen of acrylonitrile (AN) can be easily deuterated by the isotope exchange reaction with deuterium oxide in the presence of calcium oxide:

$$CH_2{=}CH{-}CN + D_2O \xrightarrow{CaO} CH_2{=}CD{-}CN \quad (1)$$

The obtained α-deuteroacrylonitrile (AN-αd_1) can be polymerized by the ordinary method for AN without reexchange with hydrogen.

PAN-d_3 can be prepared by the method shown in eqs. (2)–(4):

$$CaC_2 + D_2O \rightarrow C_2D_2 \quad (2)$$

$$KCN + D_2SO_4 \rightarrow DCN \quad (3)$$

$$C_2D_2 + DCN \rightarrow CD_2{=}CD{-}CN \rightarrow \text{-}(\text{-}CD_2{-}\underset{\displaystyle CN}{\underset{|}{CD}}\text{-})_n \quad (4)$$

Figure 1 shows schematically the apparatus used for the synthesis of α,β,β-trideuteroacrylonitrile (AN-d_3). This apparatus was made by modifying the apparatus for the synthesis of α,β,β-trideuterovinyl acetate.[6] The system can be highly evacuated by using a mercury diffusion pump and rotary pump. Vessel B_1 made of Telex glass (borosilicate glass manufactured by Tôshiba Electric Co., Ltd.) contained calcium carbide

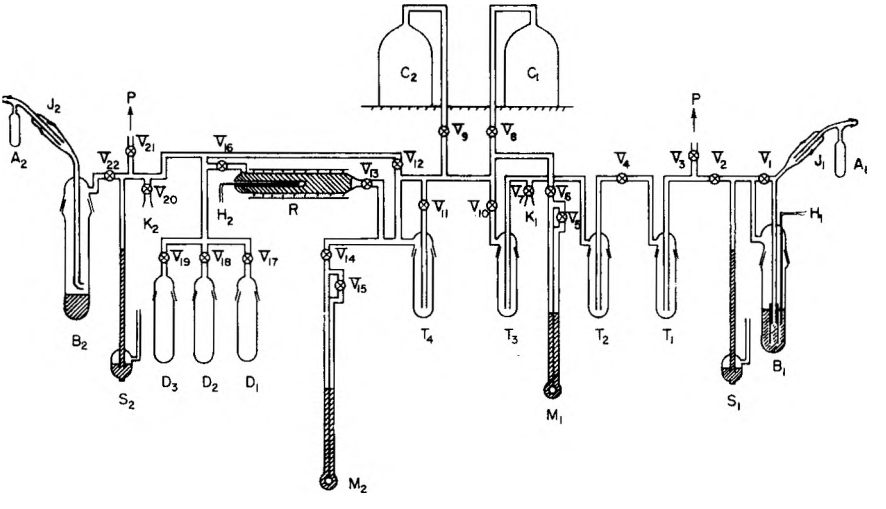

Fig. 1. The apparatus for the synthesis of α,β,β-trideuteroacrylonitrile: (A_1) D_2O; (B_1) CaC_2 (vessel made of Telex); (C_1) gas vessel for C_2D_2 (20 l.); (A_2) D_2SO_4; (B_2) KCN (vessel made of Telex); (C_2) gas vessel for DCN (20 l.); (D_1, D_2, D_3) traps for product; (H_1, H_2) thermocouples; (J_1, J_2) joints; (K_1, K_2) gas cells for infrared measurements; (M_1, M_2) mercury manometers; (P) vacuum pump; (R) reaction tube (made of Telex); (S_1, S_2) safety valves: (T_1, T_2, T_3) traps; (T_4) trap for liquidized DCN; (V_1–V_{22}) stopcocks.

which was dried at about 550°C. for about 4 hr. under high vacuum (10^{-4} mm. Hg or below). The container of deuterium oxide A_1 was rotated at joint J_1 and acetylene-d_2 was generated by dropping deuterium oxide into B_1. The generated acetylene-d_2 was transferred to the trap T_1 cooled with liquid nitrogen, and then warmed up to the Dry Ice temperature by exchanging the refrigerant. The same procedure was repeated at trap T_2 and the acetylene-d_2 was then transferred to trap T_3 cooled with liquid nitrogen. In this way impurities and excess deuterium oxide were eliminated from the acetylene-d_2. The acetylene-d_2 was then stored in the gas vessel C_1 (about 20 l.).

Deuterium cyanide was prepared by a procedure similar to the above for acetylene-d_2 from potassium cyanide and sulfuric acid-d_2 (Shôwa Denkô Co., Ltd.; deuterium concentration 98%). Deuterium cyanide was generated by dropping sulfuric acid-d_2 into vessel B_2 containing potassium cyanide previously dried at about 300°C. for about 10 hr. In this procedure the vessel B_2 was cooled by water in order to avoid the generation of sulfur dioxide by the elevation of the temperature during the reaction. In order to eliminate carbon dioxide and other impurities, the generated deuterium cyanide was transferred to the trap T_3, which is cooled with Dry Ice–acetone-mixture. Then the deuterium cyanide was stored in the gas vessel C_2 (about 20 l.).

The isotopic purities of the acetylene-d_2 and deuterium cyanide were checked by measuring the infrared spectra by use of a gas cell K. The deuterium cyanide and the acetylene-d_2 were mixed at a volume ratio of 1:2.4 by passing the acetylene-d_2 gas over the deuterium cyanide condensed in the trap T_3. The mixed gas was introduced into a reaction tube containing zinc oxide catalyst (kindly supplied by Dr. S. Morimoto[7]) and heated at 430°C. The rate of flow was about 40 cc./min. The reaction mixture was trapped into D_1, D_2, or D_3 cooled by liquid nitrogen, and then the unreacted acetylene-d_2 was removed by changing the refrigerant to Dry Ice. When the refrigerant was again changed to a sodium chloride–ice mixture, most of the unreacted deuterium cyanide could be removed. The obtained AN-d_3 was purified by distillation[10] on a concentric distillation column (Taika Kôgyô Co., Ltd., Osaka) with small amount of toluene. Toluene does not form an azeotropic mixture with acrylonitrile and remains in the distillation column after almost all AN-d_3 distilled off.

The polymerization of AN-d_3 was carried out in a sealed glass tube with ammonium persulfate catalyst at 60°C. for about 3 hr. The small amount of toluene and deuterium cyanide contained in AN-d_3 did not prevent the polymerization reaction.

Infrared Spectra of Intermediate Products

The measurements of the infrared spectra were carried out with a Hitachi EPI-2 double-beam spectrophotometer and partly with a Shimadzu AR-275 IIS double-beam spectrophotometer. Figure 2 shows the infrared spectra of AN-αd_1 prepared by the isotope exchange reaction. The degree

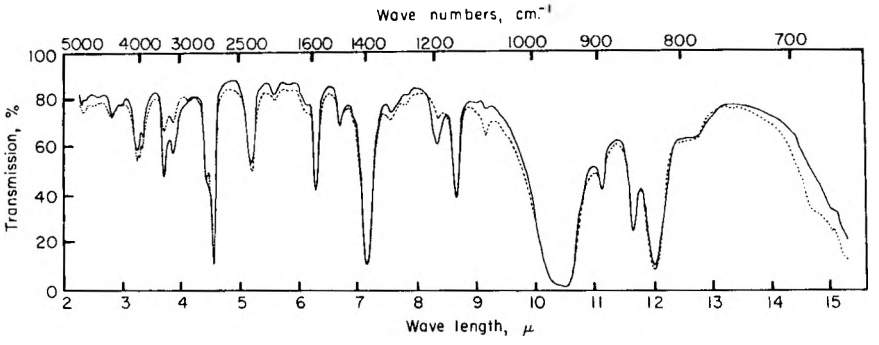

Fig. 2. Infrared spectra of α-deuteroacrylonitrile: (- -) degree of deuteration 85%; (——) degree of deuteration 95%.

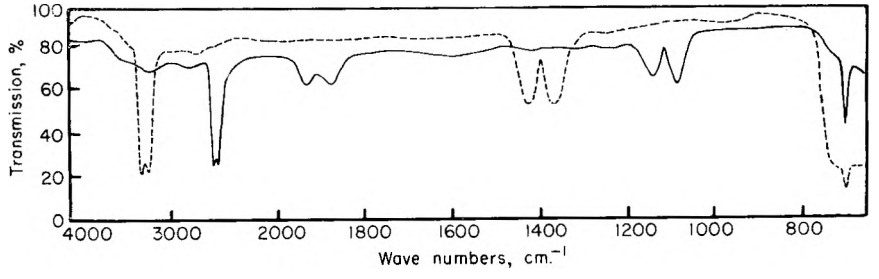

Fig. 3. Infrared spectra of (——) deuterium cyanide and (- -) hydrogen cyanide at 100 mm. Hg.

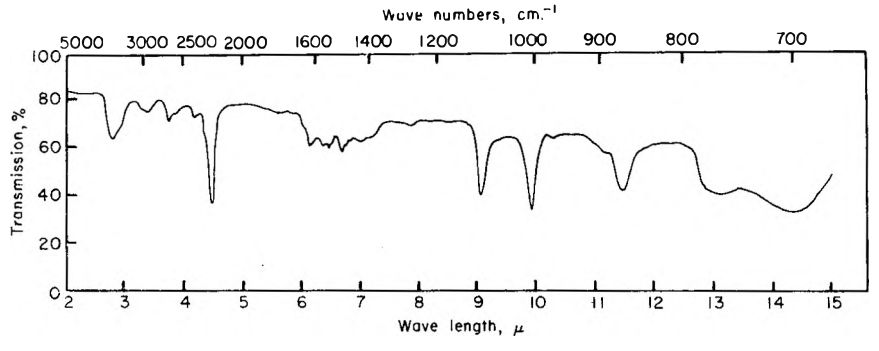

Fig. 4. Infrared spectrum of α,β,β-trideuteroacrylonitrile purified by gas chromatography.

of deuteration was estimated by using the 1093 cm.$^{-1}$ band in the infrared spectra or by mass spectrometry. (Measurements of mass spectra were kindly carried out by Mr. M. Hatada of Osaka Laboratory, Japanese Association for Radiation Research on Polymers.) In Figure 2 the broken and the solid curves represent the spectra of AN-αd_1 having the degrees of deuteration of 85% and 95%, respectively. The former sample was pre-

pared by distillation after reflux of the mixture of AN and D_2O (1:1 in volume) with CaO for 7 hr., and the latter was prepared by further reflux of the former sample with an equal volume of D_2O for 3 hr. In the spectra of Figure 2 the 2724, 2622, and 1211 cm.$^{-1}$ bands are due to the small amount of D_2O remaining in the AN-αd_1. The spectrum of the sample (95% deuteration) is in good agreement with the spectrum reported by Cochburn and Hubbey.[4]

The infrared spectrum of the acetylene-d_2 prepared by the above method has been reported in a previous paper.[6] Figure 3 shows the infrared spectra of the DCN prepared by the above-mentioned method (solid line) and HCN for reference (broken line) measured in a 10 cm. gas cell at 100 mm. Hg. The CH stretching and deformation bands of HCN at 3321 and 712 cm.$^{-1}$, respectively, are very weak in the spectrum of the prepared DCN. The spectrum obtained here is in good agreement with previous reports.[8,9] The degree of deuteration was estimated from the band at 712 cm.$^{-1}$ to be about 97%.

In Figure 4 the infrared spectrum of the AN-d_3 purified by gas chromatography is shown. The conditions for the gas chromatographic separation of AN-d_3 from DCN and toluene were as follows: carrier gas, He at 50 ml./min.; temperature, 70°C.; chromatographic column, 20 mm. in diameter, 1.56 m. in length, and packed with β,β'-oxydipropionitrile. Under these conditions, the retention times of AN-d_3, DCN, and toluene are 16, 6.5, and more than 20 min., respectively; thus AN-d_3 can be separated almost completely.

Infrared Spectra of PAN, PAN-αd_1 and PAN-d_3

The polarized infrared spectra of PAN, PAN-αd_1 and PAN-d_3 are shown in Figures 5, 6, and 7, respectively. The solid and broken curves represent the spectra obtained with radiation polarized perpendicular and parallel to the direction of elongation, respectively. The wave numbers, relative intensities, and dichroism of the absorption bands for PAN and deuterated PAN's are given in Tables I and II. The films for the infrared measurements were prepared from the dimethylformamide solution at about 60°C. The small amount of solvent remaining in the films was removed by treat-

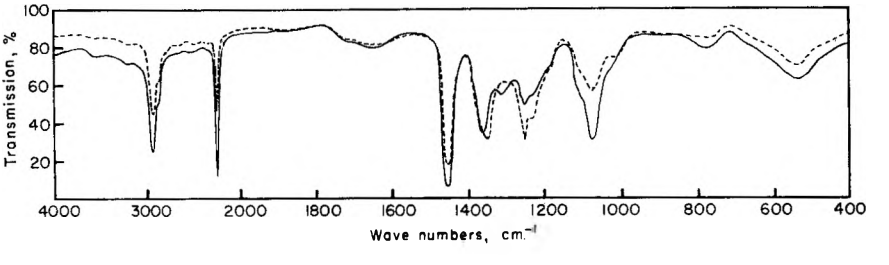

Fig. 5. Infrared dichroism of polyacrylonitrile: (——) electric vector perpendicular to elongation; (- -) electric vector parallel to elongation.

TABLE I

Observed Data, Calculated Frequencies, and Tentative Assignments for PAN

Observed			Calculated	
Frequency, cm.$^{-1}$	Intensity	Dichroism[a]	Frequency, cm.$^{-1}$	Tentative assignments[b]
2950	vs	σ	2935	$\nu_a(CH_2)$ (B_1) (B_2)
2930	(sh)	σ	2929	$\nu(CH)$ (A_1) (B_1)
2870	m	σ	2886	$\nu_s(CH_2)$ (A_1)
2810	vw	π		
2237	vs	σ	2237	$\nu(CN)$ (A_1) (B_1)
1447	vs	σ	1453	$\delta(CH_2)$ (A_1)
			1396	$w(CH_2)$ (B_1)
1362	m	σ	1362	$\delta(CH)$ (A_1)
1355	m	π	1357	$w(CH_2)$ (B_2)
1310	w	σ	1309	$\delta(CH)$ (B_1)
1247	s	π	1189	$w(CH) - \nu(CC)$ (B_2)
1227	w	π		
1175	(sh)	π		
1115	(sh)	σ	1101	$\nu(CC)$ (A_1)
1073	vs	σ	1080	$\nu(CC)$ (B_1)
			1066	$r(CH_2)$ (B_1)
1015	(sh)	π	1018	$w(CH) + \nu(CC)$ (B_2)
			999	$t(CH_2)$ (A_1)
865	vw	π	847	$r(CH_2)$ (B_2)
778	m	σ	796	$\nu(C—CN)$ (A_1)
			764	$\nu(C—CN)$ (B_1)
570	(sh)	σ	551	$\delta(C—C—CN) - \delta(C—C—N)$ (B_1)[c]
537	m	σ	518	$\delta(C—C—CN) - \delta(C—C—N)$ (A_1)
520	(sh)		524	$w(C—C—CN) - w(C—C—N)$ (B_2)
			357	$\delta(C—C—C)$ (B_1)
			271	$\delta(C—C—CN) + \delta(C—C—N)$ (B_1)[d]
			246	$\delta(C—C—CN) + \delta(C—C—N)$ (A_1)
			204	$w(C—C—CN) + w(C—C—N)$ (B_2)

[a] σ = perpendicular band; π = parallel band.

[b] Here ν = stretching; ν_s = symmetric stretching; ν_a = antisymmetric stretching. δ = bending or deformation perpendicular to the chain axis; w = wagging or deformation parallel to the chain axis; r = rocking; t = twisting. The signs denote the phase relations of the coupling.

[c] Here, $\delta(C—C—CN) - \delta(C—C—N)$ or $w(C—C—CN) - w(C—C—N)$ denotes:

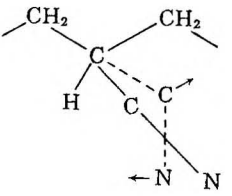

[d] Here, $\delta(C—C—CN) + \delta(C—C—N)$ or $w(C—C—CN) + w(C—C—N)$ denotes:

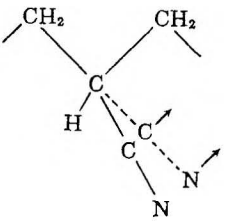

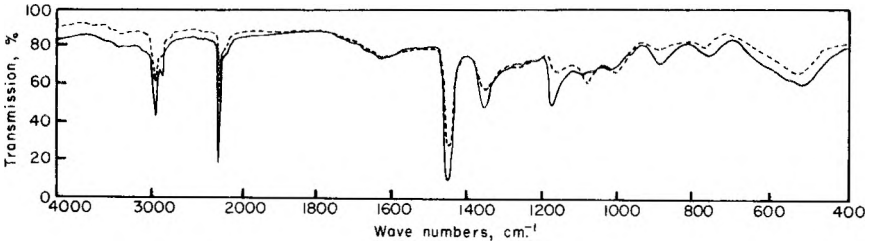

Fig. 6. Infrared dichroism of poly-α-deuteroacrylonitrile: (——) electric vector perpendicular to elongation; (- -) electric vector parallel to elongation.

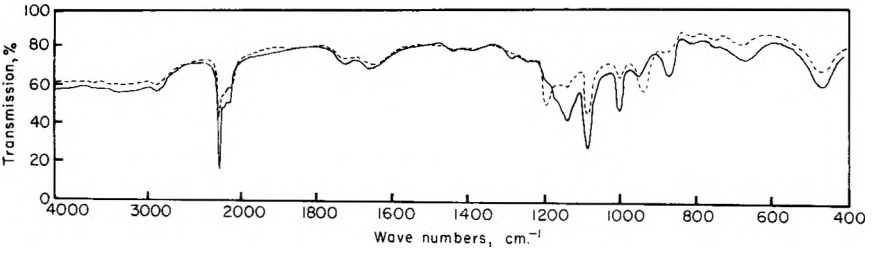

Fig. 7. Infrared dichroism of poly-α,β,β-trideuteroacrylonitrile: (——) electric vector perpendicular to elongation; (- -) electric vector parallel to elongation.

TABLE II
Infrared Data for PAN-αd_1 and PAN-d_3

PAN-αd_1			PAN-d_3		
Frequency, cm.$^{-1}$	Intensity	Dichroism	Frequency, cm.$^{-1}$	Intensity	Dichroism
2950	vs	σ	2240	vs	σ
2870	m	σ	2180	w	σ
2810	vw	π	2130	w	σ
2237	vs	σ	1292	w	σ
2170	w	σ	1198	m	π
1447	vs	σ	1142	s	σ
1355	m	σ	1085	vs	σ
1176	s	σ	1003	s	σ
1087	m	π	957	m	σ
1020	m	σ	942	m	π
1014	m	π	873	m	σ
969	vw	σ	807	vw	π
894	m	π	685	m	σ
889	m	σ	678	m	σ
765	m	π	502	(sh)	σ
755	m	σ	480	m	σ
563	(sh)	σ			
532	m	σ			

ing in boiling water for 1 hr. The films were oriented by stretching in an air bath at about 130°C. to about three times the original length. The samples obtained by this method[10] give good polarization spectra.

From these spectra it is clear that the prepared samples of PAN-αd_1 and PAN-d_3 have satisfactorily high degrees of deuteration. The strong bands at 1247 and 1073 cm.$^{-1}$ in the spectrum of PAN are absent in the spectrum of PAN-αd_1, and only very weak absorption bands remain in the CH-stretching (2800–3000 cm.$^{-1}$) and the CH_2-bending regions (1447 cm.$^{-1}$) of the spectrum of PAN-d_3.

DISCUSSION

The crystal structure of PAN has not been determined definitely because of the poor x-ray diffraction patterns. Liang and Krimm[1] have shown that the analysis based upon the atactic configuration is in agreement with the observed infrared spectra of PAN. On the other hand, Stéfani et al.[11,12] have reported from x-ray studies the coexistence of two (crystalline) phases formed by the association of the syndiotactic or isotactic short segments along the linear chains. Menčik[13] has present a slightly twisted planar zigzag model of PAN from his x-ray studies, but has not drawn any conclusions regarding the tactic structure of the chain. Kakudo[14] suggested on the basis of his x-ray results for PAN that the possibility of the syndiotactic sequence in the short range cannot be excluded. Quite recently, Bohn et al.[15] presented a new model of laterally ordered polymer for PAN and reported that the PAN molecule is believed to have no regularity along the longitudinal direction. Thus the determination of the structure of PAN is an unsettled problem at present. The purposes of the present studies are to obtain possible information for (1) the interpretation of the infrared spectrum of PAN, and (2) the clarification of the tactic structure of PAN, if possible.

Spectral Bands in the 4000–1400 cm.$^{-1}$ Region

In Figure 8 the spectra of PAN and PAN-αd_1 in the CH and CD stretching regions measured with LiF optics are shown for the convenience of discussion. The weak band at 2810 cm.$^{-1}$ has been previously assigned by Liang and Krimm[1] to the CH stretching vibration. However, the dichroism of this band was found to be parallel to the direction of elongation by the present experiment on a highly oriented PAN film. Moreover, the band found at 2930 cm.$^{-1}$ as a shoulder in the spectrum of PAN disappears and shifts to 2170 cm.$^{-1}$ in the spectrum of PAN-αd_1. The wave number ratio is 1.35. The 2810 cm.$^{-1}$ band remains without remarkable shift in the spectrum of PAN-αd_1. From these results the CH stretching vibration of PAN should be assigned to the 2930 cm.$^{-1}$ band instead of the 2810 cm.$^{-1}$ band. This conclusion agrees with the one reported recently by Liang et al.[3]

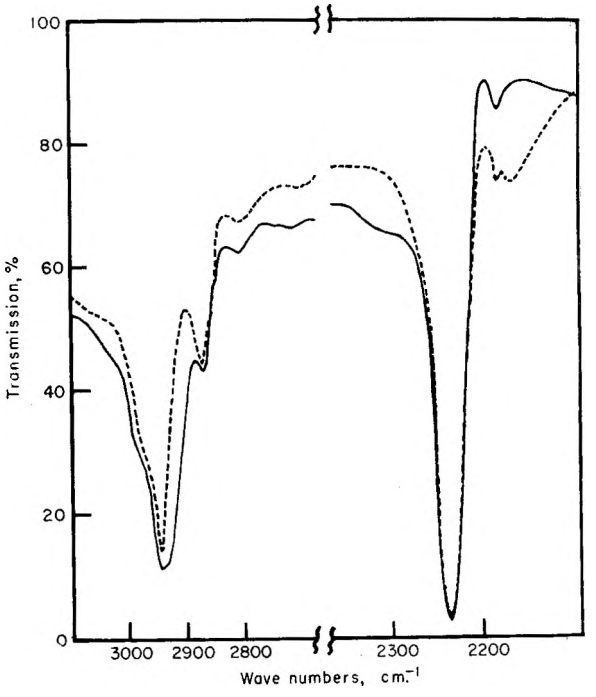

Fig. 8. Infrared spectra of (——) PAN and (- -) PAN-αd_1 in the C-H and C-D stretching regions.

The bands at 2950 and 2870 cm.$^{-1}$ in the spectrum of PAN shift to 2180 and 2130 cm.$^{-1}$, respectively, in the spectrum of PAN-d_3. These bands may be assigned to the CH_2 (or CD_2) antisymmetric and symmetric stretching modes, respectively. The wave number ratios are 1.35 for both these two modes.

The bands due to the C≡N stretching vibration of PAN and the deuterated PAN's are all found at about 2237 cm.$^{-1}$ with no appreciable change. From this fact the coupling of the C≡N stretching with the other vibrational modes may be considered to be negligibly small. Moreover, the possibility of hydrogen bonding between the CN and CH groups, as suggested by several authors,[12, 16–18] may be excluded.

The band at 1447 cm.$^{-1}$ of PAN may be assigned to the CH_2 bending mode, since this band remains at the same position for PAN-αd_1 and shifts to 1085 cm.$^{-1}$ for PAN-d_3 with wave number ratio of 1.33.

Spectral Bands in the 1400–400 cm.$^{-1}$ Region

It is difficult to discuss the assignments of the bands in the 1400–400 cm.$^{-1}$ region on the basis of only the spectral data of PAN and the deuterated PAN's obtained at present, since there is marked mixing of the group vibrations in this region. To overcome these difficulties, the calculation of the normal vibrations of a syndiotactic planar zigzag model of

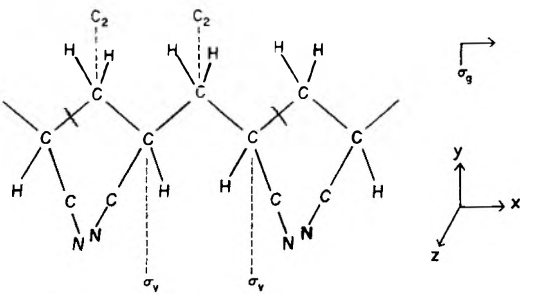

Fig. 9. Unit cell of syndiotactic polyacrylonitrile.

PAN has been made. This model was assumed here, because this is the most simple model for calculation, although the tactic structure of PAN has not been clearly determined.

Here the assumption and the results of the calculation for PAN will be given for reference to the interpretation of the spectra, and the detailed procedure and the results of the calculation (including those for the deuterated PAN's) will be published elsewhere. The infinitely extended planar zigzag chain of the syndiotactic PAN may be analyzed with a one-dimensional space group, the factor group of which is isomorphous with the point group C_{2v} (Figure 9). The symmetry species, character table, numbers of normal modes, and selection rules are obtained from the factor group analysis and are given in Table III. Here n_i is the number of total normal modes under each symmetry species, T_x, T_y, and T_z are pure translations parallel to each direction, and R_x pure rotation about the chain axis; n is the number of the genuine vibrational modes. The 30 vibrational modes which belong to A_1, B_1, and B_2 species are active in the infrared spectrum. The A_1 and B_1 modes are perpendicular to the molecular chain axis and B_2 modes are parallel to this axis.

In the present calculation[22] the Urey-Bradley force field was used, and the torsional coordinates were omitted. The method of the approximation of high frequency separations was applied for the C—H and C≡N stretching modes. The assumed values of the molecular constants are given in Table IV. The values of the force constants most appropriate at present are given in Table V. These values were transferred at first from poly-

TABLE III
Character Table, Number of Normal Modes, and Selection Rules for Syndiotactic Polyacrylonitrile

C_{2v}	E	C_2	σ_v	σ_g	n_i	T, R	n	IR[a]	R[a]
A_1	1	1	1	1	12	T_y	11	$a(\sigma)$	a
A_2	1	1	−1	−1	8	—	8	f	a
B_1	1	−1	1	−1	13	T_z, R_x	11	$a(\sigma)$	a
B_2	1	−1	−1	1	9	T_x	8	$a(\pi)$	a

[a] a = active; f = forbidden.

vinyl chloride,[19] acetonitrile,[20] and succinonitrile[21] and were modified so as to explain the observed infrared bands. The results are given in Table I, which shows a fairly good agreement between the observed and calculated frequencies. The dichroism and the intensity of the bands seems to be explainable quite well by the results of this calculation with a few exceptions. The tentative assignments of the bands are also given in Table I.

As to the bands in the 4000–1400 cm.$^{-1}$ region, the assignments described in the last section were confirmed by the calculation. The splitting of the frequencies of the modes belonging to the different species cannot be discussed in the present calculation because of the application of the high frequency splitting approximation.

TABLE IV
Molecular Constants[a]

Bond[b]	r, A.
C—C	1.54
C—H	1.09
C′—N	1.16
C—C′	1.45

[a] <C—C—N = 180°; all other bond angles 109° 28′.
[b] C′ represents the carbon atom in the CN group.

TABLE V
Force Constants and Intramolecular Tension[a]

	Force constants, mdyne/A.			Intramolecular tension
	K	H	F	κ, mdyne·A.
CC	3.00		0.45	
CC′	3.20		0.45	
CH	4.19		0.41	
CH′	3.97		0.40	
C′H′	—		0.625	
HH	—		0.06	
CN	—		0.50	
C′N	18.55		—	
CCC		0.21		
CCC′		0.25		
HCH		0.37		
CCH		0.11		
CCH′		0.10		
C′CH		0.232		
CC′N		0.141		
(—CHH—)				0.20
(—CH—) | CN				0.20

[a] C′ represents the carbon atom in the CN group, and H′ the hydrogen atom in CHCN group; F' is assumed to be $-0.1\,F$.

The 1359 cm.$^{-1}$ band of PAN which has been reported as a single parallel band by Liang and Krimm,[1] is found as a doublet consisting of two bands 1362 (σ) and 1355 cm.$^{-1}$ (π) in the present measurements. The vibrational calculation has led to the following assignments: the perpendicular band at 1362 cm.$^{-1}$ to $\delta(CH)(A_1)$, and the parallel band at 1355 cm.$^{-1}$ to $w(CH_2)(B_2)$. The $w(CH_2)(B_1)$ band calculated to be at 1396 cm.$^{-1}$ was not observed in the spectrum, and this may be explained by the very weak intensity expected from the vibrational form. Thus these bands of PAN seem to be interpreted by the present assignments, but there remains some difficulty in the interpretation of the 1355 cm.$^{-1}$ band in the spectra of PAN-αd_1. This band exhibits perpendicular polarization, although this band is expected to be a parallel band from the assignments described above. On deuteration of the α-hydrogen, the CH bending band at 1362 cm.$^{-1}$ (σ) should shift to lower frequency, and the CH_2 wagging band at 1355 cm.$^{-1}$ (π) may remain at the same position. The perpendicular polarization of the 1355 cm.$^{-1}$ band might be due to the deviation from the planar configuration of the syndiotactic zigzag chain (as Menčik and Kakudo have suggested), or to the existence of the gauche form of the main chain (isotactic or syndiotactic configuration). The explanation of this fact will be an interesting problem. The perpendicular band at 1310 cm.$^{-1}$ of PAN which disappears in the spectra of PAN-αd_1 and of PAN-d_3 is assigned to the CH bending mode (B_1).

The sharp band at 1247 cm.$^{-1}$ which shows strong parallel dichroism in the spectrum of PAN was assigned to the CH wagging mode by Liang and Krimm,[1] but the shift of this band in the spectra of the deuterated PAN's cannot be explained by the above assignment. This band is considered to be due to the coupling of the CH wagging and the CC stretching modes (B_2). The strong perpendicular band at 1073 cm.$^{-1}$ of PAN may be assigned to the superposition of the CC stretching (B_1) and the CH_2 rocking modes (B_1) from the result of calculation, although it has been assigned to the CC stretching and other combination by Liang and Krimm,[1] and to the CH bending and the CH_2 rocking modes recently by Liang et al.[3] The CH_2 rocking (B_2) mode calculated to be at 847 cm.$^{-1}$ is expected to be of weak intensity from the vibration form, and is observed as a very weak band at 865 cm.$^{-1}$.

The 537 cm^{-1} band of PAN which was assigned to C—C—CN bending by Liang and Krimm,[1] is due to the coupling of the C—C—CN bending and and C—C—N bending as shown in Table I. This band is found at about the same position (532 cm.$^{-1}$) in the spectrum of PAN-αd_1, but shifts to 490 cm.$^{-1}$ in the PAN-d_3 spectrum. This fact suggests the increase of coupling with the methylene rocking modes in the case of PAN-d_3.

From the results of the present studies, the assignments of the spectral bands of PAN, could be made considerably well. But, it is still difficult to discuss from the present data the tactic structure of PAN. However, it may be considered that the exclusion of the possibility of the syndiotactic sequence model for PAN is not necessarily adequate.

The authors wish to express their sincere thanks to Professor S. Seki of this Faculty for helpful advice and criticism, to Dr. S. Morimoto and Dr. K. Adachi of this Faculty for kindly providing the catalyst, performing gas chromatographic separation, and giving helpful advice, and to Director S. Morimoto of Textile Research Institute of Tôyô Spinning Co., Ltd., for his encouragement throughout this research.

References

1. Liang, C. Y., and S. Krimm, *J. Polymer Sci.*, **31**, 513 (1958).
2. Yamadera, R., *J. Polymer Sci.*, **50**, S4 (1961).
3. Liang, C. Y., F. G. Pearson, and R. H. Marchessault, *Spectrochim. Acta*, **17**, 568 (1961).
4. Cochburn, W. F., and C. E. Hubbey, *Appl. Spectroscopy*, **11**, 188 (1957).
5. Leitch, L. C., *Can. J. Chem.*, **35**, 345 (1957).
6. Tadokoro, H., H. Nagai, S. Seki, and I. Nitta, *Bull. Chem. Soc. Japan*, **34**, 1504 (1961).
7. Morimoto, S., et al., *Ann. Report Inst. Fiber Research (Osaka Univ.)*, **No. 9**, 82 (1956); M. Nakagawa, et al., *ibid.*, **No. 10**, 112 (1957).
8. Bartunek, P. F. and E. F. Barker, *Phys. Rev.*, **48**, 516 (1935).
9. Checkland, P. B., and H. W. Thompson, *Trans. Faraday Soc.*, **51**, 1 (1956).
10. Yamadera, R., *Kôbunshi Kagaku*, **19**, 135 (1962).
11. Stéfani, R., M. Chevreton, J. Terrier, and C. Eyraud, *Compt. Rend.*, **248**, 2006 (1959).
12. Stéfani, R., M. Chevreton, M. Garnier, and C. Eyraud, *Compt. Rend.*, **251**, 2174 (1960).
13. Menčik, Z., *Vysokomolekul. Soedin.*, **2**, 1635 (1960).
14. Kakudo, M., private communication.
15. Bohn, C. R., J. R. Schaefgen, and W. O. Statton, *J. Polymer Sci.*, **55**, 531 (1961).
16. Kern, W., *J. Prakt. Chem.*, **160**, 281 (1942).
17. Schildknecht, C. E., *Vinyl and Related Polymers*, Wiley, New York, 1952, p. 276.
18. Stanton, G. W., *Textile Res. J.*, **27**, 703 (1957).
19. Shimanouchi, T., and M. Tasumi, *Bull. Chem. Soc. Japan*, **34**, 359 (1961).
20. Nakagawa, I., *Kagaku-no-Ryôiki Zôkan*, **37**, 37 (1959).
21. Matsubara, I., *Bull. Chem. Soc. Japan*, **34**, 1710 (1961).
22. The calculation was carried out according to the Wilson's **GF** matrix method. E. B. Wilson, Jr., J. C. Decius, and P. C. Cross, *Molecular Vibrations*, McGraw-Hill, New York, 1955.

Résumé

On a synthétisé le poly-α-deutéroacrylonitrile et le poly-α,β,β-trideutéro-acrylonitrile. L'α-déutéro-acrylonitrile a été préparé par la réaction d'échange de deutérium entre l'acrylonitrile et D_2O en présence de CaO. L'α-β,β-trideutéroacrylonitrile a été préparé par la réaction d'addition de C_2D_2 et DCN. Les spectres infra-rouges du polyacrylonitrile, des polyacrylonitriles deutérés, et des produits intermédiaires de synthèse ont été mesurés dans la région 4000–400 cm.$^{-1}$ et discutés. Les spectres à la lumière polarisée d'échantillon de polymères orientés ont également été mesurés. Le bandes de PAN dans la région de vibration de CH montre des déplacements notables dans les spectres des polymères deutérés, tandis que la vibration de la bande C≡N ne montre pas de déplacement appréciable. Les bandes dans la région inférieure à 1400 cm.$^{-1}$ montrent un comportement compliqué par deutération. On a fait le calcul des vibrations normales du polyacrylonitrile, en tenant compte d'une chaîne syndiotactique plane en zigzag comme étant le modèle le plus simple pour le calcul. On a également discuté les attributions des bandes.

Zusammenfassung

Poly-α-deuteroacrylnitril und Poly-α,β,β-trideuteroacrylnitril wurden synthetisiert. α-Deuteroacrylnitril wurde durch Deuteriumaustausch von Acrylnitril mit D_2O in Gegenwart von CaO dargestellt. α,β,β-Trideuteroacrylnitril wurde durch die Addition von C_2D_2 an DCN dargestellt. Die Infrarotspektren von Polyacrylnitril, der deuterierten Polyacrylnitrile und der Synthesezwischenprodukte wurden im 4000–400 cm.$^{-1}$-Bereich gemessen und diskutiert. Auch die Polarisationsspektren der orientierten Polymerproben wurden gemessen. Die PAN-Banden im CH-Valenzbereich zeigen in den Spektren der deuterierten Polymeren die zu erwartende Verschiebung, während die C≡N-Valenzbande keine nennenswerte Verschiebung aufweist. Die Banden im Bereich unterhalb 1400 cm.$^{-1}$ zeigen bei der Deuterierung ein kompliziertes Verhalten. Die Normalschwingungen von Polyacrylnitril wurden unter der Annahme einer syndiotaktischen, ebenen Zickzackkette als einfachstes Modell berechnet. Die Bandenzuordnung wird diskutiert.

Received March 28, 1962
Revised June 22, 1962

JOURNAL OF POLYMER SCIENCE: PART A VOL. 1, PP. 3043–3065 (1963)

The Branching Reaction. III. Polymeric Transfer Constants of Vinyl Acetate with Styrene and Methyl Methacrylate

MAURICE MORTON and IRJA PIIRMA, *Institute of Rubber Research, University of Akron, Akron, Ohio*

Synopsis

A study has been carried out to determine the polymeric transfer constants of poly(vinyl acetate), polystyrene, and poly(methyl methacrylate) in the polymerization of vinyl acetate, as well as the similar transfer constants of poly(vinyl acetate) in the polymerization of styrene and methyl methacrylate. As before, this was accomplished by polymerizing each monomer in the presence of varying amounts of the desired oligomer and separating the resulting polymers. The effect of oligomer endgroups was checked by using oligomers of different molecular weight (1000–5000). As found previously for styrene and methyl methacrylate, there was no noticeable effect of polymeric endgroups on transfer activity, hence the transfer constants found refer to the interior units in the chain. The values of the various transfer constants are given. As expected, the vinyl acetate radical showed a reactivity in hydrogen abstraction which was several orders of magnitude greater than that of the styrene radical, and at least one order of magnitude greater than that of methyl methacrylate. The absolute values of the activation energy for the transfer step were remarkably similar, the difference in transfer activity being largely due to the difference in activation energy of the propagation reaction, and also to steric considerations.

INTRODUCTION

In the previous paper of this series,[1] data were given on the transfer constants of polystyrene and poly(methyl methacrylate) in the homopolymerization and graft copolymerization of styrene and methyl methacrylate. This paper reports similar results for the homopolymerization of vinyl acetate, as well as for the graft copolymerization of this monomer with styrene and methyl methacrylate, respectively.

The approach used was the same as previously described,[1] and involved the polymerization of a given monomer in the presence of a low polymer (oligomer) of itself or of another monomer, followed by separation of polymer and oligomer. The effect of the presence of the oligomer on the chain length of the polymer thus yielded the transfer constant of the given oligomer. In this way it has been found possible to determine the transfer constant of the vinyl acetate radical with respect to poly(vinyl acetate), polystyrene and poly(methyl methacrylate), as well as the transfer constant of both styrene and methyl methacrylate radicals with respect to poly(vinyl

acetate). This represents all possible combinations. Furthermore, from the known values of the propagation rate constants of the three monomers, it has been possible to calculate the absolute values of the transfer reaction rate constants in all cases.

EXPERIMENTAL PROCEDURES

Materials

Vinyl acetate, supplied by Carbide and Carbon Chemical Co., was freed from inhibitor by distillation through a 500 mm. Vigreux column, and the fraction boiling at 71–72°C. was used.

Methyl methacrylate, supplied by Rohm and Haas Co., was freed from inhibitor by distillation under 100 mm. pressure of nitrogen, through a 500 mm. Vigreux column, and the fraction boiling at 46°C. was used.

Styrene supplied by Dow Chemical Co. was freed from inhibitor by distillation under 20 mm. pressure of nitrogen, through a 200 mm. Vigreux column to give a product which boiled at 46°C.

2,2′-Azobisisobutyronitrile, supplied by Distillation Products Inc., was recrystallized from ethanol.

2-Methyl-2-propanethiol (Distillation Products Inc.) was distilled through a 300 mm. column packed with helices, and the fraction which boiled at 62°C. was used.

Benzenethiol (Evans Chemetics Inc.) was distilled through a 200 mm. Vigreux column under 15 mm. pressure of nitrogen, and the fraction boiling at 71°C. was used.

1-Butanol (Fisher Scientific Co., reagent grade) was used as received.

Acetone, Merck reagent grade, was used as received.

Benzene, Baker's reagent grade, was used in most cases as received. For the cryoscopic molecular weight determinations, it was dried over sodium and distilled. For use as a solvent in polymerizations, the benzene was recrystallized three times, dried over anhydrous calcium chloride or sodium sulfate and distilled.

Methanol (Dupont, synthetic) and petroleum benzin (Merck, boiling range 30–36°C.) were both used as received.

2,6-Dichloro-*p*-quinone (Distillation Products Inc.) was used as received.

Nitrogen used throughout was Airco high purity.

Polymerization Reactions

The polymerizations were carried out in a 300 ml. two-necked flask, equipped with a condenser. The sidearm of the flask had a thermometer and a hypodermic needle inserted through a cork. The 6 in. needle, which reached to the bottom of the flask, served as a nitrogen inlet tube and was also used to withdraw polymer samples during the reaction.

In the solution polymerizations of vinyl acetate, benzene was used as a solvent. Previous to the polymerization, the required amount of benzene

was placed in the polymerization flask and was degassed under 1 mm. pressure at Dry Ice temperature. In the polymerizations where oligomer was present it was first dissolved in benzene and the solution treated in the same way as benzene alone.

The prepolymerizations, for the purification of the vinyl acetate monomer, were done in a 500 ml. three-necked flask. The flask was equipped with a nitrogen inlet tube and a thermometer, and was connected to the usual monomer distillation assembly. For the prepolymerization of vinyl acetate, 3.5 moles of the inhibitor-free monomer and 3×10^{-5} moles AIBN were heated at 72°C. until quite viscous, which required 15–20 min. Inhibitor (2,6-dichloro-*p*-quinone) was then added, and the unreacted vinyl acetate was distilled directly into the polymerization flask, containing benzene or benzene–oligomer solution, and initiator.

In the polymerizations of vinyl acetate where the oligomer was not present, the per cent conversion was determined by coagulating the weighed sample in petroleum benzin, and drying the filtered polymer in a 90°C. oven for 30 min., or in a vacuum oven at 40°C. overnight. The separations of poly(vinyl acetate) and oligomers, when oligomers were present during the polymerization, are described separately.

The polymerizations of styrene and methyl methacrylate have been previously described.

Preparation and Characterization of Oligomers

a. Oligo(vinyl Acetate). Thiols were first tested as possible chain transfer agents in the preparation of oligo(vinyl acetate.) The transfer constant of 1-butanethiol had been determined by Walling,[2] and found to be 48 ± 14 at 60°C. Since this thiol was not available at first, others like 2-methyl-2-propanethiol and benzenethiol were tried. No transfer constants were found in the literature for these thiols, however, they were expected to be less reactive than 1-butanethiol. The polymerization reactions were carried out in bulk and also in solution, using various amounts of the thiols. These experiments were not successful, the presence of the thiols introduced long induction periods (up to 5 hr. at 60°C.), and the molecular weights of the polymers were not as low as expected.

Subsequently, 1-butanethiol was received and also used as a transfer agent in the preparation of oligo(vinyl acetate). The polymerization in benzene solution at 60°C. gave results similar to the ones obtained with the other thiols. The polymerization rate was normal (2%/hr.), the presence of thiol, however, introduced an induction period whose length was dependent on the thiol charge, i.e., a higher thiol charge gave a longer induction period. The molecular weight of the polymer was found to increase with conversion and was independent of the initial thiol charge, as can be seen from the examples shown below. Using 7.66 moles/l. vinyl acetate and 7.6×10^{-4} moles/l. AIBN, the results shown in Table I were obtained. It is obvious from these results, that the preparation of larger amounts of

TABLE I

1-Butanethiol, (moles/l.) $\times 10^2$	Conversion %	$[\eta]$
1.11	0.90	0.15
"	2.04	0.40
"	3.05	0.56
1.66	1.25	0.23
"	4.44	0.85

oligo(vinyl acetate) by the chain transfer activity of thiols was rather inconvenient if not impossible.

Benzoyl peroxide was then used both as an initiator and as a transfer agent. 5.2 Moles of vinyl acetate, 5.6 moles of benzene, and 0.4 moles of benzoyl peroxide were reacted for 30 min. at 50°C. The conversion was 10% and the molecular weight was approximately 10,000. The purification of this polymer was done by first precipitating it in petroleum benzin together with the unreacted benzoyl peroxide. The latter was then removed by three successive diethyl ether extractions. To check the reactivity of the end-groups of the polymer thus prepared, it was dissolved in benzene and added to freshly distilled styrene on a base molar ratio of polymer/styrene = 0.45. The styrene was polymerized at 100°C. for 2 hr., during which time samples were taken and coagulated in methanol. Since poly(vinyl acetate) is soluble in methanol, it was expected to remain in solution. However, evaporation of the supernatant methanol did not show any traces of polymer, and the methanol extraction of the precipitated polymer also gave negative results. Presumable, the endgroups of the poly(vinyl acetate), prepared with the benzoyl peroxide as transfer agent, were extremely reactive and a block polymer was obtained with styrene. Hence, this poly(vinyl acetate) could not be used in the branching study.

In order to obtain oligo(vinyl acetate) suitable for this study (i.e., having inactive endgroups) another approach for the problem was tried. Vinyl acetate polymerizations were carried out in a great excess of solvent, using high initiator charge. Benzene and toluene were both used as diluents and AIBN was used as the initiator, since it is not supposed to undergo any chain transfer. The polymerization charges were as shown in Table II. The polymerizations were carried to 10–15% conversion, which required

TABLE II

Material	Amount, moles	
	I	II
Benzene	13.5	—
Toluene	—	11.3
Vinyl acetate	3.7	3.7
AIBN	0.152	0.152

3–4 hr. at 60°C. The intrinsic viscosities, determined in acetone at 25°C., were 0.174 for the oligomer prepared in benzene solution, and 0.102 for oligomer prepared in toluene. For the purification of the oligomer, the latter was first precipitated in petroleum benzin, together with the residual AIBN. The gummy solid was dried for an hour at 110°C. It was then dissolved in acetone and recoagulated in boiling water, to decompose all of the AIBN. The polymer was again dried at 110°C. and then extracted with ethyl ether for 24 hr. The oligo(vinyl acetate) was then finally purified by reprecipitation from water or petroleum benzin. It was dried at 110°C. to a glassy solid. To check the purity of the product, it was dissolved in benzene and added to freshly distilled styrene in a molar ratio of oligomer/styrene = 0.45. The styrene was polymerized at 100°C. for 2 hr., during which time samples were taken to determine the conversion. Any acceleration of the rate due to residual AIBN resulted in a faster polymerization rate. Whenever an acceleration of the rate was found, the oligomer was again extracted with ethyl ether. Lower molecular weight oligomers were obtained by fractional precipitations of the above two oligomers.

The molecular weights of the oligo(vinyl acetates) were not determined cryoscopically. As will be seen later, these oligomers did not show any noticeable endgroup effect, hence the various molecular weights were identified only by their intrinsic viscosities, as shown above.

b. Oligostyrene and Oligo(methyl Methacrylate). In the preparation of the oligostyrene (molecular weight range 1,500–5,000), 2-methyl-2-propanethiol was used as chain transfer agent. Benzenethiol was used in the preparation of the oligo(methyl methacrylate.) The polymerization procedures for these two oligomers were described in the previous publication.[1]

Viscosity and Molecular Weight Determinations

The viscosity of each polymer solution was determined in an Ubbelohde dilution viscometer. A plot of η_{sp}/c versus c and ln η_r/c versus c gave the intrinsic viscosity when extrapolated to zero concentration.

Acetone was used as the solvent for poly(vinyl acetate) and the measurements were carried out at 25°C. The viscosities of polystyrene and poly(methyl methacrylate) were determined in benzene solution at 30°C.

From the intrinsic viscosity values, the number-average degree of polymerization ($\bar{P}_n$) of the poly(vinyl acetate) was calculated by means of the equation of Stockmayer, published by Fuhrman and Mesrobian.[3]

$$\bar{P}_n = 2.57[\eta]^{1.45}$$

The number-average degree of polymerization of polystyrene was calculated by means of the equation[4]

$$\bar{P}_n = 1.604 \times 10^3[\eta]^{1.37}$$

The number-average degree of polymerization of poly(methyl methacrylate) was calculated by means of the equation of Schuele, Kinsiger, and Fox, published by O'Brien and Gornick[5]

$$\bar{P}_n = 2.22 \times 10^3[\eta]^{1.32}$$

In the last two equations the intrinsic viscosities are expressed in the conventional units of deciliter per gram.

Fractionation and Separation of Oligomers and Polymers

a. Oligo(vinyl Acetate) and Poly(vinyl Acetate.) Precipitation distribution curves were determined for poly(vinyl acetate) and oligo(vinyl acetate) to investigate the possibilities of their separation. In the search of a suitable solvent–coagulant system for the PVA, solvents like acetone and benzene were used at first. The precipitations were done with water or different ratios of methanol-water mixtures. None of these was found to be satisfactory, since the supernatant liquid remained turbid even after centrifugation. Of the alcohols, however, 1-butanol was found to be a good coagulant. The precipitation distribution curves obtained with benzene–1-butanol are shown in Figure 1. The addition of 10% water to 1-butanol converted it to a solvent for PVA; and using the system 1-butanol/water (90/10)–1-butanol, a much better precipitation of the polymers was achieved, as can be seen in Figure 1. The OVA used in these separation studies had an $[\eta] = 0.174$ and the PVA had an $[\eta] = 1.49$. There was still a certain amount of overlapping in the precipitation distribution curves

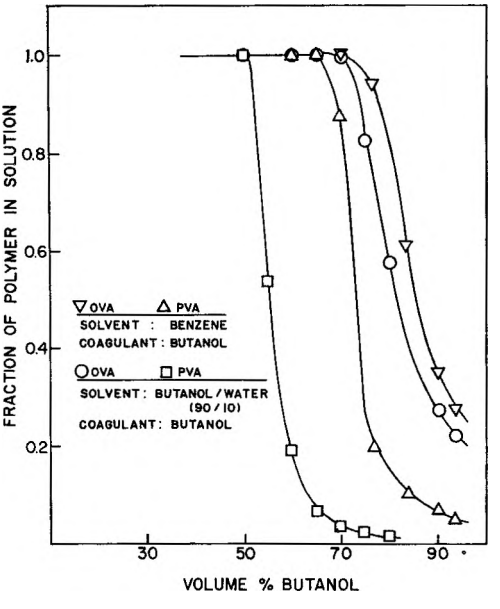

Fig. 1. Precipitation curves for oligo(vinyl acetate) and poly(vinyl acetate).

of the oligomer and polymer due to the spread in their molecular weight distribution. Hence, a fractionation of the oligo(vinyl acetate) was thought necessary. For this fractionation, a 5% solution of the oligomer in butanol/water (90/10) was used, and the higher molecular weight fraction was precipitated by adding sufficient butanol to reach a final butanol concentration of 83 vol.-%. This allowed the lower molecular weight ends to remain in solution. The oligomer in the supernatant liquid was recovered by first evaporating most of the solvent and then coagulating the oligo(vinyl acetate) in distilled water. The oligomer was dried at 110°C. to a glassy solid, which gave an $[\eta] = 0.07$ in acetone at 25°C.

For the separation of the poly(vinyl acetate) and the oligo(vinyl acetate) fraction with $[\eta] = 0.07$, several solutions of these polymers were made in butanol/water (90/10). The poly(vinyl acetate) in each solution was precipitated by the addition of 80 vol.-% butanol. The intrinsic viscosities of the recovered PVA's were determined, and are shown together with the initial values in Table III. It can be seen that the recovery of the

TABLE III
Separation of Oligo(vinyl Acetate) and Poly(vinyl Acetate)

Original solution			Recovered	
Wt. OVA, g.	Wt. PVA, g.	$[\eta]$	Wt., g.	$[\eta]$
—	0.4240	1.53	0.4150	1.52
0.4595	0.6307	1.06	0.6405	1.05
0.6425	0.6755	1.83	0.6695	1.83
0.5000	0.7000	1.32	0.6665	1.36
0.5000	0.4000	1.06	0.3795	1.08

poly(vinyl acetate) and the reproducibility of the intrinsic viscosity after the fractionation is excellent. It was found later, however, that this method of separation was not satisfactory after an actual polymerization reaction. Due to the comparatively high reactivity of the vinyl acetate radical toward its own polymer, the molecular weight of the newly formed polymer remained low, and too close to the molecular weight of the oligo(vinyl acetate). Hence, a separation was impossible. Due to this difficulty, another way had to be found, to determine the molecular weight of the poly(vinyl acetate). A method used by Schulz et al.[6] was adopted. The polymer and the oligomer were not separated, instead their combined intrinsic viscosity was determined and the intrinsic viscosity of the polymer was calculated by means of the following equation:

$$[\eta]_{PVA} = \frac{[\eta]_{Total} - (W_{OVA} \times [\eta]_{OVA})}{W_{PVA}},$$

where W_{OVA} = weight fraction of the oligomer and W_{PVA} = weight fraction of the polymer. Several solutions of the oligo(vinyl acetate) and poly(vinyl

acetate) were made in acetone, and their combined viscosities determined, to check the validity of the above equation in the range of molecular weights used in this work. As can be seen from the results shown in Table IV, the calculated intrinsic viscosity values are in good agreement with the initially determined values for the PVA.

TABLE IV

Original solution					
OVA		PVA			Calculated
Wt., g.	$[\eta]$	Wt., g.	$[\eta]$	$[\eta]_{Total}$	$[\eta]_{PVA}$
0.4500	0.174	0.1500	1.49	0.503	1.49
0.4003	0.170	0.2002	1.44	0.613	1.46
0.4003	0.104	0.3000	1.35	0.624	1.39
0.4008	0.170	0.5503	0.94	0.563	0.94
0.4000	0.104	0.1515	0.94	0.254	0.95
0.4002	0.104	0.4005	0.94	0.477	0.95

b. Oligostyrene and Poly(vinyl Acetate). For the separation studies of the poly(vinyl acetate) from the oligostyrene (M.W. 1,500) the two were dissolved in benzene. Some vinyl acetate was added to reproduce conditions which would prevail during an actual polymerization at about 2% conversion. This benzene solution of polymers (60 ml.) was poured into 500 ml. petroleum benzin to precipitate the poly(vinyl acetate). It was found previously, that this oligostyrene alone would not precipitate in this system. One sample of the precipitated PVA was filtered, dried at 90°C. for 30 min., weighed and a viscosity sample prepared in acetone. Another filtered sample was redissolved in benzene, reprecipitated in petroleum benzin, again filtered, dried and weighed, and the viscosity determined. The results are shown in Table V. It is obvious from these results that the second precipitation of the poly(vinyl acetate) is not necessary, but may be desirable to yield a complete separation of the oligostyrene and the poly(vinyl acetate). It should be pointed out here, that an oligostyrene of molecular weight higher than 5,000 was not completely soluble in petroleum benzin, and could not be used in these experiments.

c. Oligo(methyl Methacrylate) and Poly(vinyl Acetate). Precipitation distribution curves were determined for the poly(vinyl acetate) and olig-

TABLE V

Separation of Oligostyrene and Poly(vinyl Acetate)[a]

1st precipitation		2nd precipitation	
Wt., g.	$[\eta]$	Wt., g.	$[\eta]$
0.3169	1.47	0.3024	1.49

[a] Original solution contains: 0.3000 g. poly(vinyl acetate), $[\eta]$ = 1.49, and 2.00 g oligostyrene (M.W. = 1,500).

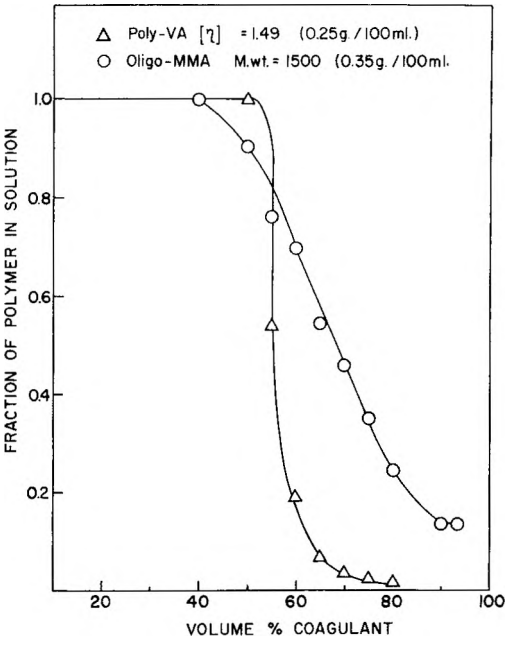

Fig. 2. Precipitation curves for poly(vinyl acetate) and oligo(methyl methacrylate). Solvent: butanol–water (90/10), coagulant: butanol.

(methyl methacrylate) to investigate the possibilities of their separation. Figure 2 shows one set of distribution curves obtained for PVA, $[\eta] = 1.49$ and oligo-(MMA), M.W. = 1,500, using a butanol/water(90/10)–butanol solvent–coagulant system. The curves show a definite overlapping due to the similarity in molecular weight distribution.

Since the poly(vinyl acetate) is completely soluble in methanol and the oligo(methyl methacrylate) can be coagulated from methanol, a mixture of the two polymers in benzene solution was poured into methanol under vigorous stirring in order to precipitate the oligo(MMA). However, due to the presence of PVA, the oligo(MMA) did not coagulate properly. The supernatant liquid remained turbid and it was impossible to separate the oligomer by filtration.

To obtain better separation, other solvent-coagulant systems were investigated. When vinyl acetate was used as solvent, instead of benzene, methanol gave a better precipitation of the oligo(MMA), although the recovery was still not quantitative. Addition of water to the methanol improved the precipitation markedly, as can be seen from the precipitation distribution curves shown in Figure 3, where two methanol/water ratios (90/10 and 80/20) were used. At the 80/20 methanol/water ratio, the oligo(MMA) was practically all precipitated, while the poly(vinyl acetate) remained in solution.

In order to avoid any difficulties in the actual separations of the poly-(vinyl acetate) and the oligo(MMA), the latter was fractionated to remove

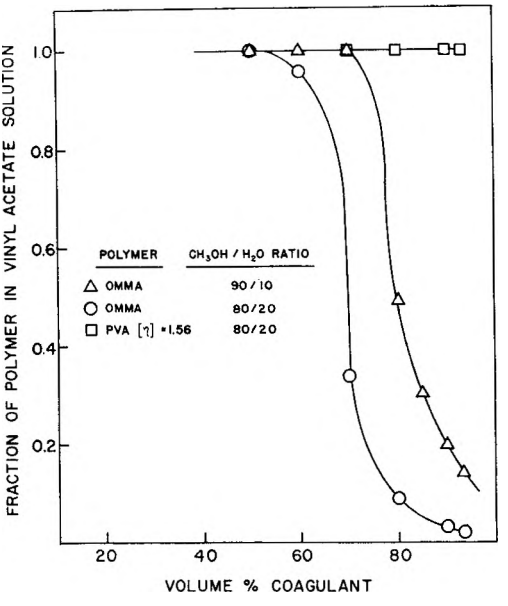

Fig. 3. Precipitation curves for oligo(methyl methacrylate) and poly(vinyl acetate).

the low molecular weight ends, which may remain in solution together with the PVA. For this fractionation, a 10% solution of the oligo(MMA) in vinyl acetate was made, and the higher molecular weight fraction was precipitated by adding methanol/water (90/10) to reach a final concentration of 80 vol.-%. This allowed the low molecular weight ends to remain dissolved. The precipitate was allowed to settle overnight and the clear supernatant liquid was decanted. The precipitated oligomer was dissolved in benzene and coagulated in petroleum benzin.

For an actual separation, the poly(vinyl acetate) and the oligo(MMA) fraction were dissolved in vinyl acetate. Three 20 ml. solutions were thus made and the oligo(MMA) precipitated with 280 ml. (93.4V%) methanol/water (80/20). The samples were left to settle for 48 hr. The clear supernatant liquid was decanted and filtered. It was then concentrated to about 50 ml., or until the first traces of poly(vinyl acetate) started precipitating. The solution was cooled, and the precipitation of PVA completed by an addition of water. The polymer was filtered, partially dried at 110°C., redissolved in acetone and recoagulated from petroleum benzin. The viscosities of the recovered poly(vinyl acetates) are shown in Table VI together with the initial values. It can be seen that the recovery of the poly(vinyl acetate) is satisfactory. Hence this separation technique was adopted in the polymerization of vinyl acetate in the presence of oligo-(methyl methacrylate).

It should be mentioned here that an attempt was also made to calculate the intrinsic viscosity of the poly(vinyl acetate) from the intrinsic viscosity of the combined oligo(MMA) and PVA. As can be seen from the data

TABLE VI
Separation of Oligo(methyl Methacrylate) and Poly(vinyl Acetate)

Original solution				
OMMA	PVA		Recovered PVA	
Wt., g.[a]	Wt., g.	$[\eta]$	Wt., g.	$[\eta]$
1.0000	0.6000	1.51	0.5705	1.50
1.0000	0.6000	1.51	0.5755	1.52
1.5000	0.5000	1.51	0.4952	1.48

[a] M.W. of oligo(MMA) = 5,000.

shown in Table VII, the results were not very good. In three experiments out of five, the calculated intrinsic viscosity of the poly(vinyl acetate) was much higher than the original intrinsic viscosity of the polymer used in the mixture. Hence, this method was thought to be too unreliable.

TABLE VII

Original solution					
OMMA		PVA		Calculated	
Wt., g.	$[\eta]$	Wt., g.	$[\eta]$	$[\eta]_{Total}$	$[\eta]_{PVA}$
0.3581	0.116	0.2420	1.62	0.809	1.84
0.5089	0.116	0.1151	1.62	0.400	1.66
0.3581	0.116	0.3642	0.94	0.550	0.98
0.4681	0.116	0.3113	0.94	0.468	1.00
0.3612	0.116	0.2203	0.94	0.424	0.93

d. Polystyrene and Oligo(vinyl Acetate). For the separation of polystyrene and oligo(vinyl acetate) a 25 ml. solution of these polymers was made in benzene containing some styrene. This polymer solution was poured into 500 ml. methanol under vigorous stirring. The precipitated polystyrene was filtered, washed with methanol and dried at 110°C. for 1 hr. The oligo(vinyl acetate) remained in solution. The intrinsic viscosities of duplicate samples of the recovered polystyrene were determined in benzene. Table VIII shows the results.

TABLE VIII
Separation of Polystyrene and Oligo(vinyl Acetate)

Original solution				
Wt., OVA,	Polystyrene		Recovered polystyrene	
g.[a]	Wt., g.	$[\eta]$	Wt., g.	$[\eta]$
0.5000	0.1500	1.41	0.1545	1.40
0.5000	0.1062	1.41	0.1099	1.41

[a] $[\eta] = 0.168$.

Again it can be seen that the recovery of the polystyrene is excellent after one precipitation.

e. Poly(methyl Methacrylate) and Oligo(vinyl Acetate). For the separation of poly(methyl methacrylate) and oligo(vinyl acetate) a 50 ml. solution of these polymers was made in vinyl acetate. The poly(MMA) was precipitated in 500 ml. methanol/water (80/20). The oligo(vinyl acetate) remained in solution. The precipitated poly(MMA) was filtered, washed with some methanol/water, and dried in a vacuum oven at 40°C. The intrinsic viscosity of the recovered poly(MMA) was determined in benzene at 30°C. The results are shown in Table IX. As indicated, the separation of the poly(methyl methacrylate) and the oligo(vinyl acetate) did not give any difficulty. Hence, this method was used in the separations, after actual polymerization reaction of the methyl methacrylate in the presence of oligo(vinyl acetate).

TABLE IX
Separation of Poly(methyl Methacrylate) and Oligo(vinyl Acetate)

Original solution				
Wt., OVA, g.[a]	Poly(MMA)		Recovered poly(MMA)	
	Wt., g.	$[\eta]$	Wt., g.	$[\eta]$
1.2500	0.5000	3.93	0.5013	3.94
1.2500	0.5000	3.93	0.4939	3.93

[a] $[\eta] = 0.174$.

RESULTS AND DISCUSSION

Chain Transfer of Vinyl Acetate with Oligo(vinyl Acetate)

The vinyl acetate polymerizations were carried out in benzene solution at three different temperatures, 40°C., 60°C., and 75°C. A molar ratio of benzene/vinyl acetate = 0.35 was used, together with AIBN (2,2′-azobisisobutyronitrile) concentrations as tabulated in Table X. Figure 4 shows the effect of conversion on rate at these temperatures. In the polymerizations where oligomers were present, they replaced the benzene on an equal volume basis, hence no change in polymerization rate should occur. In some of the polymerization reactions carried out in the presence of oligomers, a short induction period was noted (especially at 40°C.), possibly due to some impurities in the oligomers. In case any acceleration or retardation of the rate was observed, the data were not used.

Due to the use of benzene as solvent in the polymerizations, it was necessary to obtain the benzene transfer constant with vinyl acetate. A value of 2.96×10^{-4} was found in the literature.[7] This value could, however, not be duplicated. A value of 1.07×10^{-4} was actually obtained for the chain transfer constant of benzene at 60°C., and a value of 1.40×10^{-4} at 75°C. The transfer activity of benzene is shown graphically in Figure 5 and the

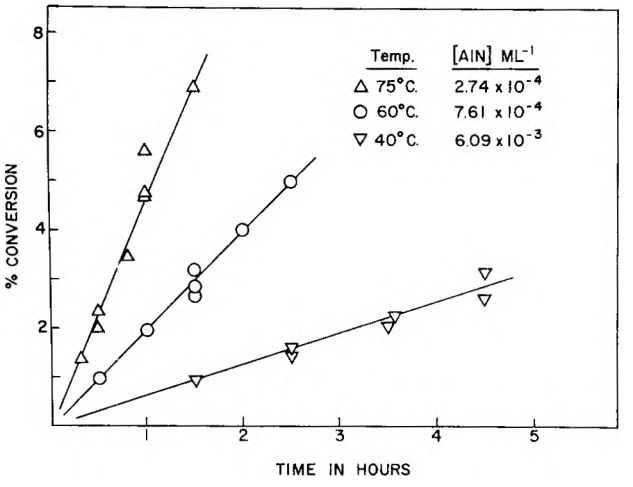

Fig. 4. Polymerization of vinyl acetate in benzene solution. [Benzene]/[vinyl acetate] = 0.35.

TABLE X

Polymerization temp., °C.	[AIBN], mole/l.	Rate, %/hr.
40	6.09×10^{-3}	0.72
60	7.61×10^{-4}	2.00
75	2.74×10^{-4}	4.60

data are tabulated in Table XI. The benzene transfer constant at 40°C. was calculated from the plot of log C versus $1/T$ and found to be 0.70×10^{-4}.

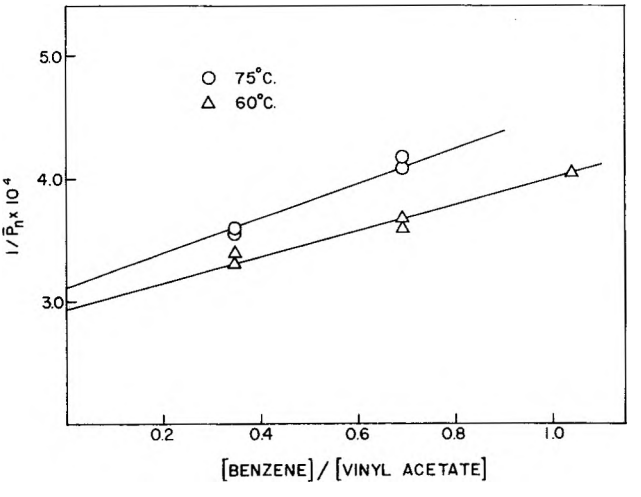

Fig. 5. Chain transfer of vinyl acetate with benzene.

TABLE XI
Polymerization of Vinyl Acetate in Benzene Solvent

Solvent: monomer ratio S/M	Temp., °C.	Max. conversion, %	$R_p \times 10^5$, mole/l./sec.	$R_p/M^2 \times 10^7$	Ave. $[\eta]$	$1/P_n \times 10^4$	$C \times 10^4$
0.35	60	4.46	4.51	6.85	1.56	3.31	1.07
0.69	60	3.87	2.91	6.90	1.45	3.66	
1.04	60	3.51	1.88	6.42	1.35	4.05	
0.35	75	6.97	10.5	15.9	1.48	3.56	1.40
0.69	75	5.89	6.40	15.2	1.33	4.14	

The polymerization of vinyl acetate in the presence of oligo(vinyl acetate) was carried out at two different temperatures, i.e., 40°C. and 60°C. No separations of the OVA and the newly formed poly(vinyl acetate) were carried out due to the experimental difficulties previously described. The vinyl acetate radical was found to be reactive to the extent that the molecular weight of the newly formed polymer was very close to that of the oligomer used, with some overlapping in the molecular weight distribution of the two. Hence a physical separation was impossible.

The weight fraction of the poly(vinyl acetate) was determined from the total weight of the polymers and the known weight of the oligo(vinyl acetate). The viscosities of the total samples were determined in acetone, and the intrinsic viscosity calculated for the poly(vinyl acetate). A correction was made in the $1/P_n$ value for the chain transfer activity of benzene, using the appropriate C_sS/M value.

The transfer activity of the oligo(vinyl acetate) at 40°C. and 60°C. is shown in Table XII. The plot of $1/P_n$ versus O/M (Fig. 6) leads to a good

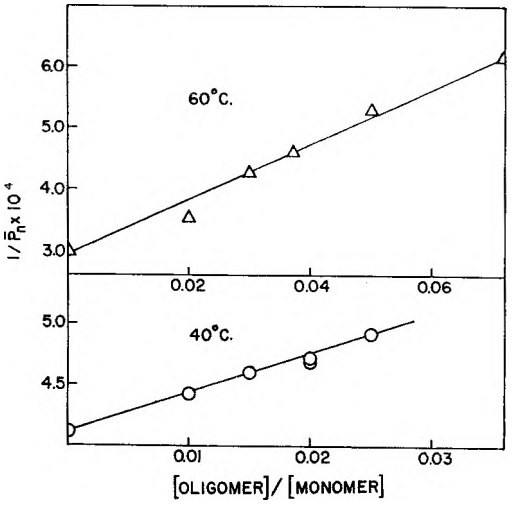

Fig. 6. Chain transfer of vinyl acetate with oligo(vinyl acetate).

TABLE XII
Polymerization of Vinyl Acetate in the Presence of Oligo(vinyl Acetate)

Temp., °C.	O/M[a]	$[\eta]$ of oligomer	S/M	C_sS/M × 10^4	Max. conversion, %	Rate, %/hr.	Ave. $[\eta]_{Pol.}$	$1/P_n$ × 10^4	Corr. $1/P_n$ × 10^4	C × 10^3
40	0	—	0.35	0.25	2.64	0.72	1.28	4.37	4.12	
40	0.01	0.104	0.34	0.24	2.43	0.81	1.22	4.67	4.43	
40	0.015	0.104	0.34	0.24	2.10	0.70	1.18	4.85	4.61	3.20
40	0.02	0.170	0.33	0.23	1.31	0.66	1.17(0)	4.95	4.72	
40	0.02	0.104	0.33	0.23	2.29	0.76	1.17(4)	4.93	4.70	
40	0.025	0.170	0.32	0.23	1.69	0.71	1.14	5.14	4.92	
60	0	—	0.35	0.37	4.00	2.00	1.56	3.31	2.94	
70	0.02	0.170	0.33	0.35	3.86	1.93	1.39	3.89	3.54	
60	0.03	0.104	0.32	0.34	4.08	2.04	1.23	4.62	4.28	4.76
60	0.037	0.104	0.31	0.33	2.53	1.99	1.17	4.95	4.62	
60	0.05	0.170	0.30	0.32	3.21	2.02	1.07	5.64	5.32	
60	0.07	0.104	0.28	0.30	2.00	2.00	0.965	6.48	6.18	

[a] Base moles oligomer/mole monomer.

straight line, from which the values of 3.20×10^{-3} and 4.7×10^{-3} were obtained for the transfer constant at 40°C. and 60°C., respectively. The value at 40°C. is in good agreement with the value of 3.09×10^{-3} obtained by Melville et al.[8] for the transfer constant of poly(vinyl acetate) toward vinyl acetate using a different experimental technique.

Chain Transfer of Vinyl Acetate with Oligostyrene

In the polymerizations of vinyl acetate in the presence of oligostyrene, benzene was used in most cases as solvent. Due to the relatively high reactivity of the vinyl acetate radical toward the oligostyrene, the molecular weight of the poly(vinyl acetate) was low and the polymerization medium remained fluid. Hence, no solvent was really needed, it was only used to adjust the total volume of the polymerization medium, in order to keep the (solvent + oligomer)/monomer volume ratio constant.

The separation of the poly(vinyl acetate) and the oligostyrene was carried out as described previously in the experimental part. No difficulties were encountered despite the branching reaction. The maximum conversion, however was kept low (2–3%) to avoid any possible influence of the oligostyrene on the viscosity determination of the PVA.

Four different oligomer/monomer charge ratios were used, and also three different molecular weight oligostyrenes (1,500, 2,300, and 5,000) to check for a possible endgroup effect. The polymerization temperatures used were 60°C. and 75°C. Two runs were carried out at 40°C., to obtain a third point for the activation energy calculations. The transfer activity of the oligostyrene is shown graphically in Figure 7 and Table XIII, from which the values of 1.5×10^{-3} and 1.9×10^{-3} were obtained at 60°C. and 75°C., respectively.

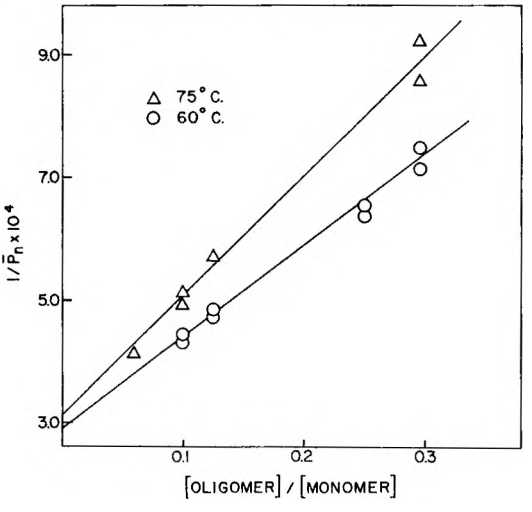

Fig. 7. Chain transfer of vinyl acetate with oligostyrene.

TABLE XIII
Polymerization of Vinyl Acetate in Presence of Oligostyrene

Temp., °C.	O/M	M.W. of oligomer	S/M	$C_sS/M \times 10^4$	Max. conversion, %	Rate, %/hr.	Ave. $[\eta]$	$1/P_n \times 10^4$	Corrected $1/P_n \times 10^4$	$C \times 10^3$
40	0	—	0.35	0.25	2.64	0.7	1.28	4.37	4.12	1.2
40	0.125	1500	0.20	0.14	1.98	0.7	1.05	5.76	5.62	
60	0	—	0.35	0.37	4.00	2.0	1.56	3.31	2.94	
60	0.10	2300	0.23	0.25	2.39	2.0	1.24	4.56	4.31	
60	0.10	1500	0.23	0.25	1.98	2.0	1.21	4.72	4.47	
60	0.125	1500	0.20	0.21	2.27	2.0	1.15	5.07	4.86	
60	0.125	5000	0.20	0.21	2.37	2.0	1.17	4.95	4.74	1.5
60	0.250	1500	0.05	0.05	3.32	2.0	0.97	6.44	6.39	
60	0.250	5000	0.05	0.05	2.64	2.0	0.95	6.63	6.58	
60	0.296	1500	—	—	1.99	2.0	0.90	7.15	7.15	
60	0.296	2300	—	—	2.34	2.0	0.86	7.50	7.50	
75	0	—	0.35	0.49	6.97	4.65	1.48	3.56	3.07	
75	0.062	1500	0.27	0.38	6.81	4.5	1.25	4.51	4.13	
75	0.10	1500	0.23	0.32	4.22	5.0	1.09	5.47	5.15	
75	0.10	2300	0.23	0.32	3.20	4.5	1.12	5.26	4.94	1.9
75	0.125	1500	0.20	0.28	4.64	4.6	1.02	6.00	5.72	
75	0.296	1500	—	—	3.21	4.8	0.75	9.25	9.25	
75	0.296	2300	—	—	4.17	4.6	0.79	8.58	8.58	

Chain Transfer of Vinyl Acetate with Oligo(methyl Methacrylate)

The polymerization of vinyl acetate in the presence of oligo(methy methacrylate), which was carried out at two different temperatures (60°C. and 75°C.), presented some difficulties. A noticeable increase in the

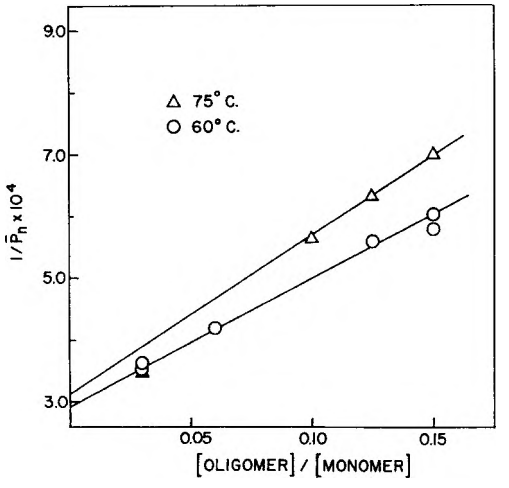

Fig. 8. Chain transfer of vinyl acetate with oligo(methyl methacrylate).

viscosity of the polymerizing mixture occurred at quite low conversions (ca. 2%), showing accelerated rates and a rise in the molecular weight of the poly(vinyl acetate). Hence higher ratios than $O/M = 0.15$ could not be used.

Another difficulty arose in the separations of the oligo(MMA) and the poly(vinyl acetate). Using the procedure described in the experimental

TABLE XIV
Polymerization of Vinyl Acetate in the Presence of Oligo(methyl Methacrylate)

Temp., °C.	O/M	M.W. of oligomer	S/M	$C_s S/M$ 10^4	Ave. $[\eta]$	$1/P_n$ $\times 10^4$	Corrected $1/P_n \times 10^4$	$C \times 10^3$
60	0	—	0.35	0.37	1.56	3.31	2.94	
60	0.03	3100	0.32	0.34	1.37	3.97	3.63	
60	0.03	5000	0.32	0.34	1.39	3.89	3.55	
60	0.06	3100	0.29	0.31	1.25	4.51	4.20	2.1
60	0.06	5000	0.29	0.31	1.21	4.72	4.41	
60	0.125	5000	0.21	0.22	1.07	5.83	5.61	
60	0.15	3100	0.18	0.19	1.02	6.00	5.81	
60	0.15	5000	0.18	0.19	0.99	6.25	6.06	
75	0	—	0.35	0.49	1.48	3.56	3.07	
75	0.03	5000	0.32	0.45	1.36	4.01	3.56	
75	0.10	5000	0.23	0.33	1.02	6.00	5.67	2.6
75	0.125	3100	0.21	0.29	0.95	6.63	6.34	
75	0.15	5000	0.18	0.25	0.89	7.26	7.01	

part, and coagulating the oligo(MMA) with methanol/water from the mixture of the two polymers in vinyl acetate, the precipitate of the oligo(MMA) did not settle properly. The solutions had to be centrifuged, so that the poly(vinyl acetate) could be recovered from the supernatant liquid.

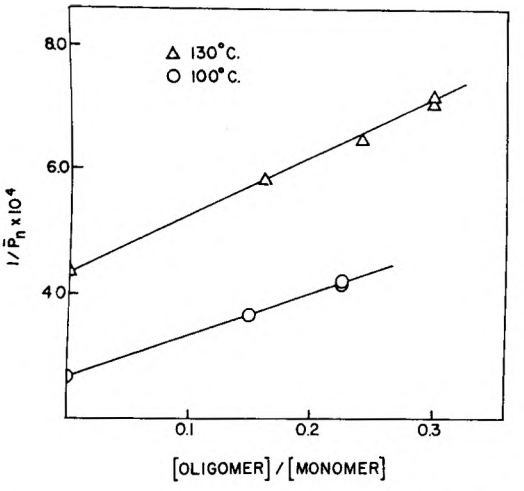

Fig. 9. Chain transfer of styrene with oligo(vinyl acetate).

The transfer activity of the oligo(methyl methacrylate) is shown graphically in Figure 8 and Table XIV, from which the values of 2.1×10^{-3} and 2.6×10^{-3} were obtained at 60°C. and 75°C., respectively. Although the plot of $1/P_n$ versus O/M gave a good straight line, the transfer constants are of questionable value, due to the difficulties encountered in the separations.

TABLE XV
Polymerization of Styrene in the Presence of Oligo(vinyl Acetate) at Benzene/Styrene = 1.5

Temp., °C.	O/M	$[\eta]$ of oligomer	Max. conversion, %	Rate, %/hr.	Ave. $[\eta]$	$1/P_n \times 10^4$	$C \times 10^4$
100	0	—	3.26	1.14	1.85	2.68	
100	0.150	0.10	3.62	1.1	1.47	3.67	
100	0.225	0.10	4.51	1.0	1.34	4.17	6.6
100	0.225	0.17	4.32	1.0	1.33	4.21	
130	0	—	8.98	16.3	1.30	4.35	
130	0.16	0.17	6.30	13.9	1.05	5.82	
130	0.24	0.10	7.18	13.9	0.97	6.49	9.2
130	0.30	0.10	10.10	13.2	0.90	7.19	
130	0.30	0.17	6.32	12.6	0.91	7.08	

Chain Transfer of Styrene with Oligo(vinyl Acetate)

To conclude the study of the branching reaction in the polymerization of styrene, methyl methacrylate and vinyl acetate, the rate of transfer between the styrene radical and the oligo(vinyl acetate) was also investigated.

In the polymerizations of styrene at 100°C., benzene was used as solvent in a molar ratio of benzene/styrene = 1.5, which gave a rate of 1.14%/hr. No solvent was used in the polymerizations at 130°C. The transfer activity of oligo(vinyl acetate) is shown graphically in Figure 9 and the corresponding data are tabulated in Table XV.

Chain Transfer of Methyl Methacrylate with Oligo(vinyl Acetate)

The methyl methacrylate polymerizations in benzene solution were carried out at two different temperatures, 60 and 80°C. A molar ratio of

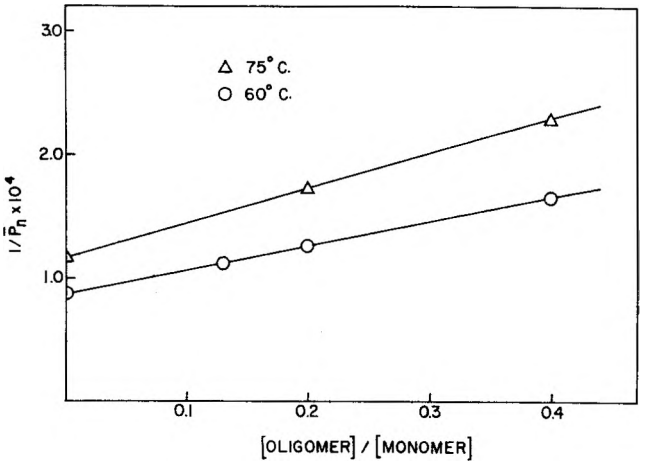

Fig. 10. Chain transfer of methyl methacrylate with oligo(vinyl acetate).

TABLE XVI
Polymerization of Methyl Methacrylate in the Presence of Oligo(vinyl Acetate)

Temp., °C.	O/M	$[\eta]$ of oligomer	S/M	$C_s S/M$	Max. conversion, %	Rate, %/hr.	Ave. $[\eta]$	$1/P_n \times 10^4$	Correction $1/P_t \times 10^4$	$C \times 10^4$
60	0	—	1.0	0.02	4.84	1.65	3.42	0.89	0.87	
60	0.13	0.10	0.89	0.02	4.80	1.60	2.82	1.15	1.13	
60	0.20	0.10	0.84	0.02	1.80	1.64	2.58	1.29	1.27	2.0
60	0.40	0.17	0.67	0.01	1.58	1.58	2.12	1.67	1.66	
80	0	—	1.0	0.08	6.32	4.50	2.65	1.24	1.17	
80	0.20	0.17	0.84	0.06	6.46	4.53	2.01	1.79	1.73	2.8
80	0.40	0.10	0.67	0.05	5.53	4.48	1.64	2.34	2.29	

TABLE XVIII
Absolute Chain Transfer Values

Radical	Polymer	Transfer constants × 10^3						$E_{tr} - E_p$, kcal.	E_{tr}, kcal.	k_{tr}, l./mole sec.	A_{tr}, l./mole sec.
		40°C.	60°C.	75°C.	80°C.	100°C.	130°C.				
VA	VA	3.2	4.8	—	—	—	—	4.0	11.3	17.6 (60°C.)	4.2×10^8
VA	Styrene	1.2	1.5	1.9	—	—	—	2.8	10.1	5.3 (60°C.)	2.5×10^7
VA	MMA	—	2.1	2.6	—	—	—	3.2	10.5	7.8 (60°C.)	6.5×10^7
Styrene	VA	—	—	—	—	0.66	0.92	3.3	11.1	0.4 (100°C.)	1.2×10^6
MMA	VA	—	0.20	—	0.28	—	—	4.2	10.5	0.1 (60°C.)	8.3×10^5

benzene/methyl methacrylate = 1.0 was used together with an AIBN concentration of 2.39×10^{-4} mole/l. for 60°C. and 7.31×10^{-5} mole/l. for 80°C., giving a rate of 1.65 and 4.50%/hr., respectively. In the polymerizations with the oligo(vinyl acetate) present, the latter replaced the benzene on an equal volume basis, hence no change in the polymerization rate was observed. The transfer activity of the oligo(vinyl acetate) is shown in Table XVI. A small correction was applied to the $1/P_n$ value, taking into consideration the transfer activity of benzene, and using $C = 0.2 \times 10^{-5}$ at 60°C.[9] and 0.75×10^{-5} at 80°C.[6] Figure 10 shows the plot of $1/P_n$ verus O/M, from which the values of the transfer constants 2.0×10^{-4} and 2.8×10^{-4} were obtained for oligo(vinyl acetate) at 60°C. and 80°C., respectively.

DISCUSSION

In order to obtain the absolute values for the chain transfer reaction, i.e., E_{tr}, k_{tr} and A_{tr}, use was made of the absolute values for the propagation rate constants, k_p, and activation energies, E_p, for the monomers used in

TABLE XVII

Monomer	k_p, l./mole sec.	E_p, kcal.	Reference
Vinyl acetate	3700 (60°C.)	7.3	10
Styrene	618 (100°C.)	7.8	11
Methyl methacrylate	573 (60°C.)	6.3	12

this work. The values used are listed in Table XVII. All the values obtained for the transfer constants together with the calculated values for the transfer rate constants, the activation energies, and the frequency factors are tabulated in Table XVIII.

References

1. Morton, M., and I. Piirma, *J. Am. Chem. Soc.*, **80**, 5596 (1958).
2. Walling, C., *J. Am. Chem. Soc.*, **70**, 2561 (1948).
3. Fuhrman, N., and R. Mesrobian, *J. Am. Chem. Soc.*, **76**, 3281 (1954).
4. Mayo, F. R., R. A. Gregg, and M. S. Matheson, *J. Am. Chem. Soc.*, **73**, 1691 (1951).
5. O'Brien, J. L., and F. Gornick, *J. Am. Chem. Soc.*, **77**, 4757 (1955).
6. Schulz, G. V., G. Henrici, and S. Olivé, *J. Polymer Sci.*, **17**, 45 (1955).
7. Palit, S. R., and S. K. Das, *Proc. Roy. Soc. (London)*, **A226**, 82 (1954).
8. Bevington, J. C., G. M. Guzman, and H. W. Melville, *Proc. Roy. Soc. (London)* **A221**, 437 (1954).
9. Basu, S., J. N. Sen, and S. R. Palit, *Proc. Roy. Soc. (London)*, **A202**, 485 (1950).
10. Matheson, M. S., E. E. Auer, E. B. Bevilacqua, and E. J. Hart, *J. Am. Chem. Soc.*, **71**, 2610 (1949).
11. Matheson, M. S., E. E. Auer, E. B. Bevilacqua, and E. J. Hart, *J. Am. Chem. Soc.*, **73**, 1700 (1951).
12. O'Brien, J. L., and F. Gornick, *J. Am. Chem. Soc.*, **77**, 4757 (1955).

Résumé

Une étude a été effectuée en vue de déterminer les constantes de transfer sur polymère d l'acétate de polyvinyle, du polystyrène et du polyméthyacrylate de méthyle, lors de la polymérisation d'acétate de vinyle, de même que les constantes de transfert analogues d'acétate de polyvinyle dans la polymérisation du styrène et du méthacrylate de méthyle. Comme précédemment ceci a été réalisé en polymérisant chaque monomère en présence de quantités variables de l'oligomère désiré et en séparant les polymères résultants. L'effet des groupes terminaux des oligomères a été vérifié en utilisant des oligomères de différents poids moléculaires (1000–5000). Comme on a trouvé auparavant pour le styrène et le méthacrylate de méthyle, il n'y a pas d'effet appréciable des groupes terminaux des polymères sur l'activité de transfert, aussi les constantes de transfert trouvées se rapportent-elles aux unités internes de la chaîne. Les valeurs de différentes constantes de transfert sont mentionnées. Comme attendu, le radical d'acétate de vinyle montre une réactivité pour arracher un hydrogène qui est de plusieurs ordres de grandeur supérieure à celle du radical styryle, et au moins d'un ordre de grandeur plus grande que celle du méthacrylate de méthyle. Les valeurs absolues de l'énergie d'activation de l'étape de transfert sont remarquablement similaires, la différence dans l'énergie de transfer étant largement due à la différence dans l'énergie d'activation de la réaction de propagation et aussi à des conditions d'ordre stérique.

Zusammenfassung

Die Polymerübertragungskonstanten für Polyvinylacetat, Polystyrol und Polymethylmethacrylat bei der Polymerisation von Vinylacetat sowie die Übertragungskonstante von Polyvinylacetat bei der Polymerisation von Styrol und Methylmethacrylat wurden bestimmt. Diese Bestimmung wurde wie früher durch Polymerisation eines jeden Monomeren in Gegenwart verschiedener Mengen des betreffenden Oligomeren und Abtrennung des gebildeten Polymeren durchgeführt. Der Einfluss von Oligomer-Endgruppen wurde durch Verwendung von Oligomeren mit verschiedenem Molekulargewicht (1000–5000) festgestellt. Wie schon früher bei Styrol und Methylmethacrylat gefunden, bestand kein merklicher Einfluss der Polymerendgruppen auf die Übertragungswirkung; die gefundenen Ubertragungskonstanten beziehen sich daher auf die inneren Kettenbausteine. Die Werte der verschiedenen Übertragungskonstanten sind angegeben. Wie erwartet zeigte das Vinylacetatrdikal bei der Wasserstoffabspaltung eine um mehrere Gröss enordnungen höhere Wirksamkeit als da Styrolradikal und eine um mindestens eine Grössenordnungh öhere als das Methylmethacrylatradikal. Die Absolutbeträge der Aktivierungsenergie des Übertragungsschrittes zeigten eine bemerkenswerte Ähnlichkeit; der Unterschied in der Übertragungswirksamkeit geht grossen Teils auf einen Unterschied in der Aktivierungsenergie der Wachstumsreaktion und auch auf sterische Verhältnisse zurück.

Received July 18, 1962

JOURNAL OF POLYMER SCIENCE: PART A VOL. 1, PP. 3067–3077 (1963)

Some Applications of Afterglow Studies of Luminescent Compounds in Solid Polymers

STEFAN CZARNECKI, *Institute of Physics, Polish Academy of Science, Warsaw,* and MARIAN KRYSZEWSKI, *Polytechnic Institute of Lodz, Lodz, Poland*

Synopsis

The afterglow (β-band luminescence) observed in polymethyl methacrylate activated with different hydrocarbons such as naphthalene and its derivatives was found to be sensitive to the influence of oxygen. The sharp boundary between the luminescent and nonluminescent area is due mainly to the diffusion of oxygen and shifts with time from the edges to the center of the specimen. The recovery of the afterglow results on H_2 diffusion into the polymer sample or after ultraviolet irradiation. An interpretation of the observed phenomena as well as the application of the afterglow moving boundary technique to the determination of diffusion coefficients of gases in polymers and to the studies of some related processes is suggested.

Introduction

Structural changes in solid polymers are usually investigated by such methods as x-ray diffraction, electron micrography, nuclear magnetic resonance, electron spin resonance, diffusion, etc. Studies of afterglow (sometimes called β-band or fluorescence of long duration) of organic compounds dissolved in solid polymers can yield some information not only on the excited states of the low molecular compound but also on the structure and its changes of the solid medium. This point of view in luminescence studies is rather new; however, numerous afterglow investigations of organic molecules in solid media have been done.

It is well known that many organic molecules show fluorescence and afterglow. The latter occurs only in a very viscous or solid medium. The afterglow is related to long-lived excited states (metastable levels) of the luminescent molecule. These states are responsible for the emission of two bands of luminescence of long duration: one at the same wavelength called the α-band,[1] and another at longer wavelength called the β- band. These phenomena can be explained on the basis of the molecular energy level diagram proposed by Jablonski.[2] The solid medium must prevent the deactivation of the luminescent molecules in the metastable state. All changes in viscosity, packing, configuration, etc., of molecules in the solid medium influence the intensity and polarization of luminescence. Thus, the studies of the volume distribution of afterglow intensity in the sample

(especially of the β-band) were carried out to investigate the changes in structure which occur in solid polymers during aging under different external conditions. Changes of the degree of polarization of fluorescent light were used in the studies of polymerization kinetics.[3]

Experimental

We have investigated the β-band of naphthalene, α-bromonaphthalene, α-iodonaphthalene, and phenanthrene (activators) dissolved in solid polymethyl methacrylate (PMMA). The α-band emission was observed only in the case of naphthalene. All studies were carried out with carefully purified monomer and fluorescent compounds.

Thermal polymerization of purified monomer with the various activators was used in all cases, because the decomposition products of aromatic peroxides themselves show afterglow (PMMA obtained by polymerization of carefully purified monomer was not itself luminescent).

Thermal polymerization of degassed monomer solutions containing known concentrations of activators were carried out in sealed vials in three steps: (a) prepolymerization at 80°C. for 2–6 hr.; (b) polymerization at 45°C. for 15–40 hr.; (c) final polymerization at 90°C. for 8 hr. All necessary corrections for the concentration of dissolved luminescent substances relative to the contraction of solutions during polymerization were taken into consideration. The final concentration c of activators was 1×10^{-3} g./cm.^{3}. In order to eliminate the fluorescence, the photographs of the afterglow were taken with the use of a mechanical phosphoroscope. A HBO 200 or HBO 500 high pressure mercury lamp was the source of exciting light.

Results

Freshly prepared samples containing activators show at room temperature a uniform intensity of afterglow throughout the whole sample. Naphthalene-activated specimens also show phosphorescence (α-band). This α-band is rather anomalous* as shown by Czarnecki.[4] The intensity (but not the dimensions of the luminescent area in a given specimen) depends slightly on the degree of conversion of monomer into polymer. With conversion of the order of 80% the intensity of afterglow is lower than that at higher conversion because of larger deactivation in the metastable state.[6] Nevertheless, the intensity of afterglow is not directly related to the degree of conversion. These phenomena are the subject of investigations presently being carried out.

Some peculiar changes in the observed afterglow are connected with aging of activated samples.

When the activated samples are kept in air for prolonged periods, the

* The activation temperatures given by Pringsheim for the hydrocarbons used are comparatively high (up to 100°C.[5]) so that the phosphorescence should not appear at room temperature.

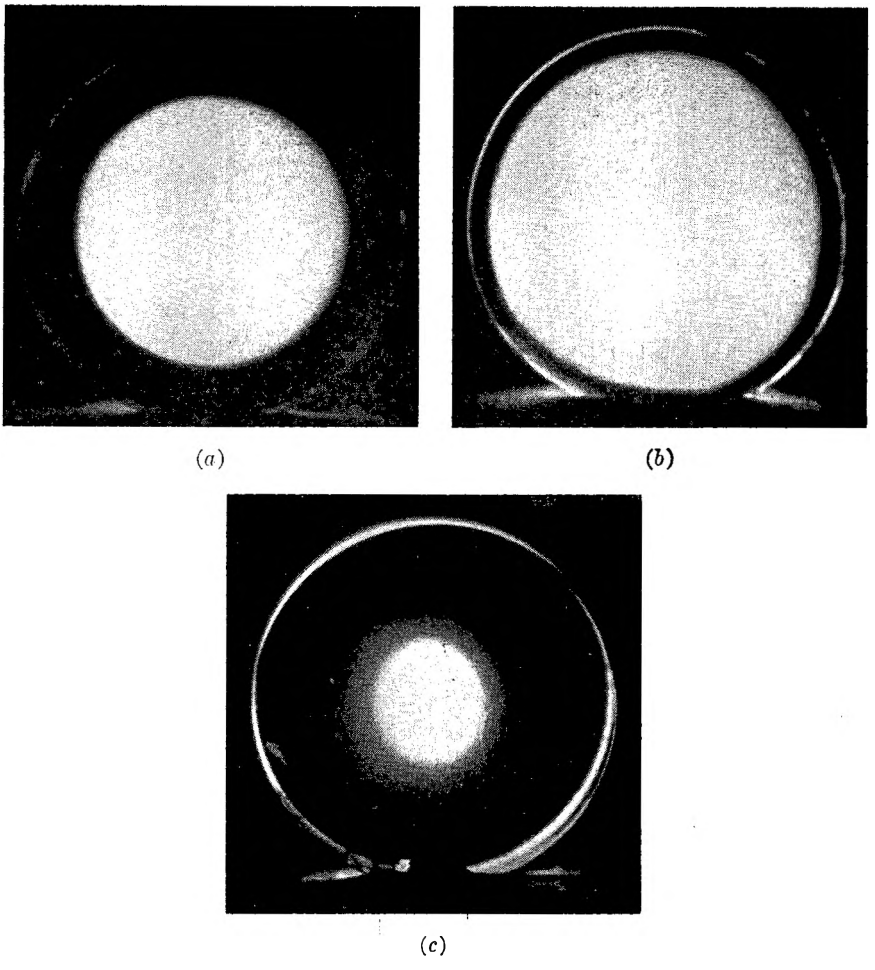

(*a*) (*b*)

(*c*)

Fig. 1. Photographs of the afterglow area in cylindrical samples of naphthalene-activated PMMA for different times of aging in air: (*a*) after 1 month; (*b*) after 2 months; (*c*) after 2 yr.

afterglow disappears, beginning at the edges of the specimen, in spite of the uniform afterglow seen in fresh samples. The phosphorescent areas decrease with time. After a sufficiently long period they are limited only to the center of the samples. This is shown in Figure 1.

The photographs of cylindrical samples with well polished, transparent walls were taken with a mechanical phosphoroscope. It should be noted that the fluorescence did not change, being uniform throughout the specimen.

The boundaries of the afterglow areas do not have a diffuse character, i.e., they are visually sharp. We assumed that the effect of afterglow decay is due to the diffusion of oxygen into the polymer, as O_2 is well known to be a quencher of phosphorescence.[7]

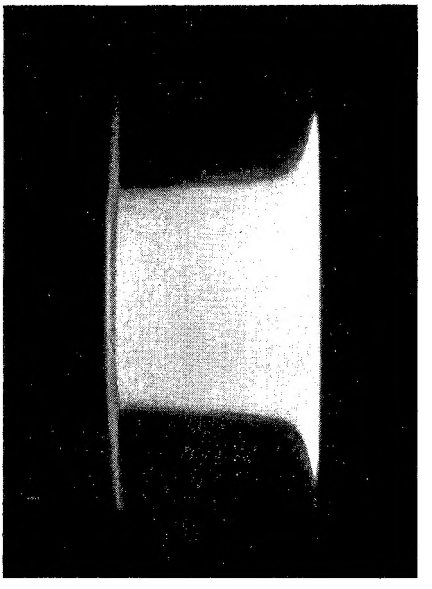

Fig. 2. Recovery of the afterglow by ultraviolet irradiation (irradiation from the right).

In order to investigate the influence of O_2 on the change of dimensions of the luminescent areas we put two identical activated samples into atmospheres of O_2 and H_2. Samples which were kept in O_2 did not show afterglow, although in those kept in H_2, no changes in luminescence were established.

In the case of those samples which show afterglow only at the center (as a result of aging in O_2) a return to a H_2 atmosphere causes the complete recovery of the afterglow which was observed in fresh samples. The recovery of the afterglow began at first at the border of the luminescent area (at the center of the specimen) and slowly extended throughout the sample, always being set off by a sharp boundary.

When the samples which were not luminescent as a result of storage in O_2 were further irradiated with strong ultraviolet light at a wavelength in the range 2890–3000 A., full recovery of the afterglow was observed. The recovery of the luminescence began at the irradiated surface (Fig. 2); subsequently, the dimension of this area increased (dark reaction). With further storage of these specimens in O_2 or in air (dark reaction) there was subsequent quenching of the afterglow as is shown in Figure 1.

There experiments indicate that the change of luminescent areas are not only related to the diffusion of oxygen, which causes afterglow quenching, but also to changes which occur in the solid medium. The diffusion of O_2 is, however, the main factor which causes the decrease of afterglow.

The influence of oxygen on the pure (without activators) thermally polymerized PMMA was studied by means of transmission changes. The ultraviolet transmission for freshly prepared samples begins at 2600 A. and reaches 50% at 2800 A. (Fig. 3), according to Pfund,[8] Robinson,[9]

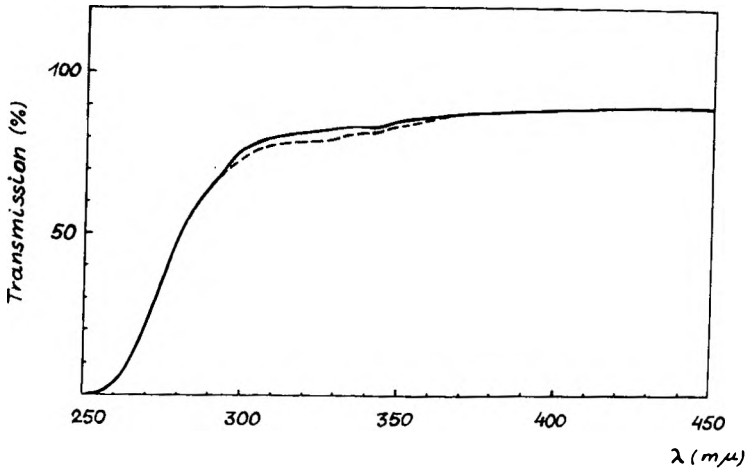

Fig. 3. Transmission vs. wavelength for pure PMMA samples; (- - -) sample kept in air; (——) sample kept in H_2.

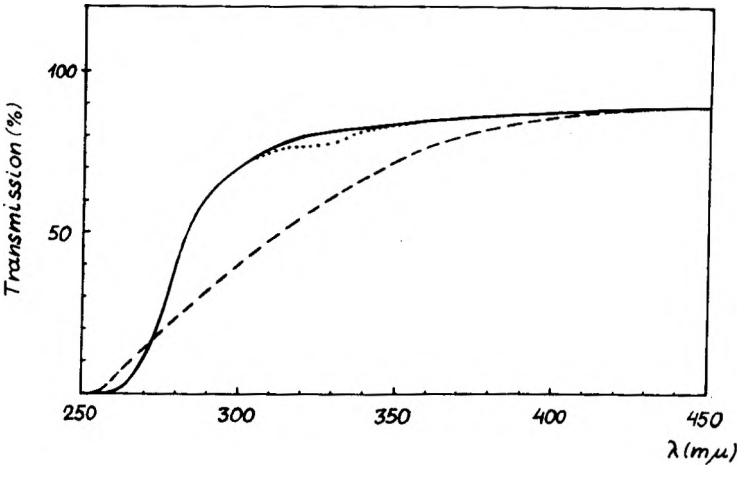

Fig. 4. Transmission vs. wavelength for pure PMMA: (· ·) sample aged in air; (- - -) after strong ultraviolet irradiation; (——) sample kept in H_2.

and others. After aging of PMMA for some weeks in the presence of O_2, a small decrease of transmission in the 3100–3500 A. range was observed. This decrease disappeared when (1) the sample was kept in an H_2 atmosphere, or (2) the sample was strongly irradiated with ultraviolet light. Prolonged irradiation of PMMA with ultraviolet light of high intensity (complete spectrum of Hg lamp) effects not only some color change of the specimen (maximum of changes in the region 3000–4300 A.) but also an increase of transmission at 2550–2700 A. (Fig. 4).

The 10% transmission loss is due to reflections on the specimen surfaces. Similar phenomena were observed by Chapiro,[10] Gross,[11] and others in

studies on ultraviolet degradation of PMMA.[12] The effect of ultraviolet irradiation on PMMA was confirmed also by infrared absorption spectra. It was established that the small absorption peak at 2.10 μ decreases (increase of transmission) after ultraviolet irradiation for a short time. In the dark this decrease of absorption went farther. The final change after a few days was of the order of $^1/_2\%$. The infrared absorption was evaluated by a differential method which guaranteed a precision of 0.01%. When the sample was kept in air, the intensity of 2.10 μ peak came back slowly to the value observed before ultraviolet light treatment. This indicates the existence of some slow processes in PMMA caused by the oxygen diffusion.

None of the above changes in infrared and ultraviolet transmission were seen when the samples were kept in a hydrogen atmosphere.

Discussion

The following interpretation of the observed phenomena is suggested.

The main factors responsible for the observed phenomena of a sharp-moving boundary of the luminescent area is the diffusion of O_2 and the changes which occur in the polymer medium.

In the solid polymer, even at a high degree of conversion, there are still monomer molecules and trapped radicals. The very high viscosity of the medium restrains the diffusion of monomer molecules to the growing chains, and some kind of dynamic equilibrium is established. The diffusion of O_2 into the solid polymer changes these conditions by the formation of different oxygen-containing compounds.[13,14] The problem of these equilibrium conditions has been discussed by Winkler,[15] Thompson,[16] Barnes,[17] and other authors. The most probable oxygen compounds formed are hydroperoxides, as has been found in oxidative degradation studies of PMMA[12] and in investigations of the reaction of O_2 with trapped radicals.[19] (It seems interesting to note that the activator molecules in the excited state can take part in oxidation reactions, as it was shown in the investigations of anthracene in liquid solutions.[20] In our case, this process is, however, of secondary importance.) The first step is the formation of peroxides which show rather fast decay giving hydroperoxides. Similar phenomena have been observed on γ-irradiation of PMMA in the presence of O_2.[18,19,21,22] When high energy radiation is applied, this reaction is much faster, depending on the dose. The terminal C=C bonds as well as trapped radicals might easily form peroxides. The physical changes which occur in polymers during the diffusion of O_2 result from either aggregative or "disaggregative" reactions (i.e., depolymerization and chain scission causing a decrease of molecular weight). The relative rates of these reactions depend upon the concentration of radicals and other active species, so the scission and crosslinking reactions occur side by side under normal conditions. In solutions, any radicals formed are kept sufficiently far apart to allow the scission reactions to predominate. In the solid polymer it is rather the scission that occurs at small concentration of O_2. Thus, the

equilibrium of aggregative and disaggregative reactions is shifted to the latter. It should be noted that the chain scission reaction as the main reaction for PMMA is more pronounced for samples of high molecular weight (above 180,000). This results in a decrease of the average molecular weight of the specimen, according to the data found in the studies of thermal and oxidative degradations of PMMA.[12]

In fact, this was confirmed by the determination of viscosity-average molecular weight $\bar{M}_v$ of specimens aged in O_2. The samples were dissolved in chloroform, and $\bar{M}_v$ was found from the intrinsic viscosity $[\eta]$ by using the relation[23]:

$$[\eta] = 4.8 \times 10^{-5} \bar{M}_v^{0.9}$$

For PMMA samples of high molecular weight ($\bar{M}_v = 7.8 \times 10^5$-$1.2 \times 10^6$) which have been kept in O_2 atmosphere for half a year, a decrease of 8–9% in molecular weight was established. These specimens show a complete disappearance of afterglow.

The increase in concentration of the low molecular species which are acting as plasticizers changes the local viscosity of the medium. As a high local viscosity is the principal condition for the appearance of afterglow, the changes of the viscosity value result in the decrease of long-term luminescence.

The H_2 recovery of the afterglow is connected with faster diffusion of H_2 molecules (in comparison with O_2) into polymer samples. As all polymers are permeable for H_2 (which has a very large diffusion coefficient), the concentration of hydrogen in the polymer increases and the amount of absorbed O_2 decreases (O_2 molecules which are not bound to the polymer are pushed out of the specimen). This does not simply imply the decomposition of hydroperoxides being formed by O_2 diffusion. The equilibrium between the formation and decomposition of hydroperoxides is, however, changed. This can be explained by the sequence of reactions (1)–(4) which include the above-mentioned reactions of hydroperoxide formation as well the reaction of radicals with O_2:

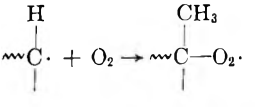

(1)

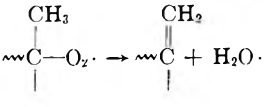

(2)

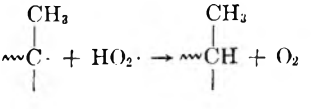

(3)

or

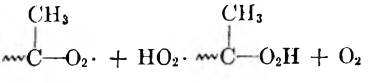

(4)

In the reactions (3) and (4) oxygen molecules are again liberated, and owing to fast diffusion of H_2 they are pushed out.

Thus, the concentration of oxygen in the sample which formerly was saturated by O_2 decreases. It should be taken into account that the increase in concentration of H_2 molecules also influences the stability of hydroperoxides. The increased stability of hydroperoxides favors the aggregative reactions and an increase of the local viscosity. However this kind of reaction is a minor one, and the recovery of afterglow in H_2 is mainly related to the decrease of O_2 quenching of the afterglow.

All samples preserved in H_2 atmosphere show no changes in $\bar{M}_v$, even on prolonged storage.

Fast recovery of afterglow as a consequence of ultraviolet irradiation should be related to the decomposition of hydroperoxides. Thus, the radicals formed under the influence of ultraviolet light initiate again the growing of the chains, and an increase of the local viscosity. PMMA is quite transparent for the near ultraviolet, so the chemical action of ultraviolet irradiation is extended throughout the whole sample. Since the initial concentration of O_2 and hydroperoxides is smaller at the center of the specimen than at the edges, the reaction of afterglow recovery starts first at the center where the oxygen concentration is too low to initiate a significant production of hydroperoxides. Generally, the methyl methacrylate peroxides are rather stable at room temperature and they decompose very little. This explains the necessity of the use of ultraviolet light for afterglow recovery.

As was stated before, the main factor which influences the afterglow is the O_2 quenching of activator molecules. These phenomena have been observed by numerous authors, e.g., Kautsky.[7] The quenching of afterglow is similar to the observed phenomena of color center disappearance formed by γ-irradiation of plastics. In fact, a sharp line of demarcation between the colored core and the border region "saturated" with O_2 has been reported by several workers.[24,25]

The visually sharp line of demarcation between the luminescent and nonluminescent area can be explained as follows. The activator molecules, trapped radicals, and C=C groups act as trapping sites for O_2; therefore the appropriate relation for the diffusion rate of O_2 into the polymer is more complicated than in the case of simple diffusion without chemical reactions. The concentration c of the diffusant in polymer depends upon the rate of flux through the surface and upon the contributions due to available trapping processes. In general, the local rate v of diffusion per unit of volume will depend on the concentration n of trapping sites of the ith type. The relation for the changes of the diffusant concentration (at constant diffusion coefficient) is given by

$$\partial c/\partial t = (D\nabla^2 c) + \Sigma v_i$$

$$= D\nabla^2 c \text{ H} - kcn \tag{5}$$

The negative second term is related to the trapping of diffusant molecules. The concentration n of trapping sites is a function of time:

$$\partial n/\partial t = -knc - k_1 n - k_2 n^2 - \ldots \quad (6)$$

where k, k_1, k_2 are constants.

The term kcn is the function which is responsible for the sharp visible demarcation line between luminescent area and the border region. In the simple case when $k_1 n$ and $k_2 n$ are small, eq. (6) may be solved approximately, and the diffusion coefficient D can be calculated. On the basis of the obtained relation it can be argued that the sharp boundary should be at a definite distance from the edge, i.e., where the concentration c reaches a threshold value c_t, to quench the luminescence. The threshold value c_t of O_2 is reached first near the edges, so the quenching of activator molecules begins there. With time, it moves towards the center of the specimen and defines the dimensions of luminescent area.

If an oxygen-saturated sample is put into a hydrogen atomosphere, fast diffusion of H_2 molecules causes a decrease of the local concentration. When, in a part of the sample the concentration of O_2 reaches a value lower than c_t, the recovery of afterglow starts at that point. This occurs first at the center because the concentration of O_2 is smaller, the greater the distance from the edges. A detailed quantitative discussion of these diffusion phenomena will be published later.

Conclusions

The phenomena described in this paper with their qualitative interpretation permit one to draw the following conclusions.

The observed moving boundary of the phosphorescent area is not limited to the particular case of PMMA with activators used in that study. In every transparent material, with luminescent molecules in the solid solution, these phenomena will occur in the similar way—the process of quenching of afterglow is general. This permits one to treat the described phenomena as a basis for a technique of studies concerning structure changes in polymers and some related phenomena.

Thus the moving boundary technique of luminescent area may be used to determine the diffusion coefficient in polymers in a rather simple way. The application of this method is not limited to O_2 only. Other gases, e.g., I_2 or Br_2, or vapors, e.g., nitrobenzene, which might act as quenchers can be used too.

The measurement of the shift rate of the afterglow boundary versus temperature will give some indications on the mobility of molecules. This is especially interesting in the temperatures close to the second-order transition temperature T_g. By means of values obtained in this manner, the activation energy for diffusion of gases and vapors, using the approach proposed by Brandt[27] one can get data related to the principal features of polymer structure.

The influence of stress on diffusion in polymers can be conveniently studied by the moving boundary of the afterglow. A comparison of the stress pattern taken through crossed polaroids with photographs of the luminescent areas of the same polymer specimen permits an evaluation of the relation between the permeation depth and stress-fringe order on the basis of photoelasticity theories.[28]

The accuracy of the technique of investigation of the luminescent boundary shift is limited to some degree by the determinations of absolute diffusion coefficients, but the method provides experimental opportunities.

Some results of the application of the moving boundary of afterglow will be published soon.

The disappearance of color centers in γ-irradiated polymers was similarly directly utilized in the study of diffusion in polymers by Zimmerman[29] and Barker and Moulton.[30] High energy irradiation, however, introduces too serious changes in the structure of investigated specimens which do not allow the extrapolation of the obtained data for unirradiated samples. This is not the case when activator molecules are introduced in low concentrations into polymer and form molecular solutions. In commercial polymers it might even not be necessary to introduce special activators, as the molecules of aromatic initiators (e.g., benzoyl peroxide) or residual stabilizer molecules can themselves cause the afterglow.

It seems that the described phenomena can offer some advantages in the studies of the polymer structure and its changes under the influence of numerous factors.

References

1. Lewis, G. N., D. Lipkin, and T. T. Mangel, *J. Am. Chem. Soc.*, **65**, 3005 (1941).
2. Jablonski, A., *Z. Physik*, **94**, 38 (1935).
3. Kryszewski, M., and B. Grossman, *J. Polymer Sci.*, **52**, 85 (1961).
4. Czarnecki, S., *Bull. Acad. Polon. Sci., Ser. Sci. Math. Astron. Phys.*, **9**, 561 (1961).
5. Pringsheim, P., *Fluorescence and Phosphorescence*, Interscience, New York–London, 1949.
6. Kryszewski, M., unpublished data.
7. Kautsky, H., *Trans. Faraday Soc.*, **35**, 291 (1939); *Z. Anorg. Chem.*, **222**, 126 (1935). Vogels, H., *Etude experimentale de la fluorescence et de la phosphorescence des colorants absorbées sur les geles colloidaux*, Paris, 1935.
8. Pfund, A. H., *J. Opt. Soc. Am.*, **29**, 291 (1939).
9. Robinson, H. A., R. Ruggy, and E. Siantz, *J. Appl. Phys.*, **15**, 343 (1943).
10. Chapiro, A., *J. Chim. Phys.*, **53**, 295 (1956).
11. Gross, B., *J. Polymer Sci.*, **27**, 135 (1958).
12. Grassie, N., and H. W. Melville, *Proc. Roy. Soc. (London)*, **A199**, 14, 24, 39 (1949).
13. Mesrobian, R. B., D. Metz, and A. V. Tobolsky, *J. Am. Chem. Soc.*, **67**, 785 (1945).
14. Mesrobian, R. B., and A. V. Tobolsky, *J. Polymer Sci.*, **2**, 463 (1947).
15. Winkler, C. A., *Can. J. Research*, **B24**, 179 (1946).
16. Thompson, J. O., *J. Phys. Colloid Chem.*, **54**, 338 (1950).
17. Barnes, C. E., *J. Am. Chem. Soc.*, **67**, 217 (1945).
18. Charlesby, A., *Atomic Radiation and Polymers*, Pergamon, London, 1960, p. 335.

19. Abraham, R., and D. H. Whiffen, *Trans. Faraday Soc.*, **54**, 1291 (1958).
20. Bowen, E. J., *Discussions Faraday Soc.*, **14**, 143 (1953).
21. Alexander, P., A. Charlesby, and W. Ross, *Proc. Roy. Soc.* (*London*), **A223**, 392 (1954).
22. Bamford, C. H., and J. C. Ward, *Trans. Faraday Soc.*, **58**, 971 (1962).
23. Bishoff, F., and V. Desreux, *Bull. Soc. Chim. Belge*, **61**, 10 (1952).
24. Charlesby, A., *Proc. Roy. Soc.* (*London*), **A215**, 187 (1952).
25. Boag, J. W., G. W. Dolphin, and J. Rotblat, *Radiation Res.*, **9**, 589 (1958).
26. Jost, W., *Diffusion*, Academic Press, New York, 1960.
27. Brandt, W. W., *J. Phys. Chem.*, **63**, 1080 (1959).
28. Forcht, M. M., *Photoelasticity*, Vol. II, Wiley, New York, **1948**.
29. Zimmerman, J., *J. Polymer Sci.*, **46**, 151 (1960).
30. Barker, R. E., Jr., W. G. Moulton, *J. Polymer Sci.*, **47**, 175 (1960).

Résumé

On a trouvé, que la bande β de phosphoresence fluorescence de longue durée des échantillons de polyméthacrylate de méthyle, activés par les hydrocarbures comme le naphtalène et ses dérivés, est sensible à l'influence de l'oxygène. Des frontières rigoureuses entre les régions phosphorescentes et non-phosphorescentes des échantillons sont liées à la diffusion de l'oxygène. Les frontières se mouvent avec le temps des bords de l'échantillon vers son centre. La régénération de la β-phosphorescence est causée par la diffusion de l'hydrogène ou par irradiation U.V. Une interprétation des phénomènes observés ainsi que la suggestion d'application de la technique de frontières mobiles de β-phosphorescence aux études des coefficients de la diffusion de gaz et aux autres processus liés avec ce phénomène, est présentée.

Zusammenfassung

Es wurde gefunden, dass die β-Phosphoreszenz (Fluoreszenz langer Dauer) des mit verschiedenen Kohlenwasserstoffen, wie Naphthalin und dessen Derivaten, aktivierten Polymethylacrylsäuremethylesters, durch Sauerstoff beeinfluss wird. Durch Sauerstoffdiffusion wird eine scharfe Grenze zwischen den phosphoreszenzfähigen und den gelöschten Bereichen verursacht. Diese Grenze verschiebt sich mit der Zeit vom Rande bis zur Mitte der Probe. Eine Regenerierung der β-Phosphoreszenz wird durch Wasserstoffdiffusion oder UV-Bestrahlung bewirkt. Eine Interpretation der beobachteten Erscheinungen wird gegeben und die Anwendung der Methode der beweglichen Grenze zur Bestimmung der Diffusionskoeffizienten von Gasen und mancher damit verbundener Prozesse wird beschrieben.

Received July 31, 1962

JOURNAL OF POLYMER SCIENCE: PART A VOL. 1, PP. 3079–3089 (1963)

Some Viscoelastic Studies on Penton

M. G. SHARMA and T. W. HAAS, *Department of Engineering Mechanics, The Pennsylvania State University, University Park, Pennsylvania*

Synopsis

Stress relaxation tests on Penton polymer were conducted at various initial strain rates and initial strains. The data indicates that Penton is a nonlinearly viscoelastic material for the range of values of stresses and strains considered. It is found that the course of the relaxation depends considerably on the initial strain rates employed to attain a particular initial strain in a relaxation test. For the range of initial strain rates considered, the relaxation function can be represented as a function of the time $\phi(t)$ and by a power function of the strain rate $\dot{\epsilon}_0$ of the type $\psi(t,\dot{\epsilon}_0) = \phi(t)(\dot{\epsilon}_0)^n$. From the relaxation tests conducted at the same initial strain rate and for various initial strains, the relaxation stress σ for Penton can be expressed by the relation: $\sigma = \sigma_0(1 - k \log t)$, where σ_0 is the stress at 1 min., t is the time, and k is a material constant.

I. Introduction

Many methods of specifying the properties of viscoelastic materials have been reviewed by Alfrey and Doty.[1] These methods can be classified into two groups according to whether the material behavior is specified in terms of mechanical models or by phenomenalogical functions such as creep functions, relaxation functions, and dynamic modulus functions as determined from experiments. In a linear viscoelastic material, all these methods can be shown to be equivalent to each other and can be transformed from one mode of representation to another. However, when the material behaves nonlinearly, it is very difficult to characterize the material in terms of mechanical models. The material whose viscoelastic properties are described in this paper is Penton. The test data indicate that this material is nonlinearly viscoelastic for the stress values considered in the investigation. Therefore, the relaxation behavior of the material described in this paper is in terms of relaxation function ψ, which is a function of not only time but also of initial strain and initial strain rates.

An ideal stress relaxation test requires that an instantaneous deformation be applied to a specimen and this deformation be held constant for the duration of the test. The load is reduced to keep this deformation constant. In practice this cannot be attained. Not only is a finite time required to attain a particular strain prior to a relaxation test, but also this value of strain is attained at various initial strain rates. This investigation was partly conducted to ascertain the effects of initial strain rates on the relaxation behavior of Penton. To our knowledge there has not been

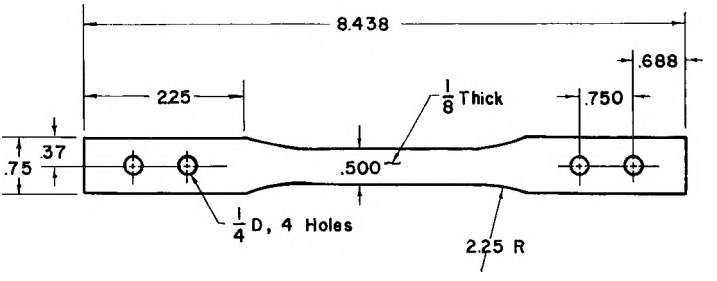

Fig. 1. Specimen of Penton.

any similar study conducted on solid polymers. However, the effect of initial strain rate on the course of relaxation has been investigated for polymeric solutions.[2] In addition, relaxation behavior of Penton has been investigated for various initial strains. These initial strains were attained at the same initial strain rates.

II. Description of the Material

The material[3] tested was Penton, chemical name 3,3-bis-(chloromethyl) oxetane. It is a linear polymer, crystalline in character, and its molecular

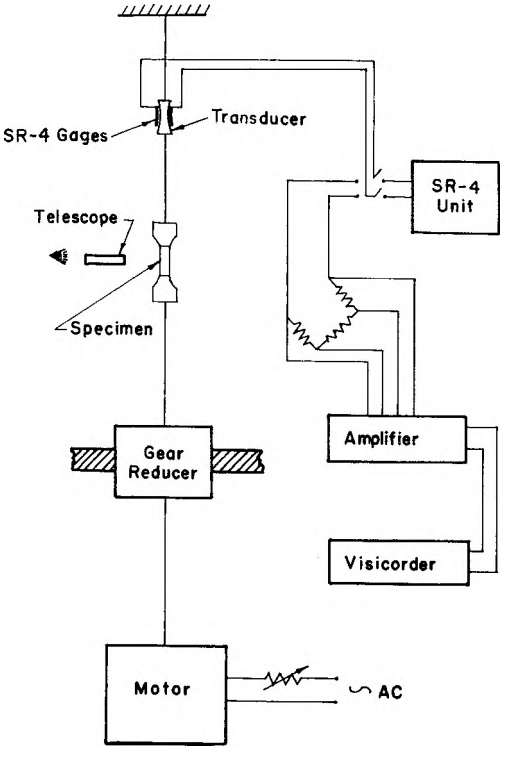

Fig. 2. Line schematic of stress relaxation unit.

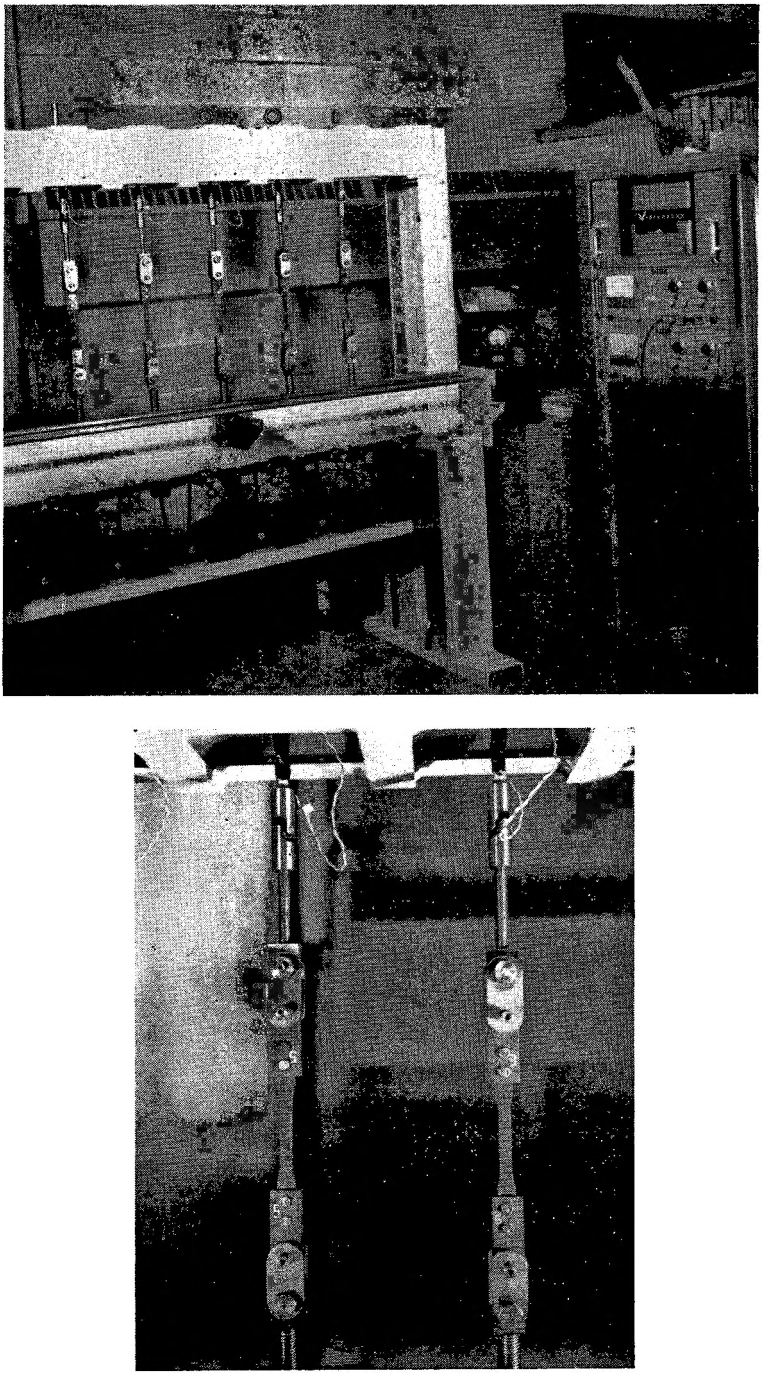

Fig. 3. Stress relaxation test arrangement.

weight ranges from 250,000 to 350,000. The material was supplied by Hercules Powder Company, Wilmington, Delaware, in the form of flat specimens as shown in Figure 1. The gage length used in all the relaxation tests was 2 in.

III. Description of the Equipment

The equipment used for these relaxation tests is shown in Figures 2 and 3. The specimen is placed in series with a transducer which has two SR-4 gages bonded to it. The transducer is calibrated to read the load at any stage of relaxation test. The other end of the specimen is connected to a variable speed motor through a system of reduction gears. The strain rate in the specimen can be varied from 0.0002 in./in./sec. to 0.0027 in./in./sec. by the variation of speed in the motor. The initial part of the stress distribution due to the initial strain history (prior to the attainment of constant strain in the specimen for relaxation) is automatically recorded in a visicorder (Fig. 3) which is capable of advancing the chart at 25 in./sec. However, for this investigation a chart speed of 0.2 in./sec. was found sufficient.

IV. Test Program

In the present investigations two types of stress relaxation tests were conducted, namely: (*a*) stress relaxation tests in which the initial strain of 2.3% was attained at twenty-two strain rates varying from 0.00023 in./in./sec. to 0.00261 in./in./sec. (Figs. 4–9); (*b*) stress relaxation tests in which the initial strains were varied. These strains were attained at the same average strain rate of 0.0022 in./in./sec. The initial strains in these tests varied from 0.0089 in./in. to 0.0329 in./in. Figure 12 shows the results of these tests for various initial stresses.

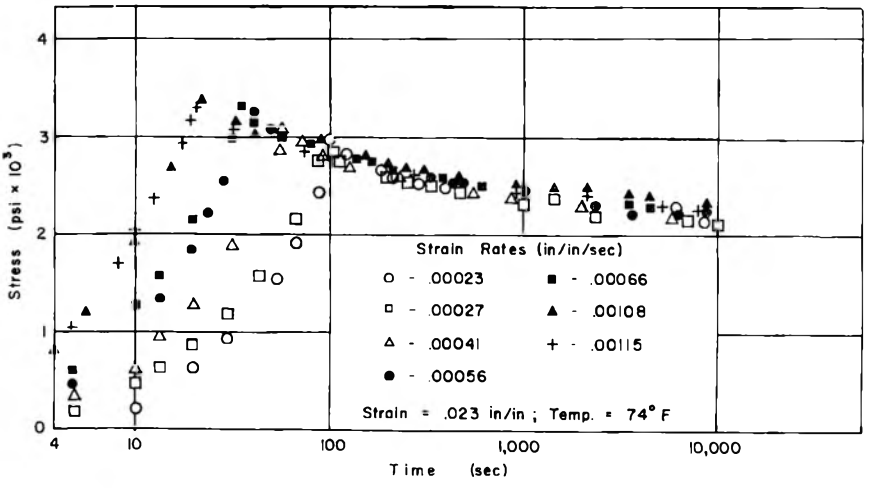

Fig. 4. Stress relaxation of Penton in tension.

V. Stress Relaxation Tests at Various Initial Strain Rates

The specimens were subjected to the same initial strain value of 0.023 in./in. This strain was attained at strain rates varying from 0.00023 in./in./sec.–0.00160 in./in./sec. In all 22 tests were conducted for the foregoing range of strains. The results of these tests are plotted in three groups corresponding to low strain rates (Figs. 4 and 5), intermediate strain rates (Figs. 6 and 7), and high strain rates (Figs. 8 and 9). The curves in each group were plotted in two parts, namely, stress relaxation curves for very short times up to 10,000 sec. (see Figs. 4, 6, and 8), and stress relaxation curves for very long times up to 10,000 min. (see Figs. 5,

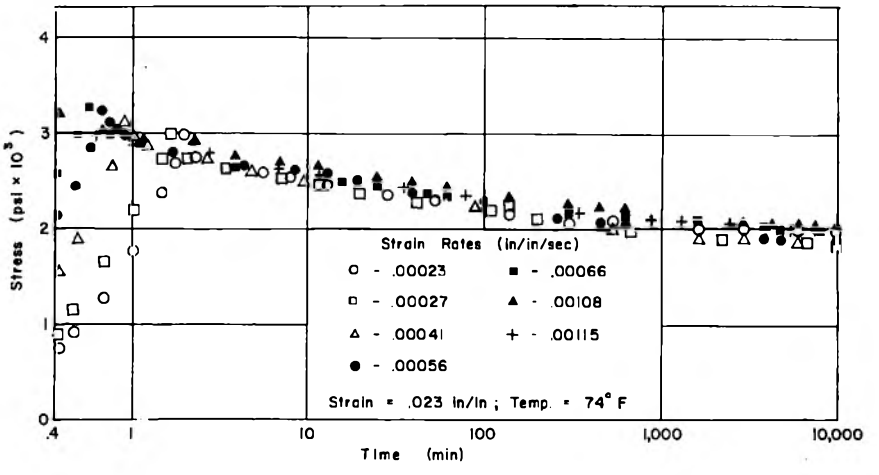

Fig. 5. Stress relaxation of Penton in tension.

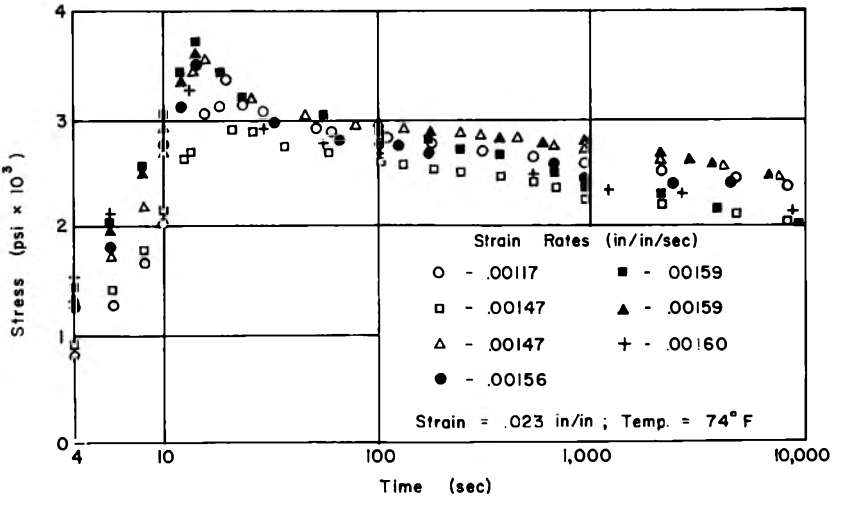

Fig. 6. Stress relaxation of Penton in tension.

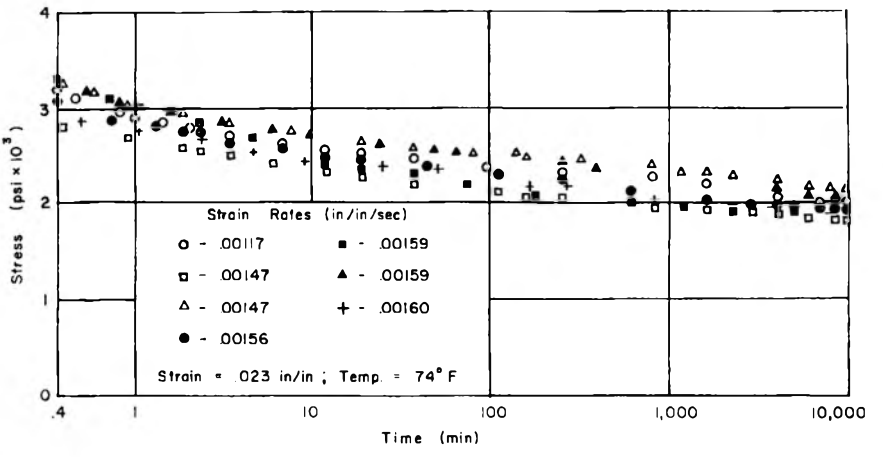

Fig. 7. Stress relaxation of Penton in tension.

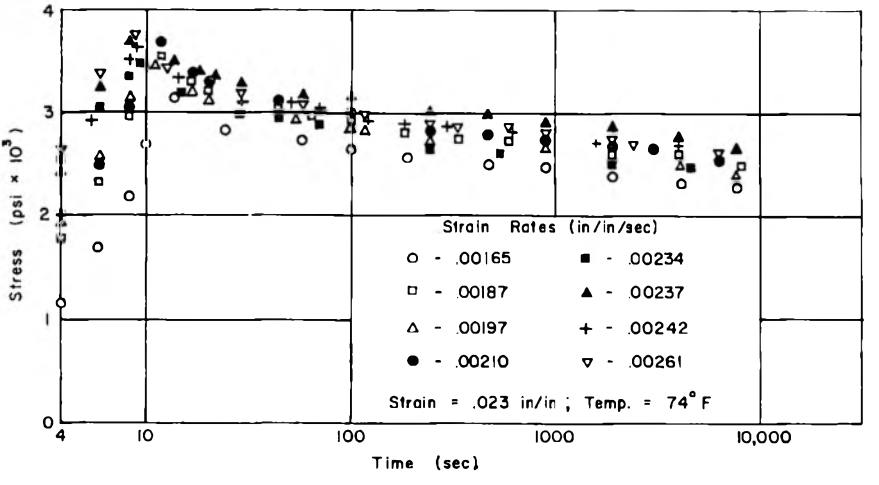

Fig. 8. Stress relaxation of Penton in tension.

7, and 9). The separation of the data for short times and for long times was necessary to determine the effect of initial strain history on the relaxation behavior of Penton. From Figures 4–9 the relaxation function $\psi(t,\dot{\epsilon}_0) = (\sigma/\epsilon_0)$, where t is time, σ is uniaxial stress, ϵ_0 is initial strain, and $\dot{\epsilon}_0$ is initial strain rate, was evaluated for various strain rates and plotted on a log–log basis, as shown in Figure 10 at specified times ranging from 0 to 10,000 min. Figure 10 shows that the relaxation function ψ is a power function of the strain rates

$$\psi(t,\dot{\epsilon}_0) = \phi(t)(\dot{\epsilon}_0)^n \tag{1}$$

where $\phi(t)$ is a function of time and $\phi(t)$ varied from 266,100 at $t = 0$ to 101,500 at $t = 10{,}000$ min.

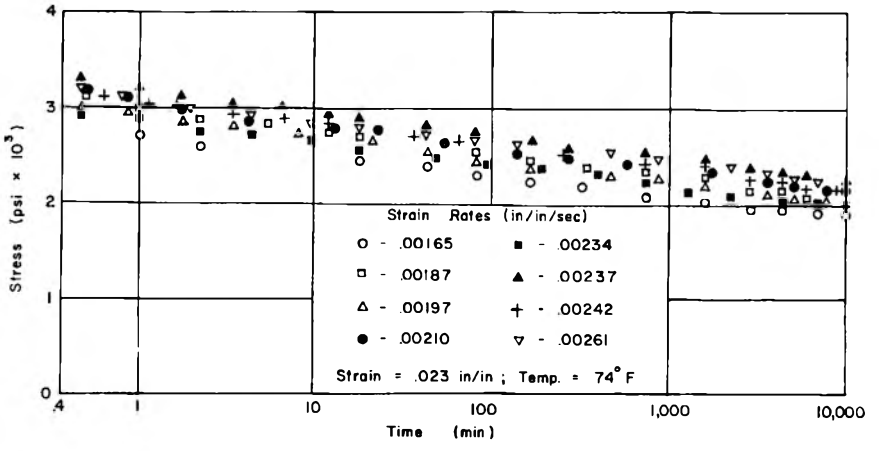

Fig. 9. Stress relaxation of Penton in tension.

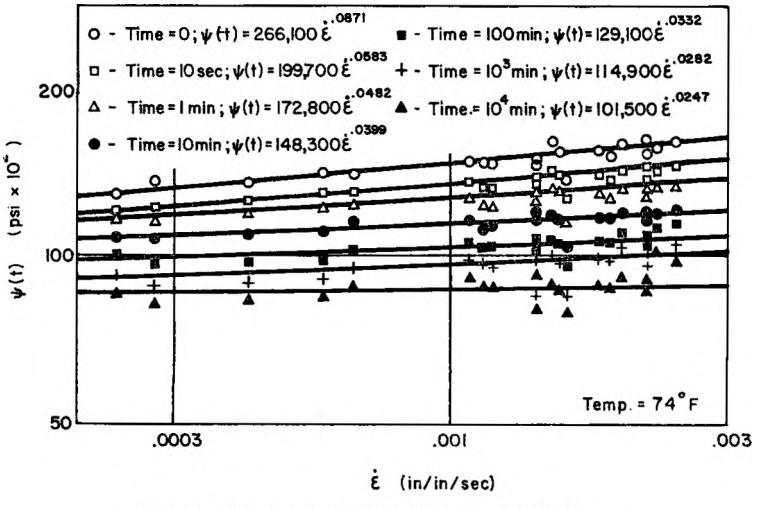

Fig. 10. Stress relaxation of Penton in tension.

The exponent n is a function of time, which varies from 0.0871 at $t = 0$ to 0.0247 at $t = 10{,}000$ min.

From Figure 10, the stress relaxation function $\psi(t,\dot{\epsilon}_0)$ is plotted in Figure 11 as a function of log t for various strain rates.

VI. Stress Relaxation Tests at Constant Strain Rate

Relaxation tests were conducted at various initial strains ranging from 0.0089 in./in. to 0.0329 in./in. These strains were attained at the same initial average strain rate of 0.0022 in./in. The test data obtained are shown in Figure 12. Figure 12 indicates that the stress relaxation behavior of Penton for the stress range considered can best be represented by eq. (2):

$$\sigma = \sigma_0(1 - k \log t) \tag{2}$$

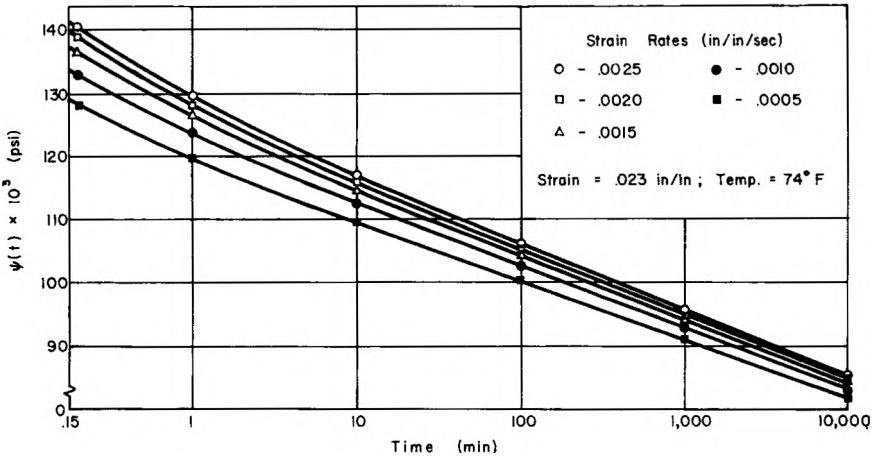

Fig. 11. Stress relaxation of Penton in tension.

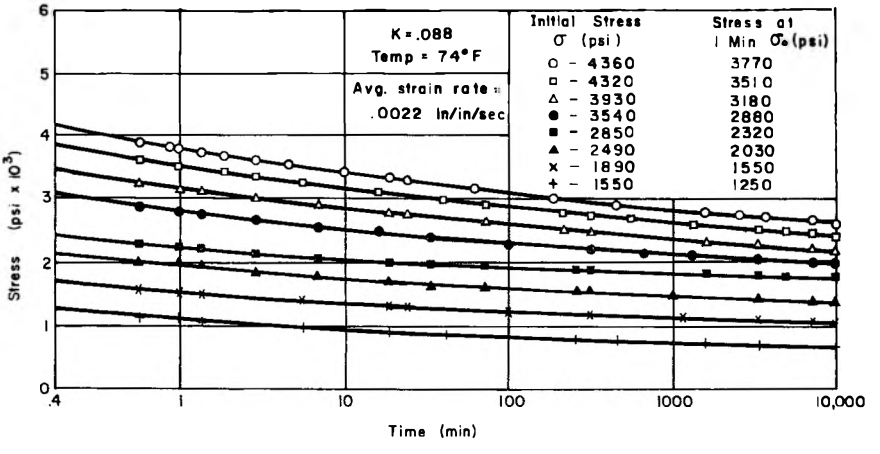

Fig. 12. Stress relaxation of Penton in tension.

where t is the time, σ is the stress, σ_0 is the stress value in a relaxation test at 1 min., and k is a material constant which is independent of stress. The values of σ_0 and k are shown in Figure 12 for various initial stress values. From Figure 12 stress and strain values were calculated for specified times and isochronous curves were drawn as shown in Figure 13. From these isochronous curves the stress relaxation function $\psi(t,\epsilon_0)$ was calculated and is shown in Figure 14 for various initial strains ϵ_0. If the material had been linearly viscoelastic, the relaxation function would have been a function of time alone and independent of initial strain ϵ_0.

VII. Discussion of Results

Figures 4–10 clearly indicate that the stress value in any relaxation test, at any time depends upon the initial strain rates employed in attaining a

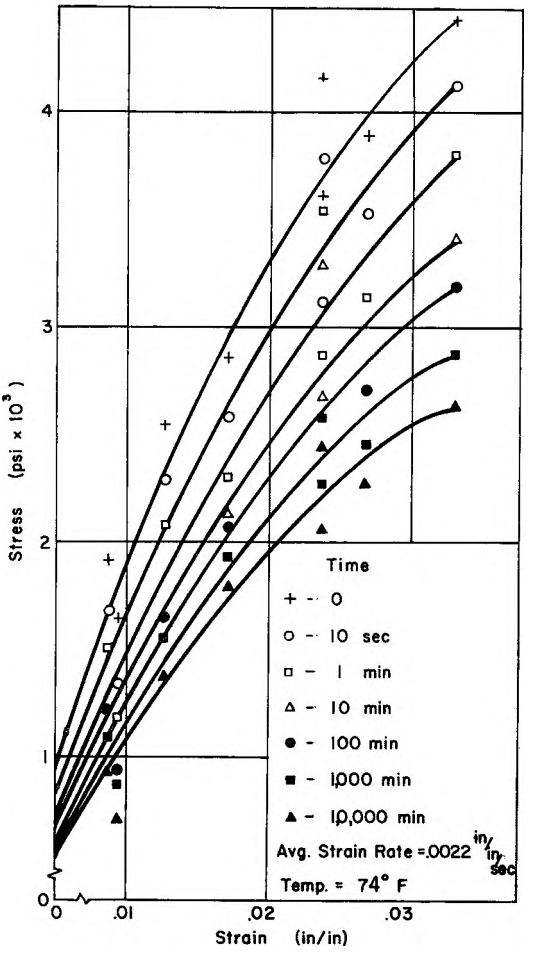

Fig. 13. Isochronous curves for Penton (from relaxation tests).

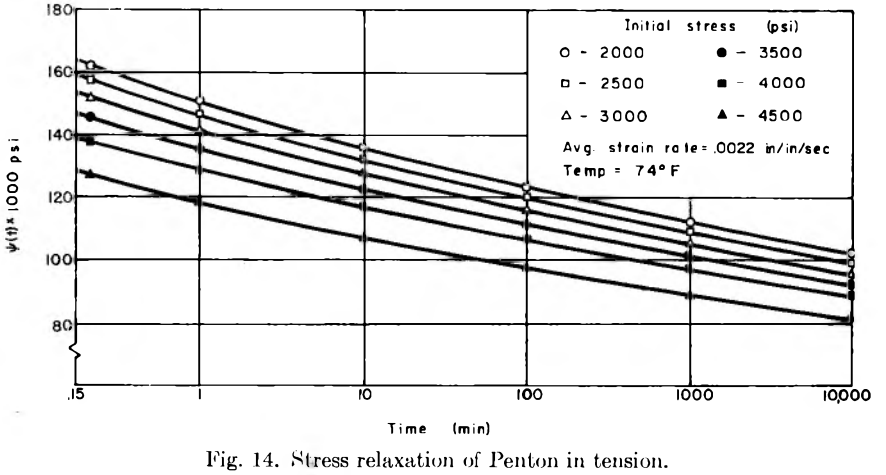

Fig. 14. Stress relaxation of Penton in tension.

particular value of initial strain prior to the relaxation test. This is also indicated by Figure 11, where relaxation function ψ is also a function of initial strain rate. The greater the initial strain rate, the higher the value of relaxation stress at a particular time. In addition, Figure 10 indicates that initial strain history in a relaxation test influences the relaxation behavior at very short times but has negligible effect at higher times. This can be observed from the tendency of the relaxation function ψ versus strain rate $\dot{\epsilon}_0$ relation (Fig. 10) to become horizontal beyond 10,000 min. Figure 11 also indicates more clearly the effect shown in Figure 10, that is, the greater the initial strain rate, the higher the value of the relaxation function ψ. As the initial strain rate is increased, there is a tendency for the relaxation function versus log t curves to coincide. This indicates that as the initial strain rate is increased, the value of the relaxation function becomes independent of the initial strain rates. The same tendency is displayed in Figure 11 at larger times of the order of 10,000 min. and beyond indicating that in relaxation behavior at large times, the effect of initial strain history can be neglected.

Figure 10 shows that the relaxation function ψ can be expressed as a power function of the strain rate. However, the constants in the power law vary according to the time under consideration. The range of variation of these constants is shown in Figure 10.

Stress relaxation tests conducted at the same initial strain rate and at various initial strains, as indicated in Figure 12, show that Penton has linear stress versus time plot on semilog graph paper for the stress range considered. Equation (2) gives the relationship between stress and time in the above type of relaxation test. Based upon the isochronous curves for various times, as shown in Figure 13, the relaxation function $\psi(t,\epsilon_0)$ was calculated for each initial strain value ϵ_0, as shown in Figure 14. These isochronous curves were necessary to eliminate the scatter in $\psi(t,\epsilon_0)$ versus log t curves. Relaxation function $\psi(t,\epsilon_0)$ variation with time in Figure 14 indicates that Penton is nonlinearly viscoelastic. This is also indicated by eq. (2). However, there is a tendency for the relaxation function $\psi(t,\epsilon_0)$ versus log t curves to coincide for smaller value of stress. This indicates that as the initial value of stress is lowered in a relaxation test, the material tends to be linearly viscoelastic.

VIII. Conclusions

The relaxation test results on Penton indicate that the curve of relaxation in any relaxation test depends on the initial strain rates used in attaining a particular value of strain prior to a relaxation test. The effects of initial strain rate are considerable at relatively short times and are negligible at long times. As the initial strain rates in any relaxation test are increased, the effect of change in initial strain rate on the relaxation behavior becomes negligible. Relaxation test data obtained at various initial strain values indicate that at low values of initial stress, the material can be considered as linearly viscoelastic.

The authors wish to thank Dr. J. Marin, Head of the Department of Engineering Mechanics of The Pennsylvania State University for his helpful suggestions in the preparation of this paper. The content of the paper is a part of the investigation sponsored by the Army Research Office Durham, Project No. 59901007. The authors are indebted to the Army Research Office for sponsoring the above project and for having made the work possible. The authors are grateful to Hercules Powder Company, Wilmington, Delaware, for supplying the Penton specimens.

References

1. Alfrey, T., and P. Doty, *J. Appl. Phys.*, **16,** 700 (1945).
2. Shremp, F. W., J. D. Ferry, and W. W. Evans, *J. Appl. Phys.*, **22,** 711 (1951).
3. *"Penton" an Engineering Polymer*, published by Hercules Powder Company, Wilmington, Delaware.

Résumé

Des tests de rélaxation de tension sur le polymère Penton ont conduit à différentes vitesses de tensions initiales et forces de tension initiales. Le résultat indique que le Penton est une matière nonlinéaire viscoélastique pour le domaine des valeurs de tension et forces de tension considérés. On trouve que l'allure de la rélaxation dépend considérablement des vitesses initiales de tension employées pour atteindre une tension initiale particulère dans un test de rélaxation. Pour le domaine de vitesse initiale de tension considéré, la fonction de rélaxation est représentée par une fonction du temps $\phi(t)$ et par une fonction potentielle de la vitesse de tension ϵ_0 du type $\phi(t, \dot{\epsilon}_0) = \phi(t)\,(\dot{\epsilon}_0)^n$. A partir des tests de rélaxation conduits à la même vitesse de tension initiale et pour différentes forces de tension initiales, la tension de rélaxation σ s'exprime par la relation suivante pour le Penton $\sigma = \sigma_0\,(1 - k \log t)$, où σ_0 = la tension à 1 min., t = le temps et k est une constante de la matière.

Zusammenfassung

Spannungsrelaxationsmessungen werden an Pentonpolymeren bei variierter Anfangsverformungsgeschwindigkeit und Afnangsverformung durchgeführt. Die Ergebnisse zeigen, dass Penton im untersuchten Spannungs- und Verformungsbereich ein Material mit nicht-linearer Viskoelastizität darstellt. Der Verlauf der Relaxation hängt stark von der bei einem Relaxationstest zur Erreichung einer bestimmten Anfangsverformung verwendeten Anfangsverformungsgeschwindigkeit ab. Im untersuchten Anfangsverformungsgeschwindigkeitsbereich kann die Relaxationsfunktion als Zeitfunktion $\phi(t)$ und durch eine Potenzfunktion der Verformungsgeschwindigkeit ϵ_0 von der Gestalt $\psi(t,\dot{\epsilon}_0) = \phi(t)\,(\dot{\epsilon}_0)^n$ dargestellt werden. Aus den bei gleicher Anfangsverformungsgeschwindigkeit und verschiedener Anfangsverformung durchgeführten Relaxationsversuchen kann die Relaxationsspannung σ für Penton durch folgende Beziehung ausgedrückt werden: $\sigma = \sigma_0\,(1 - k \log t)$, wo σ_0 die Spannung nach 1 min, t die Zeit und k eine Materialkonstante ist.

Received July 31, 1962

JOURNAL OF POLYMER SCIENCE: PART A VOL. 1, PP. 3091–3103 (1963)

Fibrous Structure in Stretched Crystalline Elastomers

M. H. WALTERS, *Central Research Division, Dunlop Rubber Company, Ltd., Erdington, Birmingham, England*

Synopsis

Stress-induced crystallinity in elastomers produces a strengthening structure, and tearing the rubber along the axis of extension leaves this structure outlined in the rupture surface. By maintaining the initial elongation, and taking replicas of this torn surface, the morphology of stress crystallinity has been examined in the electron microscope. The crystallites were found to be closely spaced fibers, rounded in section, and oriented in the direction of elongation. The fibers were usually between 100 and 1000 A. in diameter, and individual crystallites could be traced for distances of several microns before disappearing beneath the exposed surface. Noncrystallizing polymers showed no structure in the rupture surface. The addition of fine particle fillers had little effect on the structures observed in crystallizing polymers. In amorphous polymers traces of structure were observed, apparently consisting of groups of carbon black particles linked by rubber molecules.

INTRODUCTION

Many high polymers of regular molecular structure crystallize if they are cooled below their freezing point, while in rubber crystallinity can also be induced at higher temperatures if they are stretched. Stress crystallinity of this type is particularly important because it imparts high strength to the polymer. The degree of crystallinity, the arrangement of the molecules in the crystal lattice, and the average size of the crystallites can be determined by the analysis of x-ray diffraction patterns. Further detailed information on the shape and arrangement of the crystallites can be obtained by examination with polarizing and electron microscopes.

The fine structure of low temperature crystallinity has been examined extensively in recent years, and studies with the polarizing microscope have shown the growth of spherulites to be the most typical effect. There is strong evidence[1] that a spherulite grows from a nucleus of parallel fibers. Successive branching from the ends of these fibers form a sheaf-like structure which finally develops into a complete spherulite which looks like a cluster of thin needles radiating from a central point. X-ray studies have shown that (in some cases at least) the molecular chains run at right angles to the fiber axes.[2]

Stress crystallinity in rubber has also been examined by x-ray methods, and in this way Bunn[3] has shown that the molecules are aligned along the axis of stress. The individual crystallites have been estimated from

the width of their x-ray diffraction spots to be about 300 A. in size. Because of the small size of the stress crystallites and the great length of rubber molecules (ca. 10,000 A.) it is usually postulated that a single molecule may pass alternately through a number of crystallites and amorphous regions.[4a] There seem to be no literature references to a microscope examination of the morphology of stress crystallinity.

Our first attempt to observe stress crystallinity in rubber was by examining surface replicas of stretched vulcanizates in the electron microscope. It was hoped that the slight contraction (10% by volume)[4b] on crystallizing would give surface irregularities large enough to be observed, but no trace of crystallinity was found. Vulcanized rubbers cannot be etched with solvent to reveal crystallinity because the crosslinks prevent the removal of dissolved material, but attempts to reveal crystallinity by differential swelling, making use of the greater oil absorption of noncrystalline material, were also unsuccessful.

A more successful method has as its basis the assumption that the path of a tear deviates around crystallites in its path. Thus, if the stress (and hence crystallinity) can be maintained after tearing has ceased, the crystallites in the torn surface can be examined with surface replicas. Crystallites in the torn surface might also be preserved by rapid freezing of the rubber, but this technique was not attempted, partly because of the difficulty of preparing replicas under these conditions, but also to avoid confusion in interpretation between stress and low temperature crystallinity.

EXPERIMENTAL PROCEDURE

To preserve the rupture surface in a state of extension after tearing had ceased, a "longitudinal" tearing procedure was used. Rectangular testpieces (10 cm. × 2 cm. × 2 cm.) were slit along half their length, and thin loops of metal tape were inserted into the slit. The specimens were stretched longitudinally to between 100% and 450% elongation, and the metal loops pulled apart (Fig. 1), so causing the tear to run along the length of the stretched specimen. (When the specimen was completely relaxed it was usually found that the tear had curved slightly off this axis). After the tearing forces F_T had been released the longitudinal extending force F_L was still maintained, thus preserving the crystallinity.

The metal loops were removed and the cut wedged open so that two-stage, gelatin–carbon replicas of the torn surfaces could be prepared by the method described by Andrews.[5] The replicas were shadowed at 60° with palladium–gold alloy before digestion of the gelatin in warm trypsin solution, and were examined in an R.C.A. EML-1B electron microscope.

In a preliminary attempt to reveal stress crystallinity in the surface of an untorn polymer by etching, drops of solvent were applied to the surface of the stretched rubber. It was found that the resultant local swelling weakened the rubber surface and caused the outer layer to tear away (Fig. 2).

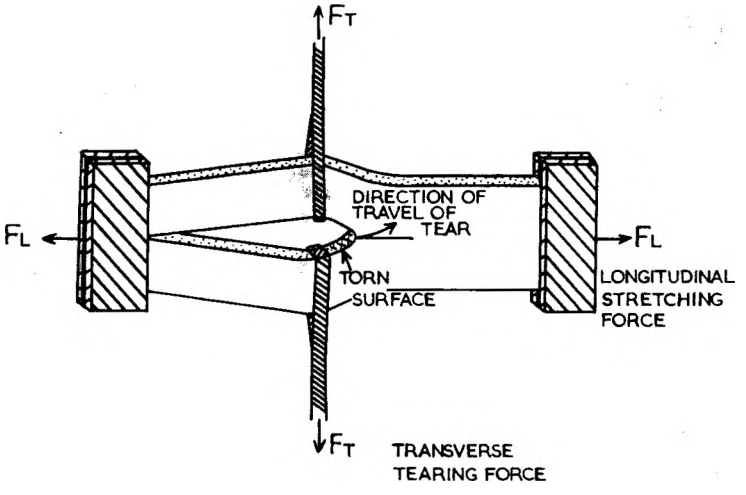

Fig. 1. Longitudinal tearing. The initial extension is applied by the stretching force F_L, and the sample torn by the transverse forces F_T. Surface replicas of the torn surface are examined in the electron microscope.

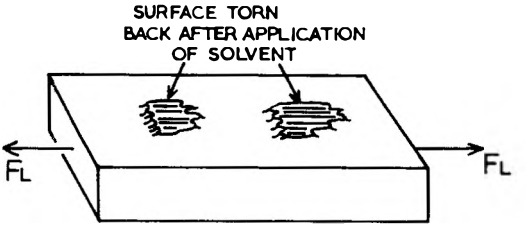

Fig. 2. Solvent tearing. Drops of solvent placed on the surface of the stretched sample cause the rubber surface to tear back. The torn surface is examined by surface replicas.

It was thought that the new surface thus revealed might also show crystalline structure without the complications to interpretation caused by the transverse tearing forces F_T in the method described above. This surface was therefore examined by a similar surface replica technique.

RESULTS

The longitudinal method of tearing differs from most other tear tests in that the rupture travels along, rather than perpendicular to, the direction of initial stress. The only reported work on these lines seems to be that of Chasset and Thirion,[6] who inferred that the tearing of natural rubber is fundamentally different from that of noncrystallizing polymers. The longitudinal tearing of natural rubber was visualized as the rupture of a fibrous material, either parallel or perpendicular to the fiber axis, while in noncrystallizing rubbers the tearing was that of an isotropic material. These concepts have been largely confirmed when the electron micrographs were assessed.

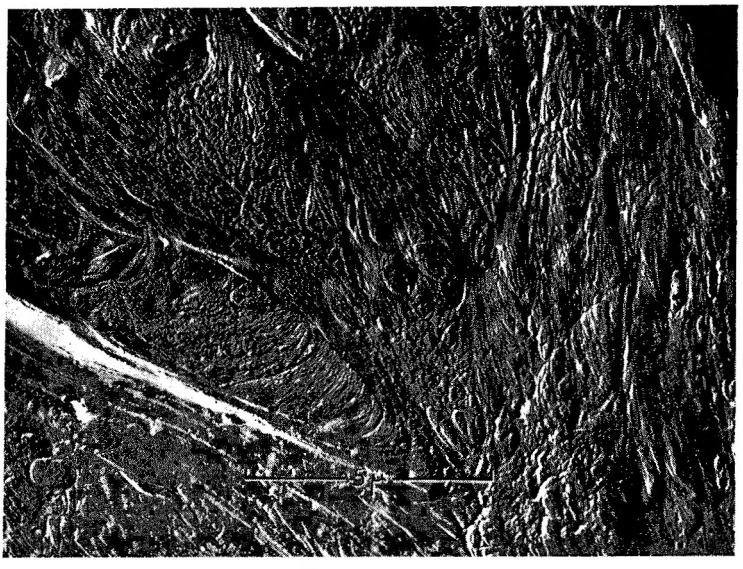

Fig. 3. Fibrous surface from longitudinally torn natural rubber, showing sheakflike pattern and layered effects. The initial extension was 350% in the direction top left to bottom right.

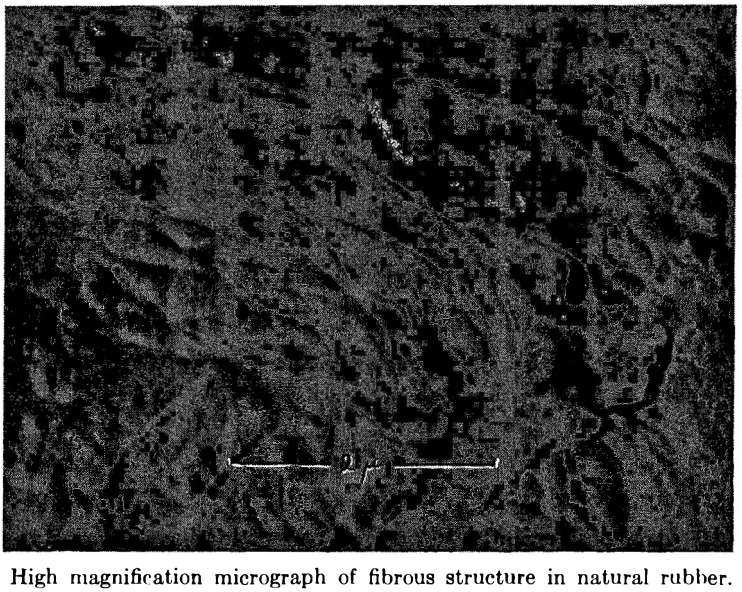

Fig. 4. High magnification micrograph of fibrous structure in natural rubber. The shadowing shows the fibers to be of rounded section.

By far the most common effect observed in micrographs of torn natural rubber gumstocks was the pronounced fibrous appearance of the surface. This could be observed over a wide range of longitudinal extensions (100–450%). In some samples this covered the whole surface, and in others the fibrous patches occurred only sparsely. The effect is well shown in Figure

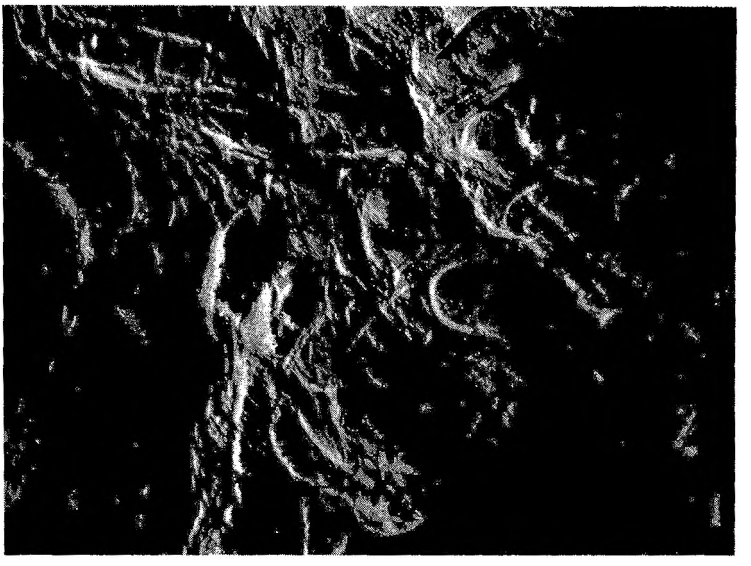

Fig. 5. Fibrous structure in polychloroprene (Neoprene W). The dark patches at the right-hand side appear to be fibrous material torn out by the replication process.

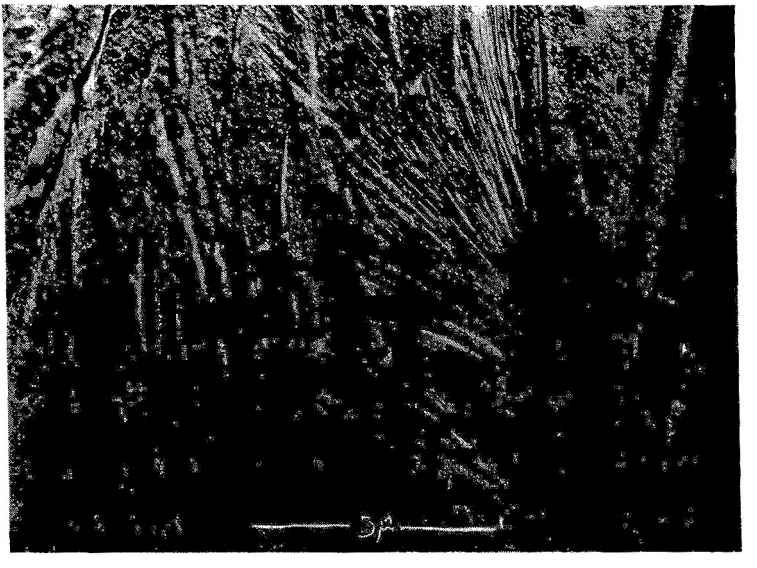

Fig. 6. A star formation from natural rubber. The stratified appearance at bottom right indicates that it is composed of radiating surfaces rather than lines. Probably a spherulite.

3. The surface is apparently composed of a mass of fibers, sometimes bunching together into sheaflike patterns, and at other places wandering more or less at random over the surface, although showing a tendency to align themselves more or less in the direction of longitudinal extension. There are also examples of layering effects, the fibers in successive layers

Fig. 7. Platelets in natural rubber. The kinks crossing the platelets are similar to those observed by Kellar in lamellar crystals of polyethylene.

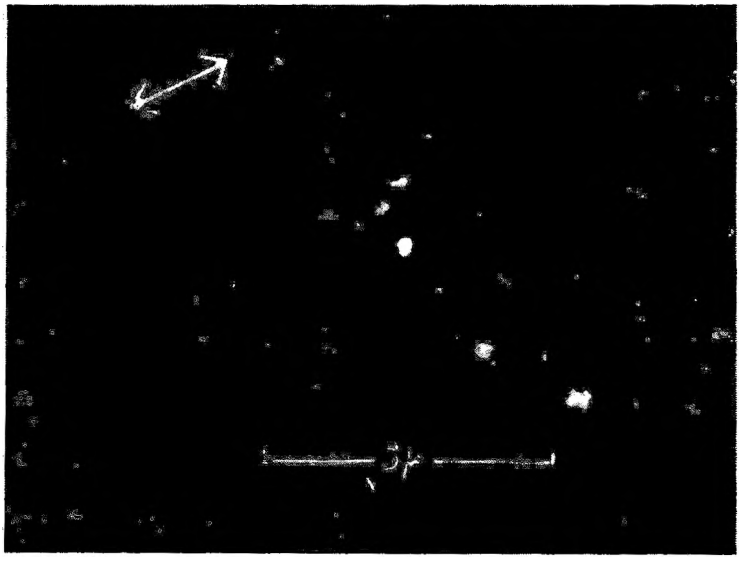

Fig. 8. Closely splaced lumps in over-cured natural rubber. Possibly due to stick-slip tearing. The arrow shows the direction of tearing.

appearing to run in different directions. When examined at high magnification the shadowing indicates that the fibers are of rounded cross section (Fig. 4). Thus the tear has deviated around complete fibers rather than passing through them via planes of easy cleavage. The fibers are usually between 100 A. and 1000 A. in diameter, and individual fibers may be fol-

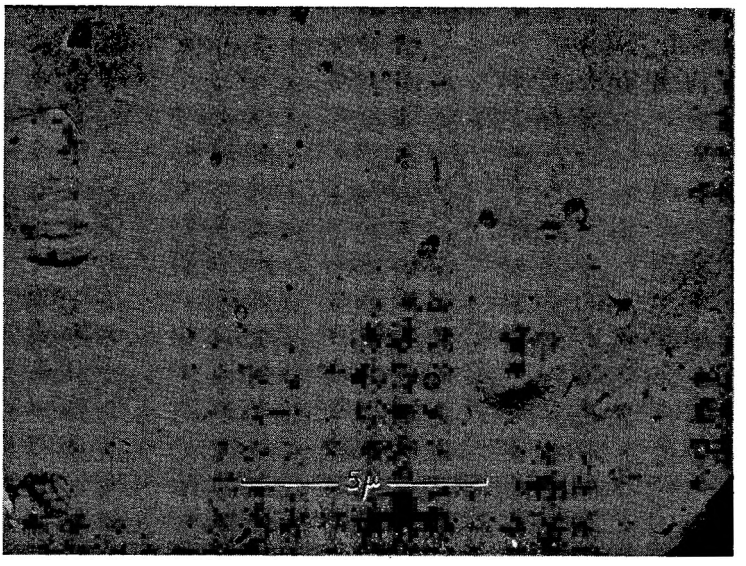

Fig. 9. Featureless surface of longitudinally torn styrene–butadiene rubber.

Fig. 10. Highly oriented structure in solvent torn natural rubber surface. The layering structure at top right shows this to be a true fibrous effect.

lowed over distances of several microns before they wind under the exposed surface, or merge into other features.

Similar fibrous effects were observed in other crystallizing polymers (e.g., polyurethane, polychloroprene) when surfaces prepared by the longitudinal stretching technique were examined. In polychloroprene

(Neoprene W) some of the fibrous structure had been pulled out of the surface by the gelatin, and can be seen in the replica (Fig. 5). Somewhat surprisingly, fibrous structure was also observed on surfaces of polypropylene prepared by cutting with scissors or by sandpapering; presumably the mechanism of formation consisted of stretching the surface of the polypropylene sufficiently to break down the normal granular crystals[7] into fibrous structure. The high degree of crystallinity and low resilience of this polymer prevents these fibers from melting as they would in a rubber when the tension is relaxed.

Other types of structure were also observed in these replicas of natural rubber. Among these were "star" formations of straight lines, either radiating outwards from a common center or bunched in a sheaflike pattern, and often with the longest lines running in the direction of the tear. In places where cracks penetrating the surface cross these patterns, the "stratified' appearance indicates that they are composed of radiating surfaces, rather than lines (Fig. 6).

At low elongation the torn surface of a natural rubber gum compound appeared over a large area to consist of flat, elongated platelets with rounded tips, often overlapping one another (Fig. 7). The surface of these platelets were so smooth as to resemble crystal faces, and many of the larger ones were crossed by the "kinks" which Keller has observed crossing lamallar crystallites of polyethylene. The platelets can sometimes be seen merging into the more usual fibrous appearance, presumably by the breakdown of the platelets under the tearing force. In some places this flaky appearance resembled the star formations observed at higher elongations, and they may result from the same cause.

Another surface effect was found in rubber which had been highly overcured. In this case the fibrous structure was replaced by rows of nearly parallel ridges, or in some cases lumps, closely spaced (0.5 μ) and running across the line of stretch. Often these ridges were crossed by strongly marked lines running in the direction of stretch (Fig. 8). This ridged effect is apparently not fibrous in nature, and the tendency for the lumps to align themselves in roughly parallel ridges suggests that excessive cure causes a stick-slip tearing process on a very small scale.

Unreinforced vulcanizates of noncrystalline rubber are too weak to be stretched to large elongations without breaking. At extensions of about 200% the surface of styrene–butadiene rubber (Krylene) was generally featureless (Fig. 9), although occasionally displaying the ridged effect described above. Other noncrystallizing polymers were similar. The absence of fibrous structure in noncrystalline rubbers is in agreement with the "amorphous" tearing characteristic (according to Chasset and Thirion) of these polymers.

The necessity, in the longitudinal tearing technique, of stretching in two directions at right angles makes it impossible to determine with an electron microscope technique the degree to which the fibrous structure follows the line of resultant stress. It was found that when a volatile solvent

(diethyl ether) was dropped onto the surface of a stretched natural rubber vulcanizate, the top layer tore back along the line of stretch. This is a form of longitudinal tearing, but without the complication caused by the transverse tearing forces. Replicas showed this freshly exposed surface to be often fibrous (Fig. 10), and the fibers are aligned amost entirely along the direction of extension. The degree of alignment was so high that when first seen they were thought to be the result of chance irregularities in the tear path being perpetuated in the direction of the running tear, but layering (as in the top right-hand corner of Fig. 10) show them to be due to a fibrous structure. The mechanism of this effect is probably that the ether is unable to penetrate far into the crystalline polymer.[8] The surface of the rubber, where swelling takes place, is weakened by the solvent, and tearing takes place under the influence of the longitudinal tearing forces, once again following the boundaries of the fibrous structure. When this technique was used with noncrystallizing polymers the solvent penetrated deeply into the sample which as a result failed completely.

DISCUSSION

When considering these observations the nature of the fibrous structure is obviously of first interest. It may be assumed that it is caused by some strengthening formations in the rubber, since, if this were not the case, the tear path would not have to deviate in outlining their shape. Fibrous structure was observed in all crystalline polymers examined, but was never observed in noncrystallizing polymers, and this is strong evidence that the fibers represent stress crystallinity in rubber. The observed diameter of the fibers (a few hundred Angstroms) is consistent with x-ray determinations[9] of crystallite dimensions, although there are no reports of crystallite lengths of several microns. In some places fibers can be seen crossing over one another, and this indicates that the long fibers are continuous crystallites, and not a succession of amorphous regions and short crystallites (of the size determined by x-ray measurements) aligned in the same direction and fortuitously represented as a single fiber by the tearing process.

In most replicas featureless areas existed alongside the fibrous effects reported here. It is possible that the fibers actually occur in patches in an amorphous continuum, and this "patchy" crystallinity could be due to some kind of nucleation effect promoting local crystallization. On the other hand, it was found that relaxing both the transverse and the longitudinal tension before preparing the replica resulted in almost complete disappearance of fibrous structure. The featureless areas on the stretched testpieces can thus be explained as the result of local relaxation of the torn surface when the transverse forces were removed, and the fibrous areas as the true structure of natural rubber. No practical experiment to differentiate these possibilities has yet been thought of.

It is surprising to find crystallinity at the low elongations (150%) at which the fibrous structure has been observed. A possible explanation is

that the crystallization is mainly caused by the high transverse tearing forces, and after relaxation of these forces the longitudinal force merely prevents melting. This explanation causes further difficulties, however, because crystallinity caused by the transverse forces should be aligned perpendicularly to the direction of longitudinal stress (in which the fibers are roughly aligned) and it is difficult to visualise how the apparent change in alignment takes place.

The micrographs of surfaces prepared by dropping solvent onto stretched samples are not subject to the complication of two perpendicular stretching forces. In these samples a very much higher degree of alignment was observed. It seems likely that this orderly arrangement is a better picture of stress crystallinity than that of randomly wandering fibers in the longitudinally stretched samples, which is probably due to the change in the direction of stress when the transverse forces are relaxed. In both the longitudinal and solvent tearing techniques higher stresses probably occur at the torn surface than in the bulk of the sample, and thus the observed structure represents the degree of crystallinity produced in rubber when it is stresses to its ultimate elongation.

The platelets and star formations seen in natural rubber (Figs. 5 and 6) appear to be different phenomena from the stress crystallinity. It seems unlikely that they are artifacts caused by the experimental technique, nor do they resemble any of the vulcanizing agents or antioxidants added to the rubber. Molecular rearrangement caused by stretching would be expected to give an aligned structure rather than these effects, and the most likely explanation is that they are the remains of spherulites, initially present in the rubber, but partially disrupted by the tearing forces. They were not observed sufficiently frequently to make more systematic study possible.

STRUCTURE CAUSED BY FILLERS

It is believed that the path of a running tear is deflected around strengthening structures in its path, and the longitudinal method of tearing is a technique for preserving this structure in the rupture surface where it can be examined by surface replicas. Apart from crystallinity, strengthening structure can be imparted to rubber compounds by the addition of fine particle fillers, such as carbon black, and there have been numerous investigations of black reinforcement.[10] Carbon black reinforces both crystalline and amorphous rubbers (the effect being greatest in the latter), and the longitudinal tearing technique was used to examine the resultant structure in both types of polymer. To avoid complications in interpretation the black loading had to be kept low (10% by volume) and a large particle size filler (SRF) was used.

In natural rubber the usual fibrous effects could be seen, but the presence of carbon black caused a greater alignment of the fibers, reminiscent of the solvent torn surface, and only a few areas showed the sheaflike fibrous

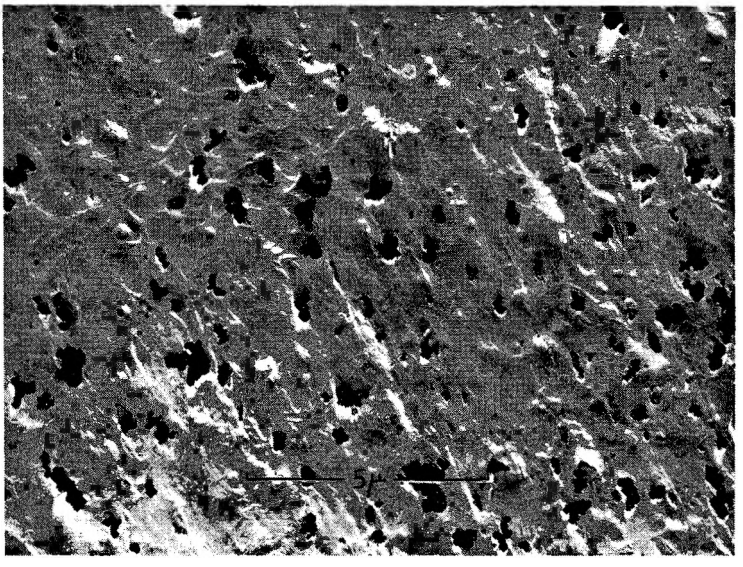

Fig. 11. Black-loaded natural rubber. The structure in crystallizing elastomers is usually much more highly aligned than this.

Fig. 12. Apparent structure in black-loaded styrene–butadiene rubber. The steaks appear to link carbon black particles beneath the rupture surface.

patterns (Fig. 11) normally expected from longitudinal tearing. For the same initial elongation it was noticed that black-loaded vulcanizates tore at lower transverse strains than gum compounds, and this might be expected to reduce the transverse crystallinity, and result in a fibrous surface highly oriented in the direction of primary elongation.

The reinforcing ability of carbon black is much greater in noncrystallizing polymers, permitting higher extensions to be used than had been possible with gum compounds. Strongly defined surface patterns, consisting of broad streaks tending to curve so as to cross the line of tear were observed in black-reinforced styrene–butadiene rubber (Fig. 12) and were unlike anything observed in the unreinforced compound. Where these streaks merge into the bulk of the surface, small projections sometimes indicate the presence of carbon black particles below the surface, and the streaks may well be composed of rubber molecules linking together groups of filler particles. Although this structure was of a coarse, blurred nature when compared with the sharply defined fibers in crystalline polymers, it must be remembered that (to avoid confusion in the replicas) only a low loading of a coarse (and therefore poorly reinforcing) filler was used. The structure imparted by the higher loadings of fine black used in most practical rubber compounds may well be much more pronounced, but further work over a range of sizes and loading is required to confirm this view. It is hoped that the longitudinal tearing technique may be of use in the study of all types of strengthening structure in rubber compounds.

The author wishes to thank the Dunlop Rubber Co., Ltd., for permission to publish this work, Mr. C. H. Leigh-Dugmore for much help and advice, and Miss Y. C. Whitfield for the considerable experimental work involved.

References

1. Kellar, A., and J. S. R. Waring, *J. Polymer Sci.*, **17**, 447 (1958).
2. Campbell, H. N., and M. D. Allen, *Rubber Chem. Technol.*, **24**, 550 (1951).
3. Bunn, C. W., *Proc. Roy. Soc. (London)*, **A180**, 40 (1942).
4. Treloar, L. R. G., *Physics of Rubber Elasticity*, Clarendon Press, 1949, (a) p. 17; (b) *ibid.*, p. 172.
5. Andrews, E. H., and A. Walsh, *Nature*, **179**, 729 (1957).
6. Chasset, R., and P. Thirion, *Proc. Intern. Rubber Conf. Washington*, **1959**, p. 349.
7. Walters, M. H., and Y. C. Whitfield, unpublished work.
8. Barrie, J. A., and B. Platt, *J. Polymer Sci.*, **54**, 261 (1961).
9. Bunn, C. W., and T. C. Adcock, *Trans. Faraday Soc.*, **41**, 317 (1949).
10. Naunton W. J. S., Ed., *The Applied Science of Rubber*, Edward Arnold, 1961, p. 414.

Résumé

La cristallinité, induite par tension, produit dans les élastomères une structure renforcée. Quand on déchire le caoutchouc suivant l'axe de l'extension, cette structure envisible à la surface de rupture. On a étudié au microscope électronique la morphologie de la cristallinité par tension, en gardant l'extension initiale. On a pris des copies de cette surface de rupture. On a trouvé que les cristallites sont des fibres fort compactes, de section ronde, et orientées suivant l'axe de l'extension. Le diamètre des fibres était généralement entre 100 et 1000 Å. Il était possible de tracer les cristallites individuels sur une longueur de plusieurs microns, avant qu'ils ne disparaissent en dessous de la surface exposée. Les polymères non-cristallisables ne possèdent pas de structure à la surface de rupture. L'addition de charge sous forme de particules fines a peu d'effet sur la structure observée dans les polymères cristallisables. On a observé des traces de structure dans les polymères amorphes, apparemment formées d'amas de particules de noir animal, liées par les molécules de caoutchouc.

Zusammenfassung

Die spannungsinduzierte Kristallinität in Elastomeren liefert eine Verfestigungsstruktur und ein Reissen des Kautschuks entlang der Dehnungsachse macht diese Struktur in der Bruchfläche erkennbar. An Abdrücken dieser Rissfläche bei aufrechterhaltener Anfangesdehnung wurde die Morphologie der Spannungskristallinität im Elektronenmikroskop untersucht. Die Kristallite erweisen sich als dicht gepackte Fasern mit abgerundetem Querschnitt und Orientierung in der Dehnungsrichtung. Die Fasern hatten gewöhnlich einen Durchmesser von 100 bis 1000 Å und die einzelnen Kristallite konnten über Distanzen bis zu einigen Mikron verfolgt werden, bevor sie unter der exponierten Oberfläche verschwanden. Nicht kristallisierende Polymere zeigten in der Bruchfläche keine Struktur. Der Zusatz von feinteiligen Füllstoffen hatte auf die bei kristallisierenden Polymeren beobachteten Strukturen wenig Einfluss. Bei amorphen Polymeren wurden Spuren einer Struktur beobachtet, die offenbar aus Gruppen von Russteilchen mit einer Verknüpfung durch Kautschukmoleküle bestanden.

Received July 30, 1962

JOURNAL OF POLYMER SCIENCE: PART A VOL. 1, PP. 3105–3134 (1963)

The Diffusion of Chrysophenine G into Viscose Sheet*

J. O. WARWICKER, *The Shirley Institute, Manchester, England*

Synopsis

An experimental investigation into the diffusion of a direct dye into the edges of a viscose sheet is described. The results of these experiments are used to test the diffusion-adsorption theory of Standing, Warwicker, and Willis. It is shown how this theory can be extended to allow for the effect of sodium chloride concentration on the diffusion coefficients.

INTRODUCTION

The process of dyeing cellulose with direct dyes involves the diffusion of the dye from an aqueous dye bath into water-swollen cellulose. Early theories[1,2] assumed this process to be governed by Fick's law, but now it is generally recognized[3–8] that the simple diffusion equation has to be modified to take account of adsorption and electrical factors known to affect the process. Several modified diffusion equations[3–8] have been given, but unfortunately there does not exist an extensive set of diffusion data by which to test them adequately. In this paper an attempt is made to fill the gap in the published data on diffusion of direct dyes into cellulose and to apply the results to one of the published theories, viz., that of Standing et al.[5]

The experimental method used consisted in making measurements of the rate of diffusion of Chrysophenine G from aqueous solution into the edge of a "never-dry" viscose sheet held in a special clamp. This is a nonsteady-state method and the time of diffusion was chosen so that the diffusion took place effectively in a semi-infinite medium. After the dyeing process the spatial distribution of dye concentration in the plane of the sheet was determined with a spectrophotometer, and the distribution curves so obtained were mathematically analyzed.

EXPERIMENTAL

The Apparatus

All the parts of the apparatus were made from stainless steel specially selected to withstand high concentrations of electrolytes. The individual components are shown in Figure 1. Essentially, there are two units, one

* Part of the contents of this paper was presented to the University of London as a Ph.D. Thesis (1947).

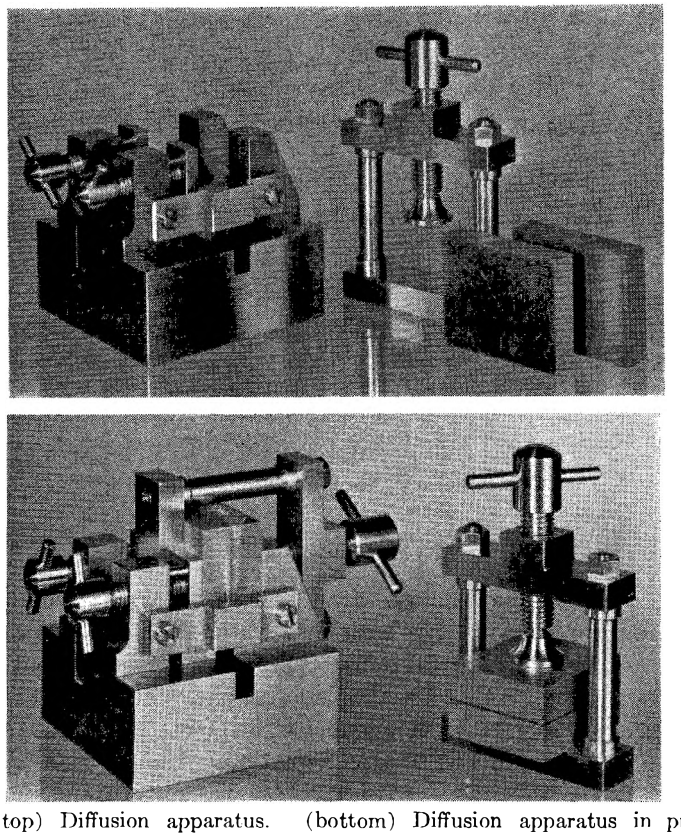

Fig. 1. (top) Diffusion apparatus. (bottom) Diffusion apparatus in process of assembly.

consisting of a frame and two blocks with ground surfaces and the other a special jig for aligning the blocks on top of one another.

The frame was first slid into the jig. Three pieces of never-dry viscose sheet oriented with the spinning direction along the long edge of the blocks were sandwiched between the two blocks and this assembly was then slid into the frame and held in exact location on the horizontal and vertical flats of the locating jig by two screw grips (Fig. 1). The screw of the frame was tightened, and the assembled unit could then be removed from the jig. The viscose sheet was trimmed flush with the edges of the blocks with a sharp razor blade, and the unit was kept in distilled water until required.

The Dye Bath

One liter of dye solution having the required concentrations of dye and electrolyte was contained in a round-bottomed flask almost completely immersed in a thermostat. The flask was closed by a ground-glass stopper fitted with a stirrer sealed by mercury and a ground-glass tap.

When the dye bath was at the required temperature (90°C.) the stopper of the flask was opened, the prepared unit lowered into the dye solution,

and the stopper replaced; almost immediately the glass tap was closed and the stirring commenced. Since the flask was almost completely immersed in the thermostat very little moisture condensed on the stopper and the use of a condenser was not found necessary.

At a prearranged time the unit was removed and rapidly cooled. The sheets were then removed and placed immediately in a saturated aqueous solution of quinine sulfate which fixed the dye and allowed measurements to be taken at some subsequent convenient time.

Measurement on the Sheets

The measurements of dye concentration in the sheets were made with a spectrophotometer specially fitted with microscope objectives and slits to provide a beam of light $^1/_8$ mm. wide.

The wet sheets were mounted between two glass plates and placed on a special carriage of the spectrophotometer. After aligning the appropriate edge of the sheet parallel to the slit the wavelength was set at $\lambda = 4200$ A. and measurements were made at $^1/_{32}$ mm. intervals until the beam was located on the edge of the sheet. Nine readings $^1/_{16}$ mm. apart were then made and were followed by readings at $^1/_8$ mm. until the undyed cellulose was reached, when several blank readings were recorded.

The optical density at any given point x is given by $\log y_0/y_x$, where y_0 is the mean transmission of the undyed cellulose and y_x is the transmission at the point x.

A calibration curve was obtained with the same optical system on uniformly dyed sheets containing known amounts of dye fixed with quinine sulfate, and this showed that optical density was directly proportional to dye concentration within the sheet. It was therefore convenient to plot the distribution curve in terms of optical density versus distance and introduce the calibration constant only where appropriate. In constructing the distribution curves the measured optical density is taken as the mean value over the area covered by the beam and therefore located on the graph at the position of the center of the beam.

In every experiment two films were each measured on all four edges; this provided quadruplicate distribution curves for diffusion along and across the spinning direction of the sheet.

Accuracy of Distribution Curves

Before analyzing the distribution curves it was necessary to check whether they truly represented the diffusion process under investigation.

Test of Optical System

The optical system can introduce errors if stray light is included in the transmitted beam, or if the light is dispersed at the edge of a sheet where a high density is in juxtaposition with a low density. Measurements were made with a linear carbon wedge that gave a straight-line plot for optical

density versus distance. Photographs of this wedge, although not linear in optical density, proved that the same distribution of density was given from a predetermined place before and after cutting of the film and measuring across the cut edge. A similar experiment with a sheet from an edgewise-diffusion experiment also showed that the same distribution curve was given from a predetermined place before and after cutting of the sheet at this place. It was thus concluded that, except for the first two readings, which can be allowed for, the cut edge of the sheet did not introduce errors into the measured distribution curve.

Fortunately, the dyed sheets soaked in saturated aqueous quinine sulfate do not show dichroism (i.e., a change of absorption with the direction of polarization), and the slight polarization of the light introduced by the optics of the instrument did not affect the results obtained in different directions.

Tests of Experimental Procedure

Errors can arise in the experimental procedure if unmodified diffusion takes place in the aqueous channels between the blocks and the sheets or between the sheets themselves. Distribution curves measured at different places along a given edge agreed with each other within the experimental error, so that any inaccuracy of the type discussed must be uniform along the edges. An experiment was carried out in which the sheets were left projecting on one edge of the blocks while on the other edges they were cut flush as usual. At the end of this experiment half the length of the projecting sheets was cut flush before demounting. Measurements were made across the normal edges, the projection, and also across the part of the edge that was cut flush at the end of the experiment. In all cases the distribution curve of the dye in the film within the block was the same within the experimental error. There was no evidence of the equilibrium absorption given by the projection piece, continued for any distance into the part of the film within the blocks.

Furthermore, although the type of distribution curve given along the spinning direction of the sheet is the same as that across it, there is a measurable difference in rate of penetration between these directions of diffusion that depends on the structure of the cellulose sheet. It would therefore seem that the measured distribution curves are representative of the diffusion process and not overlaid by unmodified diffusion.

One difficulty, however, does remain. When the screws of the frame are tightened the pressure exerted on the sheets extrudes them slightly, causing the sheets within the blocks to be slightly thinner than the uncompressed sheets. If nonuniform recovery takes place when the pressure is released, then the distribution curves will not be representative of the actual diffusion process. It is difficult to prove conclusively that the pressure effects are uniform and that a true distribution curve is thereby obtained, but all the experimental evidence seems to justify such a conclusion. However, owing to the orientation of the molecular chains in the sheets the effects of

pressure might be expected to be different in the directions across and in those parallel to the chains. Except for a difference in penetration, which may be expected on consideration of the structure, no difference in shape of the distribution curves is found for the two directions of diffusion. Furthermore, repeat experiments under the same experimental conditions agreed within the experimental error, and all experiments for different times of dyeing gave consistent results amongst themselves. Again, the shape of the distribution curves altered in accordance with dye bath conditions in a consistent manner. All these facts suggest that consistency in the experimental data would not have been obtained if any appreciable non-uniformity had been present.

Errors Arising from Diffusion Process

In the experiments described, dye and salt diffuse together, but calculation shows that, owing to the rapidity of the diffusion of the salt and the relatively slow diffusion of the dye, the sodium chloride concentration is substantially at equilibrium across the sheet during the main diffusion of the dye (minimum time studied, 24 hr.). As a first approximation, therefore, the dye can be taken to be diffusing in the presence of a uniform concentration of sodium chloride. Prior soaking of the sheets in sodium chloride solution gave no measurable difference in the subsequent distribution curves. A similar argument also applies to the back-diffusion of hydrogen ions liberated from the carboxyl groups in the cellulose.

It was thus concluded that the edgewise diffusion experiments are consistent amongst themselves and typical of the process being studied, but may not be directly comparable to experiments done under other experimental conditions.

Typical distribution curves are shown in Figure 2.

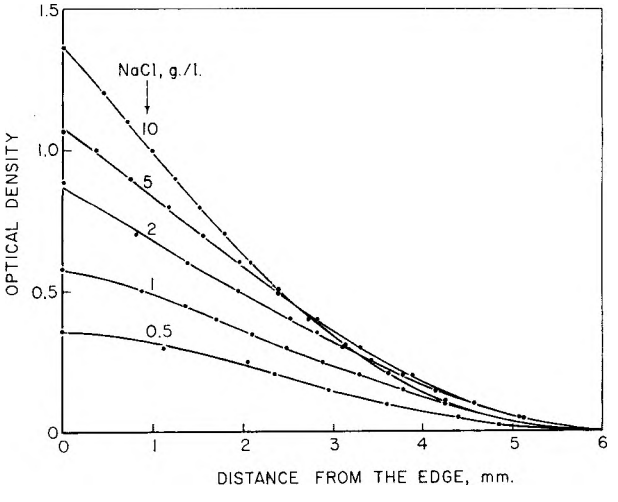

Fig. 2. Typical distribution curves: Chrysophenine G, 0.1 g./l.; time, 48 hr.

CALCULATIONS AND RESULTS

The Differential Diffusion Coefficients

It is required to find the variation of the differential diffusion coefficient with the dye concentration within the cellulose from the measured distribution curves. The differential diffusion coefficient is defined by the equation

$$D_c = [(dS/dt)/(dC/dx)]_c \tag{1}$$

where dS/dt is the flux of dye across the plane at which the concentration is C, dC/dx is the concentration gradient across this plane, and s is the total amount of dye that has crossed a unit area of a given plane perpendicular to the x axis.

Several values of the differential diffusion coefficients are possible under the definition of the concentration. Unless otherwise stated, the one calculated refers to the total concentration of dye at the given point and is therefore the total differential diffusion coefficient.

Two methods are available for this calculation, that of Garvie and Neale[3] and one based on the method of Boltzmann.[9,10] The first method depends on finding dS/dt for each concentration from a curve of s versus t derived from the distribution curves for any given set of experimental conditions, and also on the measurement of dC/dx on the original distribution curves for the given concentration. Although the method does not involve any assumptions, it is very laborious and subject to large errors.

The second method, based on that of Boltzmann,[9,10] assumes that the distance penetrated by a given concentration of dye is proportional to the square root of the time of diffusion. This assumption has been found valid for all the experiments recorded here, and so the Boltzmann method can be applied to these results. The method has the advantage that a complete analysis can be applied to each distribution curve without reference to derived curves, and hence several values of D_c for a given concentration can be derived from the distribution curves for different times of diffusion under given experimental conditions. Mean values of D_c for different concentrations can thus be derived, and the variation of D_c versus C for the given conditions can be obtained.

As a check, some of the data were analyzed by both methods, and the mean D_c versus C curve derived from the Boltzmann analysis was shown to lie within the scatter of points of D_c versus C produced by the method of Garvie and Neale. The two methods are substantially in agreement, but the Boltzmann method gives results that are more accurate and more readily compared and it was therefore used throughout this work.

In the Boltzmann method[9,10] the diffusion equation, in which the diffusion coefficient varies with the concentration, can be written

$$\partial C/\partial t = (\partial/\partial x)[D_c(\partial C/\partial x)] \tag{2}$$

The boundary conditions for the edgewise-diffusion experiments are $C = 0$ where $x > 0$ for $t = 0$, and $C = E$ where $x = 0$ for all t.

If the distance of penetration x of any concentration is proportional to the square root of the time of diffusion t it can be shown that for the given boundary conditions

$$D_c = -(1/2t)(dx/dC)\int_0^C x dC \tag{3}$$

In these experiments all the distribution curves were given in terms of the optical density Δ, which was shown to be directly proportional to the concentration. The equation then becomes

$$D_c = -(1/2t)(dx/d\Delta)\int_0^\Delta x d\Delta \tag{4}$$

Since the distribution curves are in fact $\Delta = f(x)$ for a given time t, simple graphical analysis enabled the values of D_c for different values of Δ (and hence C) to be obtained. In the experiments four distribution curves for each direction of diffusion for a given time of diffusion were available, so that a mean of four values of D_c for a given value of Δ could be obtained for each direction of diffusion. Finally, since the same variation of D_c with Δ should be given for the different times of diffusion under the given experimental conditions, the mean D_c for all the experiments could be plotted against Δ. The results of this analysis are given in Tables I–VI, and a plot of the variation of D_c with optical density for a given dye concentration but with different sodium chloride concentrations (for one given

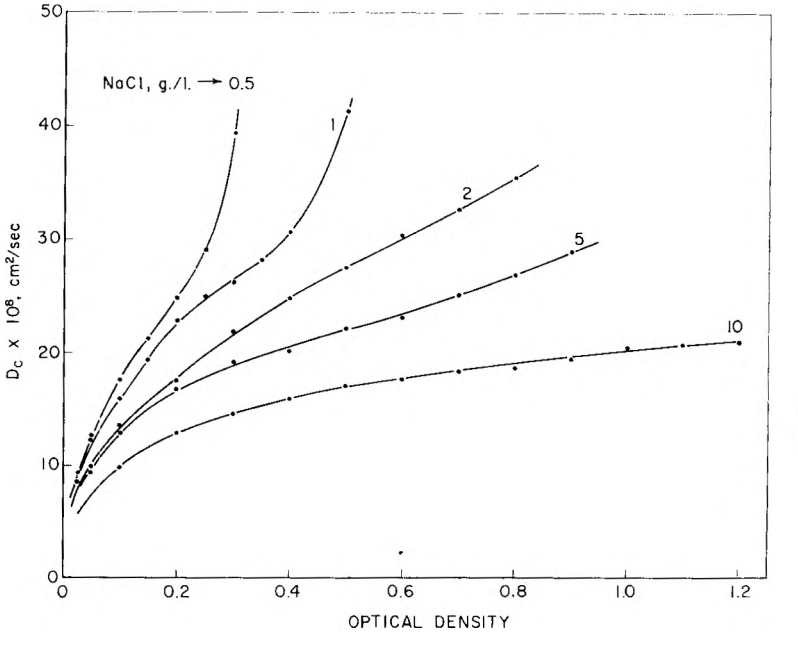

Fig. 3. Differential diffusion coefficient vs. optical density at various NaCl concentrations (diffusion perpendicular to spinning direction): Chrysophenine G, 0.1 g /1.

TABLE I

Edgewise Diffusion of Chrysophenine G into Viscose Sheet: Diffusion Perpendicular to Spinning Direction of Sheet (at 90°C.)

	Diffusion coefficient × 10^8, cm.²/sec.																			
	Dye bath concn. 0.1 g./l., NaCl concn. 0.5 g./l., at:							Dye bath concn. 0.1 g./l., NaCl concn. 1.0 g./l., at:							Dye bath concn. 0.1 g./l., NaCl concn. 2.0 g./l., at:			
Opt. dens.	24 hr.		48 hr.		72 hr.		Mean	24 hr.		48 hr.		72 hr.	Mean		24 hr.	48 hr.	72 hr.	Mean
0.025	7.8	10.4	10.6	10.6	8.1	9.1	9.4	8.1	—	8.0	10.5	8.6	8.8		—	—	—	—
0.05	10.8	13.2	13.6	13.7	12.5	11.3	12.5	11.0	14.6	11.0	12.5	12.5	12.3		10.4	9.4	9.7	9.8
0.1	15.8	19.3	19.2	16.5	18.0	17.3	17.7	14.7	17.6	14.2	15.9	16.5	15.8		14.3	13.1	13.5	13.6
0.15	20.1	21.3	23.2	19.4	22.1	22.0	21.3	17.5	20.7	18.2	20.6	19.6	19.3		—	—	—	—
0.2	23.2	24.7	26.1	24.2	26.3	24.3	24.8	20.6	24.2	22.2	23.7	23.4	22.8		18.4	16.5	17.5	17.5
0.25	27.2	28.9	31.2	27.2	29.4	30.2	29.0	22.7	25.4	24.4	26.3	26.1	25.0		—	—	—	—
0.3	44.0	42.4	38.1	33.2	39.9	39.6	39.5	24.2	26.8	25.8	26.2	27.7	26.2		22.7	22.0	20.9	21.9
0.35								27.1	27.6	28.5	27.9	29.6	28.2		—	—	—	—
0.4								27.8	31.0	30.5	30.7	33.0	30.6		25.1	25.4	23.9	24.8
0.45								30.2	34.4	36.5	35.2	38.6	35.0		—	—	—	—
0.5								35.9	43.1	42 0	42.2	43.5	41.3		27.5	29.3	25.8	27.5
0.6															31.2	31.3	28.4	30.3
0.7															33.9	33.1	31.2	32.7
0.8															38.3	33.8	34.4	35.5

TABLE II

Edgewise Diffusion of Chrysophenine G into Viscose Sheet: Diffusion Perpendicular to Spinning Direction of Sheet (at 90°C.)

	Diffusion coefficient × 10^8, cm.²/sec.													
	Dye bath concn. 0.05 g./l., NaCl concn. 5.0 g./l., at:				Dye bath concn. 0.1 g./l., NaCl concn. 5.0 g./l., at:					Dye bath concn. 0.3 g./l., NaCl concn. 5.0 g./l., at:				
Opt. dens.	17 hr.	42 hr.		Mean	24 hr.	40 hr.	48 hr.	64 hr.	Mean	17 hr.	18 hr.	42 hr.	48 hr.	Mean
0.025	8.1													
0.05	11.1	9.9	8.9	9.9	8.7	10.3	10.5	8.8	9.6					
0.1	13.3	13.7	12.9	13.3	13.2	13.3	12.8	12.2	12.9	11.8	12.1	12.6	12.4	12.2
0.15														
0.2	17.3	17.1	17.1	17.2	16.5	17.3	16.8	16.5	16.8	15.3	14.3	16.3	15.0	15.2
0.25														
0.3	19.9	18.9	18.5	19.1	19.0	19.9	19.2	18.6	19.2					
0.35														
0.4	21.8	18.4	20.3	20.2	20.0	21.5	20.8	20.0	20.1	18.1	18.8	20.6	20.8	19.6
0.45														
0.5	24.2	17.6	22.7	21.5	21.3	23.1	21.9	22.1	22.1					
0.6	27.7	18.2	23.9	23.3	21.3	23.7	24.0	23.8	23.2	20.0	21.2	23.6	22.9	21.9
0.7					23.8	25.2	26.1	25.8	25.2					
0.8					25.6	27.4	27.6	27.2	26.9	22.2	25.4	28.0	26.2	24.1
0.9					27.5	30.7	28.8	28.1	28.8					
1.0					31.2		29.3			24.4	25.4	28.0	26.2	26.0
1.1														
1.2										26.3	27.7	30.7	28.7	28.3
1.4										28.6	29.8	33.2	30.9	30.6
1.6										30.8	31.7	35.1	32.0	32.4
1.8										32.2	32.7	36.5	40.2	35.4
2.0										34.8	33.3	37.3		

TABLE III

Edgewise Diffusion of Chrysophenine G into Viscose Sheet: Diffusion Perpendicular to Spinning Direction of Sheet (at 90°C.)

	Diffusion coefficient × 10^8, cm.²/sec.												
	Dye bath concn. 0.025 g./l., NaCl concn. 10.0 g./l., at:			Dye bath concn. 0.05 g./l., NaCl concn. 10.0 g./l., at:			Dye bath concn. 0.1 g./l., NaCl concn. 10.0 g./l., at:				Dye bath concn. 0.15 g./l., NaCl concn. 10.0 g./l., at:		
Opt. dens.	24 hr.	48 hr.	Mean	20 hr.	42 hr.	Mean	24 hr.	48 hr.	72 hr.	Mean	24 hr.	48 hr.	Mean
0.025	6.9	6.4	6.7										
0.05	8.9	8.9	8.9	8.3	8.9	8.6							
0.1	12.2	12.1	12.1	10.5	11.1	10.8	9.5	9.8	10.1	9.8	9.7	11.0	10.3
0.15	13.2	14.1	13.6										
0.2	13.5	15.3	14.4	13.5	13.7	13.6	12.0	12.7	13.9	12.9	13.3	13.4	13.3
0.25	14.6	15.8	15.2										
0.3	15.9	16.0	16.0	15.0	15.3	15.2	13.8	14.0	15.9	14.6			
0.35	16.8	16.6	16.7										
0.4	17.4	17.2	17.3	15.6	16.9	16.3	15.0	15.4	17.2	15.9	15.4	16.7	16.0
0.5				17.2	17.2	17.2	16.1	16.3	18.9	17.1			
0.6				18.8	16.6	17.7	16.5	17.0	19.3	17.6	16.6	18.3	17.5
0.7							17.2	17.5	20.1	18.3			
0.8							17.6	18.3	20.3	18.7	18.2	20.5	19.3
0.9							18.7	19.0	20.8	19.5			
1.0							19.6	19.8	21.2	20.5	19.3	21.6	20.4
1.1							20.2	20.5	21.1	20.6			
1.2							20.7	20.9	21.2	20.9	19.7	22.0	20.9
1.4											20.0	21.5	20.8

TABLE IV

Edgewise Diffusion of Chrysophenine G into Viscose Sheet: Diffusion Parallel to Spinning Direction of Sheet (at 90°C.)

	Diffusion coefficient × 10^8, cm.²/sec.																			
	Dye bath concn. 0.1 g./l., NaCl concn. 0.5 g./l., at:							Dye bath concn. 0.1 g./l., NaCl concn. 1.0 g./l., at:							Dye bath concn. 0.1 g./l., NaCl concn. 2.0 g./l., at:			
Opt. dens.	24 hr.		48 hr.		74 hr.		Mean	24 hr.		48 hr.		72 hr.		Mean	24 hr.	48 hr.	72 hr.	Mean
0.025	10.2	10.7	11.9	11.6	9.4	11.9	11.0	9.6	12.5	9.2	12.8	10.1	10.8		—	—	—	—
0.05	14.1	14.5	16.6	15.6	14.7	15.7	15.4	13.8	15.1	11.5	17.4	19.3	14.4		14.1	11.2	12.0	12.4
0.1	21.3	21.9	22.5	22.3	21.7	22.0	22.0	17.9	21.3	17.2	22.3	20.6	19.9		17.5	15.5	16.5	16.5
0.15	26.6	26.9	27.8	26.0	25.6	26.5	26.6	20.9	25.6	21.4	24.3	24.9	23.4		—	—	—	—
0.2	29.5	30.7	32.4	30.9	30.7	30.8	30.8	23.7	28.3	24.9	28.1	27.3	26.5		22.7	22.3	22.2	22.4
0.25	34.3	38.4	38.3	35.0	36.5	37.6	36.7	27.3	29.0	28.9	31.0	30.3	29.3		—	—	—	—
0.3	48.7	59.9	49.4	48.0	49.2	51.3	51.0	28.0	31.6	31.1	32.9	32.3	31.2		26.8	26.6	26.2	26.5
0.35								28.5	35.5	33.3	35.1	36.4	33.9		—	—	—	—
0.4								33.7	38.6	37.3	39.1	42.0	38.2		29.6	30.4	29.0	29.7
0.45								38.6	45.8	42.4	44.1	48.6	43.9		—	—	—	—
0.5								45.4	57.8	50.3	55.6	53.7	52.6		31.3	33.1	32.2	32.2
0.6															36.5	38.0	35.6	36.7
0.7															42.6	41.6	38.8	41.0
0.8															52.5	43.9	41.2	45.9
0.9																		

TABLE V

Edgewise Diffusion of Chrysophenine G into Viscose Sheet: Diffusion Parallel to Spinning Direction of Sheet (at 90°C.)

Opt. dens.	Diffusion coefficient × 10^8, cm.²/sec.													
	Dye bath concn. 0.05 g./l., NaCl concn. 5.0 g./l., at:				Dye bath concn. 0.1 g./l., NaCl concn. 5.0 g./l., at:					Dye bath concn. 0.3 g./l., NaCl concn. 5.0 g./l., at:				
	17 hr.	42 hr.		Mean	24 hr.	40 hr.	48 hr.	64 hr.	Mean	17 hr.	18 hr.	42 hr.	48 hr.	Mean
0.05	12.3	11.5	10.7	11.5	11.1	10.7	11.5	12.2	11.4					
0.1	15.7	15.5	14.7	15.3	15.2	13.4	15.8	15.2	14.9	13.6	13.7	13.8	13.6	13.7
0.2	19.7	18.8	18.3	18.9	19.1	20.0	19.9	19.8	19.7	18.1	16.5	18.4	16.9	17.5
0.3	23.2	20.5	21.4	21.7	22.1	22.7	22.5	22.5	22.4					
0.4	24.7	21.9	23.7	23.4	23.9	25.8	23.8	25.4	24.7	21.8	21.1	22.7	22.5	22.0
0.5	28.9	20.3	26.3	25.2	25.9	27.1	25.8	28.1	26.7					
0.6	35.2	38.5	29.9	34.5	27.4	27.6	28.3	27.5	27.7	24.1	24.8	25.8	26.3	25.2
0.7					28.7	29.7	31.1	30.7	30.0					
0.8					31.1	33.7	33.5	33.2	32.9	25.7	26.0	28.8	28.1	27.1
0.9					33.7	38.7	35.3	35.9	35.9					
1.0					36.9	42.6	36.5	37.6	38.4	28.7	28.9	31.1	31.1	29.9
1.2										31.6	31.9	33.9	33.4	32.7
1.4										34.7	33.7	37.6	33.9	35.2
1.6										37.1	36.4	39.1	37.4	37.5
1.8										38.8	37.6	40.6	50.0	41.7
2.0										41.1	38.2	41.5		

TABLE VI

Edgewise Diffusion of Chrysophenine G into Viscose Sheet: Diffusion Parallel to Spinning Direction of Sheet (at 90°C.)

Opt. dens.	Diffusion coefficient × 10^8, cm.²/sec.												
	0.025 and 10.0 g./l.,[a] at:			0.05 and 10.0 g./l.,[a] at:			0.1 and 10.0 g./l.,[a] at:				0.15 and 10.0 g./l.,[a] at:		
	24 hr.	48 hr.	Mean	20 hr.	42 hr.	Mean	24 hr.	48 hr.	72 hr.	Mean	24 hr.	48 hr.	Mean
0.025	6.9	6.4	6.7										
0.05	8.9	8.9	8.9	9.2	8.6	8.9							
0.1	12.1	12.1	12.1	12.3	11.5	11.9	10.9	10.7	10.9	10.8	11.1	12.2	11.6
0.15	13.2	14.1	13.6										
0.2	13.5	15.3	14.4	14.9	14.3	14.6	14.0	14.0	15.2	14.4	14.7	15.3	15.0
0.25	14.6	15.8	15.2										
0.3	15.9	16.0	16.0	17.0	16.0	16.5	15.8	16.5	18.5	16.9			
0.35	16.8	16.6	16.7										
0.4	17.4	17.2	17.3	18.4	17.4	17.9	17.2	17.5	19.6	18.1	17.5	18.4	18.0
0.5				19.7	18.5	19.1	18.6	18.7	21.2	19.5			
0.6				22.4	18.8	20.6	19.7	19.4	21.3	20.1	19.8	20.7	20.2
0.7							20.4	20.0	22.3	20.9			
0.8							20.8	20.7	23.2	21.6	21.5	22.9	22.2
0.9							22.0	21.5	24.3	22.6			
1.0							23.1	22.4	24.9	23.5	23.0	25.3	24.1
1.1							24.2	23.1	25.6	24.3			
1.2							24.5	23.7	26.1	24.8	23.9	26.2	25.0
1.4											25.0	25.2	25.1

[a] Dye bath and sodium chloride concentrations, respectively.

direction of diffusion, i.e. perpendicular to the spinning direction of the sheet) is shown in Figure 3.

Validity of Fick's Law

Figure 2 shows some typical distribution curves, and from the fact that they are not convex to the x axis over all their length it can be inferred that the diffusion coefficient is not constant. This inference is confirmed by an inspection of the variation of the differential diffusion coefficient with optical density, the latter being proportional to the concentration of dye within the sheet (Fig. 3). At no salt concentration is a constant diffusion coefficient, as required by Fick's law, obtained.

Nevertheless, it is found that if the total mass of dye diffused into the sheet be plotted against the square root of the time, a straight line through the origin is obtained for each salt concentration, as would be predicted by Fick's law. Hence, for problems in which the interest lies in the total mass of dye diffused rather than in the distribution of the dye in the medium, an "effective value" for the diffusion coefficient can be assigned to each salt concentration, derived from the slope of the S versus $\sqrt{t}$ lines.

Thus for the given boundary conditions a solution of Fick's law is[11]:

$$S = 2E\sqrt{Dt/\pi} \tag{5}$$

where S is the total amount of dye diffused across unit cross section in time t into an infinite slab, from a boundary maintained at a constant concentration E. In the edgewise-diffusion experiments S can be derived from the area under the distribution curves and E is related to the optical density at the edge of the sheet. Diffusion coefficients derived in this way have been designated D_F to distinguish them from diffusion coefficients derived by other methods.

For comparison with these experiments, absorption-kinetic experiments were carried out in the way described by Neale and Stringfellow,[1] but instead of estimating the dye in the dyed sheet by extraction it was determined from the mean optical density of the sheets soaked in saturated aqueous quinine sulfate. Otherwise, the experimental details and the method of calculating the results were identical with Neale's and need not be described here. The apparent diffusion coefficient found by this method is written D_N, to distinguish it from the apparent diffusion coefficient D_F found from edgewise-diffusion experiments.

Since it has been suggested by Standing et al.[5] that the integral diffusion coefficient, defined as

$$\bar{D} = (1/E)\int_0^E D_c dC \tag{6}$$

where D_c is the differential diffusion coefficient, is equivalent to the apparent diffusion coefficient found by the method of Neale,[1] it was decided to include this diffusion coefficient in the comparison. The integral diffusion coefficients for each set of dye bath conditions can be readily obtained from

the area under the D_e versus optical density curves given by the edgewise-diffusion experiments.

Table VII shows a comparison of the diffusion coefficients discussed above, and a plot of some of them versus sodium chloride concentration is shown in Figure 4. Contrary to the results found by Neale et al.[13] for other dyes, only a slight, or no, maximum is found in the curve of D_N versus sodium chloride concentration. In the region over which D_N remains substantially constant, electrical forces and adsorption forces presumably counteract each other, but at high salt concentrations the adsorption forces take predominance.

TABLE VII
Comparison of Different Diffusion Coefficients (at 90°C.)

Dye bath concn., g./l.	NaCl concn., g./l.	Diffusion coefficient × 10^6, cm.²/sec.[a]				
		D_F (perp.)	D_F (para.)	$\bar{D}$ (perp.)	$\bar{D}$ (para.)	D_N
0.1	0.25					19.6
0.1	0.5	35.0	47.1	25.3	32.3	19.6
0.1	0.75					19.8
0.1	1.0	32.3	39.9	27.3	33.0	19.5
0.1	1.5					19.1
0.1	2.0	27.5	34.8	26.7	30.4	19.8
0.1	2.5					17.9
0.1	5.0	24.6	30.8	22.0	26.3	15.8
0.1	10.0	18.0	20.5	16.9	19.7	13.4
0.05	5.0	21.2	24.5	17.6	20.9	
0.3	5.0	30.8	35.2	26.3	30.2	
0.025	10.0	13.0	15.5	11.9	13.5	
0.05	10.0	16.1	19.0	15.5	16.6	
0.15	10.0	19.6	22.7	16.9	21.1	
0.25	0.25					23.0
0.25	0.5					23.6
0.25	1.0					23.3
0.25	1.5					23.6
0.25	2.0					22.0
0.25	2.5					20.4
0.25	5.0					16.3
0.25	10.0					12.5

[a] D_F = apparent diffusion coefficient based on eq. (5); $\bar{D}$ = integral diffusion coefficient; $\bar{D}_N$ = values derived from experiments based on the method of Neale and Stringfellow.[1]

In Figure 4 comparison is also made with corresponding curves for $\bar{D}$ and D_F. It is not certain whether the curve for $\bar{D}$ has a slight maximum or not, but its general tendency is certainly similar to that of D_N, an identity of absolute values of D not being expected since two different directions of diffusion are involved. The curve for D_F, on the other hand, shows a steady decrease of D with increasing salt concentration.

It therefore seems evident that the integral diffusion coefficient is not identical with D_N, so that tests of the diffusion-adsorption theory relying on this identity must be treated with caution.

The fact that a diffusion coefficient based on Fick's law can be worked out for these results shows that the total mass of dye diffusing into the sheet is the same as that predicted by Fick's law by the use of the appropriate diffusion coefficient. However, since the detailed analysis shows that Fick's law is not valid, the distribution of dye within the sheet must be different from that predicted by Fick's law, as indeed is shown by the distribution curves.

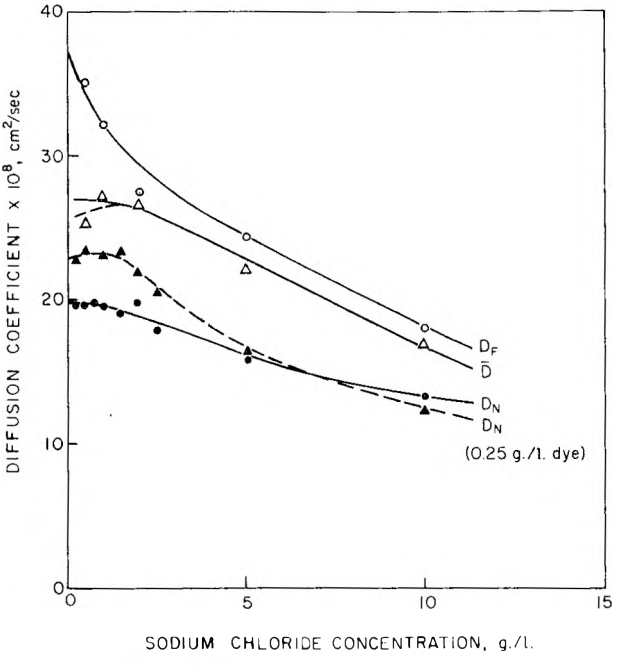

Fig. 4. Chrysophenine G, 0.1 g./l. Variation of diffusion coefficients with sodium chloride concentration: D_F and $\bar{D}$ are given for diffusion perpendicular to the spinning direction of the sheet; D_N refers to diffusion normal to the plane of the sheet.

A confirmation of the invalidity of Fick's law is provided by the increase in D_F and $\bar{D}$ with increasing dye bath concentration (Fig. 5), although at the salt concentrations used D_N does not appear to vary greatly in the range of dye concentrations studied (Fig. 4). It can be concluded that, although the application of Fick's law to the dye process can lead to a parameter that may be useful from an experimental standpoint, its real theoretical significance and value are still obscure. Further discussion will therefore be confined to a study of the differential diffusion coefficient, which can be precisely defined and experimentally measured.

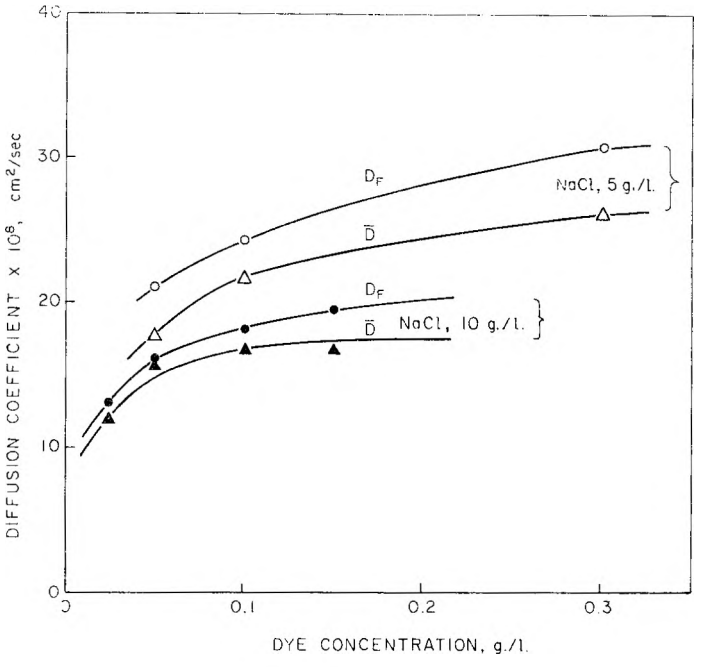

Fig. 5. Illustrating increase in D_F and $\bar{D}$ with increasing dye bath concentration; diffusion perpendicular to spinning direction.

TESTING OF THE DIFFUSION-ADSORPTION THEORY

In the theory of Standing et al.[5] it was shown that the differential diffusion coefficient D_c was given as

$$D_c = \alpha(D_0 - D_a)(dP/dC) + D_a \tag{7}$$

where D_0 is the aqueous diffusion coefficient of the dye in the pores of the cellulose, D_a the diffusion coefficients of the dye diffusing in the adsorbed state without intermediate solution, P the dye concentration in the pore where the total concentration is C, and α the ratio of the pore volume of the total volume of cellulose.

If it is assumed that the relation between P and C is given by the corresponding absorption isotherm with the equation $C = kC_0^m$ where $C_0 = P$, then the equation can be rewritten:

$$D_c = \alpha(D_0 - D_a)(C_0/mC) + D_a \tag{8}$$

If $n = 1/m$ this equation can be rewritten[5]:

$$D_c = \alpha(D_0 - D_a)(n/k^n)C^{n-1} + D_a \tag{9}$$

If now

$$B = \alpha(D_0 - D_a)(n/K^n)$$

Then

$$D_e - D_a = BC^{n-1} \tag{10}$$

Another form[5] of the diffusion-adsorption equation, in terms of the integral diffusion coefficient defined in eq. (6), can be derived:

$$\bar{D} = \alpha(D_0 - D_a)\,(C_0/E) + D_a \tag{11}$$

where E is the equilibrium absorption for a particular dye bath condition and C_0 is the concentration of dye in the bath.

The result of the application of eq. (11) to the edgewise-diffusion data is given in Table VIII. In this table E is the equilibrium boundary concentration in the edge of the sheet appropriate to the given experimental conditions. It will be seen that the value of $\bar{D}E/C_0$ increases with increasing sodium chloride concentration up to 2 g./l. but thereafter, within the experimental error, attains a constant value. This observation is consistent with the view that up to a sodium chloride concentration of 2 g./l. electrical effects are being eliminated, and with the view that the value of D_a must be negligibly small or zero. It is therefore reasonable to assume that D_a is zero and to work out a value for α, the fractional pore volume.

TABLE VIII

Test of the Diffusion-Adsorption Theory: Use of the Integral Diffusion Coefficient $\bar{D}$

Dye bath concn. C_0, g./l.	NaCl concn., g./l.	$\bar{D} \times 10^6$, cm.²/sec.		E, mg./g.		$\bar{D}E/C_0 \times 10^{6}$ [a]		α	
		Perp.	Para.	Perp.	Para.	Perp.	Para.	Perp.	Para.
0.1	0.5	25.3	32.3	1.71	1.72	433	556	0.095	0.122
0.1	1.0	27.3	33.0	2.77	2.74	756	904	0.166	0.199
0.1	2.0	26.7	30.4	4.23	4.17	1129	1268	0.248	0.279
0.05	5.0	17.6	20.9	3.05	2.97	1074	1241	0.236	0.273
0.1	5.0	22.0	26.3	5.11	5.15	1124	1354	0.247	0.298
0.3	5.0	26.3	30.2	10.32	10.27	905	1034	0.199	0.227
0.025	10.0	11.9	13.5	2.16	2.14	1028	1156	0.226	0.254
0.05	10.0	15.5	16.6	3.84	3.80	1190	1262	0.262	0.278
0.1	10.0	16.9	19.7	6.53	6.55	1104	1290	0.243	0.283
0.15	10.0	16.9	21.1	8.11	8.26	914	1162	0.201	0.256

[a] $\bar{D}E/C_0 = \alpha D_0/\rho$ where $D_0 = 1 \times 10^{-5}$ cm.²/sec. and $\rho = 0.22$ g./ml. of wet cellulose.

In computing the value for α it must be noted that the concentration E is given in milligrams per gram of dry cellulose and, in consequence, the factor ρ, the number of grams of dry cellulose per milliliter of wet cellulose, has to be introduced to obtain α in terms of volume. Thus:

$$\bar{D}E/C_0 = \alpha\,(D_0/\rho) \tag{12}$$

where D_0 is the aqueous diffusion coefficient, taken here to be independent of sodium chloride concentration and equal to 1×10^{-5} cm.²/sec.[14]

Values of α can be computed from eq. (12), and these values are included in Table VIII. It will be seen that, for a given dye bath concentration, α increases with increasing salt concentration up to a salt concentration of about 2 g./l. and thereafter decreases slightly (Fig. 6). For sodium chloride concentrations great enough to overcome the electrical effects, α increases with dye bath concentration, reaches a maximum, and then decreases (Fig. 7).

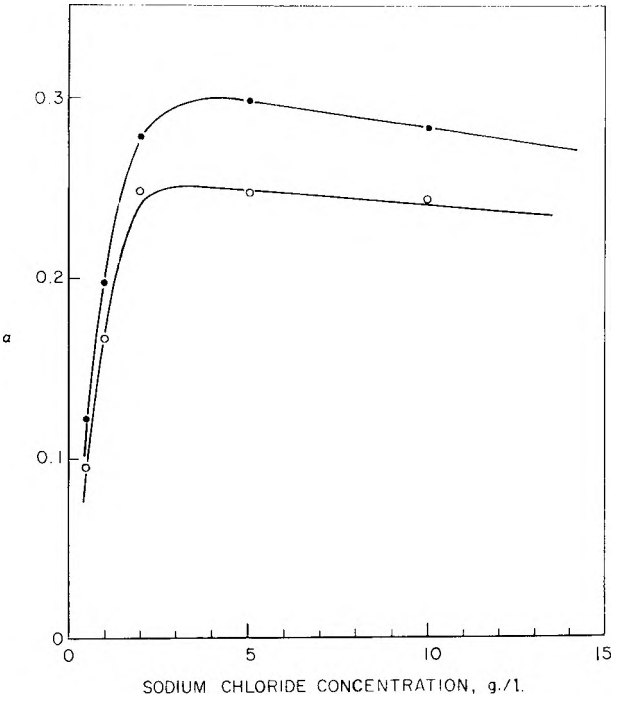

Fig. 6. Fractional pore volume α vs. salt concentration, Chrysophenine G: (●) diffusion parallel to spinning direction; (○) diffusion perpendicular to spinning direction.

On the basis of the assumptions of the diffusion-adsorption theory, α is the ratio of the volume free for diffusion to the total volume, and so the volume free for diffusion should vary with salt and dye concentration in the manner described if the diffusion-adsorption theory is to account fully for the variation of $\bar{D}$ with these variables. One method of testing this concept is to relate α to that volume of water within the cellulose that is uninfluenced by the electrical double layer due to the cellulose and adsorbed dye. This volume varies with salt and dye concentration, tending to increase as the width of the double layer decreases. On the other hand, a build-up of adsorbed dye will decrease the value of α, thus counteracting some of the effect of salt concentration on the double layer.

A modification of the diffusion-adsorption theory, taking account of these variations of available volume, is discussed in a later section.

Equation (12) is similar to Crank's equation,[6] viz.:

$$D = D_0 f\omega(C_B/S) \tag{13}$$

where D is the apparent diffusion coefficient, D_0 the true unimpeded diffusion coefficient within cellulose, C_B the concentration of the dye bath, S the corresponding equilibrium absorption of dye given in grams per 100 g. of cellulose, and w the number of liters of water per 100 g. of cellulose.

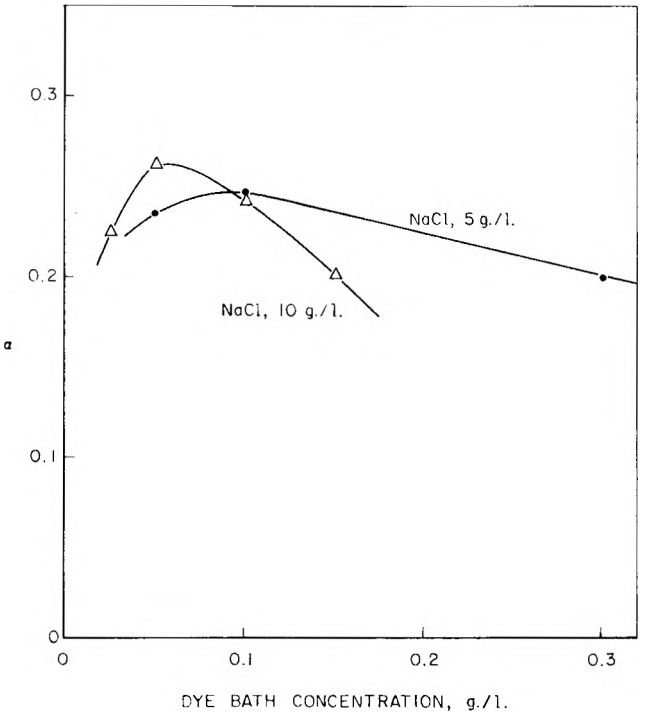

Fig. 7. Fractional pore volume α vs. dye batch concentration; diffusion perpendicular to spinning direction.

The difference between the equations lies in the interpretation of α and f, if it is assumed that the apparent diffusion coefficient is the same as the integral diffusion coefficient. On the basis of Crank's theory, f is the fraction of dye molecules having the requisite activation energy to surmount the electrical potential barrier to diffusion. It is clear that f will vary with dye and salt concentration in the same way as α if Crank's equation is applied to the experimental results.

Thus the experimental results cannot distinguish between these theories unless a theoretical solution for the variation of f with salt and dye concentration can be shown to accord better with experiment than a theoretical treatment of the corresponding variation of α. This theory is yet to be fully developed.

It should be noted in passing that the apparent α is larger for diffusion parallel to the chain direction than for diffusion perpendicular to the chains. This means that per unit area the mean pore diameter is greater in the one direction than the other, which is compatible with the fine structure of cellulose that is here envisaged. Thus there must be an obstruction factor as well as α if the theory is to account for experiment.

The chief test of the theory, however, is in the application of eqs. (9), (10), and (11) to the values of the differential diffusion coefficient found from the edgewise-diffusion experiments.

These equations can be written in simpler form because the evidence just discussed has shown that the value of D_a is probably zero. Hence we have:

$$D_c = \alpha D_0(C_0/mC) \tag{14}$$

$$D_c = \alpha D_0\,(n/K^n)C^{n-1} \tag{15}$$

That is,

$$D_c = B'\,C^{n-1} \tag{16}$$

where

$$B' = \alpha D_0(n/K^n)$$

It is convenient to discuss eq. (16) first. A plot of log D_c versus log optical density should produce a straight line with an intercept equal to log B' and the slope of the line should give a value from which m can be derived.

Application of this procedure to the results for a constant dye bath concentration gives a reasonable agreement between experiment and theory for the lower concentrations of adsorbed dye, i.e., for dye concentrations at positions within the sheet away from the edge (Table IX and Fig. 8). Near the edge the relation fails, especially with the lower salt concentrations. The most probable factor that would lead to such a breakdown is that, near the edge of the sheet, equilibrium is being approached and the rate of attainment of equilibrium here may be comparable to the speed of diffusion of the free dye.

TABLE IX
Chrysophenine G, 0.1 g./l.[a]

Salt concn., g./l.	$n-1$ (perp.)	log B' (perp.)	$n-1$ (para.)	log B' (para.)	m (Perp.)	m (Para.)	m Mean	m Isoth.
0.5	0.471	1.7176	0.496	1.8348	0.68	0.67	0.675	0.67
1.0	0.44	1.6568	0.431	1.7242	0.69	0.70	0.695	0.67
2.0	0.451	1.5752	0.496	1.7205	0.69	0.67	0.68	0.72
5.0	0.353	1.4582	0.353	1.5296	0.74	0.74	0.74	0.69
10.0	0.278	1.3033	0.300	1.369	0.79	0.77	0.78	0.72

[a] Log D_c = n − 1 log optical density + log B'.

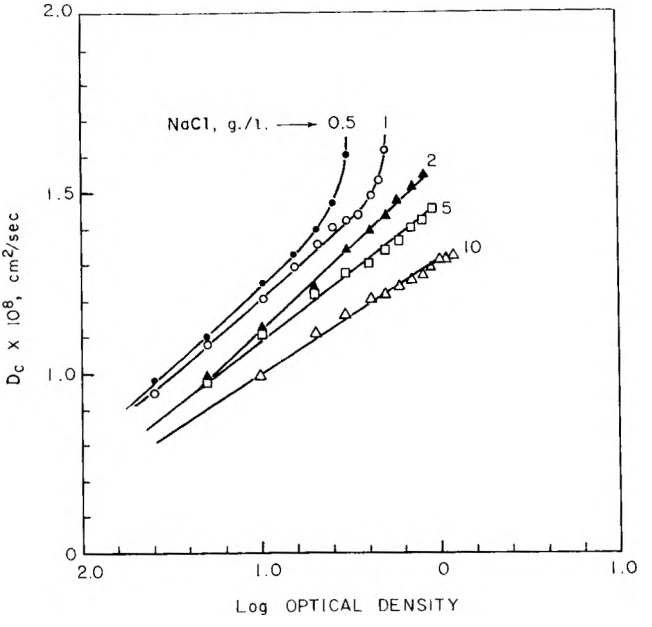

Fig. 8. Differential diffusion coefficient vs. log optical density, Chrysophenine G, 0.1 g./l.; diffusion perpendicular to spinning direction.

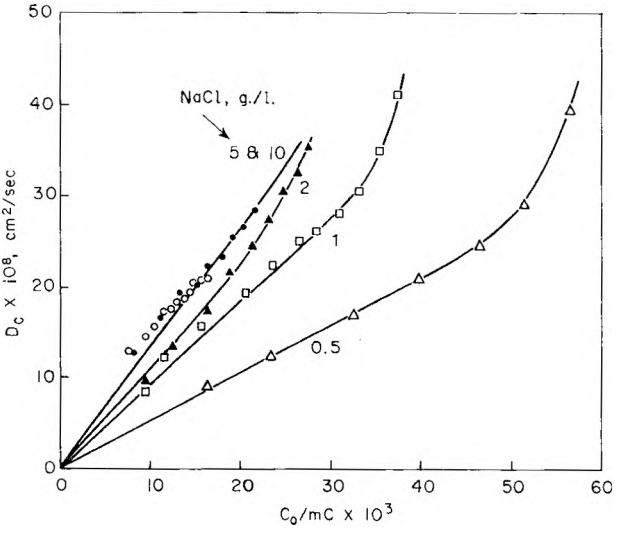

Fig. 9. Chrysophenine G, 0.1 g./l.; differential diffusion coefficient vs. $C_0/mC \times 10^3$ at various salt concentrations.

For the dye concentrations within the sheet for which the logarithmic relation is valid, reasonable agreement is also found between the exponent m in the isotherm equation derived from the theory and that obtained experimentally. It would seem that if the diffusion-adsorption theory is applied

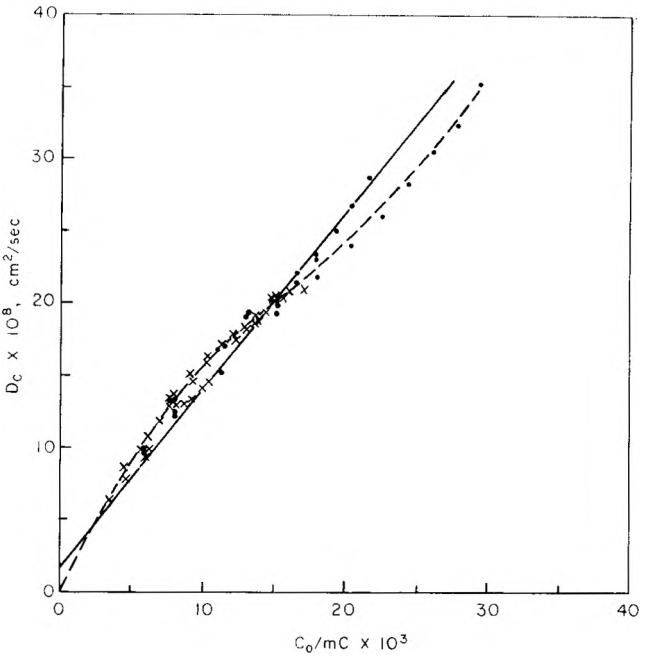

Fig. 10. Differential diffusion coefficient vs. C_0/mC for various salt and dye concentrations; diffusion perpendicular to spinning direction. (●) .05, .1, and .3 g./l. Chrysophenine G: 5.0 g./l. salt; (×) .025, .05, .1, and .15 g./l. Chrysophenine G: 10.0 g./l. salt.

to diffusion coefficients that are capable of precise definition then the objections raised by Crank[7] are no longer tenable.

A further test of the theory may be obtained by applying eq. (14). According to this equation, a plot of D_c versus C_0/mC should generate a unique straight line for all values of dye and salt concentration in the dye bath. In computing the values used for Figures 9 and 10 the concentration C originally expressed in milligrams per gram was multiplied by the factor ρ (defined earlier) in order to convert it into grams per liter: C_0 is in grams per liter. The value of m was that found experimentally from the appropriate isotherm.

Figure 9 shows the results for a constant dye bath concentration of 0.1 g./l. of Chrysophenine G. It is clear that a common line is only generated for the results with 5.0 g./l. and 10.0 g./l. of sodium chloride in the dye bath. The deviation of the other lines from this line would seem attributable to the effect of factors other than those of adsorption on the diffusion process. The slope of the lines should be proportional to αD_0 and, assuming that D_0 remains constant throughout, must be proportional to α, the ratio of the free space for diffusion to the total volume. The variation of the slopes shows that α increases with increasing sodium chloride concentration, and this means that as the salt concentration increases the free volume for diffusion must increase. This is quite consistent with the

concept that, as the ζ potential on the walls of the channels through which diffusion takes place is suppressed by the increase of the ionic strength of the dye bath, the volume unaffected by the potential will increase. Thus the variation of the slope of these lines is quite consistent with the view that initially salt suppresses the ζ potential and that only when this is virtually eliminated can the full effect of the simple diffusion-adsorption theory be seen.

Further proof of the essential validity of the theory when the ζ potential is eliminated is shown by a plot of D_c versus C_0/mC for the following salt and dye concentrations in the dye bath: (*1*) salt 5.0 g./l. with dye 0.05, 0.1, and 0.3 g./l., and (*2*) salt 10. g./l. with dye 0.025, 0.05, 0.1, and 0.15 g./l. All these results fall on the same curve (Fig. 10), deviations being found only for the higher adsorbed-dye concentrations near the edge of the sheet. Although the common curve is not perfectly straight, as demanded by theory, the results can be fitted reasonably well by a straight line having an intercept on the D_c axis. The intercept can be interpreted either as a small diffusion coefficient D_a neglected by the simple equation or as a measure of the deviation of the real line from linearity, since the actual curve seems to pass through the origin.

Thus, at high salt concentrations the experimental results are in reasonable agreement with the diffusion-adsorption theory for a region in the cellulose remote from the edge. It is thought that a breakdown of the theory, for near the edge, results from the breakdown in the condition that the adsorption at any given point be virtually instantaneous.

Any extension of the theory must therefore take account of the divergence of the experimental results at lower salt concentrations from those predicted by theory. One concept that allows this to be done is the assumption that the variation with salt concentration may be directly related to a variation in the value of α with salt concentration. Since in the derivation of C_0/mC, the concentrations C_0 and C were expressed in different units, to get α in terms of a volume ratio it is necessary to introduce the constant ρ, the ratio of the weight of dry cellulose to wet. Thus

$$\alpha' = \alpha/\rho \tag{17}$$

gives the constant α' in the correct units of volume.

If it is now assumed that the cellulose phase is that volume of solution within the cellulose over which the electrical double layer operates, plus the volume of the cellulose chains, a variation in α' with salt concentration can be explained. Thus α can be defined as:

$$\alpha = V_w/(V_c + V_z + V_w) \tag{18}$$

where V_w is the volume for free diffusion, V_c is the volume of cellulose chains, and V_z is the volume of the electrical double-layer region. As the sodium chloride is raised, V_z will diminish until in the limit $\alpha = V_w/(V_c + V_w)$, which should be a constant for a given cellulose, and when this limit is reached the diffusion-adsorption theory should then apply.

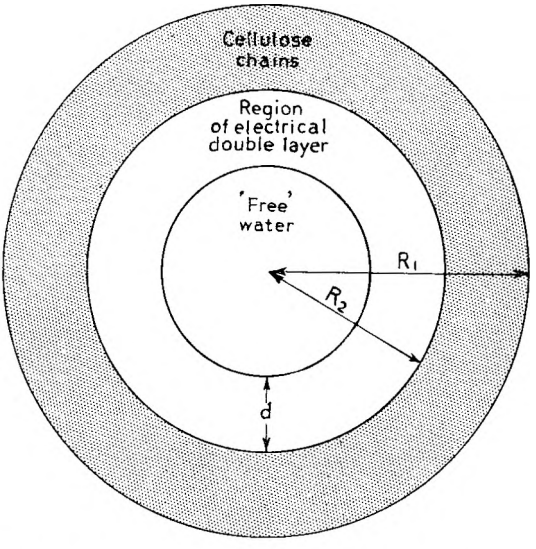

Fig. 11. Proposed cross section of cellulose capillary.

The extended diffusion-adsorption equation can then be written:

$$D_c = (D_0/\rho)[V_w/(V_w + V_c + V_z)](C_0/mC) \tag{19}$$

One method of evaluating the quantity $V_w/(V_w + V_c + V_z)$ is to assume that the cellulose is made up of a random set of capillaries with circular cross sections. Such an assumption is, clearly, an idealized picture of the cellulose structure but it can serve to give an indication of the variation likely to occur in the actual structure. Figure 11 gives a view of a cross section of a capillary of the type envisaged, and in this type of capillary it can easily be shown that:

$$\alpha = (R_2 - d)^2/R_1^2 \tag{20}$$

where R_1 and R_2 are the external and internal radii of the capillary, respectively, and d is the thickness of the electrical double layer. That is

$$\alpha = (L - Nd)^2 \tag{21}$$

where L and N are constants. Thus α becomes dependent on d and, hence, on the salt concentration. According to the theory of Debye and Hückel, the radius of an "ionic atmosphere" is proportional to $\mu^{-1/2}$, where μ is the ionic strength of the solution. For the ionic double layer postulated in the cellulose system it is therefore assumed that the thickness d is proportional to $\mu^{-1/2}$, where μ refers to the dye bath. Thus,

$$\alpha = (L - Q/\sqrt{\mu})^2 \tag{22}$$

where L and Q are constants. Since by definition $\mu = {}^1/_2\Sigma Cz^2$, eq. (22) predicts that α is a function of the concentration and valency of the ionic

TABLE X

0.1 g./l. of Chrysophenine G plus 0.5 g./l. of Sodium Chloride at 90°C.[a]

Opt. dens.	C_0/mC	$D_c \times 10^8$ (perp.) cm.²/sec.	$D_c(mC/C_0)$	$D_c \times 10^8$ (para.), cm.²/sec.	$D_c(mC/C_0)$
0.025	0.01629	9.4	577	11.0	675
0.05	0.02303	12.5	542	15.4	669
0.1	0.03256	17.7	543	22.0	676
0.15	0.03988	21.3	534	26.6	667
0.2	0.04605	24.8	539	30.8	669
0.255	0.05149	29.0	563	36.7	713
0.3	0.05651	39.5	699	51.0	902

[a] C_0 is given as grams per liter; C is in milligrams per gram.

TABLE XI

0.1 g./l. of Chrysophenine G plus 1.0 g./l. of Sodium Chloride at 90°C.[a]

Opt. dens.	C_0/mC	$D_c \times 10^8$ (perp.), cm.²/sec.	$D_c(mC/C_0)$	$D_c \times 10^8$ (para.), cm.²/sec.	$D_c(mC/C_0)$
0.025	0.00823	9.3	1130	10.8	1312
0.05	0.01165	12.3	1056	14.4	1236
0.1	0.0155	15.8	1019	19.9	1282
0.15	0.02023	19.3	954	23.4	1157
0.2	0.02338	22.8	975	26.5	1133
0.25	0.02615	25.0	956	29.3	1120
0.3	0.02867	26.2	914	31.2	1088
0.35	0.03095	28.2	911	33.9	1095
0.4	0.03312	30.6	924	38.2	1153
0.45	0.03514	35.0	996	43.9	1249
0.5	0.03703	41.3	1116	52.6	1420

[a] See footnote, Table X.

TABLE XII

0.1 g./l. of Chrysophenine G plus 2.0 g./l. of Sodium Chloride at 90°C.[a]

Opt. dens.	C_0/mC	$D_c \times 10^8$ (perp.), cm.²/sec.	$D_c(mC/C_0)$	$D_c \times 10^8$ (para.), cm.²/sec.	$D_c(mC/C_0)$
0.05	0.0094	9.8	1053	12.4	1319
0.1	0.01231	13.6	1105	16.5	1341
0.2	0.01612	17.5	1086	22.4	1390
0.3	0.01888	21.9	1160	26.5	1404
0.4	0.02112	24.8	1174	29.7	1406
0.5	0.02304	27.5	1193	32.2	1398
0.6	0.02474	30.3	1225	36.7	1483
0.7	0.02626	32.7	1245	41.0	1561
0.8	0.02766	35.5	1283	45.9	1659

[a] See footnote, Table X.

TABLE XIII

0.1 g./l. of Chrysophenine G plus 5.0 g./l. of Sodium Chloride at 90°C.[a]

Opt. dens.	C_0/mC	$D_c \times 10^6$ (perp.) cm.²/sec.	$D_c(mC/C_0)$	$D_c \times 10^6$ (para.), cm.²/sec.	$D_c(mC/C_0)$
0.05	0.005971	9.6	1608	11.4	1909
0.1	0.008123	12.9	1588	14.9	1834
0.2	0.01105	16.8	1520	19.7	1783
0.3	0.01323	19.2	1451	22.4	1693
0.4	0.01503	20.1	1337	24.7	1643
0.5	0.01659	22.1	1332	26.7	1609
0.6	0.018	23.2	1289	27.7	1539
0.7	0.01927	25.2	1308	30.0	1557
0.8	0.02045	26.9	1315	32.9	1609
0.9	0.02155	28.8	1336	35.9	1666
1.0	0.02258			38.4	1701

[a] See footnote, Table X.

TABLE XIV

0.1 g./l. of Chrysophenine G plus 10.0 g./l. of Sodium Chloride at 90°C.[a]

Opt. dens.	C_0/mC	$D_c \times 10^6$ (perp.), cm.²/sec.	$D_c(mC/C_0)$	$D_c \times 10^6$ (para.), cm.²/sec.	$D_c(mC/C_0)$
0.1	0.006008	9.8	1631	10.8	1798
0.2	0.00791	12.9	1631	14.4	1820
0.3	0.009289	14.6	1572	16.9	1819
0.4	0.01041	15.9	1527	18.1	1739
0.5	0.01137	17.1	1504	19.5	1715
0.6	0.01223	17.6	1439	20.1	1644
0.7	0.01299	18.3	1409	20.9	1609
0.8	0.0137	18.7	1365	21.6	1577
0.9	0.01435	19.5	1359	22.6	1575
1.0	0.01497	20.5	1369	23.5	1570
1.1	0.01555	20.6	1325	24.3	1563
1.2	0.01609	20.9	1299	24.8	1541

[a] See footnote, Table X.

species in the dye bath. It is now necessary to see whether this extended theory bears any relation to the experimental facts.

The new equation is thus:

$$D_c = (D_0/\rho)(L - Q/\sqrt{\mu})^2(C_0/mC) \tag{23}$$

To find the apparent α, the quantity $D_c mC/C_0$ was calculated for all the points for each salt concentration at which the D_c versus C_0/mC graph is a straight line (Tables X–XV). It is then a simple matter to calculate α from this mean value, and a plot of $\sqrt{\alpha}$ versus $1/\sqrt{\mu}$ should give a straight line from which L and Q can be derived.

It should be emphasized that the experimental value of the apparent α includes an obstruction factor since its value is different for the different

TABLE XV

NaCl concn., g./l.	α	$\sqrt{\alpha}$	μ	$1/\sqrt{\mu}$
	Diffus. perpendicular to spinning direction			
0.5	0.12	0.3464	0.009	10.54
1.0	0.21	0.4583	0.0175	7.559
2.0	0.25	0.5000	0.0346	5.376
5.0	0.31	0.5568	0.0859	3.412
10.0	0.32	0.5657	0.1714	2.421
	Diffus. parallel to spinning direction			
0.5	0.15	0.3873	0.009	10.54
1.0	0.26	0.5099	0.0175	7.559
2.0	0.31	0.5568	0.0346	5.376
5.0	0.37	0.6083	0.0859	3.412
10.0	0.37	0.6083	0.1714	2.421

directions of diffusion under given conditions. The obstruction factor is a constant and depends only on the type of cellulose sheet used. Figure 12 shows that within the experimental error $\sqrt{\alpha}$ is linearly related to $1/\sqrt{\mu}$ and hence eq. (23) is valid for the diffusion process under discussion. It is clear that this extended theory applies only to the region in the cellulose

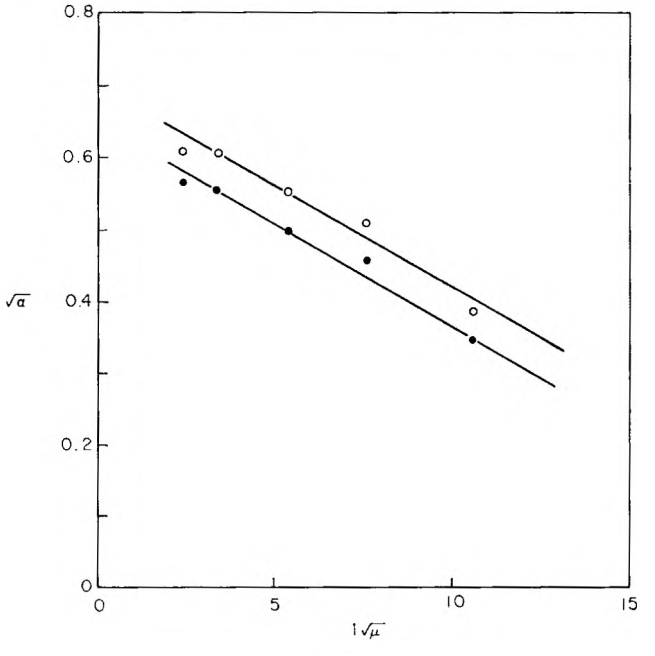

Fig. 12. Fractional pore volume α vs. $1/\sqrt{\mu}$; μ = ionic strength of solution. (○) Parallel to spinning direction; (●) perpendicular to spinning direction.

remote from the dye bath, and does not apply to the region close to the cellulose-dye bath interface. It has already been mentioned that in the latter region other factors cause a breakdown in the conditions necessary for the application of the straightforward diffusion-adsorption theory.

Another outcome of this analysis is that no overall diffusion coefficient can be expected to fit either the diffusion-adsorption theory or the foregoing extension of it, because such coefficients are complex and must include factors associated with regions in the cellulose over which the theory is invalid. Thus it is not surprising that no justification for the theory could be found by means of its application to the diffusion coefficients calculated according to the Neale method or to other methods that imply a constant diffusion coefficient for the whole process.

Although this extended theory is still incomplete for the total diffusion process, it is adequate to indicate the role of the different factors in the diffusion of direct dyes into viscose sheet.

APPENDIX

Materials. Details of the dye Chrysophenine G (C.I. Direct Yellow 12) and the never-dry viscose sheet are given in a paper by Standing and Warwicker.[12]

Constants for the Sheet. The never-dry viscose sheets were sorted into a batch of sheets of thickness $(40 \pm 0.5) \times 10^{-4}$ in. with a Mercer gauge. The actual thickness was determined by a specific-gravity method.

Thickness = 0.0984 mm.
Specific gravity of the sheet = 1.096 g./cc.
Wet weight per unit area = 0.01079 g./cm.^{2}.
Dry weight per unit area = 0.00259 g./cm.^{2}.
Weight of dry cellulose per unit volume of wet cellulose = ρ = 0.22 mg./cc.
Weight of water per gram of dry cellulose = 3.16 g./g.

Calibration Curve for Dyed Sheet. A series of uniformly dyed sheets of different dye content was obtained from appropriate equilibrium-absorption experiments. The dye content was estimated colorimetrically from aqueous pyridine extracts of known quantities of dyed sheet; the optical densities of corresponding dyed sheets soaked in saturated aqueous quinine sulfate were obtained with the spectrophotometer under the same conditions as those used for the edgewise-diffusion measurements (wavelength, 4200 A.). A plot of optical density versus dye concentration in milligrams per gram of sheet was a straight line, the equation of which was optical density $\times$ 4.8 = concentration (in milligrams per gram) of dye in the sheet.

Absorption Isotherms. Four films of the never-dry viscose sheet measuring 1 cm. $\times$ 1 1/4 cm. (i.e., 0.01295 g. of cellulose) were used with 100 ml. of dye liquor for each concentration of dye at a constant salt concentration. The concentration of the dye within the sheet was determined by measuring the optical density of the dyed sheets soaked in saturated aqueous quinine sulfate. The equations of these isotherms were:

0.5 g./l. of sodium chloride.	$C = 10.07\ C_0^{0.6667}$
1.0 g./l. of sodium chloride.	$C = 15.76\ C_0^{0.6657}$
2.0 g./l. of sodium chloride.	$C = 24.43\ C_0^{0.7197}$
5.0 g./l. of sodium chloride.	$C = 28.84\ C_0^{0.6925}$
10.0 g./l. of sodium chloride.	$C = 40.18\ C_0^{0.7161}$

The author thanks Dr. H. A. Standing for his help and encouragement during the course of this work.

References

1. Neale, S. M., and W. A. Stringfellow, *Trans. Faraday Soc.*, **29**, 1167 (1933).
2. Boulton, J., A. E. Delph, F. Fothergill, and T. H. Morton, *J. Textile Inst.*, **24**, P113 (1933).
3. Garvie, W. M., and S. M. Neale, *Trans. Faraday Soc.*, **34**, 335 (1938).
4. Morton, T. H., *Trans. Faraday Soc.*, **31**, 262 (1935).
5. Standing, H. A., J. O. Warwicker, and H. F. Willis, *Shirley Inst. Mem.*, **20**, 145 (1946), or *J. Textile Inst.*, **38**, T335 (1947).
6. Crank, J., *J. Soc. Dyers Colourists*, **63**, 412 (1947).
7. Crank, J., *J. Soc. Dyers Colourists*, **66**, 366 (1950).
8. Peters, R. H., J. H. Petropoulos, and R. McGregor, *J. Soc. Dyers Colourists*, **77**, 704 (1961).
9. Boltzmann, L., *Ann. Physik.*, **53**, 959 (1894).
10. Matano, C., *Japan J. Physiol.*, **8**, 109 (1932).
11. Ward, A. F. H., *Proc. Roy. Soc.*, **A133**, 522 (1931).
12. Standing, H. A., and J. O. Warwicker, *Shirley Inst. Mem.*, **22**, 45 (1948), or *J. Textile Inst.*, **40**, T175 (1949).
13. Garvie, W. M., L. H. Griffiths, and S. M. Neale, *Trans. Faraday Soc.*, **30**, 273 (1934).
14. Holmes, F. H., and H. A. Standing, *Shirley Inst. Mem.*, **19**, 260 (1944); *Trans. Faraday Soc.*, **41**, 542 (1945).

Résumé

On décrit l'étude expérimentale concernant la diffusion d'un colorant direct dans les bords d'un film de viscose. Les résultats de ces expériences ont été utilisés pour vérifier la théorie de diffusion—absorption de Standing, Warwicker et Willis. On a démontré que cette théorie peut etre étendue pour prendre en considération l'effet de la concentration en chlorure sodique sur les coefficients de diffusion.

Zusammenfassung

Eine Experimentaluntersuchung der Diffusion eines Direktfabrstoffs in die Kanten einer Viskosefolie wird beschrieben. Mit den Ergebnissen dieser Versuche wird die Diffusions-Adsorptionstheorie von Standing, Warwicker und Willis überprüft. Eine Erweiterung dieser Theorie zur Berücksichtigung des Einflusses der Natriumchloridkonzentration auf die Diffusionskoeffizienten wird vorgenommen.

Received July 30, 1962

JOURNAL OF POLYMER SCIENCE: PART A VOL. 1, PP. 3135–3150 (1963)

Aromatic Polyimides*

G. M. BOWER and L. W. FROST, *Westinghouse Materials Research Laboratories, Pittsburgh, Pennsylvania*

Synopsis

Aromatic polyimides were prepared in two steps. Pyromellitic dianhydride was added to a solution of an aromatic diamine in a highly polar solvent, such as dimethylformamide, dimethylacetamide, dimethyl sulfoxide, or *N*-methyl-2-pyrrolidone, until a high molecular weight polypyromellitamic acid was obtained. The amount of pyromellitic dianhydride required was determined by the rate of viscosity increase with addition of the reagent, and it corresponded fairly closely to the stoichiometric quantity. Inherent viscosity of the polypyromellitamic acids in dimethylacetamide ranged from 0.54 to 3.22. Upon standing at room temperature, the viscosity of these solutions gradually declines. This viscosity decline is rapidly accelerated by an increase in temperature and is negligible at 0°C. Water and excess pyromellitic dianhydride result in a more rapid decline in viscosity. The polypyromellitimides were formed from the amide acids by heating. The solvent could be removed during the imidization step or earlier under vacuum at a lower temperature. Polypyromellitimides were prepared from *m*-phenylenediamine, benzidine, 4,4′-diaminodiphenyl ether, 3,4′-diaminodiphenyl ether, 4,4′-diaminodiphenyl sulfide, methylene dianiline, isopropylidene dianiline, several diaminobenzanilides, 4,4′-diaminophenyl benzoate, and other amine-terminated low molecular weight aromatic esters and amides. Polyimides cast in the form of thin films were for the most part clear, tough, flexible, insoluble, and infusible. Thick sections tended to be brittle and opaque. Several of the polymers in the form of films suffered less than 10% weight loss after aging 400 hr. at 325°C. in air. Most of these films were still intact and moderately flexible after this treatment.

INTRODUCTION

The intrinsic thermal and oxidative stability of aromatic structures has long been recognized, and a variety of polymers have been made in which benzene rings are linked together in chains or networks. In most cases, the connecting groups are less stable than the rings, and the stability of the polymer is determined largely by the nature of these groups. Among the more stable linking groups that have been used to make high polymers with film-forming properties are amide,[1] ester,[2] and imide.[3] The present paper is concerned with the preparation and properties of a series of resins in which benzene rings are linked by imide groups to give linear polymers of very high thermal stability. Most of these polymers also include other connecting groups between rings, and the effects of these groups upon physical properties and thermal stability are reported.

* Presented at 144th Meeting of the American Chemical Society, Los Angeles, California, April, 1963.

DISCUSSION

The reaction of pyromellitic dianhydride (PMDA) with a primary diamine proceeds according to the equation:

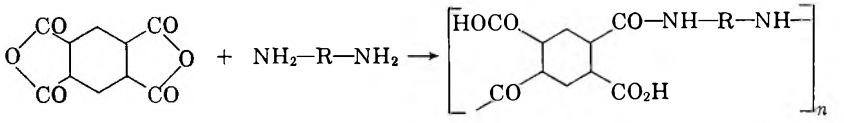

When the polypyromellitamic acid is heated or treated with a dehydrating agent, cyclization occurs with the formation of a polyimide:

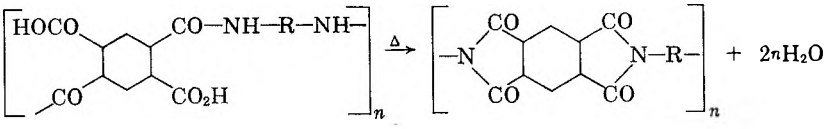

Polyimides derived from aliphatic diamines are generally soluble and thermoplastic and can be conveniently prepared by a fusion reaction of a salt of the diamine with a diester of pyromellitic acid.[4] The polyimide is produced in one step and can then be fabricated. Aromatic amines, however, are generally not basic enough to form well-defined salts. Moreover, the aromatic polyimides are usually infusible and insoluble, so that when the reactants are heated together the mixture becomes solid before a high molecular weight is reached. However, when the reaction is carried out at moderate temperatures in a solvent it is possible to attain a very high molecular weight while the polymer is in the soluble amide form. The polymer can then be applied from solution to form films, laminates, varnish coatings, etc. The imidization reaction occurs during or after solvent removal.

Highly polar solvents are necessary to dissolve the polymers, and these solvents associate strongly with both the polymer and the reactants. This association probably accelerates the reaction. One of the best solvents is *N*,*N*-dimethylacetamide (DMAC). The interaction of DMAC with various aromatic compounds in solution has been demonstrated spectroscopically by Hatton and Richards,[5] and we have isolated crystalline 1:1 complexes of DMAC with PMDA and with isophthal(3-aminoanilide). These adducts apparently involve association between the nitrogen atom and the aromatic ring. A different type of complex is formed between DMAC and pyromellitic acid. In this case 4 moles of DMAC are required, and the carboxyl groups are involved. The formation of similar complexes between aromatic dicarboxylic acids and DMAC has been reported by Ham and Beindorff.[6] The carboxyl groups of the polymer are probably associated with DMAC in a similar way, although the solvent is not sufficiently basic to cause appreciable ionization. A stronger base, such as triethylamine, removes a proton from the carboxyl group of the polymer, forming a salt.

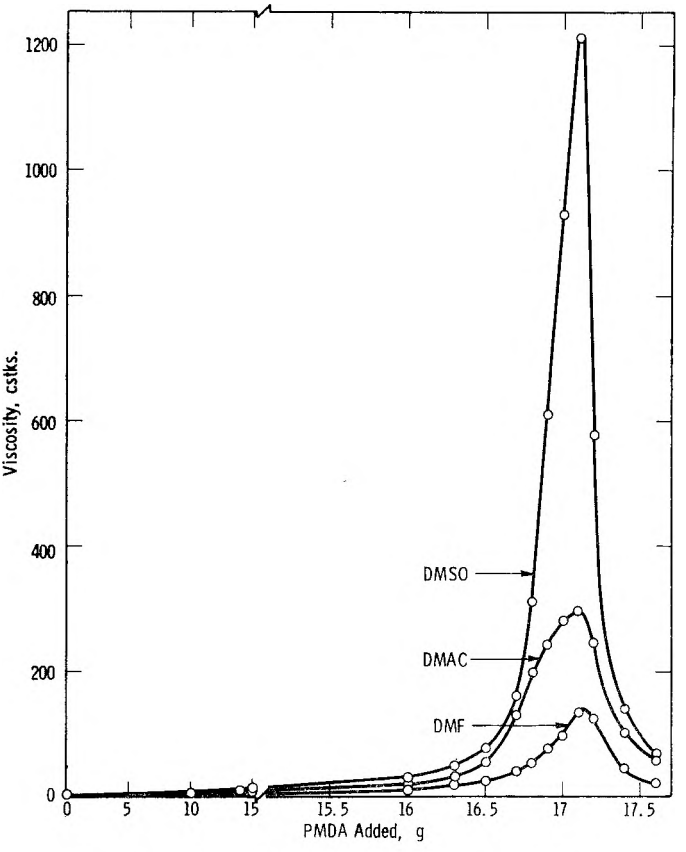

Fig. 1. Reaction of PMDA with MDA in three solvents.

It is characteristic of condensation polymers that the attainment of a high molecular weight depends upon a very close approach to equivalence in the reactant ratio. The proper ratio is conveniently determined in the present case by observing the viscosity rise as PMDA is added slowly to a solution of diamine. This method is usually more accurate than determining the equivalent quantity from molecular weights, unless the reactants are extremely pure.

Surprisingly, the addition of more than the equivalent quantity of PMDA causes a decrease in viscosity, as shown in Figure 1. The molecular weight of the resin in solution at the maximum viscosity is estimated to be in the range of 10^5–10^6, but the molecular weight and viscosity decline with time, as shown in Table II and Figure 2. The rate of decline increases with increasing temperature, and the high rate at 70°C. is indicated in Figure 3. At 0°C. the solution can be stored for several weeks without a noticeable change in viscosity.

Apparently, the imidization reaction occurs very slowly in solution at moderate temperatures. After 55 hr. at 35°C. the formation of imide

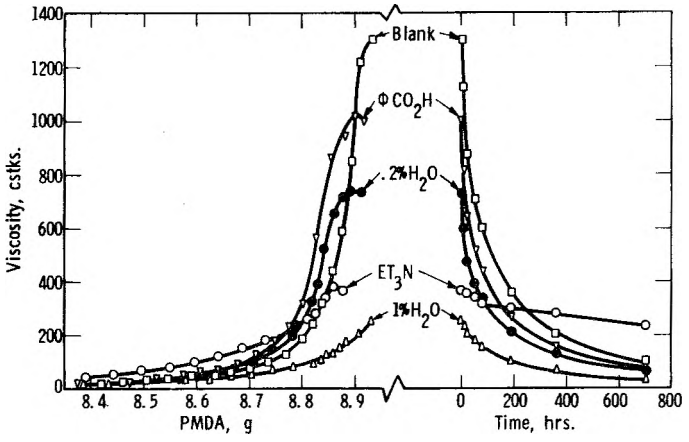

Fig. 2. Viscosity changes of DAPE–PMDA solutions prepared in the presence of various additives.

could not be detected by titration of residual carboxyl groups, nor did the infrared spectrum show any evidence of imide groups. However, when the solution was heated to the boiling point the insoluble polyimide precipitated in a few minutes.

When the order of addition was reversed, and the diamine was added slowly to a solution or suspension of PMDA, a high viscosity was not attained. These observations suggest that anhydrides degrade the polymer if present in excess. This and other degradation reactions will be discussed in a separate paper.

Table I includes a comparison of polyimides prepared from a variety of diamines, most of which include other linking groups. The data are not conclusive, but an approximate order of thermal stability for the groups studied is imide > ether, sulfide, direct phenyl–phenyl bond > amide, ester > methylene > isopropylidene. Orientation of groups on the benzene ring did not generally have a great effect on stability, but was a factor in flexibility and viscosity. The greatest flexibility was observed in films containing both *meta* and *para* substitution, and the highest inherent viscosities occurred in solutions of polymers high in *para* substitution. In a few cases, products high in *para* substitution were found to be essentially insoluble, and were not investigated.

Amide-imide copolymers are of particular interest because of their ease of preparation and the range of compositions and properties available. Those prepared from pure diamines containing internal amide groups are of regular structure and many of them have excellent physical properties and thermal stability. A wider range of amide/imide ratios is available in the random polymers prepared from amine-terminated polyamides and PMDA.

The polyamide portion can be prepared by either interfacial or homogeneous reaction of a diacyl chloride, such as isophthaloyl chloride, with an

TABLE I. Properties of Polyimides

Diamine	Inherent visc.	Film properties[a]	Weight loss at 325°C.,[b] %			
			100 hr.	200 hr.	300 hr.	400 hr.
m-Phenylenediamine	1.19	Brit	3.3	4.3	5.0	5.6
Benzidine	3.22	Flex	2.2	3.6	5.1	6.5
4,4′-Diaminodiphenyl ether	2.45	Flex	3.3	4.0	5.2	6.6
3,4′-Diaminodiphenyl ether	1.31	Flex	3.4	3.8	5.1	7.2
4,4′-Diaminodiphenyl sulfide	1.83	Flex	4.8	5.8	6.8	7.9
4,4′-Methylene dianiline	1.86	Brit	9.4	12.9	14.7	16.8
4,4′-Diaminobenzanilide	2.20	Brit	5.7	8.4	11.9	12.1
4,4′-Isopropylidene dianiline	1.48	Flex	16.1	26.2	31.0	36.0
4,3′-Diaminobenzanilide	1.55	Flex	4.3	7.8	10.8	11.9
3,4′-Diaminobenzanilide	2.19	Flex	2.0	4.2	6.9	9.8
3,3′-Diaminobenzanilide	1.18	Flex	3.2	6.5	9.8	11.2
3,5-Diaminobenzanilide	1.29	No film, just crumbs				
Isophthal(4-aminoanilide)	1.46	Flex	6.9	9.4	14.4	20.4
N,N′-m-Phenylene-bis(4-aminobenzamide)	1.48	Flex	6.0	9.2	12.5	15.6
Isophthal(3-aminoanilide)	1.48	Flex	6.8	8.1	10.5	13.2
N,N′-m-Phenylene-bis(3-aminobenzamide)	1.07	Flex	6.2	8.3	14.0	20.3
N,N′-bis(3-Aminobenzoyl)-2,4-diamino-diphenyl ether	0.54	Flex	24.1	31.5	38.6	44.3
N,O-bis(3-Aminobenzoyl)-*p*-aminophenol	1.22	Flex	12	17	21	27
bis(4-Aminophenyl)isophthalate	0.93	Flex (shrunk)	3.6	6.7	10.9	15.0
4,4′-Diaminophenyl benzoate	1.21	Brit	3.3	5.5	7.6	9.7
Resorcinol-bis(3-aminobenzoate)	0.78	Brit	9.5	13.3	17.3	22.7
$MPD_{7.2}IP_{6.25}$[c]	1.16	Flex	6.7	16.5	29.8	
$MPD_{7.6}IP_{4.98}TP_{1.66}$[c]	1.21	Flex	8.5	22.4	44.4	

[a] The samples consisted of films approximately 1 mil thick adhering to aluminum. The film was judged to be flexible if it could be creased without cracking; brittle if it cracked on creasing. Brit = brittle, Flex = flexible. [b] The values at 100 hr. intervals were obtained from plots of weight loss vs. time. [c] MPD = *m*-phenylenediamine units; IP = isophthalic units; TP = terephthalic units.

excess of a diamine, such as *m*-phenylenediamine (MPD). The interfacial procedure[7,8] provides a good method of preparing polymers with a high amide/imide ratio. Some control over polyamide chain length is possible through variation in reactant ratio and concentrations, but the method is

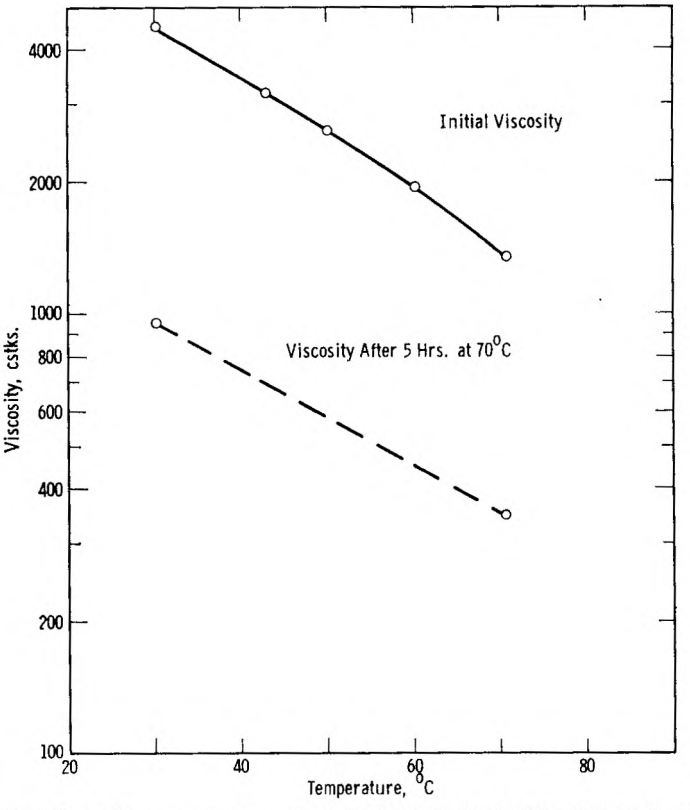

Fig. 3. Effect of temperature on viscosity of 11% DAPE–PMDA in DMAC.

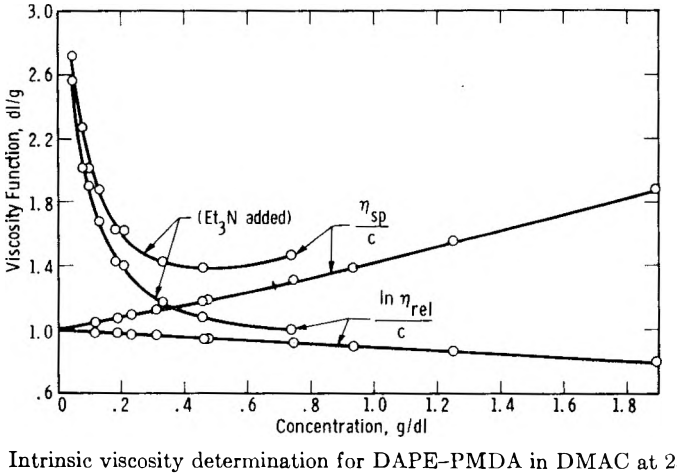

Fig. 4. Intrinsic viscosity determination for DAPE–PMDA in DMAC at 25.0°C.

not well adapted to preparing the short-chain polyamides needed for polymers high in imide content. When the reaction is conducted in solution, any average ratio desired is easily obtained. A third method of preparation involves the initial reaction of PMDA with excess diamine, followed by reaction of the resulting low polymer with a diacyl chloride. The second step can be done interfacially to give the uncured copolymer in the form of a solvent-free powder. In some cases, this is an advantage over the other methods, in which the polymer is obtained as a viscous solution.

The deleterious effect of an excess of PMDA has been mentioned. Some effects of other added materials upon the course of the reaction and the stability of the product are shown in Figure 2. Benzoic acid had only a small effect upon the maximum viscosity or the rate of viscosity decline. Water prevented the attainment of a high viscosity and also degraded the polymer rapidly. The rapid hydrolysis of *o*-carboxyamide groups has been studied by Bender et al.,[9] and a mechanism similar to the one they propose is probably operative in this case. Hydrolysis of one of the anhydride groups of the PMDA would also give an end-blocking structure that would limit the molecular weight of the polymer.

Triethylamine forms a salt with the carboxyl groups along the polymer chain. When an equivalent quantity is added to a solution of the polymer, the viscosity rises immediately by as much as 13 times, and the conductance about 20 times. The intrinsic-viscosity plot, Figure 4, shows the upturn at low concentration that is characteristic of polyelectrolyte solutions.[10] If the triethylamine is present during the preparation of the polymer, a high viscosity is not reached, as shown in Figure 2, although the resulting solution has a high conductance. Apparently, the product in this case is a polyelectrolyte of low molecular weight.

The curing of aromatic polyimide resins presents certain problems. Thin films of excellent clarity and toughness are obtained from many of the polymers simply by spreading the solution on a flat surface and baking at 150°C. for an hour or two. As the thickness is increased, however, the film becomes more brittle and less clear, until the cured resin is obtained in the form of brittle opaque fragments, shiny on the upper surface, powdery beneath. This effect is most noticeable in polymers high in imide. The effect can be minimized by removing most of the solvent at low temperature, preferably under vacuum, and completing the cure with a slowly rising temperature. Toughness and flexibility of the polymers high in imide groups can often be improved markedly by heating the film to a temperature of about 300°C. for a few minutes.

As the ratio of amide to imide is increased, the flexibility of the films after curing at 150°C. generally increases, but the films high in amide tend to degrade and become brittle when heated for any length of time at 300°C. Films of the more stable polyimides, such as those prepared from 4,4′-diaminodiphenyl sulfide or ether (DAPE), or from one of the diaminobenzanilides, remain a clear amber and flexible after several hundred hours of aging at 325°C. in air.

EXPERIMENTAL

Materials

In most cases satisfactory results were obtained by using commercial reagents without further purification. Higher molecular weights were obtained, however, by using purified reagents and anhydrous solvents. Samples used for inherent viscosity and weight loss determinations were prepared from diamines which had been recrystallized or sublimed and, in most cases, had melting ranges of less than 1°C. Many of the diamines were synthesized by us for this project. The preparation of those that have not been reported before will be the subject of a separate paper.

PMDA was obtained from the Explosives Department, E. I. du Pont de Nemours & Co., Inc. Both granular and micropulverized grades were used successfully. The former is less susceptible to hydrolysis in storage and is preferable when maximum molecular weight is desired. Iso and terephthaloyl chlorides were obtained from the Hooker Electrochemical Co., and were used without further purification.

Preparation of Polymers

General

The simplest method of preparation is the slow addition of solid PMDA to a stirred solution of a diamine until maximum viscosity is attained. The reaction, which is somewhat exothermic, has been run successfully at temperatures from −20 to +70°C. Suitable solvents are DMAC; *N*,*N*-dimethylformamide (DMF), *N*-methyl-2-pyrrolidone (NMP), and dimethyl sulfoxide (DMSO). Up to about 40% of a diluent such as xylene can be included. Rapid addition of the total quantity of PMDA or the addition of a mixture of PMDA and diamine to the solvent gave satisfactory results when the reactant ratio was accurately controlled, but the addition of diamine to a solution of PMDA gave products of low molecular weight. Amide–imide copolymers were also prepared by the reaction of a diacyl chloride with the reaction product of PMDA and excess diamine. Examples of these methods follow.

Reaction of PMDA and MDA

Simultaneous preparations were made in three solvents, DMF, DMAC, and DMSO. In each case, 14.84 g. (0.075 mole) of 4,4′-methylenedianiline (MDA) in 281 g. of solvent was stirred rapidly in a Waring blender while 10.00 g. (0.0459 mole) of PMDA was added. When this had dissolved, an additional 4.00 g. (0.0184 mole) was added, followed by smaller increments as the equivalent quantity was approached. After each addition, viscosity measurements were made by observing the efflux time from a 2 ml. pipet which had been calibrated against solutions of known viscosity. The temperature was held at 35–40°C. throughout the run, and the viscosity meas-

urements were made at 40°C. Solvent was added when necessary to replace losses by evaporation.

In the early stages of the run there was little change in viscosity. When about 95% of the PMDA had been added, a rapid rise in viscosity was observed after each addition, reaching a constant value in 10–15 min. The time required to become constant increased to several hours as the end point was approached. Finally, when the PMDA exceeded 17.1 g. (0.0785 mole), the viscosity began to decrease with time. Additional PMDA increased the rate of viscosity decline.

The maximum viscosity after each addition of PMDA was recorded until the viscosity began to decrease. Thereafter, viscosity readings were made arbitrarily 23 hr. after each addition. These viscosity values are plotted in Figure 1 for the three solvents. Small samples were removed when 17.0 g. (0.078 mole) of PMDA had been added, and 1-mil films were cast by baking in aluminum dishes for 1 hr. at 150°C. and 1 hr. at 200°C. The sample prepared in DMAC gave a clear film which could be creased without cracking. The other two samples were cracked and brittle.

If the addition of PMDA was stopped short of maximum viscosity, a stable solution was obtained which could be stored for several weeks without apparent change. Addition of PMDA to the aged solution gave the expected viscosity increase. When excess PMDA was added, the viscosity decreased rapidly with time, and the addition of diamine did not restore it. When the reaction was carried out by adding the diamine to a solution of PMDA, the viscosity rise was small and indefinite, and satisfactory films were not obtained.

The amount of PMDA required to give maximum viscosity was about 5% more than that calculated, probably because of partial hydrolysis of the PMDA in storage. Once the optimum ratio was determined for a given batch of reactants, the total amount of PMDA could be added at one time, or a mixture of the dry ingredients could be added to the stirred solvent. The final viscosity and the film characteristics were about the same for the three procedures.

DMAC Complexes

Preparation. A mixture of 250 g. of PMDA and 500 g. of DMAC was heated to 105°C. to give a clear solution, which was allowed to cool slowly. Large crystals formed, from which the supernatant solution was decanted. DMAC was added to the residue to give a total weight of 750 g., and the crystallization process was repeated four times. The product was dried under vacuum at 25°C. for 12 days to give coarse colorless crystals of PMDA–DMAC weighing 198 g. (57% yield).

ANAL. Calcd. for $C_{14}H_{11}O_7N$: C 55.1, H 3.61, N 4.59. Found: C 54.6, H 4.06, N 4.95.

The infrared spectrum of the complex was found to be similar to that of PMDA, with no change in the anhydride bands at 5.3 to 5.8 μ. Most of

the absorption bands of DMAC were also present in the spectrum of the complex, although they were weak compared with the PMDA spectrum. The carbonyl band of the DMAC was shifted to 6.2 μ from its normal position at 6.1 μ. A similar shift was noted by Schmulbach and Drago[11] for the I_2–DMAC complex.

A complex was prepared from DMAC and pyromellitic acid by the same procedure. A similar shift in carbonyl absorption was observed in the infrared spectrum. In this case, the composition of the complex was PMA–4DMAC.

ANAL. Calcd. for $C_{26}H_{42}O_{12}N_{14}$: C 51.8, H 6.97, N 9.30. Found: C 51.7, H 6.85, N 9.35.

A sample of isophthal(3-aminoanilide), m.p. 239–240°C., was dissolved in the minimum quantity of DMAC. The solution became slightly warm and a crystalline solid separated in a few minutes. The solid was filtered off, washed with DMAC, and dried for 24 hr. at 50°C. and 10 mm. Hg pressure, to give a 1:1 complex.

ANAL. Calcd. for $C_{24}H_{27}N_5O_3$: C 66.5, H 6.24, N 16.17. Found: C 66.2, H 6.03, N 16.04.

Polymers from PMDA–DMAC. A solution of 1.43 g. (0.00722 mole) of MDA in 17 g. of DMAC was stirred while PMDA–DMAC was added in small portions. A maximum viscosity of 3390 cstokes at 25°C. was reached when 2.57 g. (0.00843 mole) of complex had been added.

A mixture of 2.57 g. (0.00843 mole) of PMDA–DMAC and 17 g. of DMAC was stirred while MDA was added slowly. The addition of MDA was continued beyond the calculated quantity, but a high viscosity was not observed at any time. The viscosity after adding 1.73 g. (0.00874 mole) of MDA was 113 cstokes.

A mixture of 1.43 g. (0.00723 mole) of MDA and 2.57 g. (0.00843 mole) of PMDA–DMAC was dissolved in 17 g. of DMAC to give a solution having a viscosity of 2150 cstokes.

Preparation of Random Amide–Imides

Interfacial Reaction. A solution of 32 g. (0.30 mole) of MPD, 75 g. (0.197 mole) of borax, 10 g. of sodium sulfite, and 1600 g. of water was stirred in a Waring blender while a solution of 15 g. (0.074 mole) of isophthaloyl chloride (IPC), 5 g. (0.025 mole) of terephthaloyl chloride (TPC), and 1000 g. of xylene was added rapidly. The mixture was stirred for 2 min. and the precipitated polymer was filtered off. An identical run was made and the products from the two runs were combined, washed twice with water and once with acetone, and dried for 1 hr. at 150°C. The product was a gray powder weighing 48 g.

A solution of 11.5 g. of the powder in 100 g. of DMAC was stirred while PMDA was added in small portions. A maximum viscosity of 760 cstokes was observed when 2.9 g. (0.0133 mole) of PMDA had been added. Films

were cast from the resulting solution by baking at 150°C. for 2–20 hr., followed by 1–4 hr. at 200°C. Clear tough films were obtained which could be stripped from the substrate and creased repeatedly without cracking. This polymer had an amide/imide ratio of about 3.

In another interfacial run a mixture of 32 g. of MPD, 43 g. of sodium carbonate, and 500 g. of water was stirred in a Waring blender while a solution of 15 g. of IPC, 5 g. of TPC, and 43 g. of xylene was added rapidly. The mixture was stirred for 1 min. and filtered. The precipitated polymer was combined with that from an identical run and the product was washed twice with water, twice with acetone, once more with water, twice more with acetone, and dried at room temperature in a stream of nitrogen. The product was a white powder weighing 43 g. A solution of 41.0 g. of the powder in 200 g. of DMAC was stirred while PMDA was added in small portions until the viscosity reached a maximum. The required amount was 6.06 g. (0.0278 mole), giving an amide/imide ratio of about 5.7. Films cast by baking the solution at 150°C. were very tough and flexible.

Homogeneous Reaction. A solution of 32.4 g. (0.300 mole) of MPD, 33.3 g. (0.300 mole) of triethylamine, and 400 g. of DMAC was stirred in a Waring blender while 30.5 g. (0.150 mole) of IPC was added slowly. The temperature rose to 64°C. When it had dropped to 30°, the solution was filtered and diluted to 531 g. with additional DMAC. The filtrate was stirred while 30 g. of PMDA was added in 5 min., followed by small increments over a period of several hours. A maximum viscosity of 1150 cstokes was reached with 31.8 g. (0.146 mole) of PMDA. Films were cast by baking for 2 hr. at 150°C. and then 1 hr. at 200°C. Films up to 2 mils thick were clear and moderately flexible. Thicker films were opaque and brittle. This polymer had an amide/imide ratio of 1.

Satisfactory results also were obtained from this general procedure when sodium carbonate was substituted for the triethylamine and when the acyl chloride was added as a solution in xylene or other inert solvent. Since triethylamine hydrochloride is somewhat soluble in the system, the sodium carbonate method gives more complete removal of hydrogen chloride.

Reverse Order of Reaction. A solution of 10.8 g. (0.100 mole) of MPD in 100 ml. of DMAC was stirred rapidly while 10.9 g. (0.0500 mole) of PMDA was slowly added. A solution of 4 g. of sodium hydroxide in 250 ml. of water was then added. The resulting clear solution was stirred rapidly in a Waring blender while a solution of 10.15 g. (0.0500 mole) of IPC in 150 ml. of xylene was added rapidly. The thick emulsion obtained was filtered, and the solid polymer was washed with xylene, water, and acetone. It was dried for 30 min. at 150°C. to give a white powder weighing 29.7 g. A film cast from a DMSO solution of the powder by baking at 200°C. was clear and moderately flexible.

Effect of Additives on Reaction

A solution of 40.0 g. (0.200 mole) of DAPE, 750 g. of DMAC, and 200 g. of xylene was distilled slowly through a 12 in. unpacked column until 270

ml. had been removed and the vapor temperature was 160°C. The residual dehydrated solution was diluted to 750 g. with DMAC and divided into five equal parts, to which were added the following materials:

A. 8.6 g. of DMAC.

B. 8.1 g. of triethylamine plus 0.4 g DMAC (2 moles amine per mole of polymer unit).

C. 9.8 g. of benzoic acid plus 8.5 g. of DMAC (2 moles of acid per mole of polymer unit).

D. 1.52 g. of water plus 6.98 g. of DMAC (1% water).

E. 0.30 g. of water plus 8.2 g. of DMAC (0.2% water).

Each sample was stirred while 8.00 g. of PMDA was added, followed by additional small portions. The temperature was held at 35°C. and the viscosity was measured about 15 min. after each addition. When the viscosities were judged to have reached maximum values, at about 8.9 g. (0.04 mole) of PMDA in each, addition of PMDA was stopped and additional measurements of viscosity were made as a function of time. The viscosity observations are shown in Figure 2.

Solution Properties

Effect of Temperature on Viscosity

A solution of 200 g. (1.00 mole) of DAPE in 3062 g. of DMAC was stirred rapidly while 216 g. of PMDA was added. When the solution was complete, 1 g. increments of PMDA were added until the viscosity had reached a maximum. The total PMDA used was 220 g. (1.01 moles). The solution was diluted to 3490 g. with DMAC, and the viscosity was measured at five temperatures, from 30.0 to 70.5°C., as rapidly as possible from the lowest temperature to the highest. The solution was then held at 70.5°C. for 5 hr. and the viscosity was measured again at 70.5 and 30.0°C. The results are shown in Figure 3.

Viscosity and Molecular Weight

A 10% solution of the DAPE–PMDA polymer in DMAC was prepared as described above. The intrinsic viscosity was determined at 25.0°C., with the use of Ubbelohde dilution pipets for the viscosity measurements and a 25 ml. pycnometer for density determinations. The solution was allowed to stand at 25°C. and additional determinations were made after 48

TABLE II
Intrinsic Viscosity Decline of DAPE–PMDA at 25°C.

Aging time, hr.	$[\eta]$, dl./g.	Approx. MW
1.5	1.25	620,000
48	1.05	560,000
164	1.00	450,000

and 164 hr. of aging. The molecular weights were estimated by the equation of Chinai[12] and are shown in Table II.

To a portion of the solution after 164 hr. of aging were added 2 moles of triethylamine per mole of polymer unit. The intrinsic viscosity determination was repeated, with the results shown in Figure 4. Because of the upturn of the polyelectrolyte curves as the concentration decreased, extrapolation to zero concentration was impossible. However, the treatment of Van Oehne and Cragg[13] gave a value of 0.81 dl./g. for $[\eta]$ of the polyelectrolyte. Their method gave 1.01 dl./g. for the normal solution, in excellent agreement with the value of 1.00 found by the usual extrapolations.

A determination of molecular weight by light scattering was made by Dr. L. S. Chang of these laboratories. Using two DAPE–PMDA polymers which had been stored for some time in solution, precipitated by water, and redissolved in DMAC, he obtained a molecular weight of 200,000 and dissymmetry factors of 1.32 and 1.12 on different samples.

Titration of Carboxyl Groups

A solution of 20.00 g. (0.1000 mole) of DAPE in 307 g. of DMAC was stirred in a Waring blender while 22.00 g. (0.1010 mole) of PMDA (quantity previously determined by slow addition to maximum viscosity) was added at once. The mixture was stirred for 1 min. and then diluted to 10.0% solids to give a clear solution with a viscosity of 970 cstokes at 35°C.

The solution was aged at 35°C. and samples were removed periodically for carboxyl determination. Weighed samples of 3–5 g. were diluted with 50 ml. of DMAC and titrated with 0.1*N* sodium hydroxide, using calomel-verus-glass electrodes. A blank determination was made on the solvent. Eight determinations over a 55 hr. period gave values of 1.94 to 2.02 equiv. per polymer unit. There was no apparent trend.

Polyelectrolyte Formation

A 10% solution of DAPE–PMDA polymer in DMAC, prepared as previously described, had a specific conductance of 8.3 μmhos/cm. at 25°C. and 60 cycles, and a viscosity of 1124 cstokes at 35°C. When 2 moles of triethylamine per mole of polymer unit was added, the viscosity rose immediately to 14,770 cstokes. The specific conductance of a similar polymer solution prepared in the presence of the same quantity of triethylamine was 363 μmhos/cm. at 25°C. but its viscosity was only 364 cstokes at 35°C.

A 1% solution of MDA–PMDA polymer in DMAC was found to have a viscosity of 3.18 cstokes and a specific conductance of 7 μmhos at 25°C. The addition of 2 moles of triethylamine per mole of polymer unit raised the viscosity to 3.63 cstokes and the conductance to 150 μmhos/cm.

Film Casting

Good films were obtained from many polymers by spreading a uniform film of solution on a glass or metal plate, baking at 150°C. for an hour or

more, and stripping off the cured film. In other cases, more satisfactory results were obtained by curing slowly in a vacuum.

Films were cast from two different solutions of DAPE–PMDA polymer. Solution A was prepared by the addition of 21.51 g. (0.09867 mole) of PMDA to a solution of 20.00 g. (0.1000 mole) of DAPE in 376 g. of DMAC. The viscosity was 3900 cstokes at 35°C. Solution B was prepared by adding 0.125 g. (0.00057 mole) of PMDA to half of solution A. It had a viscosity of 5700 cstokes at 35°C. The following curing schedules were used to cast film samples in 55 mm. diameter aluminum dishes:

Cure I. 16 hr. at 150°C. in air.

Cure II. 22 hr. at 25°C. and 10 mm. pressure, 6 hr. at 50°C. and 10 mm. pressure, 19 hr. at 100°C. and 10 mm. pressure, and 4 hr. at 150°C. and 10 mm. pressure.

The resulting films had the following properties:

Solution A, Cure I:

< 1 mil: Clear, continuous; dish could be creased without cracking film; could not be stripped from dish.

1.5 mils: Clear, cracked at edges; could not be creased.

2.5–4 mils: Small clear brittle pieces.

5–8 mils: Brittle pieces with yellow powder on under side.

Solution A, Cure II:

1–4 mils: Clear, continuous; could be stripped from dish intact; free film could be creased in alternate directions along the same line about ten times before cracking.

Solution B, Cure I:

0.5–1 mil: Clear, cracked; could not be creased.

1.5–4 mils: Small clear brittle pieces.

5–8 mils: Brittle pieces with yellow powder on under side.

Solution B, Cure II:

< 1 mil: Clear, continuous; dish could be creased without cracking film; could not be stripped from dish.

1.5–2.5 mils: Clear, continuous; could be stripped from dish intact; free film could be creased in alternate directions one to five times before cracking.

4 mils: Clear, brittle, badly cracked.

The films that could be stripped from the dishes were baked for 18 hr. at 300°C. in air. There was no apparent change in appearance or flexibility.

Comparison of Polymers

A series of polymers was made by slow addition of PMDA to solutions of various diamines in DMAC until the viscosity was judged to be at, or near, a maximum. The concentration of resin was chosen to give a viscosity of 1000–5000 cstokes. It varied from 7 to 20%, depending upon the diamine used. A sample of each solution was diluted to 0.5% solids with DMAC and the inherent viscosity was determined at 25.0°C.

Films were cast in 55 mm. diameter aluminum dishes, using sufficient

solution to give 0.1 g. of resin (film thickness = ca. 1 mil). The curing schedule was as follows:

24 hr. at 50°C. in vacuum
1 hr. at 100°C. in air
1 hr. at 150°C. in air
1 hr. at 200°C. in air
2 hr. at 250°C. in air
2 hr. at 300°C. in air

One sample of each resin was creased and flexed to determine its film-forming ability. Two other samples of each were aged at 325°C. in air in a forced-draft oven, and the average weight loss was plotted against time for 400 hr. Values for each 100 hr. of aging were read from the curves. Weight loss, nature of film, and inherent viscosity are given in Table I for the polymers tested.

References

1. Fedotova, O. Y., I. P. Losev, Y. P. Bryzin, and N. F. Pugachevskaya, *Vysokomolekul. Soedin.*, **2**, 899 (1960).
2. Conix, A., *Ind. Eng. Chem.*, **51**, 147 (1959).
3. E. I. du Pont de Nemours and Co., Austral. Pat. Applic. 58424, Case F-661-A/661-B/661-C (1960).
4. Edwards, W. M., and I. M. Robinson, U.S. Pat. 2,710,853 (1955) and 2,867,609 (1959).
5. Hatton, J. V., and R. E. Richards, *Mol. Phys.*, **3**, 253 (1960).
6. Ham, G. E., and A. B. Beindorft, U.S. Pat. 2,811,548 (1957).
7. Wittbecker, E. L., and P. W. Morgan, *J. Polymer Sci.*, **40**, 289 (1959).
8. Morgan, P. W., and S. L. Kwolek, *J. Polymer Sci.*, **40**, 299 (1959).
9. Bender, M. L., Y.-L. Chow, and F. Chloupek, *J. Am. Chem. Soc.*, **80**, 5380 (1958).
10. Flory, P. J., *Principles of Polymer Chemistry*, Cornell Univ. Press, Ithaca, 1953, p. 635.
11. Schmulbach, C. D., and R. S. Drago, *J. Am. Chem. Soc.*, **82**, 4484 (1960).
12. Chinai, S. N., *Ind. Eng. Chem.*, **49**, 303 (1957).
13. van Oehne, H., and L. H. Cragg, *Nature*, **191**, 1160 (1961).

Résumé

On a préparé des polyimides aromatiques en deux étapes. On additionne des dianhydrides pyromellitiques à une solution d'une diamine aromatique dans un solvant de polarité élevée comme le diméthylformamide, le diméthylacétamide, la diméthylsulfoxyde ou la *N*-méthyl-2-pyrrolidone jusqu'à obtention d'un acide polypyromellitamique de haut poids moléculaire. La quantité de dianhydride pyromellitique nécessaire est déterminée par la vitesse d'augmentation de viscosité avec l'addition du réactif et correspond étroitement à la quantité stoéchiométrique. La viscosité intrinsèque des acides polypyromellitamiques dans la diméthylacétamide s'étend de 0.54 à 3.22. En restant à température de chambre; la viscosité de ces solutions décline graduellement. Cette diminution de viscosité de ces solutions s'accélère rapidement par augmentation de température; elle est négligeable à 0°C. L'eau et le dianhydride pyromellitique en excès donne une chute plus rapide dans la viscosité. Les polypyromellitimides sont formées à partir des amides d'acides par chauffage. Le solvant peut être enlevé soit durant l'étape d'imidification ou plus tard sous vide à plus faible température. Les polypyromellitimides sont préparées à partir de *m*-phénylène diamine, de benzidine, d'éther

4,4′-diaminodiphényl, d'éther 3,4′-diaminodiphényl, de sulfure 4,4′-diaminodiphényle, de méthylène dianiline, d'isopropylidène dianiline, de plusieurs diaminobenzanilide, de benzoate de 4,4′-diaminophényle, et d'autres esters et amides aromatiques de faible poids moléculaire de terminaison amine. Les coulées de polyamides en forme de films fins sont pour la plupart claires, souples, flexibles, insolubles et infusibles. Les sections épaisses tendent à etre fragiles et opaques. Plusieurs polymèresven forme de films subissent moins de 10% de perte en poids après usage de 400 heures à 325°C dans l'air. La plupart de ces films sont encore intacts et modérément flexibles après ce traitement.

Zusammenfassung

Aromatische Polyimide wurden in zwei Stufen dargestellt. Pyromellithsäuredianhydrid wurde einer Lösung eines aromatischen Diamins in einem hochpolaren Lösungsmittel, wie Dimethylformamid, Dimethylacetamid, Dimethylsulfoxyd oder *N*-Methyl-2-pyrrolidon, bis zur Bildung eines hochmolekularen Polypyromellithsäureamids zugesetzt. Die erforderliche Menge an Pyromellithsäuredianhydride wurde aus der Geschwindigkeit der Viskositätszunahme beim Zusatz des Reagens bestimmt und entsprach ziemlich genau dem stöchiometrischen Verhältnis. Die Viskositätszahl des Polypyromellithsäureamids in Dimethylacetamid lag im Bereich von 0,54 bis 3,22. Beim Stehen bei Raumtemperatur nimmt die Viskosität der Lösungen allmählich ab. Die Viskositätsabnahme wird durch Temperaturerhöhung stark beschleunigt und ist bei 0°C vernachlässigbar. Wasser und überschüssiges Pyromellithdianhydrid führen zu einer rascheren Viskositätsabnahme. Die Polypyromellithimide wurden aus den Säureamiden durch Erhitzen gebildet. Das Lösungsmittel konnte entweder während der Imidisierung oder schon früher bei niedrigerer Temperatur unter Vakuum entfernt werden. Polypyromellithimide wurden aus *m*-Phenylendiamin, Benzidin, 4,4′-Diaminodiphenyläther, 3,4′-Diaminodiphenyläther, 4,4′-Diaminodiphenylsulfide, Methylendianilin, Isopropylidendianilin, einigen Diaminobenzaniliden, 4,4′-Diaminophenylbenzoat und anderen niedermolekularen Estern und Amiden mit endständiger Aminogruppe dargestellt. Dünne Folien aus Polyimiden waren grösstenteils klar, zähe, biegsam, unlöslich und unschmelzbar. Dicke Abschnitte neigten zur Sprödigkeit und Opazität. Einige Polymerfolien zeigten nach einer Alterung durch 400 Stunden bei 325°C in Luft einen Gewichtsverlust von weniger als 10%. Die meisten Folien waren nach dieser Behandlung noch intakt und zeigten eine gewisse Biegsamkeit.

Received August 7, 1962

JOURNAL OF POLYMER SCIENCE: PART A VOL. 1, PP. 3151-3161 (1963)

Resonance Effect of Amide Group on the Polymerizability of Lactam Derivatives. III. Polymerization of Many-Membered Lactams Ring*

NAOYA OGATA,† *Nagoya Laboratory, Research Department, Toyo Rayon Co., Nagoya, Japan*

Synopsis

The polymerization rate of many-membered lactams in the presence of water and the equilibrium constant of the addition reaction between lactam and hydrogen chloride were measured to investigate the relationship between the conformation, resonance effect, and polymerizability of lactams. The polymerization velocity of lactams in the presence of the same amount of water is in the following order: 8-membered lactam > 7-membered lactam > 11-membered lactam ≫ 5- and 6-membered lactams. The polymerizability reaches a maximum with the 8-membered lactam. The equilibrium constant K of the addition reaction between lactam and hydrogen chloride reaches a maximum with the 7-membered lactam and the basicity of the lactams is highest with the 7- or 8-membered lactam. The conformation of the amide group of the less than 6-membered lactam is a *cis* form, while that of the 6- to 8-membered lactam is a mixture of the *cis* and *trans* forms, and an equal number of *cis* and *trans* forms is found in the 8-membered lactam in the infrared spectrum. From these results it is concluded that when the two conformations of the amide group become equal, the resonance effect of the amide group decreases, resulting in an increase in the polymerizability of lactam.

INTRODUCTION

It is known[1] that an amide group has a planar structure which causes two rotational isomers, the *trans* and *cis* isomers. The *trans* form is more stable than the *cis* form.[2] It is said[1] that the conformation of the amide group of lactams having rings of less than 7 members is the *cis* form, while lactams with rings of more than 8 members are of the *trans* form because of the increase in freedom of chain conformation.

The conformation of amide groups among the 6- and 9-membered lactams is expected to be a mixture of both *trans* and *cis*. As the resonance effect of the amide group is affected by the conformation, the polymerizability of lactams should be influenced by the conformation as well as by the strain of ring. In this work lactams having many-membered rings have been synthesized and the polymerizability of lactams has been systematically investigated.

* For Part II, see Ogata, N., *Bull. Chem. Soc. Japan*, **34**, 248 (1961).

† Present address: Polytechnic Institute of Brooklyn, Brooklyn, New York.

EXPERIMENTAL

Synthesis of Many-Membered Lactams

Lactams of 5, 6, and 7-Membered Rings

Commercial α-pyrollidone, α-piperidone, and ϵ-caprolactam were purified by fractional distillation in the presence of a small amount of sodium hydroxide.

Lactam of 8-Membered Ring

Cycloheptanone was synthesized[3] by the reaction of cyclohexanone with diazomethane, and was transformed into ζ-enantholactam by oxime formation followed by a Beckmann rearrangement.[4]

Lactam of 11-Membered Ring

Ring oxyketone was synthesized[5] from ethyl ester of dibasic acid by means of acyloin synthesis. The lactam was synthesized by reduction of the oxyketone to the ketone, followed by oxime formation and Beckmann rearrangement, as shown in the following equations.

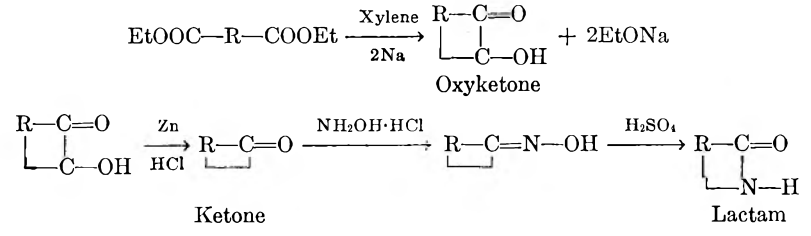

It is necessary in the acyloin synthesis to stir the reaction medium vigorously in order to disperse metallic sodium colloidally. Therefore, the acyloin synthesis was carried out in a steel reaction vessel with a high-speed stirrer, shown in Figure 1.

Synthesis of Oxyketone. A 1450 ml. portion of purified xylene and 83 g. (3.6 moles) of metallic sodium were put into a reaction vessel under prepurified nitrogen. By refluxing the xylene and stirring at 4,000–5,000 rpm for 15 min., sodium was dispersed colloidally. A mixed solution of 206 g. (0.8 mole) of ethyl sebacate in 900 ml. of xylene was added dropwise over a period of 27 hr. under nitrogen atmosphere, followed by stirring at 3,000–3,500 rpm for 1 hr. after the addition of the solution. After cooling the reaction product with ice, a mixed solution of 220 ml. of glacial acetic acid and 220 ml. of xylene was added dropwise over a period of 30–40 min. The whole solution was then diluted with 500 ml. of water and filtered. The xylene solution was separated from the aqueous phase. The aqueous solution was washed with 100 ml. of xylene. The xylene solutions were combined, dried over magnesium sulfate, and then distilled under vacuum. Sebacoin: b.p. = 115–180°C. at 6–9 mm Hg; yield 34.5 g. (25%), n_D^{25} = 1.4940.

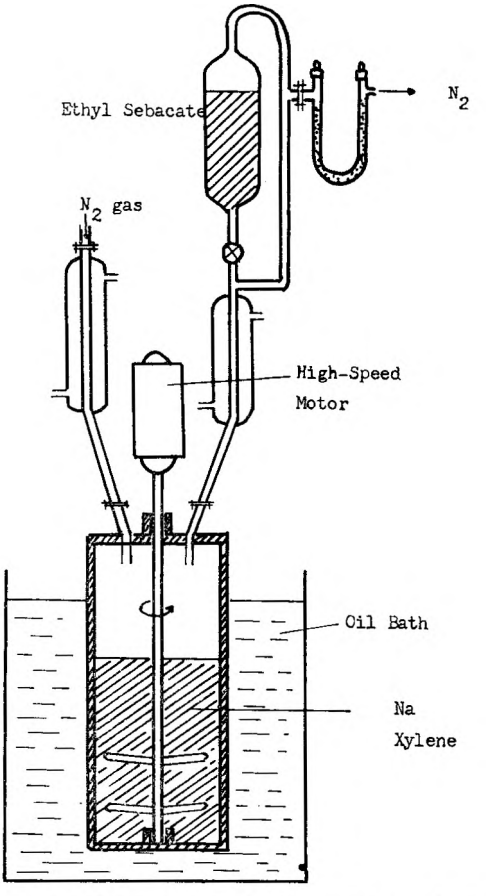

Fig. 1. Reaction apparatus for the acyloin synthesis.

Reduction of Oxyketone. A 32.5 g. (0.5 mole) portion of zinc powder, 80 g. (1.3 moles) of glacial acetic acid, and 34 g. (0.2 mole) of sebacoin were placed in a four-necked flask which was heated at 75–80°C. in an oil bath, and 72 ml. of concentrated HCl was added dropwise with stirring over a period of 10 min. After 30 min., 72 ml. more of concentrated HCl was added, and the whole solution was stirred for 1 hr. The supernatant was decanted and the residue washed twice with 250 ml. portions of ether. The supernatant was diluted with 560 ml. of water saturated with NaCl and washed 4 times with 250 ml. portions of ether.

The ether extracts of the residue and the supernatant were combined and washed with 250 ml. of water saturated with NaCl, then washed three times with a 10% Na_2CO_3 solution and finally washed with 250 ml. of water saturated with NaCl. The ether solution was dried over magnesium sulfate and distilled. Cyclodecanone: b.p. = 96–115°C. at 16 mm. Hg; yield 12.2 g. (39.5%) n_D^{25} = 1.4820–1.4832.

Synthesis of Lactam. A 43 g. (0.28 mole) portion of cyclodecanone, 22 g. (0.315 mole) of hydroxylamine hydrochloride, and 75 ml. of ethanol were placed in a 250 ml. three-necked flask, and 60 ml. of an aqueous solution containing 122 g. of K_2CO_3 was added dropwise to the solution. The oximation was done at 50–55°C. for 3 hr. with stirring. Oxime was extracted by chloroform and dried. Cyclodecanone oxime: m.p. = 79.5°C.; yield 38.9 g. (81%).

A 51 g. (0.52 mole) portion of fuming sulfuric acid containing 8% of free SO_3 and an equal amount of cyclohexane were placed in a three-necked flask, and 150 ml. of cyclohexane containing 38 g. (0.225 mole) of cyclodecanone oxime was added over a period of 1 hr., the temperature being kept in the range of 45–50°C. The reaction continued for 2 hr. at the same temperature. After cooling to room temperature, the aqueous solution was separated from the cyclohexane and neutralized with NaOH. Crude lactam was obtained by extracting the neutralized solution with chloroform. Lactam was purified by recrystallization in petroleum ether. ω-Decanolactam: m.p. = 128–135°C.; yield 33 g. (80%).

Polymerization of Lactams

The water content of the lactams was adjusted to the desired amount by adding a certain amount of water to the lactam and measuring the water content by the Karl Fischer method. Lactam in 1 g. portions was placed in tubes and the tubes were sealed under nitrogen and heated at 257°C. for a given period. After the products had been dried in a desiccator over P_2O_5, monomer was extracted by chloroform and the polymers were weighed. The end groups of the polymers and the relative viscosity of the 1% polymer solution in 98% H_2SO_4 were measured.

Basicity of Lactams

Dry hydrogen chloride gas was dissolved in 0.02*M* solutions of many-membered lactams, resulting in a concentration of 0.2–2.0 × 10^{-2} mole/l. of HCl. The equilibrium constant for the following reaction was measured, as reported in the previous paper[6]:

$$—NHCO— + H^+ \overset{K}{\rightleftarrows} —NH_2{}^+CO—$$

RESULTS

Rate of Polymerization of Lactams

The rate of polymerization of many-membered lactams and the analytical results are shown in Figures 2 and 3 and Table I. The polymerization rates of lactams containing the same amount of water are in the following order: ζ-enantholactam (8-membered lactam) > ε-caprolactam (7-membered lactam)> ω-decanolactam (11-membered lactam). α-Pyrollidone

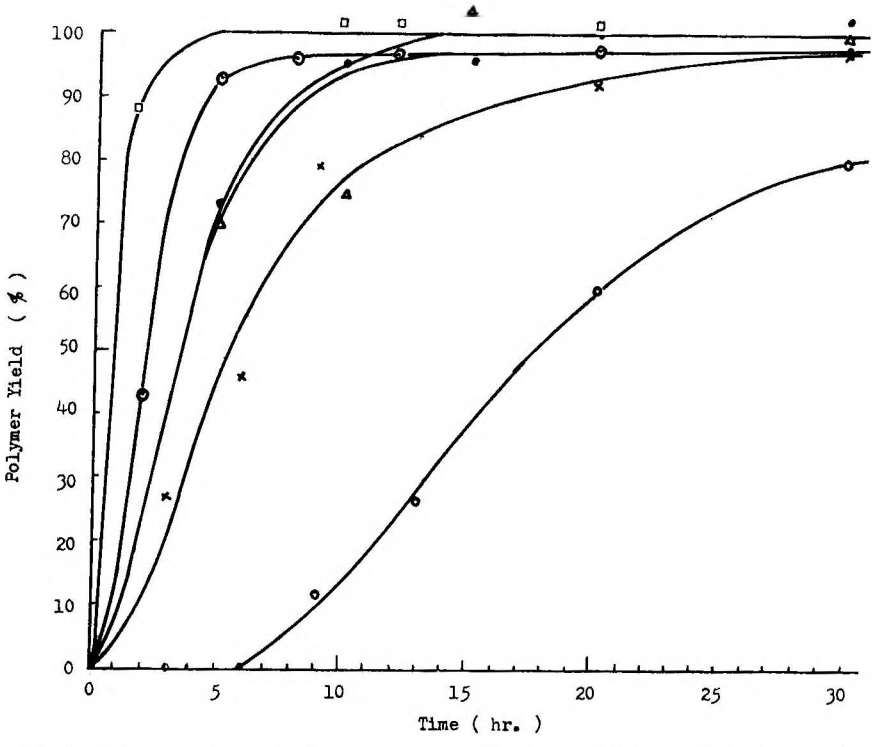

Fig. 2. Polymerization rate of many-membered lactams: (□) ζ-enantholactam, water 1.20%; (⊙) ε-caprolactam, water 1.10%; (●) ε-caprolactam, water 0.54%; (△) ρ-enantholactam, water 0.56%; (×) ζ-enantholactam, water 0.267%; (○) ε-caprolactam, water 0.26%.

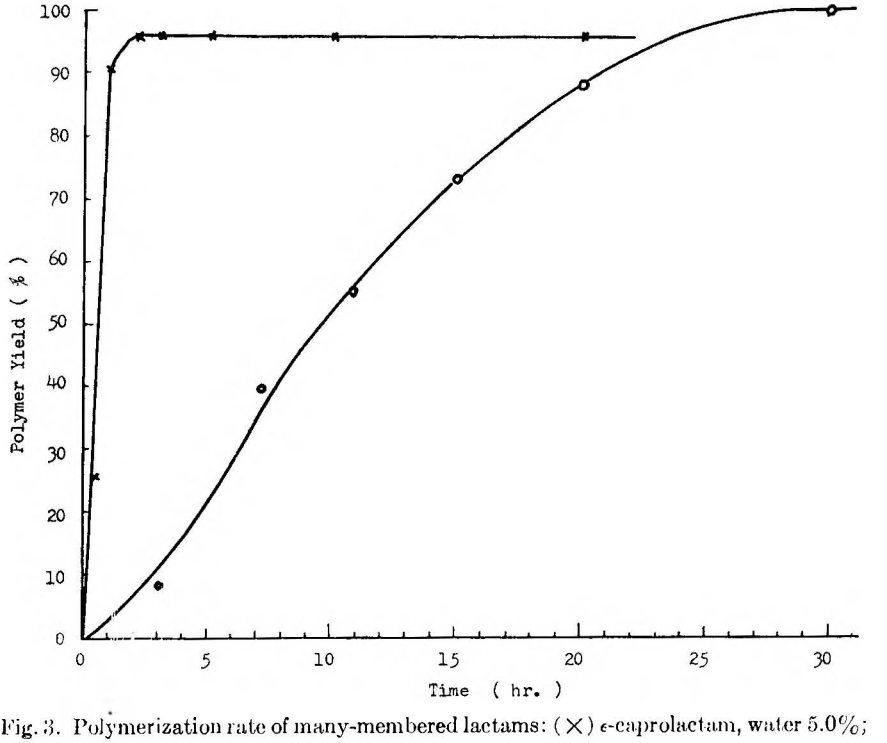

Fig. 3. Polymerization rate of many-membered lactams: (×) ε-caprolactam, water 5.0%; (○) ω-decanolactam, water 5.0%.

TABLE I
Polymerization of Many-Membered Lactams

Water content %	Time, hr.	Polymer, %	η, in H_2SO_4	$-NH_2$, $\times 10^{-3}$ mole/mole	$-COOH$, $\times 10^{-3}$ mole/mole
		α-Pyrollidone			
1.0	50	0	—	—	—
		α-Piperidone			
1.0	50	0	—	—	—
0.26	3	0	—	—	—
	6	0	—	—	—
	9	12.2	—	—	—
	13	26.5	1.68	—	—
	20	60.4	2.36	2.93	8.31
	30	80.0	3.41	2.58	5.38
0.54	5	72.8	2.02	7.49	16.19
	7	—	2.31	6.49	9.64
	10	94.8	2.44	5.65	8.47
	15	96.2	2.49	5.50	8.06
	20	99.6	2.50	5.39	8.16
	30	105.0	2.41	4.95	8.24
		ε-Caprolactam			
1.10	2	42.8	1.69	11.49	—
	5	93.1	2.36	1.51	13.40
	8	96.2	2.47	1.00	12.42
	12	97.0	2.45	0.52	12.24
	20	97.7	2.37	2.79	11.94
	30	96.7	2.40	1.13	12.06
5.00	0.5	25.8	1.13	—	—
	1	90.7	1.50	24.90	23.51
	2	96.4	1.55	21.31	21.02
	3	96.2	1.53	20.92	21.25
	5	96.2	1.53	20.76	21.15
	10	96.0	1.56	20.27	21.00
	20	95.7	1.53	20.71	20.41

(*continued*)

and α-piperidone did not polymerize at all. The difference in the polymerization velocities among these lactams becomes much greater with decreasing water content in lactams. ω-Decanolactam did not polymerize when heated at 257°C. for 50 hr. in the presence of 1 wt.-% of water, while in the presence of 5 wt.-% of water at the same temperature the polymer yield reached 99% in 30 hr. On the other hand, the polymerization of ε-caprolactam in the presence of 5 wt.-% of water reached equilibrium after 2 hr. of heating at 257°C. The polymerization velocity of the 11-membered lactam decreased remarkedly compared with that of the 7-membered lactam.

TABLE I (*continued*)

Water content %	Time, hr.	Polymer, %	η_r in H_3SO_4	$-NH_3$, $\times 10^{-3}$ mole/mole	$-COOH$, $\times 10^{-3}$ mole/mole
		ζ-Enantholactam			
0.27	3	27.2	—	8.62	—
	6	46.1	1.76	—	—
	9	79.4	1.97	5.25	—
	13	83.8	2.24	2.08	12.00
	20	92.3	2.40	1.41	9.88
	30	97.4	2.51	1.15	8.58
0.56	5	70.4	1.76	5.11	21.56
	10	75.1	1.96	3.80	12.82
	15	104.5	1.97	3.66	11.74
	20	103.8	2.05	3.10	11.39
		ζ-Enantholactam			
1.20	2	88.0	1.88	3.10	22.80
	5	101.5	2.05	1.56	17.43
	8	102.2	2.07	2.97	16.95
	12	102.7	2.09	2.19	16.76
	20	101.4	2.09	1.62	16.30
	30	100.7	2.45	0.91	9.10
		ω-Decanolactam			
5.00	3	8.0	—	—	—
	7	40.0	1.32	—	—
	11	54.9	1.42	34.69	31.99
	15	73.0	1.52	29.78	31.32
	20	88.3	1.57	23.93	22.69
	30	99.2	1.59	23.32	24.90

The number of amino groups in the polymers is smaller than that of the carboxyl groups, and the difference becomes greater with decreasing water content, as shown in Table I. The cause is not clear; perhaps it is some deamination reaction. The polymer yield of lactams with more than 8 members reached about 99% and the equilibrium between polymer and monomer shifted toward polymer as the lactam ring enlarged.

Basicity of Lactams

The equilibrium constants K for the addition between the many-membered lactams and hydrogen chloride decrease with enlarging lactam ring, as shown in Tables II and III. Table IV shows the comparison with values for the less than 7-membered lactams and for chain amide compounds. The K value for many-membered lactams reaches a maximum at ε-caprolactam and then decreases, approaching the K value of chain *trans* amide compounds. The heat of the addition reaction becomes lower in the less-membered lactams.

TABLE II. K Values for ζ-Enantholactam–HCl Addition Reaction

Temp., °C.	[HCl], × 10^{-3} mole/l.	Absorb. at 1653 $cm.^{-1}$	[—NH-CO—], × 10^{-2} mole/l.	$[H^+]$, × 10^{-3} mole/l.	$[NH_2$-CO—], × 10^{-2} mole/l.	K	K
20	2.96	0.554	1.80	0.96	0.20	115.8	
	5.76	0.498	1.65	2.26	0.35	93.9	
	11.56	0.373	1.20	3.56	0.80	187.4	
	23.56	0.262	0.85	12.06	1.15	112.2	107
40	2.76	0.572	1.85	1.26	0.15	64.4	
	5.68	0.533	1.75	3.18	0.25	44.9	
	10.92	0.409	1.35	4.42	0.65	109.0	
	22.08	0.280	0.90	11.08	1.10	110.3	82
55	2.72	0.561	1.85	1.22	0.15	66.4	
	5.00	0.514	1.70	2.00	0.30	88.2	
	9.96	0.423	1.40	3.96	0.60	108.2	
	19.84	0.269	0.90	8.84	1.10	138.3	100

TABLE III. K Values for ω-Decanolactam-HCl Addition Reaction

Temp., °C.	[HCl], × 10^{-3} mole/l.	Absorb. at 1660 $cm.^{-1}$	[—NH-CO—], × 10^{-2} mole/l.	$[H^+]$, × 10^{-3} mole/l.	$[—NH_2$-CO—], × 10^{-2} mole/l.	K	$\bar{K}$
20	8.76	0.331	1.20	6.42	0.50	91.7	
	13.42	0.266	1.20	9.54	0.70	90.9	
	17.04	0.277	1.10	6.28	0.75	65.6	83
40	2.44	0.409	1.80	1.44	0.10	38.6	
	4.60	0.385	1.70	2.60	0.20	45.3	
	9.20	0.335	1.50	5.20	0.40	51.3	
	18.20	0.288	1.25	11.70	0.65	44.5	45
60	2.60	0.382	1.70	1.60	0.10	36.8	
	4.84	0.366	1.60	2.84	0.20	44.0	
	9.56	0.328	1.45	4.06	0.55	93.4	
	18.44	0.287	1.25	10.94	0.75	54.9	45

TABLE IV. K Values of Various Amide Compounds and Heat of Reaction

Amide compound	K 20°C.	K 40°C.	K 55°C.	$-\Delta H$, kcal./mole
α-Pyrollidone	159	68	—	7.64
α-Piperidone	164	79	—	6.58
ε-Caprolactam	177	124	91	3.15
ζ-Enantholactam	107	82	82	1.63
ω-Decanolactam	83	45	45	3.70
N-Methyl-α-piperidone	49	38	—	2.34
N-Methyl-ε-caprolactam	35	20	12	5.12
N,*N*-Dibutylacetamide	35	22	—	4.14
N-Hexylacetamide	58	48	—	2.16

DISCUSSION

It is well known that 5- or 6-membered ring compounds are remarkedly stable compared with other ring compounds, owing to less strain in bond angles. α-Pyrollidone and α-Piperidone do not polymerize at all by the usual method used commercially for ε-caprolactam.

When a ring compound contains an amide group within the ring, the steric conformation of the amide group influences the resonance effect, resulting in a change of the stability of ring structure. In the previous paper[6] the increase in the stability of the lactam ring caused by *N*-methylation was explained by the resonance effect of the amide group.

It is said[1] that the conformation of the amide group consisting of less than 7-membered lactams is *cis*, while that of the more than 8-membered lactams is *trans*, the form preferred in chain amide compounds because of the increase in freedom of movement of the chain within the chain. Strong support for deciding the conformation of the amide group is obtained by measuring the infrared spectrum in a region of the N—H stretching vibration.

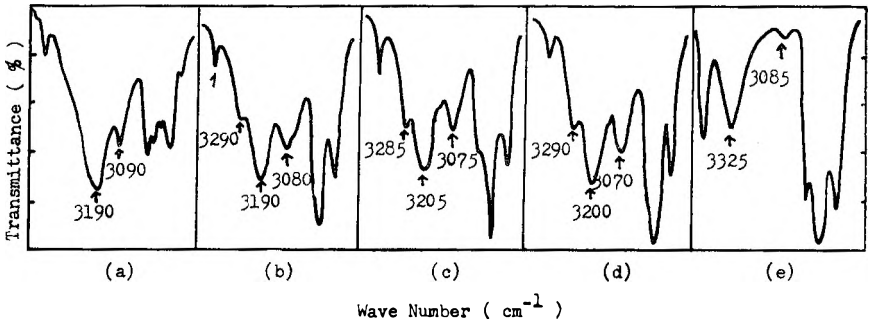

Fig. 4. N—H absorption bands (wave numbers in cm.$^{-1}$) of various lactams (concentration of lactams = 0.6 mole/l. CCl_4): (*a*) α-pyrollidone; (*b*) α-piperidone; (*c*) ε-caprolactam; (*d*) ζ-enantholactam; (*e*) ω-decanolactam.

The infrared spectra of various lactams were measured in the region of 4,000 to 3,000 cm.$^{-1}$ with a LiF prism. Results are shown in Figure 4. The N—H absorption band due to the *cis* amide, which usually appears at about 3,200 cm.$^{-1}$, is found in α-pyrollidone, while a shoulder absorption appears at 3,290 cm.$^{-1}$ near the 3,290 cm.$^{-1}$ absorption region in the case of α-piperidone. This 3,200 cm.$^{-1}$ absorption becomes stronger in ε-caprolactam; ζ-enantholactam shows the same absorption strength for 3,200 and 3,290 cm.$^{-1}$; and ω-decanolactam has no 3,200 cm.$^{-1}$, but only 3,290 cm.$^{-1}$ absorption which also appears in chain amide compounds, R—CONH—R′, having the *trans* form of the amide group.[7]

From these results it is found that lactams having the less than 6-membered rings contain the *cis* amide, while both *cis* and *trans* amides coexist in

lactams having 6- to 8-membered rings. According to the absorption strength, ϵ-caprolactam and ζ-enantholactam are expected to have almost the same number of the *cis* forms as *trans* forms of the amide group.

That the polymerization velocity of ζ-enantholactam is the greatest among the lactams may be ascribed to the decrease in the resonance effect of the amide group, caused by the random conformation of the amide group. This is also supported by the result that the basicity of lactams reaches a maximum with 7- and 8-membered lactams. As the conformation of the amide groups shifts toward the *trans* form with enlarging ring size, the stability of the ring increases again, owing to the increase in the resonance effect of the amide groups; this is seen in the much slower polymerization rate of ω-decanolactam.

The equilibrium constants of the following reaction are shown in Table V.

$$—NHCO— + H_2O \overset{K}{\rightleftharpoons} —NH_2 + —COOH$$

TABLE V
Equilibrium Constant between Polyamide and Water

Fundamental struct. unit	Water content, %	K	$\bar{K}$
ϵ-Caprolactam	0.54	480	
	1.10	440	
	5.00	610	510
ζ-Enantholactam	0.27	208	
	0.56	275	
	1.20	284	260
ω-Decanolactam	5.00	770	700

The values of K fluctuate somewhat but are similar to those of nylon 6, 66, and 610.[8-10] The chemical equilibrium between polymer and water is not affected by the change in the fundamental structural unit.

Grateful acknowledgement is made to Dr. H. Kobayashi for permission to publish this work. The author is indebted to Messrs. M. Nakata and T. Ishikawa for their cooperation in carrying out the experiments.

References

1. Huisgen, R., H. Walz, *Chem. Ber.*, **89**, 2616 (1956).
2. Mizushima, S., et al., *J. Am. Chem. Soc.*, **72**, 3490 (1950).
3. Doering, W. E., and D. B. Denney, *J. Am. Chem. Soc.*, **77**, 4619 (1955).
4. Coffman, D. D., et al., *J. Polymer Sci.*, **3**, 85 (1948).
5. Prelog, V., et al., *Helv. Chim. Acta*, **30**, 1741 (1947).
6. Ogata, N., *Bull. Chem. Soc. Japan*, **34**, 245, 248 (1961).
7. Tsuboi, M., *Bull. Chem. Soc. Japan*, **22**, 215 (1949).
8. Fukumoto, O., *J. Polymer Sci.*, **22**, 263 (1956).
9. Ogata, N., *Makromol. Chem.*, **42**, 52 (1960).
10. Fukumoto, O., *Chem. High Polymer (Tokyo)*, **18**, 25 (1961).

Résumé

La vitesse de polymérisation des lactams à plusieurs membres en présence d'eau et la constante d'équilibre de la réaction secondaire entre le lactame et le chlorure d'hydrogène ont été mesurées pour trouver la relation entre la conformation du monomère, l'effet de résonance et l'aptitude des lactames à polymériser. La vitesse de polymérisation de ces lactames en présence de la même quantité d'eau, decroit dans l'ordre suivant: lactames à 8 membres > lactames à 7 membres > lactames à 11 membres ≫ lactames à 5 et 6 membres. La polymérisation atteint un maximum chez le lactame à 8 membres. La constante d'équilibre, K, de la réaction secondaire, entre le lactame et le chlorure d'hydrogène, atteint un maximum chez le lactame à 7 membres et ce sont les lactames à 7 et 8 membres qui ont le caractère le plus basique. La conformation du groupe amide des lactames à moins de 6 membres a la forme *cis*, alors que celle des lactames à 6–8 membres est un mélange de *cis* et *trans* formes. Un nombre équivalent de *cis* et *trans* formes a été trouvé chez les lactames à 8 membres à l'aide du spectre infrarouge. On a pu conclure de ces resultats que lorsque deux conformations du groupe amide deviennent égales l'effet de résonance diminue et l'aptitude à polymérisation des lactames augmente.

Zusammenfassung

Die Polymerisationsgeschwindigkeit von vielgliedrigen Lactamen in Gegenwart von Wasser und die Gleichgewichtskonstante der Additionsreaktion von Lactam und Chlorwasserstoff wurden gemessen, um das Verhältnis zwischen Konformation, Resonanzeffekten und der Polymerisationshfähigkeit der Lactame zu bestimmen. Die Reihenfolge der Polymerisationsgeschwindigkeiten der Lactame in Gegenwart der gleichen Menge Wasser ist die folgende: 8-gliedriges Lactam > 7-gliedriges Lactam > 11-gliedriges Lactam ≫ 5 und 6-gliedrige Lactame. Die Fähigkeit zur Polymerisation hat beim 8-gliedrigen Lactam ein Maximum. Die Gleichgewichtskonstante K der Additionsreaktion zwischen Lactam und Chlorwasserstoff erreicht beim 7-gliedrigen Lactam ein Maximum und die Basizität ist beim 7 order 8-gliedrigen Lactam am höchsten. Die Konformation der Amidgruppe bei kleineren as 6-gliedrigen Lactamen ist die einer *cis*-Form, während bei 6–8-gliedrigen Lactamen eine Mischung von *cis*- und *trans*-Form besteht. Beim 8-gliedrigen Lactam wird durch Infrarotmessungen die gleiche Anzahl von *cis*- und *trans*-Formen gefunden. Aus diesen Ergebnissen muss man folgern, dass der Resonanzeffekt der Amidgruppe abnimmt, wenn *cis*- und *trans*-Formen in gleicher Menge in Polymeren vorkommen. Mit der Abnahme der Resonanz steigt die Polymerisationsfähigkeit der Lactame.

Received August 7, 1962

JOURNAL OF POLYMER SCIENCE: PART A VOL. 1, PP. 3163-3173 (1963)

Zone-Refining Fractionation of Polymers

JOSEPH D. LOCONTI and JOHN W. CAHILL,* *Pioneering Research Division, Quartermaster Research and Engineering Center, U.S. Army, Natick, Massachusetts*

Synopsis

The unidirectional freezing of dilute solutions of polystyrene in benzene yields a frozen charge with a high concentration gradient, low in the first part frozen and highest in the last. A substantial heterogeneity in molecular weights is also noted, the highest molecular weight being found in the first part and progressively lower molecular weights toward the terminal end of the charge. Both concentration and molecular weight changes are strongly dependent upon freezing rate, low rates favoring maximum concentration changes and intermediate rates favoring maximum molecular weight separation. The application of these observations to a polymer fractionation system is reported.

In 1952, W. G. Pfann[1] invented the excellent zone-refining process for the production of extremely pure semiconductor materials required in the manufacture of transistors. The method is based on the principle that a soluble impurity in a material will distribute itself between the solid and liquid phases of that material in a certain ratio, the distribution ratio, which generally differs from unity. If, for example, impure germanium is melted and a portion of it allowed to solidify slowly, the concentration of impurity in the molten phase is usually higher than that in the solid phase. This is the principle by which materials are purified by fractional crystallization.

In his method Pfann melted a narrow zone at one end of an elongated ingot of impure germanium by means of an encircling ring-shaped induction heater. By slowly moving the heater toward the other end of the ingot the molten zone was caused to move with it as germanium melted at the leading interface and solidified at the trailing face. Because the concentration of impurity was somewhat higher in the molten zone than in the trailing crystallized phase, a single pass of the heater resulted in the net transfer of a small amount of impurity to the end of the ingot. Repeated passes of the heater caused additional increments of impurity to be moved to the end of the charge. In this manner it was possible to obtain germanium with less than 1 part of impurity in 10 billion.

The ability of the zone-refining process to achieve such high degrees of purity shows it to have a very fine sense of discrimination between molecular species. If such a process could distinguish between adjacent molecular-

* Present address: Globe Manufacturing Co., Fall River, Massachusetts.

weight species of a polymer it would serve as a new method of fractionating polymers.

If we zone-refine a dilute solution of polymer in a solid solvent, we have a system analogous to that of germanium and its impurity, the solvent being the germanium counterpart while polymer represents impurity. We would expect polymer to move with the molten zone (or in the opposite direction if its distribution coefficient, defined as the ratio of concentrations of solute in the solid to the molten phases, is greater than unity). There is one important difference, however. The polymer, consisting of a large number of different molecular-weight species, should behave not as a single impurity but as a mixture of impurities. Each of these molecular species should have its own distribution coefficient differing from those of its neighbors, and therefore each should migrate with the molten zone at a different rate. If the differences in these distribution coefficients is finite, then there should be a theoretical basis, at least, for the occurrence of separation. Cutting up the ingot in sections should then give different molecular-weight fractions. That this does happen has been shown by Peaker and Robb[2] and by ourselves,[3] with different systems. Peaker and Robb zone-refined a solution of polystyrene in naphthalene and showed molecular weight differences in different parts of the naphthalene ingot by turbidity measurements. Our work showed substantial separation in single-stage freezing of benzene solutions of polystyrene. In the present work we report the results of our studies of the dependence of the distribution coefficient on molecular weight and of the fractionation of polystyrene in frozen benzene by zone-refining and normal freezing methods.

Experimental

Two experimental procedures were used. The zone-refining separations were carried out with an automatic zone melter patterned after one built at the National Bureau of Standards,[4] with certain modifications. It consisted of a motor-driven heater carriage which could be moved slowly along a track to a predetermined point, from which it was rapidly returned automatically to the starting point for a repeat cycle. The length, direction, and speed of a pass could be varied at will. The carriage carried one or more ring heaters which encircled the charge contained in a 1 in. i.d. $\times$ 20 in. long glass tube. During the course of zone refining the tube rotated slowly so that a uniform molten zone was maintained. A Teflon catheter, sealed at one end, was inserted along the axis of the tube. This relieved pressure buildup caused by liquid expansion and thus prevented breakage of the glass tube. Separations were conducted in a -20°C. refrigerator, to keep the benzene solution solid during zone refining.

The tube was charged with pure benzene and frozen to a height of 19 in. The remaining 1 in. was filled with a 5% solution of polystyrene in benzene, which was then also frozen. Zone melting was started at the end of the tube containing polymer. The zone width was 1 in. and the rate of travel was 2 in./hr.

TABLE I
Molecular Weights of Monodisperse Polystyrenes

Sample no.	$\bar{M}_n$ (McCormick ultracentrifuge)	$\bar{M}_w/M_n$ (McCormick)	$\bar{M}_w$ (single point)
S102	82,000	1.05	80,000
S105	153,000	1.04	155,000
S108	267,000	1.08	260,000
S1159	570,000	1.09	590,000

Measurement of distribution coefficients was made by the normal freezing technique. In this method a $^5/_8$-in. i.d. × 14 in. long glass tube filled with a 0.3% solution of polystyrene in benzene was lowered at the rate of 1.25 in./hr. into an alcohol-dry ice bath until the entire charge was solidified. The liquid phase was continuously stirred, to maintain homogeneity. The solidified charge was then removed from the tube and cut into sections, and the polystyrene concentrations in the various fractions were determined by evaporation of the solvent. When desired, molecular weight measurements were made on these same fractions. In some experiments the freezing rate was varied between 0.2 and 4.8 in./hr.

When normal freezing was used specifically as a fractionation procedure a 1 $^3/_8$ in. i.d. × 24 in. tube was employed. This was filled to a height of 10 in. with a 0.05% solution of polystyrene in benzene. As freezing progressed, benzene was continuously added with a constant-level device, to maintain a 10 in. liquid layer. When the tube became filled, benzene addition was stopped but freezing was continued until the entire charge was frozen. Since the frozen portion of the charge always had a lower concentration of polymer than the liquid phase from which it was frozen, continuous addition of solvent prevented polymer buildup in the liquid phase. This was necessary, since increased concentration appeared to impair fractionation efficiency.

The polystyrenes used in this work were Dow Styron 666-K27, having a weight-average molecular weight of 305,000, and four monodisperse polystyrenes obtained from Dr. H. W. McCormick of The Dow Chemical Company. The latter were prepared by the Szwarc anionic polymerization technique and had the molecular weights given in Table I.

Viscosities of the fractionated samples were measured at 30°C. in toluene at a single concentration of about 0.3%. Intrinsic viscosities were calculated according to Hart,[5] and molecular weights from the data of Alfrey et al.[6] The validity of this short-cut procedure was confirmed by the excellent agreement between our values and McCormick's ultracentrifuge values (Table I).

Results and Discussion

The key to a successful molecular weight separation of polymers by a zone-refining process lies in the existence of a finite dependence of distribu-

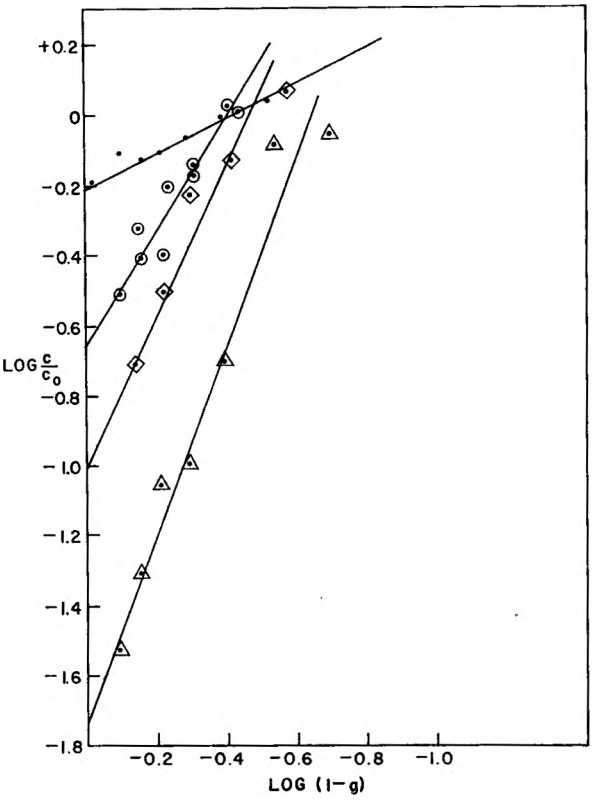

Fig. 1. Polystyrene concentration versus fraction of charge solidified during normal freezing: (●) MW 570,000; (⊙) MW 267,000; (⊡) MW 153,000; (◬) MW 82,000.

tion coefficient on molecular weight. Four nearly monodisperse polystyrenes were, therefore, subjected to normal freezing at the rate of 1.25 in./hr. and the concentration of polymer along the charge was determined. Figure 1 shows the curves for polymer concentration versus fraction of charge solidified. Segregation caused by normal freezing is described by the equations.[7]

$$C = kC_0 (1 - g)^{k-1}$$

$$\log C/C_0 = \log k + (k - 1)\log(1 - g)$$

where C = concentration of polystyrene in the frozen benzene at a point where fraction g of the original solution has been solidified, C_0 = original polystyrene concentration, and k = effective distribution coefficient; when $g = 0$, then $C/C_0 = k$.

Thus, extrapolation of the curves to zero gives k directly. These k values, plotted against molecular weight in Figure 2, reveal an unexpectedly great molecular weight dependence, up to about half a million, and immediately suggests that fractionation should occur most readily below

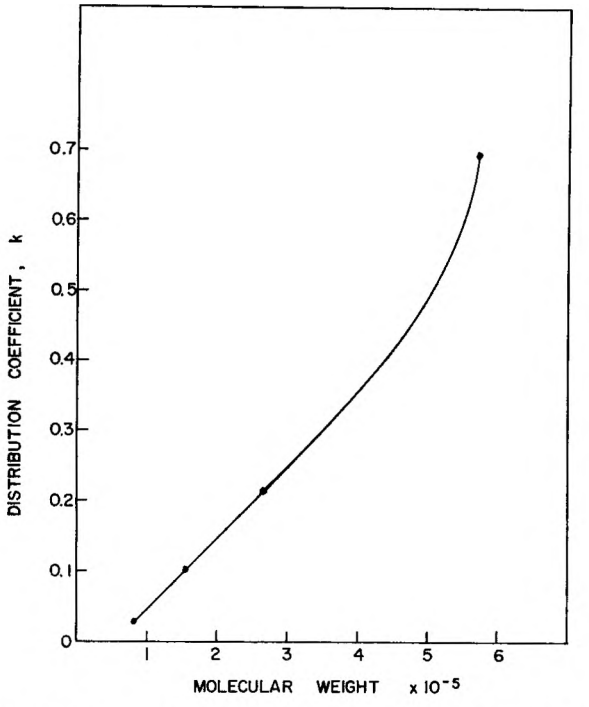

Fig. 2. Dependence of distribution coefficient on molecular weight.

500,000. In fact, it tells us that it would be difficult to maintain homogeneity during the freezing of a solution of polystyrene in benzene.

Ideally, measurement of distribution coefficients should be made on single molecular species. Since these are not available for high molecular weight polymers, samples of narrow molecular weight distribution were used. Thus, the coefficients are due to a limited range of molecular species. The presence of molecules of a size smaller than the average will result in lower values, while larger species will have the opposite effect. These will at least in part cancel, but it is not possible with the data available to determine the precise effect. Certainly the shape of the molecular distribution curve will be important.

Because of the marked dependence of k on molecular weight, fractionation was expected during the single-stage freezing process. This was shown to occur[3] for a broad distribution polystyrene with a molecular weight of 305,000. Separation was achieved up to MW 400,000, beyond which no further fractionation was observed. That molecular weights above 400,000 are separable in this system was shown by the fractionation of a similar polystyrene of MW 530,000. In this instance fractions were obtained in the range of 400,000–750,000, but molecular species above or below this range were not observed although known to be present.

When the normal freezing process was applied to one of the monodisperse polystyrenes, separation was obtained as shown in Figure 3. The distribu-

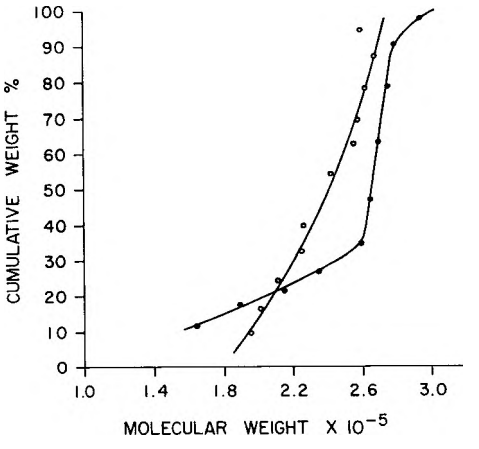

Fig. 3. Fractionation of nearly monodisperse polystyrene, MW 267,000: (O) normal freezing fractionation; (●) chromatographic fractionation.

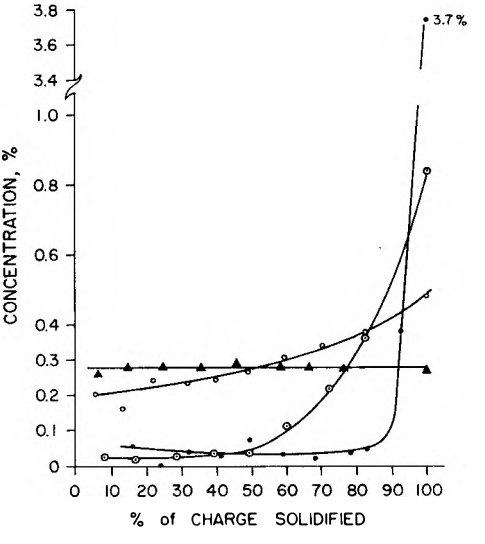

Fig. 4. Effect of normal freezing rate on polystyrene concentration: (●) MW 570,000, 0.2 in./hr., $k \cong 0$; (⊙) MW 82,000, 1.25 in./hr., $k = 0.027$; (O) MW 570,000, 1.25 in./hr., $k = 0.70$; (▲) MW 82,000, 4.8 in./hr., $k = 1.0$.

tion obtained on the same sample by thermal gradient chromatographic fractionation is also shown for comparison. The freezing process is not as efficient as the chromatographic method but, considering it is a single-pass process, the amount of separation achieved is considerable.

It must be emphasized that the distribution coefficients and the separations just discussed have been obtained at a freezing rate of 1.25 in./hr. and are to be regarded as effective or apparent distribution coefficients. These values, both absolutely and probably relatively, will change with freezing rate. If the rate is extremely slow, the k values for different

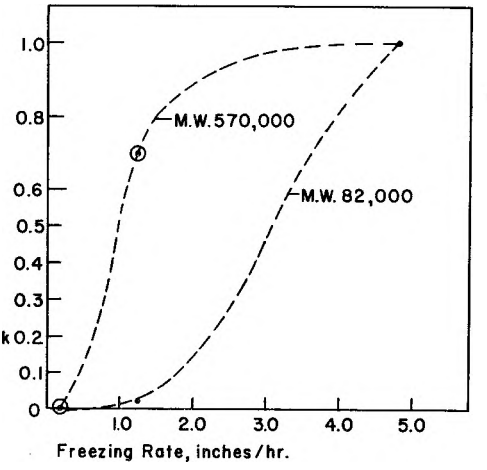

Fig. 5. Effect of freezing rate on k values for different molecular weights.

molecular weights will approach zero, while at high freezing rates they approach unity. The true distribution coefficient is an equilibrium value which is not attained in any of the experiments in this report. It appears that the true coefficient is very close to zero for all molecular species and, therefore, very slow freezing under conditions approaching equilibrium would result in little or no separation.

This effect is shown in Figure 4, in which concentration of polystyrene is plotted against distance along the charge for different freezing rates, starting with 0.3% solutions in benzene. When a sample of MW 82,000 is frozen at the fast rate of 4.8 in./hr. there is no concentration change along the charge and, accordingly, $k = 1$. When the freezing rate is dropped to 1.25 in./hr. the freezing benzene has time to reject much polymer, with a resultant $k = 0.027$, while at 0.2 in./hr. k is expected to be approximately zero.

When a solution of 570,000 MW polymer is frozen at the rate of 1.25 in./hr. we find that much more is entrapped by the freezing benzene than in the comparable low molecular weight run. At 0.2 in./hr. the k for 570,000 is approximately zero and at 4.8 in./hr. it would be close to unity.

Figure 5 shows limited data of k values versus freezing rate for these two polymers. Freezing rates between 1.25 and 2.25 in./hr. appear to be optimal for the separation of these samples.

Since fractionation is dependent upon molecular weight, freezing rate, and concentration, a system of separation was devised to take advantage of these parameters. For a broad distribution polymer it is evident that a given freezing rate will be optimal for one molecular species but progressively poorer for molecular weights further removed from this. Ideally, a continuously changing freezing rate would give a better separation than would a single rate. Starting with an initially low freezing rate, the higher molecular weights would be preferentially entrapped in the solid phase. As

these are removed and the freezing rate slowly increases, succeeding higher molecular weights would be entrapped. Perhaps the best separation could be achieved by using a rate of change in freezing which corresponds exactly to the optimum for the various molecular species present. This, of course, means one should have the answer before solving the problem.

As an initial step in this direction, an experiment was conducted in which freezing rate was continuously varied linearly with time. This was done with a cone-shaped pulley having a spirally wound groove. The cord which was attached to the tube containing polymer solution was wound along this groove. Thus, as the clock unwound the cord, the tube was lowered into the freezing bath initially at the rate of 0.2 in./hr. and

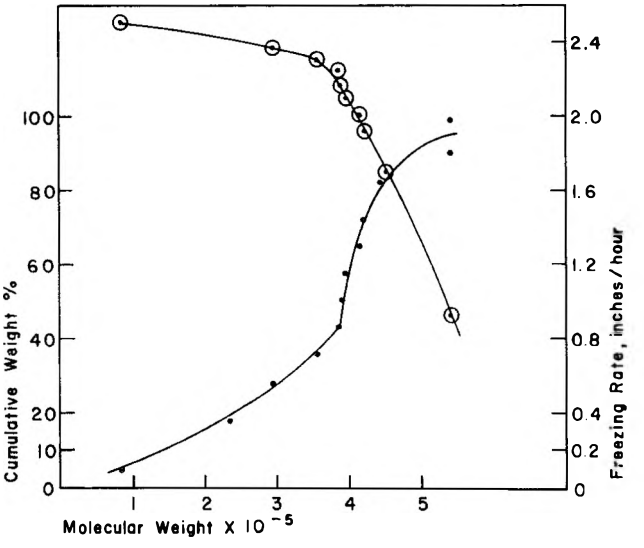

Fig. 6. Normal freezing fractionation with variable freezing rate: (⊙) right ordinate; (●) left ordinate.

terminally at the rate of 2.5 in./hr. In this way most of the polymer was initially rejected by the freezing benzene but, as the rate increased, first the highest, and then successively lower molecular weights, were selectively entrapped.

In addition to the changing freezing rate, solvent was continuously added as freezing progressed. In previous experiments it was shown that polymer concentration built up in the last 10% of the charge frozen, even in those experiments in which fractionation was achieved. Since fractionation efficiency was poorer at higher concentrations, solvent was added to prevent the buildup. This was done by means of a separatory funnel which fed solvent into the tube as soon as the liquid level fell below the outlet tube of the funnel.

The results of this fractionation are shown in Figure 6 for Styron 666-K27. Compared with the fractionation previously reported,[3] an improved

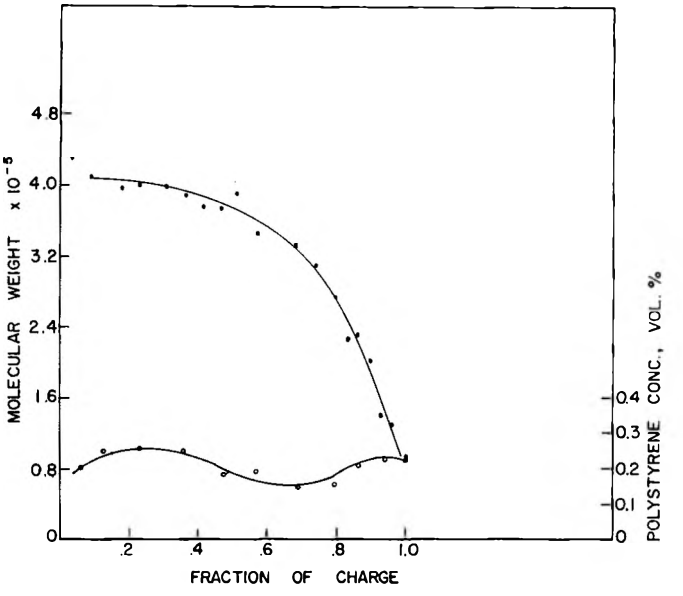

Fig. 7. Zone refining fractionation of Dow Styron, MW 305,000, ten passes: (O) left ordinate; (●) right ordinate.

separation is obtained by continuously changing the freezing rate and by addition of solvent.

Figure 7 shows the separation achieved by the zone-refining method on a broad distribution polystyrene. This was the same polymer fractionated by the normal freezing method shown in Figure 6. The lower curve gives the concentration of polymer along the charge after ten passes of the molten zone. Initially, the polymer concentration was 5% in the first 5% of the charge, while the remaining 95% of the charge was pure benzene.

In the upper curve molecular weight is plotted as a function of distance along the charge. The range of molecular weights, 100,000 to 400,000, is quite similar to that obtained by the single-stage normal freezing method. In considering why ten passes in the zone-refining method gave no better separation than the freezing method one must look at the mechanics of the former. A sharp narrow zone enhances separation. This was not achieved but, rather, a somewhat broad, irregular cone-shaped zone was observed. Equilibrium of the solute between the liquid and solid phases was not attained probably because of inadequate mixing in the molten zone. Finally, speeds other than the 2 in./hr. used may improve fractionation, especially if a speed gradient, slow at first and gradually increasing in the latter stages, is used. It is probable that improving experimental conditions will result in greatly enhanced fractionation.

The dependence of k upon freezing rate raises the question of the actual mechanism involved in the movement of polymer molecules. If the

migration is due to differences in solubility of polymer between the liquid and solid phases of benzene, then concentration equilibrium plays a part. Maintaining the equilibrium, as presumably is done by stirring during normal freezing, should yield a k which is independent of freezing rate. If, however, a thin liquid layer at the solid interface does not enter into mixing with the rest of the liquid phase, a concentration gradient would be formed across this layer. This would cause k to vary with freezing rate.

A second possible mechanism is the occurrence of thermal diffusion at the solid–liquid interface. While stirring would minimize diffusion, the existence of a stable liquid layer would decrease the effectiveness of stirring. Thus, ordinary diffusion could occur through this liquid layer. Since there is a temperature difference between the liquid and solid phases, thermal diffusion can also occur. In such an instance the higher molecular species would preferentially migrate to the cold surface.

Fractionation may also occur because of chain entanglement and chain trapping. A segment of a polymer chain may become mechanically entrapped or adsorbed on the actively growing crystal front. Slow freezing makes escape more probable and therefore leads to low k values. Since the probability of entrapment increases with the number of segments in the molecule and the probability of escape decreases with increasing molecular weight because of slower diffusion rate, the preferential freezing out of the higher molecular species is favored. Further, when one molecule becomes firmly entrapped it may be entangled with a second molecule. The probability of initial entanglement and subsequent escape is dependent on molecular weight.

All these mechanisms are consistent with the observed dependence of the distribution coefficient on freezing rate and the fact that the freezing front incorporates the larger molecules first.

References

1. Pfann, W. G., *Trans. Am. Inst. Mining Met. Eng.*, **194**, 747 (1952).
2. Peaker, F. W., and J. C. Robb, *Nature*, **182**, 1591 (1958).
3. Loconti, J. D., and J. W. Cahill, *J. Polymer Sci.*, **49**, S2 (1961).
4. Natl. Bur. Std. *U. S. Tech. News Bull.*, **39**, 81 (1955).
5. Hart, V. E., *J. Polymer Sci.*, **17**, 215 (1955).
6. Alfrey, T., A. Bartovics, and H. Mark, *J. Am. Chem. Soc.*, **65**, 2319 (1943).
7. Pfann, W. G., *Zone Melting*, Wiley, New York, 1958, p. 19.

Résumé

La congélation en une seule direction des solutions diluées benzéniques de polystyrène produisent une charge congelée à gradient de concentration important, bas dans la première partie congelée et le plus élevé dans la dernière partie. Une hétérogénéité substancielle a été également constatée pour les poids moléculaires; les poids moléculaires les plus élevés se retrouvent dans la première partie et les poids moléculaires décroissent progressivement vers la partie terminale de la charge. Tant la concentration que les variations de poids moléculaire dépendent fortement de la vitesse de congélation; des vitesse faibles favorisent des variations maxima de concentration; des vitesse intermédiaires favorisent la séparation maximum des poids moléculaire. L'attention

est attirée sur l'application de ces observations au fractionnement d'un système polymérique.

Zusammenfassung

Das gerichtete Gefrieren von verdünnten Polystyrollösungen in Benzol liefert eine gefrorene Masse mit einem hohen Konzentrations-gradienten, wobei die Konzentration im zuerst gefrorenen Teil niedrig und im zueletzt gefrorenen Teil am höchsten ist. Auch eine merkliche Molekulargewichtsheterogenität wurde festgestellt; das höchste Molekulargewicht fand sich im ersten Teil und fortschreitend niedrigere Molekulargewichte gegen das Ende der gefrorenen Masse. Sowohl Konzentrations- als auch Molekulargewichtsänderungen hängen weitgehend von der Gefriergeschwindigkeit ab; kleine Geschwindigkeiten sind für eine maximale Konzentrationsänderung günstig, mittlere Geschwindigkeiten begünstigen eine maximale Molekulargewichtstrennung. Die Anwendung der beobachteten Erscheinungen zur Polymerfraktionierung wird beschrieben.

Received August 10, 1962

JOURNAL OF POLYMER SCIENCE: PART A VOL. 1, PP. 3175–3182 (1963)

Evaluation of Molecular Weight Averages Resulting from Random Crosslinking and Chain Scission Processes for Wide Schulz-Zimm Distributions

A. M. KOTLIAR, *Chemicals Research Division, Esso Research and Engineering Company, Linden, New Jersey*

Synopsis

The Monte Carlo sampling technique was used to evaluate the resulting molecular weight averages and the intrinsic viscosity for wide Schulz-Zimm distribution polymers, in the range $\bar{P}_w/\bar{P}_n \leqq 11$, undergoing random chain scission and crosslinking processes. The results may also be used to evaluate the initial distribution and are generally more reliable than the use of fractionation data.

Introduction

The preceding papers[1–7] in this series have evaluated the resulting molecular size distributions, molecular weight averages, and the intrinsic viscosity as a function of random crosslinking and chain-scission processes for narrow initial Schulz-Zimm[8] distributions, i.e., $\bar{P}_w/\bar{P}_n \leqq 2$.

The present work applies the Monte Carlo sampling technique to generate quasi-experimental data of the resulting molecular sizes for wide Schulz-Zimm distributions undergoing random chain scission and crosslinking processes.

Theory I: Random Degradation

When random chain scissions are introduced, the resulting distribution of molecular sizes may be evaluated by playing the following statistical game (Monte Carlo). Two numbers are selected at random, ϕ (molecular size) and θ (weighing factor) from a population equidistributed in the range 0–1. The operation will be considered a success if θ is less than $g(\phi)$, the distribution function under which a choice is to be made; otherwise it is a failure. Since the probability that a molecule of size P will be involved in a scission is equal to its weight fraction, we relate ϕ to P and the condition for success to

$$Pf(P_t,S_t) > \theta \tag{1}$$

where $Pf\ (P_t,S_t)$ is the weight fraction of size P at an instantaneous scission index S_t, the number of scissions per original number-average molecule. A third random number ρ is then generated to determine the size of the re-

sulting fragments, ρP and $(1 - \rho) P$. The computer is then instructed to substract a normalized increment, $P/N\bar{P}_{n,0}\Delta P$, from the storage location associated with size P and to add $\rho P/N\bar{P}_{n,0}\Delta P$ and $(1 - \rho) P/N \bar{P}_{n,0} \Delta P$ to the storage locations associated with size ρP and $(1 - \rho)P$, where N is the total number of original chains, ΔP is the size increment between storage locations, and $P_{n,0}$ is the initial number-average degree of polymerization. This process is repeated until the required number of scissions per original number-average molecule is obtained.

With wide molecular weight distributions and a limited number of chains sampled, e.g., 4×10^4, it was found that a fraction of the storage locations containing the high molecular weight tail went negative even when N was made as large 8×10^4. It appears that an increase is N by a factor of 10 is necessary to make this effect negligible, but this is prohibitive in machine time. An alternative procedure was therefore adopted. The computer was instructed to set equal to zero any negative value in the summation step, the particular storage location still retaining the negative value. Runs were then made at 10^4, 2×10^4, 4×10^4, and 8×10^4, and an exponential extrapolation was assumed.

This approximation is based on the following considerations. We can assume, to a good degree of approximation, that the true resulting distribution after S scissions is again a Schulz-Zimm type[3] and that $\bar{P}_{w,s}$ is therefore given by

$$\bar{P}_{w,s} = \frac{y^{a+1}}{\Gamma(a+1)} \int_0^\infty P^{a+1} e^{-yP} dP \tag{2}$$

If we further assume that, in taking a relatively small number of molecules for our sample and setting the value of the storage location equal to zero when negative, the error is an exponential factor of the type $e^{EP/N}$ where E is a constant and N is the number of molecules taken as a statistical sample, then

$$(\bar{P}_{w,s})_{\text{M.C.}} = \frac{y^{a+1}}{\Gamma(a+1)} \int_0^\infty P^{a+1} e^{-(y-E/N)P} dP \tag{3}$$

and

$$(\bar{P}_{w,s})_{\text{M.C.}}/(\bar{P}_{w,s})_{\text{True}} = \frac{1}{(1 - E/Ny)^{a+2}} \cong e^{\bar{P}_{z,s}E/N} \tag{4}$$

Setting $\bar{P}_{z,s} E = F$, we have

$$(\bar{P}_{w,s})_{\text{True}} = (\bar{P}_{w,s})\, e_{\text{M.C.}}{}^{-F/N} \tag{5}$$

According to the above, F should be a constant and not a function of N. Unfortunately, comparison of values at $N = 10^4$, 2×10^4, 4×10^4 and 8×10^4 does not yield a constant value for F. Therefore, some error, probably less than 10%, is introduced.

Theory II: Random Crosslinking without Cyclization

The procedure employed has been described elsewhere[4] and the reader is referred to the original paper. The values for $g'(m)$ were taken as 0.79 and 0.72 for $m = 1$ and $m > 1$, respectively.

Theory III: Random Scission and Crosslinking Occurring Simultaneously without Cyclization

If we assume that the two processes are independent of each other and perform the scission process first, the crosslinking index γ_s, the number of crosslinked units per resulting number-average primary molecule is then

$$\gamma_s = \gamma/(1 + S) \tag{6}$$

It has been shown[3] that for an initial Schulz-Zimm distribution, the resulting distribution after S scissions may be assumed to be the same type, with relatively minor error, by the relationship

$$(a_s + 2)/a_s = \bar{P}_{z,s}/\bar{P}_{n,s} \tag{7}$$

where

$$\bar{P}_{n,s} = \bar{P}_{n,0}/(1 + S) \tag{8}$$

However, since the exponential extrapolation introduces a larger error in $\bar{P}_{z,s}$ than in $\bar{P}_{w,s}$, it is probably better to evaluate a, the width parameter, by

$$(a_s + 1)/a_s = \bar{P}_{w,s}/\bar{P}_{n,s} \tag{9}$$

Results and Discussion

The results of random degradation of wide Schulz-Zimm type distributions, given by

$$W(P) = [y^{a+1}/\Gamma(a + 1)]P^a e^{-yP} \tag{10}$$

where

$$y = a/\bar{P}_n = (a + 1)/\bar{P}_w = (a + 2)/\bar{P}_z$$

and $W(P)$ is the weight fraction of size P, are listed in Table I. In addition to evaluating the extent of degradation, the results may be used to evaluate the parameters of the distribution as shown in Figure 1. Although this technique is not extremely sensitive to differences between distributions, it is more sensitive and accurate than the evaluation of the distribution from fractionation data using the Schulz-Dinglinger[9] method of computing the cumulative sum of the fractions. An analysis of this method (to be published) shows it to be a rather poor approximation with wide distributions, particularly for the very important first and last fractions. In addition, the analysis further shows that one cannot distinguish from viscosity data alone, between $\bar{M}_w/\bar{M}_n$ values in the range of 4–21 and the

TABLE I

				$[\eta]_s/[\eta]_0\alpha$ Values[a]				
a	s	$\bar{P}_{w,s}/\bar{P}_{w,0}$	$\bar{P}_{z,s}/\bar{P}_{z,0}$	0.5	0.6	0.7	0.8	0.9
0.1	0.5	0.26	0.24	0.54	0.47	0.40	0.35	0.30
0.1	1.0	0.15	0.11	0.41	0.34	0.28	0.23	0.19
0.1	1.5	0.11	0.10	0.36	0.28	0.23	0.18	0.14
0.1	2.0	0.09	0.08	0.32	0.25	0.19	0.15	0.12
0.1	2.5	0.08	0.08[c]	0.29	0.22	0.17	0.13	0.10
0.1	3.0	0.07	0.09[c]	0.27	0.21	0.15	0.12	0.09
0.01	3.5	0.06	0.08[c]	0.26	0.19	0.14	0.11	0.08
0.1	4.0	0.05	0.05[c]	0.24	0.18	0.13	0.10	0.07
0.2	0.5	0.40	0.34	0.64	0.58	0.53	0.48	0.43
0.2	1.0	0.25	0.23	0.50	0.44	0.38	0.33	0.28
0.2	1.5	0.18	0.16	0.44	0.37	0.31	0.26	0.21
0.2	2.0	0.14	0.12	0.39	0.32	0.26	0.21	0.17
0.2	2.5	0.12	0.12[c]	0.36	0.29	0.23	0.19	0.15
0.2	3.0	0.11	0.11[c]	0.33	0.27	0.21	0.17	0.13
0.2	3.5	0.09	0.10[c]	0.31	0.25	0.19	0.15	0.12
0.2	4.0	0.08	0.10[c]	0.30	0.23	0.18	0.14	0.11
0.3	0.5	0.43	0.42	0.69	0.64	0.59	0.54	0.50
0.3	1.0	0.29	0.24	0.56	0.46	0.44	0.39	0.34
0.3	1.5	0.22	0.17	0.49	0.42	0.36	0.32	0.26
0.3	2.0	0.17	0.13	0.43	0.36	0.31	0.26	0.21
0.3	2.5	0.14	0.12	0.39	0.33	0.27	0.22	0.18
0.3	3.0	0.12	0.11	0.37	0.30	0.24	0.20	0.16
0.3	3.5	0.11	0.10	0.35	0.28	0.22	0.19	0.14
0.3	4.0	0.10	0.09	0.33	0.26	0.21	0.16	0.13
0.5	0.5	0.56	0.54	0.77	0.73	0.69	0.65	0.62
0.5	1.0	0.39	0.38	0.65	0.59	0.54	0.50	0.45
0.5	1.5	0.31	0.30	0.58	0.51	0.46	0.41	0.37
0.5	2.0	0.25	0.24	0.52	0.46	0.40	0.35	0.31
0.5	2.5	0.21	0.20	0.48	0.41	0.36	0.31	0.26
0.5	3.0	0.17	0.18	0.45	0.38	0.32	0.28	0.23
0.5	3.5	0.16	0.15	0.42	0.36	0.30	0.25	0.21
0.5	4.0	0.15	0.13	0.40	0.33	0.28	0.23	0.19
1.0	0.5	0.66	0.64	0.82	0.79	0.76	0.73	0.70
1.0	1.0	0.50	0.49	0.72	0.67	0.63	0.59	0.55
1.0	1.5	0.41	0.40	0.65	0.59	0.54	0.50	0.46
1.0	2.0	0.34	0.35	0.59	0.54	0.48	0.43	0.39
1.0	2.5	0.29	0.30	0.55	0.49	0.43	0.38	0.34
1.0	3.0	0.26	0.26	0.51	0.45	0.39	0.34	0.30
1.0	3.5	0.23	0.24	0.49	0.42	0.37	0.32	0.27
1.0	4.0	0.21	0.21	0.46	0.40	0.34	0.29	0.25
1.0[b]	0.5	0.67	0.67	0.82	0.78	0.75	0.72	0.69
1.0[b]	1.0	0.50	0.50	0.71	0.66	0.62	0.57	0.54
1.0[b]	1.5	0.40	0.40	0.63	0.58	0.53	0.48	0.44
1.0[b]	2.0	0.33	0.33	0.58	0.52	0.46	0.42	0.37
1.0[b]	2.5	0.29	0.29	0.54	0.47	0.42	0.37	0.32
1.0[b]	3.0	0.25	0.25	0.50	0.44	0.38	0.33	0.29
1.0[b]	3.5	0.22	0.22	0.47	0.41	0.35	0.30	0.26
1.0[b]	4.0	0.20	0.20	0.45	0.38	0.32	0.28	0.24

[a] α is the exponent in the Mark-Houwink expression $[\eta] = KM^{\alpha}$.

[b] Exact computations.

[c] These values are questionable.

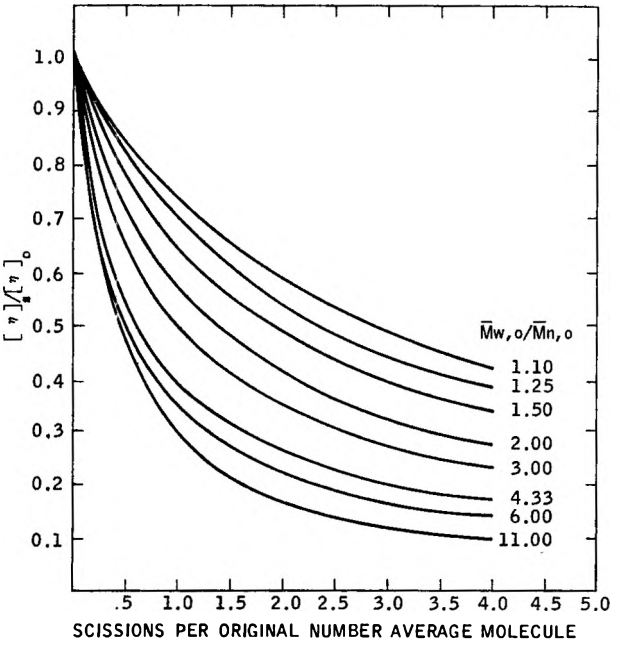

Fig. 1. The ratio of the degraded intrinsic viscosity $[\eta]_s$ to the initial intrinsic viscosity $[\eta]_0$ as a function of the scission index s for $\alpha = 0.8$.

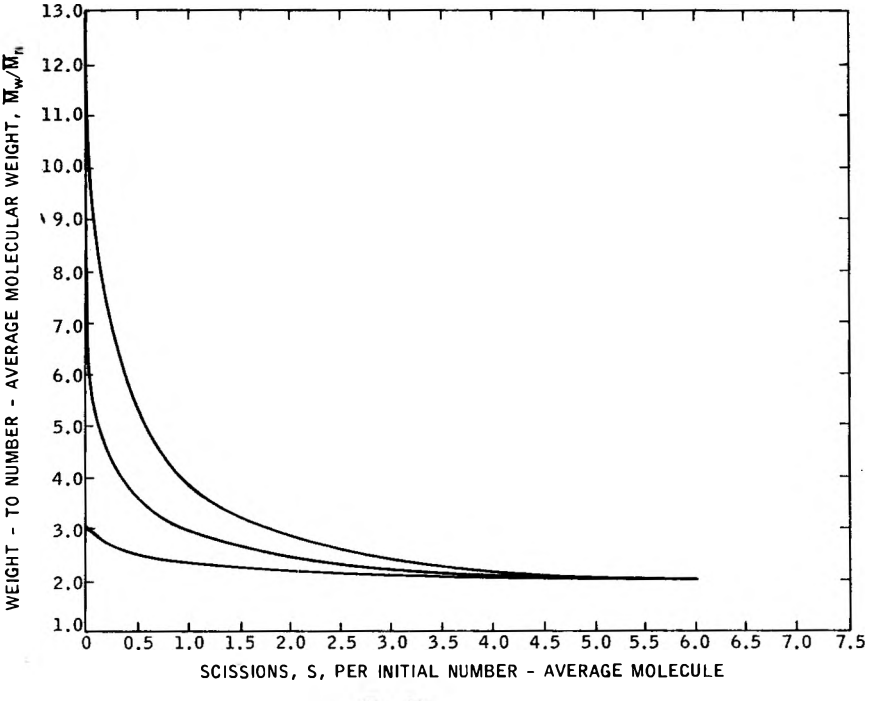

Fig. 2. The change in the $\bar{M}_w/\bar{M}_n$ ratio as a function of degradation.

TABLE II

		α				
a	γ	0.5	0.6	0.7	0.8	0.9
0.1	0.012	1.07	1.09	1.11	1.12	1.14
0.1	0.024	1.12	1.16	1.19	1.22	1.27
0.1	0.036	1.21	1.24	1.30	1.37	1.45
0.1	0.048	1.29	1.36	1.46	1.58	1.72
0.1	0.060	1.44	1.53	1.69	1.90	2.17
0.1	0.072	1.57	1.78	2.03	2.53	3.10
0.1	0.084	1.96	2.49	3.14	4.58	6.62
0.2	0.022	1.08	1.08	1.10	1.11	1.13
0.2	0.044	1.13	1.15	1.19	1.22	1.27
0.2	0.066	1.20	1.24	1.30	1.36	1.45
0.2	0.088	1.27	1.35	1.45	1.57	1.73
0.2	0.110	1.39	1.52	1.68	1.89	2.17
0.2	0.132	1.55	1.80	2.11	2.52	3.10
0.2	0.154	1.96	2.44	3.31	4.58	6.64
0.3	0.030	1.07	1.08	1.09	1.11	1.13
0.3	0.060	1.12	1.15	1.18	1.22	1.26
0.3	0.090	1.18	1.24	1.29	1.36	1.43
0.3	0.120	1.25	1.35	1.44	1.56	1.69
0.3	0.150	1.32	1.51	1.66	1.86	2.11
0.3	0.180	1.53	1.75	2.04	2.43	2.95
0.3	0.210	1.90	2.36	3.07	4.14	5.81
0.5	0.042	1.07	1.08	1.09	1.11	1.12
0.5	0.084	1.12	1.14	1.17	1.21	1.25
0.5	0.126	1.17	1.22	1.28	1.34	1.41
0.5	0.168	1.25	1.32	1.41	1.52	1.65
0.5	0.210	1.35	1.47	1.62	1.80	2.03
0.5	0.252	1.50	1.70	1.95	2.29	2.73
0.5	0.294	1.73	2.16	2.71	3.51	4.71
1.0	0.100	1.03	1.05	1.07	1.10	
1.0	0.200	1.09	1.14	1.18	1.26	
1.0	0.300	1.21	1.32	1.44	1.60	
1.0	0.400	1.46	1.73	2.02	2.46	
2.0	0.100	1.02	1.03	1.04	1.06	
2.0	0.200	1.06	1.09	1.12	1.17	
2.0	0.300	1.12	1.18	1.25	1.33	
2.0	0.400	1.22	1.33	1.46	1.61	
2.0	0.500	1.40	1.60	1.85	2.17	
4.0	0.200	1.04	1.07	1.10	1.13	
4.0	0.400	1.16	1.23	1.32	1.42	
4.0	0.600	1.39	1.59	1.83	2.16	
7.0	0.200	1.05	1.06	1.09	1.12	
7.0	0.400	1.13	1.19	1.27	1.35	
7.0	0.600	1.32	1.47	1.66	1.89	
7.0	0.800	1.84	2.35	3.12	4.21	
10.0	0.200	1.04	1.06	1.09	1.11	
10.0	0.400	1.13	1.19	1.26	1.34	
10.0	0.600	1.29	1.43	1.59	1.80	
10.0	0.800	1.70	2.09	2.63	3.41	

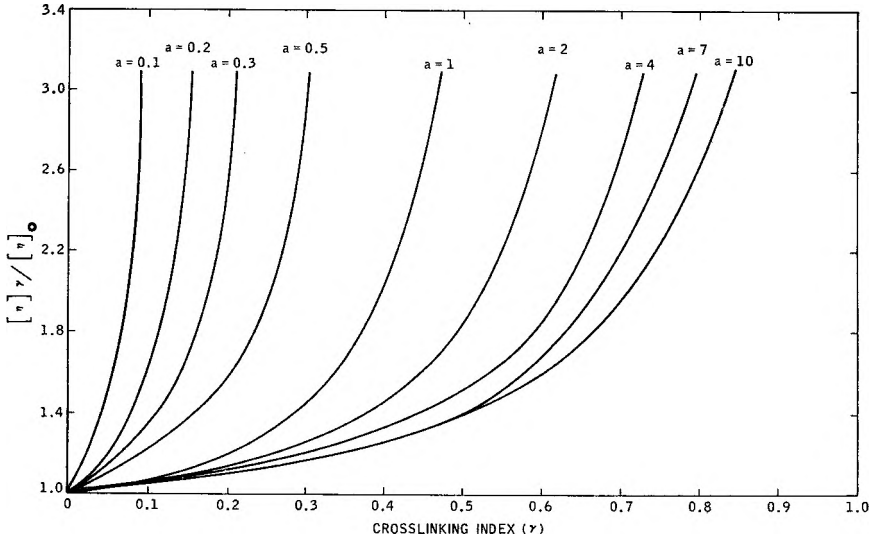

Fig. 3. The ratio of the branched intrinsic viscosity $[\eta]_\gamma$ to the initial intrinsic viscosity $[\eta]_0$ as a function of the crosslinking index γ for $\alpha = 0.7$.

results can yield $\bar{M}_w/\bar{M}_n$ values less than 2 when the fractionation data for a Schulz-Zimm distribution of $\bar{M}_w/\bar{M}_n$ of 21 is plotted on a Tung[10] plot.

Figure 2 shows how rapidly these wide distributions approach the asymptotic value of $\bar{M}_w/\bar{M}_n = 2$.

The results for random crosslinking are shown in Table II and Figure 3. Since the crosslinking index γ_c at incipient gelation is given by

$$\gamma_c = a/(a + 1) \tag{11}$$

this method may also be used to evaluate the width parameter of a Schulz-Zimm distribution. However, since wide distributions change very rapidly with small amounts of degradation and the point of incipient gelation is difficult to accurately evaluate experimentally, this method should be used with considerable caution.

References

1. Kotliar, A. M., *J. Applied Polymer Sci.*, **2,** 134 (1959).
2. Kotliar, A. M., and A. D. Anderson, *J. Polymer Sci.*, **45,** 541 (1960).
3. Kotliar, A. M., *J. Polymer Sci.*, **51,** 563 (1961).
4. Kotliar, A. M., and S. Podgor, *J. Polymer Sci.*, **55,** 423 (1961).
5. Kotliar, A. M., and S. Podgor, *J. Polymer Sci.*, **62,** S177 (1962).
6. Kotliar, A. M., *J. Polymer Sci.*, **61,** S25 (1962).
7. Kotliar, A. M., *J. Polymer Sci.*, **51,** S63 (1961).
8. Schulz, G. V., *Z. Physik. Chem.*, **B43,** 25 (1939); B. H. Zimm, *J. Chem. Phys.*, **16,** 1099 (1948).
9. Schulz, G. V., and A. Dinglinger, *Z. Physik. Chem.*, **B43,** 47 (1939).
10. Tung, L. H., *J. Polymer Sci.*, **40,** 495 (1956).

Résumé

La technique d'échantillonage dite "Monte Carlo" a été employée afin d'évaluer les moyennes de poids moléculaires en résultant et la viscosité intrinsèque pour des polymères ayant une large distribution de Schulz-Zimm, dans le domaine $\bar{P}_w/\bar{P}_n \leqq 11$, et subissant des coupures de chaîne statistiques et des processus de pontage. Les résultats peuvent être utilisées afin d'évaluer la distribution initiale et sont généralement plus sûrs que ceux obtenus par l'usage des données de fractionnement.

Zusammenfassung

Das Monte Carlo-Verfahren zur Probennahme wurde zur Ermittlung der Molekulargewichtsmittelwerte und der Viskositätszahl von Polymeren mit breiter Schulz-Zimmverteilung in Bereich von $\bar{P}_w/\bar{P}_n \leqq 11$, wie sie bei statistischer Kettenspaltung und Vernetzung entstehen, angewendet. Die Ergebnisse können auch zur Ermittlung der Anfangsverteilung herangezogen werden und sind im allgemeinen verlässlicher als Fraktionierungsdaten.

Received August 21, 1962

JOURNAL OF POLYMER SCIENCE: PART A VOL. 1, PP. 3183–3197 (1963)

General Theory of Stationary Random Sequences with Applications to the Tacticity of Polymers*

BERNARD D. COLEMAN and THOMAS G FOX, *Mellon Institute, Pittsburgh, Pennsylvania*

Synopsis

When, in a poly-α-olefin, the probability that a given placement be isotactic depends upon the tacticity of only a finite number of immediate predecessors, the resulting diastereosequence distribution obeys the theory of Markoff chains. When this is not the case, one says that the resulting diastereosequence distribution is non-Markoffian. A special case of a Markoffian distribution is given by a *simple* Markoff chain in which the tacticity of a given placement is assumed to be affected by only the tacticity of the immediately preceding placement. Another special case is, of course, the Bernoulli trial distribution in which the probability that a given placement be isotactic is independent of the tacticity of all other placements. A high resolution NMR spectrum can sometimes yield a quantitative determination of the concentrations of isotactic and syndiotactic placements and the concentrations of the three types of possible adjacent pairs of such placements (i.e., isotactic, syndiotactic, and heterotactic pairs). When this is the case, the spectrum can be used to determine whether or not a given diastereosequence distribution is Bernoullian. However, because the longest diastereosequences whose concentration can be measured by NMR spectroscopy involve only two placements, an NMR spectrum cannot check whether a given non-Bernoullian distribution be simple Markoffian or Markoffian in general. In fact, non-Markoffian distributions are compatible with existing NMR spectra on polymers prepared by anionic polymerizations. In this paper we work within the framework of Kac's theory of stationary statistical processes and point out some general results which are valid for both Markoffian and non-Markoffian processes. The results are applied to NMR spectroscopy and it is pointed out which calculations used to check the self-consistency of NMR data and to obtain the mean length of closed diastereosequences are valid for both Markoffian and non-Markoffian distributions.

Introduction

Let us consider a polymer molecule formed by head-to-tail addition polymerization of an unsymmetrical α-olefin. Assuming that the end-groups of this molecule are distinguishable, every second carbon atom in its principal (backbone) chain is an asymmetric carbon atom. We number these asymmetric carbon atoms in the order in which they were added during polymerization and use the following notation:[1] if the mth and $(m+1)$th asymmetric chain atoms have the same stereoconfiguration then we say that the mth *placement* of our polymer molecule is *isotactic;* if these

*Paper presented at the 142nd Meeting of the American Chemical Society, Atlantic City, New Jersey, September 1962.

two asymmetric atoms have opposite stereoconfigurations we say that the mth *placement* is *syndiotactic.* The property of being isotactic or syndiotactic is called "tacticity."

We define a *diastereosequence* of length n to be an ordered set of n consecutive placements, say, the mth, $(m + 1)$th, . . . , $(m + n - 1)$th placements which express, respectively, the stereorelationship between the mth and the $(m + 1)$th, the $(m + 1)$th and $(m + 2)$th, . . . , the $(m + n - 1)$th and the $(m + n)$th asymmetric chain atoms. Thus, a diastereosequence of length n involves $n + 1$ monomer units and a poly-α-olefin of degree of polymerization D constitutes a diastereosequence of length $D - 1$.

There are 2^{D-1} possible distinct diastereosequences of length $D-1$: The first placement may be isotactic or syndiotactic, in either case the second placement may be isotactic or syndiotactic, and so on, for $D-1$ times. Usually, each of these 2^{D-1} stereosequences constitutes a distinct diastereoisomer of our polymer. If the end groups are not distinguishable, the number of distinct diastereoisomers may be less than 2^{D-1}, but it is always of this order of magnitude.

Since D is often greater than a thousand or even ten thousand, if there is the slightest amount of randomness involved in the formation of successive placements, there is little hope of isolating in pure form every diastereoisomer resulting from a given polymerization, even when the molecular weight distribution is perfectly sharp. Furthermore, when the molecular weight is high and formation of successive placements is governed by processes which are strongly random (for example, by a process which can be represented by a game in which the tacticity of each placement is determined by an independent toss of a not-too-biased coin, i.e., by Bernoulli trials) so many distinct diastereoisomers of nearly equal probability are possible that most of them must be absent from any sample of reasonable size and the concentration of those present can hardly exceed one molecule per sample.

The situation just described is the rule rather than the exception for free radical polymerizations;[1-4] for anionic polymerizations the coin-tossing analogy breaks down, but there is usually still sufficient randomness to make the general conclusion valid.

Thus we see that even if we ignore dispersion in molecular weight, the stereochemistry of addition polymers must differ markedly in concepts and techniques from classical stereochemistry.

The sort of questions which are meaningful here are questions of the following types. What is the probability that the diastereosequence of length n which runs from the mth through the $(m + n - 1)$th placement has a particular pattern (say, contains only isotactic placements or consists of an alternating sequence of isotactic and syndiotactic placements)? What is the mean number of isotactic placements between successive syndiotactic placements? This second question is related to questions of "mean recurrence times."[5,6]

There is a large mathematical literature dealing with questions of these

types, but, with one notable exception,[5,6] (unfortunately, unknown to us until the present investigation was completed) it is restricted to cases in which the sequences under consideration are generated by either Bernoulli trials or by Markoff chains. True, for *free radical polymerizations* it has been proposed,[1,2] on the basis of experience with the magnitude of penultimate effects in copolymer polymerization kinetics, that to a high approximation diastereosequences should be generated by Bernoulli trials, and this has recently been confirmed, for methyl methacrylate, by high resolution nuclear magnetic resonance spectroscopy.[3] However, NMR spectra indicate that polymers prepared by anionic polymerizations do not obey Bernoulli trial statistics,[3,7] and there is no evidence supporting Markoff chain statistics for those polymers. A recent theoretical study of plausible mechanisms indicates that non-Markoffian distributions may occur frequently in anionic polymerizations.[8] Thus, if we are to have a theory in which we can discuss the questions of interest in sufficient generality to insure applicability of our results to all polymerizations of α-olefins, including anionic polymerizations, then we must leave behind Bernoullian and Markoffian simplifications and examine afresh the theory of random sequences.

The terms "Bernoullian," "Markoffian," and "non-Markoffian" will be precisely defined below. For the present we note that since an NMR spectrum determines the concentrations of only the diastereosequences which have length less than three it cannot be used to check for statistical interactions extending beyond two placements. NMR data alone can rule out Bernoullian statistics but cannot establish Markoffian statistics.

Fortunately, a diastereosequence is a binary sequence; there are only two possibilities for each component element: a given element can be either an isotactic placement or a syndiotactic placement. When this fact is combined with but one statistical assumption, that of stationarity, a rich general theory is obtained in which much can be said without further assumptions.

To explain the chemical significance of statistical stationarity, let us note that since we are here interested in polymers of high molecular weight it is reasonable to neglect end effects. One part of such neglect is the assumption that the finite diastereosequences mentioned in our questions are always finite pieces of random diastereosequences of infinite length: this is the assumption that every placement has both successors and predecessors. Related to the physical notion that end effects should be unimportant is the assertion that the probability that the mth placement of a polymer is isotactic (given no information about the tacticity of other placements) should be independent of m and should be equal to the probability that a placement selected at random is isotactic. This assertion can be strengthened by assuming that, for each n, the probability that the diastereosequence of length n running from the mth to the $(m + n - 1)$th placement has a particular pattern is independent of m (if no information is given about the tacticity of the placements preceding and succeeding the sequence): this is the essence of our assumption of the statistical stationarity. It should be emphasized that to have stationarity one need not as-

sume that the probability that the mth placement is isotactic be unaffected by a knowledge of the tacticity of the $(m - 1)$th placement; nor need it be assumed that there exists a fixed integer N, such that the probability that the mth placement is isotactic be affected by knowledge of the tacticity of placements $m - 1, m - 2, \ldots, m - N$ but given such knowledge, be then independent of the tacticity of placement $m - N - 1$. In the former case the present theory would reduce to that of Bernoulli trials while in the latter to that of stationary Markoff processes.

Definitions and Postulates

Let us replace the polymer molecule by an infinite sequence $\mathfrak{s}$ of letters S and I, where S plays the role of a syndiotactic placement and I an isotactic placement. The observations made in the previous section about diastereosequence distributions are equivalent to the assertion that the occurrence of the letters S and I in $\mathfrak{s}$ are governed by statistical laws which, though stationary along $\mathfrak{s}$, are not necessarily given by independent Bernoulli trials or even finite Markoff chains.

One way of developing our present theory would be to consider a sample space in which the entire sequence $\mathfrak{s}$ is taken as the basic random variable. Such a procedure involves some subtle concepts, because in it the basic sample space, i.e., the space of all sequences $\mathfrak{s}$ of binary digits, is an infinite and nondenumerable sample space. We shall here avoid mentioning these subtle concepts by axiomatizing our theory in such a way that we refer only to probability distributions p_n over finite sample spaces. Although we shall have an infinite (yet countable) number of these finite distributions p_n the procedures we use here do not require any sophisticated mathematical concepts.

We denote finite sequences of letters (to be interpreted as consecutive subsequences of $\mathfrak{s}$) as follows: S represents, of course, the single letter S; SI represents an I followed by an S; etc. (This convention of building up sequences from right to left is motivated by applications of the theory to the example of Fox and Coleman[8] in which the basic probabilities are given by algorithms involving matrix products. This convention also has certain advantages when one manipulates conditional probabilities.) We use the symbols $U^{(n)}$, $V^{(n)}$, $W^{(n)}$ to denote unspecified consecutive sequences of length n. For example, $U^{(1)}$ may be either S or I; $U^{(2)}$ may be II, SI, IS, or SS. etc. Since all sequences which we consider are consecutive, for short we call $U^{(n)}$ simply a *sequence* of length n. We can combine the symbols S and I with the symbols $U^{(n)}$ and $V^{(n)}$. For example $IU^{(2)}S$ represents a sequence of length four about which we specify only that it begin with an S and end with an I; i.e., $IU^{(2)}S$ may be any one of the following: $IIIS$, $IISS$, $ISIS$, $ISSS$. We use the following abbreviation: I^k represents k I's and S^k, k S's; hence SI^3S^2 is short for $SIIISS$. In order to state some of our propositions concisely, it is convenient to assign a meaning to the superscript k in $U^{(k)}$, I^k, and S^k when $k = 0$. The symbols

$U^{(0)}$, $I^{(0)}$, and $S^{(0)}$ always occur in sequences involving other symbols and always have the same meaning, namely,

$$U^{(0)}V^{(m)} = V^{(m)}U^{(0)} = I^0V^{(m)} = V^{(m)}I^0 = S^0V^{(m)} = V^{(m)}S^0 = V^{(m)}$$

The symbol $p_n\{U^{(n)}\}$ denotes the probability of occurrence of the sequence $U^{(n)}$; e.g., $p_3\{IIS\}$ is the probability that a given sequence of length three consists of an S followed by an I which is, in turn, followed by an I. (It is implicit in our notation that $p_n\{U^{(n)}\}$ is independent of the position of $U^{(n)}$ along s: the random sequences s covered by our theory are stationary.)

We assume that for every n the function p_n exists and is indeed a probaability distribution. It follows from this that

$$0 \leq p_n\{U^{(n)}\} \leq 1 \tag{1}$$

and that the summation of $p_n\{U^{(n)}\}$, over the 2^n different ways of forming $U^{(n)}$ from sequences of S's and I's, is unity:

$$p_1\{I\} + p_1\{S\} = 1 \tag{2a}$$

$$p_2\{II\} + p_2\{IS\} + p_2\{SI\} + p_2\{SS\} = 1 \tag{2b}$$

$$\vdots$$

etc.

We assume that for each n the probability distribution p_n is related to the distribution p_{n+1} by means of the formulae

$$p_{n+1}\{U^{(n)}I\} + p_{n+1}\{U^{(n)}S\} = p_n\{U^{(n)}\} \tag{3a}$$

$$p_{n+1}\{IU^{(n)}\} + p_{n+1}\{SU^{(n)}\} = p_n\{U^{(n)}\} \tag{3b}$$

The identities (3) hold for every fixed sequence $U^{(n)}$. They say that no matter what the length of a sequence $U^{(n)}$, it may be regarded as a contraction of a sequence one letter longer. In particular, eq. (3a) says that $U^{(n)}I$ (the sequence $U^{(n)}$ preceded by an I) and $U^{(n)}S$ (the sequence $U^{(n)}$ preceded by an S) give two mutually exclusive (and exhaustive) ways of preceding $U^{(n)}$ with another letter; while eq. (3b) says that $SU^{(n)}$ and $IU^{(n)}$ are two mutually exclusive (and exhaustive) ways of following $U^{(n)}$ with another letter.

Note that eqs. (3) tell us that if the function p_n is known for all $U^{(n)}$ then p_{n-1} is determined for all $U^{(n-1)}$, but not (in general) conversely.

In order to avoid vacuous theorems, we assume further that

$$p_1\{I\} \neq 0 \text{ and } p_1\{S\} \neq 0 \tag{4}$$

Our postulates have now been stated: everything that we do henceforth shall follow from the equations and inequalities (1)–(4). We note that these axioms are symmetric in the symbols S and I. Hence, every proposition we prove will remain valid if in it one replaces each S by an I and each I by an S.

Application of a theory based on stationarity assumptions to a real polymer sample always involves an idealization. Indeed, if we interpret $p_n\{U^{(n)}\}$ as the probability that a partial diastereosequence, of known distance m from the initiating end, is of type $U^{(n)}$, then we must face the fact that every imaginable mechanism of synthesis yields a dependence of $p_n\{U^{(n)}\}$ on m. Usually this dependence on m falls off rapidly with increasing m and becomes unimportant for samples of high molecular weight.

It seems possible to increase the scope of applicability of the present theory by interpreting $p_n\{U^n\}$ as the probability that a diastereosequence *selected at random* is of type $U^{(n)}$. Such an interpretation suggests that the present theory can be applied even in circumstances in which end effects are not negligible, i.e., in circumstances in which $p_n\{U^{(n)}\}$, when given the interpretation of our previous paragraph, is strongly dependent on m even for large m. Yet an idealization is involved even here. Under our present interpretation, for polymer chains of finite length, eq. (3) neglects the probability that a randomly selected placement involves an endgroup and is thus lacking a successor or a predecessor. For chains which are really of infinite length the expression "randomly selected" becomes devoid of precise meaning.

We now give definitions of conditional probabilities and then Markoffian, Bernoullian, and non-Markoffian sets of distributions, p_n.

Now $p_{q+r}\{V^{(r)}U^{(q)}\}$ is the probability that a particular sequence $U^{(q)}$ of length q occurs and is immediately followed by a certain sequence $V^{(r)}$ of length r. The conditional probability $p_{r|q}\{V^{(r)}|U^{(q)}\}$ that the sequence $V^{(r)}$ occupies the positions $q + 1, q + 2, \ldots, q +$ r, given that $U^{(q)}$ occupies the positions $1,2, \ldots, q$, is defined by

$$p_{r|q}\{V^{(r)}|U^{(q)}\}p_q\{U^{(q)}\} = p_{q+r}\{V^{(r)}U^{(q)}\} \qquad (5)$$

where $p_q(U^q)$ is, of course, the probability of occurrence of the sequence $U^{(q)}$.

We say that our set of probability distributions p_n is Markoffian if there exists an integer N such that for each sequence $V^{(N)}$ of length N

$$p_{n|N}\{U^{(q)}|V^{(N)}\} = p_{n|N+m}\{U^{(n)}|V^{(N)}|W^{(m)}\}; \qquad (6)$$

this equation is to be interpreted as an identity holding for all integers n and m and all sequences $U^{(n)}$ and $W^{(m)}$.

If the identity (6) holds for N then it holds for all $m > N$. If N is the smallest integer for which eq. (6) holds, then we say that the set of distributions p_n is Markoffian of order N. In other words, if our collection of distributions is Markoffian of order N, then the probability of occurrence of a sequence $U^{(n)}$ is, in general, affected by a knowledge of the first preceding N letters, but if these first preceding N letters are known, then a knowledge of any other preceding letters does not further affect the probability of $U^{(n)}$. If eq. (6) holds for $N = 1$ then the p_n are said to form a simple Markoff chain.

If, for all pairs of sequences $W^{(m)}$ and $U^{(n)}$ we have

$$p_{n|m}\{U^{(n)}|W^{(m)}\} = p_n\{U^{(n)}\} \tag{7}$$

then we say that our set of distributions p_n is Bernoullian. Of course, if eq. (7) holds, then eq. (6) holds for every N.

If the identity (7) does not hold, and if there does not exist a finite integer N for which the identity (6) holds, then we say that our set of distributions is non-Markoffian. The theory which we present here, because it rests on only our postulates (1)–(4), applies whether the set of distributions p_n is Bernoullian, Markoffian, or non-Markoffian.

Elementary Propositions

On putting $n = 1$ and $U^{(1)} = S$ in the eqs. (3) we obtain

$$p_2\{SI\} + p_2\{SS\} = p_1\{S\} \tag{8a}$$

$$p_2\{IS\} + p_2\{SS\} = p_1\{S\} \tag{8b}$$

from which we read off Proposition 1.

Proposition 1:

$$p_2\{IS\} = p_2\{SI\} \tag{9}$$

i.e., the probability that a letter selected at random is an S preceded by an I is equal to the probability that it is an S followed by an I. This observation has the following generalization which was pointed out by Professor Morris De Groot.

Proposition 2: For all $m \geq 1$,

$$p_{m+1}\{I^mS\} = p_{m+1}\{SI^m\} \tag{10}$$

Proof: On putting $U^{(n)} = SI^{n-1}$ in eq. (3a), and then $U^{(n)} = I^{n-1}S$ in eq. (3b), we get

$$p_n\{SI^{n-1}\} = p_{n+1}\{SI^n\} + p_{n+1}\{SI^{n-1}S\} \tag{11a}$$

$$p_n\{I^{n-1}S\} = p_{n+1}\{I^nS\} + p_{n+1}\{SI^{n-1}S\} \tag{11b}$$

from which it is obvious that if eq. (10) holds for $m = n - 1$ then it holds for $m = n$; hence by induction it holds for all m; q.e.d.

Proposition 3: The two limits

$$\lim_{N\to\infty} p_N\{I^N\} = q \tag{12a}$$

and

$$\lim_{N\to\infty} \sum_{n=1}^{N} p_{n+1}\{I^nS\} \tag{12b}$$

exist and are related by

$$\sum_{n=1}^{\infty} p_{n+1}\{I^nS\} = p_1\{I\} - q \tag{13}$$

Proof: Equation (3a) tells us that

$$p_1\{I\} = p_2\{IS\} + p_2\{I^2\}$$
$$p_2\{I^2\} = p_3\{I^2S\} + p_3\{I^3\}$$
$$\cdot$$
$$\cdot$$
$$\cdot$$
$$p_n\{I^n\} = p_{n+1}\{I^nS\} + p_{n+1}\{I^{n+1}\}$$

and on adding these equations we get the intuitively evident formula

$$p_1\{I\} = \sum_{n=1}^{N} p_{n+1}\{I^nS\} + p_{N+1}\{I^{N+1}\} \tag{14}$$

From eqs. (14) and (1) we have

$$1 \geq \sum_{n=1}^{N} p_{n+1}\{I^nS\} \geq 0 \tag{15}$$

In other words, the series $\sum p_{n+1}\{I^nS\}$, consisting of positive terms, has a sum which is bounded. Hence, this series converges, i.e., the limit (12b) exists. It then follows from eq. (14) that the limit (12a) exists and that eq. (13) holds; q.e.d.

One might expect that our assumption $p_1\{S\} \neq 0$ gives us $q = 0$. Although this is true when the distributions are Bernoullian, it is not true in general. The following example, suggested by Professor De Groot, is compatible with postulates (1)–(4) yet does not yield $q = 0$. Suppose we toss a coin, and whenever we get heads we put all the letters in s equal to I and whenever we get tails we put all these letters equal to S. Then, $p_N\{I^N\} = p_1\{I\}$ for all N and thus $q = p_1\{I\} \neq 0$.

It is expected, however, that in all the applications of the present theory to real polymerization problems, we shall have $q = 0$.

The existence of the limit (12b) has the corollary

$$\lim_{n\to\infty} p_{n+1}\{I^nS\} = 0 \tag{16}$$

which is generalized in Proposition 4.

Proposition 4: Let $U^{(r)}$ and $V^{(q)}$ be two arbitrary fixed sequences such that the letter S occurs at least once in either $U^{(r)}$ or $V^{(r)}$, then

$$\lim_{n\to\infty} p_{q+n+r}\{V^{(q)}I^nU^{(r)}\} = 0 \tag{17}$$

Proof: If $V^{(q)}$ or $U^{(r)}$ has an S then $p_{q+n+r}\{V^{(q)}I^nU^{(r)}\}$ can be rewritten in either the form $p_{q+n+r}\{V^{(q)}I^{n+t}SW^{(r-t-1)}\}$ or the form $p_{q+n+r}\{W^{(q-t-1)}SI^{(n+t)}U^{(r)}\}$. Also, it follows from eqs. (1) and (3) that for any three sequences $U^{(x)}$, $V^{(y)}$, $W^{(z)}$, with $x \geq 0$, $y \geq 1$, $z \geq 0$,

$$p_{x+y+z}\{U^{(x)}V^{(y)}W^{(z)}\} \leq p_y\{V^{(y)}\} \tag{18}$$

On noting eq. (18), we see that eq. (17) now follows immediately from eq. (16).

We shall now use Proposition 4 to obtain a useful lemma.

Proposition 5. For any sequence $V^{(n)}$ which contains the letter S at least once, and for every integer $M \geq 0$,

$$\sum_{k=M}^{\infty} p_{n+k+1}\{SI^kV^{(n)}\} = p_{n+M}\{I^MV^{(n)}\} \tag{19}$$

Proof: From eq. (3b) we get

$$p_{n+k+1}\{SI^kV^{(n)}\} + p_{n+k+1}\{II^kV^{(n)}\} = p_{n+k}\{I^kV^{(n)}\} \tag{20}$$

Solving this for the first term on the left and then summing over k we find

$$\begin{aligned}\sum_{k=M}^{N} p_{n+k+1}\{SI^kV^{(n)}\} &= \sum_{k=M}^{N} [p_{n+k}\{I^kV^{(n)}\} - p_{n+k+1}\{I^{k+1}V^{(n)}\}] \\ &= p_{n+M}\{I^MV^{(n)}\} - p_{n+N+1}\{I^{N+1}V^{(n)}\}\end{aligned} \tag{21}$$

If we now let $N \to \infty$ and note that, by Proposition 4,

$$\lim_{N\to\infty} p_{n+N+1}\{I^{N+1}V^{(n)}\} = 0 \tag{22}$$

we see that the proposition is proved.

When $V^{(n)}$ is just the letter S this lemma yields the formulae

$$\sum_{k=M}^{\infty} p_{k+2}\{SI^kS\} = p_{M+1}\{I^MS\} \tag{23}$$

$$\sum_{k=0}^{\infty} p_{k+2}\{SI^kS\} = p_1\{S\} \tag{24}$$

Theorems

We can now use the mathematical apparatus assembled in the previous section to write short proofs for some apparently nontrivial theorems on recurrence times and sequence lengths. In their present generality, these theorems were first proved by Kac.[5,6]

Let us consider the numbers f_n, $n \geq 1$, defined by

$$f_n = p_{n|1}\{SI^{n-1}|S\} \tag{25}$$

If, as we move along the sequence S, we observe that an S has occurred at a particular position, say position m, and are given no other information, then f_n tells us the probability that the positions $m + 1$, $m + 2$, ... $m + n - 1$ are occupied by I's and that the next S to occur occupies the position $m + n$, i.e., f_n is the probability that the recurrence time for S has length n.

Theorem 1:

$$\sum_{n=1}^{\infty} f_n = 1 \tag{26}$$

Proof: By eqs. (25), (5), and the inequalities (4),

$$f_n = p_{n+1}\{SI^{n-1}S\}/p_1\{S\} \tag{27}$$

On summing we get

$$\sum_{n=1}^{\infty} f_n = \sum_{n=1}^{\infty} p_{n+1}\{SI^{n-1}S\} \Big/ p_1\{S\} = \sum_{k=0}^{\infty} p_{k+2}\{SI^kS\} \Big/ p_1\{S\} \tag{28}$$

The theorem now follows immediately from eq. (24).

The quantity $\chi\{S\}$ defined as

$$\chi\{S\} = \sum_{n=1}^{\infty} nf_n \tag{29}$$

may be called the *mean recurrence time* for the letter S.

Theorem 2:

$$\chi\{S\} = \frac{1-q}{p_1\{S\}} \tag{30}$$

Proof: By eqs. (29) and (28),

$$p_1\{S\}\chi\{S\} = \sum_{n=1}^{\infty} np_{n+1}\{SI^{n-1}S\} = \sum_{m=0}^{\infty} (m+1)p_{m+2}\{SI^mS\}$$

$$= \sum_{m=0}^{\infty} mp_{m+2}\{SI^mS\} + \sum_{m=0}^{\infty} p_{m+2}\{SI^mS\} \tag{31}$$

For the first summation in eq. (31) we write

$$\sum_{m=0}^{\infty} mp_{m+2}\{SI^mS\} = \sum_{M=1}^{\infty} \sum_{k=M}^{\infty} p_{k+2}\{SI^kS\} \tag{32}$$

and, on combining eqs. (23) and (13) we find that

$$\sum_{m=0}^{\infty} mp_{m+2}\{SI^mS\} = \sum_{M=1}^{\infty} p_{M+1}\{I^MS\} \tag{33}$$

$$= p_1\{I\} - q \tag{34}$$

Since the two summations on the right in eq. (32) are now both seen to be convergent (and, of course, absolutely convergent), eq. (32) is justified.

On putting eq. (34) into eq. (31) and noting that, by eq. (24), the second summation in eq. (31) is $p_1\{S\}$, we obtain

$$p_1\{S\}\chi\{S\} = p_1\{I\} - q + p_1\{S\} = 1 - q \tag{35}$$

which completes the proof.

When $q = 0$, eq. (30) reduces to the formula

$$\chi\{S\} = \frac{1}{p_1\{S\}} \tag{36}$$

Equation (36) states that the mean recurrence time for the letter S is equal to the reciprocal of the probability of an S, a plausible result.

For the coin-tossing same of Professor De Groot, mentioned above, eq. (30) yields $\chi\{S\} = 1$, which is, for that special case, also a plausible result.

A closed sequence of I's is a sequence of $n + 2$ letters, $n > 1$, which has an S at each end and n I's in the middle. Let us denote by u_n the probability that a given closed sequence of I's contains exactly n I's. In other words u_n is the probability, given the letter S and given that S is immediately followed by I, that exactly n I's occur before another S occurs. Now, the probability that a given letter S is followed by exactly n I's before the next S occurs, given no other information, is just f_{n+1}. The probability that a given letter S is immediately followed by an I is $1 - f_1$. Hence

$$(1 - f_1)u_n = f_{n+1} \tag{37}$$

and when $f_1 \neq 1$

$$u_n = \frac{f_{n+1}}{1 - f_1} \tag{38}$$

Of course, when $f_1 = 1$ there are no closed sequences of I's. When the quantity $\mu\{I\}$, defined as

$$\mu\{I\} = \frac{\sum_{n=1}^{\infty} nf_{n+1}}{1 - f_1} = \sum_{n=1}^{\infty} nu_n \tag{39}$$

exists, it may be interpreted as the *mean length of closed sequences of the letter I.*

On noting that

$$\sum_{n=1}^{\infty} nf_{n+1} = \sum_{m=2}^{\infty} (m - 1)f_m = \sum_{m=1}^{\infty} (m - 1)f_m = \sum_{m=1}^{\infty} mf_m - \sum_{m=1}^{\infty} f_m \tag{40}$$

and using eqs. (26), (27), and (29), we find

$$\mu\{I\} = \frac{\chi\{S\} - 1}{1 - p_2\{SS\}/p_1\{S\}} \tag{41}$$

This formula and Theorem 2 yield

Theorem 3:

$$\mu\{I\} = \frac{p_1\{I\} - q}{p_1\{S\} - p_2\{SS\}} \tag{42}$$

In the case of De Groot's coin tossing game, i.e., when $q = p_1\{I\}$ and $p_1\{S\} = p_2\{SS\}$, eq. (42) is indeterminate, and it should be, for in that game there are no closed sequences of I's.

Diastereosequences

In considering diastereosequences in an actual sample of a poly-α-olefin, the quantity $p_1\{I\}$ (or $p_1\{S\}$) may be interpreted as the concentration of

asymmetric chain atoms which are in isotactic (or syndiotactic) placement with respect to their immediate predecessors, i.e., "the concentration of isotactic (or syndiotactic) placements." Similarly, $p_2\{I^2\}$ (or $p_2\{S^2\}$) may be interpreted as the concentration of asymmetric chain atoms which are in isotactic (or syndiotactic) placement with respect to both their immediate predecessor and their immediate successor, i.e., "the concentration of isotactic (or syndiotactic) pairs." The quantity

$$p\{IS_VSI\} = p_2\{IS\} + p_2\{SI\} \tag{43}$$

is, in the mathematical theory, the probability that a pair of adjacent letters selected at random is either the sequence SI or the sequence IS. In the application under consideration, $p\{IS_VSI\}$ is to be interpreted as the concentration of asymmetric chain atoms in isotactic placement with one nearest neighbor and in syndiotactic with the other, i.e., "the concentration of heterotactic pairs." We call $p_1\{I\}$, $p_1\{S\}$ *placement concentrations* and $p_2\{I^2\}$, $p_2\{S^2\}$, $p\{IS_VSI\}$, *pair concentrations.*

The experiments of Bovey and Tiers on poly(methyl methacrylate) show that for this polymer placement concentrations and pair concentrations can be measured by high resolution NMR.[3]

Now $p_1\{I\}$ and $p_1\{S\}$ are, of course, related by eq. (2a) and it follows from eqs. (2b) and (43) that

$$p_2\{II\} + p_2\{SS\} + p\{IS_VSI\} = 1 \tag{2b'}$$

The equations (2a) and (2b') are not verified by NMR measurements, but are used instead to normalize the data before it is presented. Thus, although the spectroscopist can report values of both of the placement concentrations $p_1\{I\}$, $p_1\{S\}$, and all three of the pair concentrations $p_2\{II\}$, $p_2\{SS\}$, $p\{IS_VSI\}$, we cannot regard all this data as being independent. The independent data obtained from spectroscopy consists of one placement concentration and two pair concentrations.

It follows from eqs. (3) that the experimentally independent data must obey some simple algebraic relations.

If one takes the independently measured quantities to be $p_1\{I\}$, $p_2\{I^2\}$, and $p\{IS_VSI\}$, then eqs. (3) yield

$$p\{IS_VSI\} = 2(p_1\{I\} - p_2\{I^2\}) \tag{44}$$

If $p_1\{I\}$, $p_2\{I^2\}$, and $p_2\{S^2\}$ are used, then

$$p_1\{I\} = {}^1/_2[1 + p_2\{I^2\} - p_2\{S^2\}] \tag{45}$$

and if $p_1\{I\}$, $p_2\{S^2\}$ and $p\{IS_VSI\}$ are used, then

$$p_1\{I\} = 1 - {}^1/_2\, p\{IS_VSI\} - p_2\{S^2\} \tag{46}$$

The other consequences of eqs. (3) for $n = 1$ can be obtained from eqs. (44)–(46), through interchange of the symbols S and I. Since for given spectroscopic measurement one set of independent data is equivalent to another, the experimenter need check only one of the equations (44)–(46):

if the equation he chooses is found to be consistent with his data, so then must all the others, and he can conclude that his measurements are consistent with eqs. (3). Under no circumstances should he regard an experimental confirmation of eqs. (44)–(46) as evidence for Markoffian statistics.

Let us now turn to Theorem 3. Clearly, in any stereochemical applications, we shall have $q = \lim_{n\to\infty} p_n\{I^n\} = 0$. Hence, Theorem 3 tells us that a knowledge of the syndiotactic placement concentration $p_1\{S\}$ and the syndiotactic pair concentration $p_2\{SS\}$ determines the mean (i.e., number-average) length $\mu\{I\}$ of closed sequences of isotactic placements through the formula

$$\mu\{I\} = \frac{p_1\{I\}}{p_1\{S\} - p_2\{S^2\}} = \frac{1 - p_1\{S\}}{p_1\{S\} - p_2\{S^2\}} \tag{47}$$

Thus, NMR spectra, although they measure only placement concentrations and pair concentrations, can yet be used to calculate mean lengths of closed sequences of isotactic (and, of course, also syndiotactic) placements. The important point here is that this observation is true even when the diastereosequence distribution is non-Markoffian.

In the Bernoullian case, eq. (47) reduces to $\mu\{I\} = (p_1\{S\})^{-1}$ and is almost obvious. A result equivalent to eq. (47) has been derived by Johnsen[7] for simple Markoff chains. (Of course, to have $q = 0$ for simple Markoff chains one must suppose not only that $p_1\{I\} \neq 1$, but also that $p_{1\mu}\{S|I\} \neq 0$.) Equations equivalent to eq. (47) have also been proposed by Bovey and Tiers[3] on the basis of a special model.

We remark that the placement and pair concentrations, by themselves, do not, in general, suffice to determine higher moments of the distribution of sequence lengths. Therefore, one cannot calculate weight-average lengths of closed sequences from NMR data unless one introduces special assumptions, such as the assumption that one is dealing with a simple Markoff chain. (This assumption was used for calculations reported by Johnsen;[7] as we remarked in the introduction, we do not believe such an assumption holds for homogeneous anionic polymerizations.)

Equations (8b), (9), and (43) may be used to rewrite eq. (47) in the perhaps more suggestive forms

$$\mu\{I\} = \frac{p_1\{I\}}{p_2\{IS\}} = \frac{2p_1\{I\}}{p\{IS_vSI\}} \tag{48}$$

Of course, in the case of Bernoulli trials, eq. (48) reduces to $\mu\{I\} = p_1\{S\}^{-1}$.

Let us consider the quantity ρ defined by

$$\rho = \mu\{I\}p_1\{S\} \tag{49}$$

From eq. (48) we have

$$\rho = \frac{2p_1\{I\}p_1\{S\}}{p\{IS_vSI\}} \tag{50}$$

It is easy to see that this same quantity ρ could also be defined by

$$\rho = \mu\{S\}p_1\{I\} \tag{51}$$

and that ρ is simply the ratio of the actual mean length of closed sequences of isotactic (or syndiotactic) placements to the mean length which one would calculate assuming that the diastereosequence distribution were Bernoullian with the same value of $p_1\{S\}$ (or $p_1\{I\}$). We call ρ the *persistence ratio*, for $\rho - 1$ measures the apparent "statistical after-effect," or departure from Bernoulli statistics. It follows from eq. (50) that ρ can be calculated from NMR data.

We are indebted to Professor Morris De Groot of the Mathematics Department, Carnegie Institute of Technology, for valuable discussions.

The research reported here was supported in part by the Air Force Office of Scientific Research under Contract AF 49(638)541.

References

1. Coleman, B. D., *J. Polymer Sci.*, **31**, 155 (1958).
2. Fox, T. G, W. E. Goode, S. Gratch, C. M. Huggett, J. F. Kincaid, A. Spell, and J. O. Stroupe, *J. Polymer Sci.*, **31**, 173 (1958).
3. Bovey, F. A., and G. B. D. Tiers, *J. Polymer Sci.*, **44**, 173 (1960).
4. Fox, T. G, and H. W. Schnecko, *Polymer*, **3**, 575 (1962).
5. Kac, M., *Probability and Related Topics in Physical Sciences*, Interscience, New York–London, 1959.
6. Kac, M., *Bull. Am. Math. Soc.*, **53**, 1012 (1947).
7. Johnsen, U., *Kolloid Z.*, **178**, 161 (1961).
8. Fox, T. G, and B. D. Coleman, paper presented to the Division of Polymer Chemistry, 142nd National Meeting of the American Chemical Society, September 1962; see also B. D. Coleman and T. G Fox, *J. Chem. Phys.*, **38**, 1065 (1963).

Résumé

Lorsque, dans une poly-α-oléfine, la probabilité d'une séquence isotactique dépend seulement d'un nombre limité de séquences précédentes, alors la distribution des segments qui en résulte suit la théorie des chaînes de Markoff. Dans l'autre cas, on dit que la distribution résultante est non-Markoffienne. Un cas spécial de cette distribution de Markoff est donné par une chaîne simple de Markoff dont la tacticité d'un placement donné est considérée comme étant influencée seulement par la séquence qui précède immédiatement. Un autre cas spécial est représenté naturellement par la distribution de Bernoulli dans laquelle la probabilté qu'un placement donné soit isotactique est indépendant de la tacticité de tout autre séquence. Un spectre NMR à haute résolution peut parfois fournir une détermination quantitative des concentrations des séquences isotactiques et syndiotactiques et des concentrations de trois types des paires adjacentes possibles de telles séquences, notamment des paires isotactique, syndiotactique et hétérotactique. Dans ce cas le spectre peut être employé pour déterminer si la distribution d'une séquence arbitraire est une distribution de Bernoulli ou pas. Pourtant, la plus longue séquence dont la concentration peut être mesurée par spectroscopie NMR consiste uniquement en deux unités; un spectre NMR ne peut pas définir dés lors si une distribution donnée non-Bernoullienne correspond à une distribution Markoffienne ou non-Markoffienne. En effet, les distributions non-Markoff sont compatibles avec des spectres de polyméres préparés par voie anionique. Dans cet article nous travaillons dans un cadre de la théorie de Kac qui traite des processus statistiques stationnaires et nous indiquons quelques résultats sui sont valables pour les deux processus: suivant

Markoff et non-Markoff. Les résultats sont appliqués à la spectroscopie NMR; on a indiqué quels calculs sont valables pour les distributions Markoffienne et non-Markoffienne descalculs employés à tester la validité des résultats NMR et à obtenir la longuer moyenne des diastériosćquences fermées.

Zusammenfassung

Falls bei einem Poly-α-Olefin die Wahrscheinlichkeit für die Isotaktizität einer gegebenen Plazierung nur von der Taktizität einer endlichen Zahl unmittelbarer Vorgänger abhängt, so gehorcht die resultierende Diastereosequenzverteilung der Theorie der Markoffketten. Wenn das nicht der Fall ist, bezeichnet man die resultierende Diastereosequenzverteilung als nicht-Markoffisch. Ein Spezialfall einer Markoffverteilung wird durch eine einfache Markoffkette gebildet, bei welcher die Taktizität einer gegebenen Plazierung als nur von der Taktizität der unmittelbar vorhergehenden Plazierung beeinflusst betrachtet wird. Einenweiteren Spezialfall bildet natürlich die Verteilung nach dem Bernoullischem Theorem, bei welcher die Wahrscheinlichkeit für die Isotaktizität einer gegebenen Plazierung unabhängig von der Taktizität aller übrigen Plazierungen ist. Ein Hochauflösungs-NMR-spektrum erlaubt manchmal eine quantitative Bestimmung der Konzentration isotaktischer und syndiotaktischer Plazierungen sowie der Konzentration der drei möglichen Typen benachbarter Paare solcher Plazierungen (nämlich isotaktische, syndiotaktische und heterotaktische Paare). In diesem Fall kann das Spektrum zur Entscheidung defür benutzt werden, ob eine gegebene Diastereosequenzverteilung vom Bernoulli-Typ ist. Da jedoch die längste Diastereosequenz, deren Konzzentration durch NMR-Spektroskopie bestimmt werden kann, nur zwei Plazierungen enthält, kann ein NMR-Spektrum nicht darüber entscheiden ob eine gegebene Nicht-Bernoulli-Verteilung vom einfachen oder allgemeinen Markoff-Typ ist. Tatsächlich sind Nicht-Markoff-Verteilungen mit den bekannten NMR-Spektren von anionisch hergestellten Polymeren verträglich. Die-vorliegende Mitteilung bewegt sich im Rahmen der Theorie von Kac und bringt einige allgemeine Ergebnisse, die sowohl für Markoff- als auch Nicht-Markoff-Prozesse gültig sind. Die Ergebnisse werden auf die NMR-Spektroskopie angewendet und es wird gezeigt, welche, bei der Überprüfung der Konsistenz der NMR-Daten und bei der Ermittlung der mittleren Länge geschlossener Diastereosequenzen verwendeten Berechnungen, sowohl für Markoff- als auch Nicht-Markoffverteilungen gültig sind.

Received August 23, 1962

JOURNAL OF POLYMER SCIENCE: PART A VOL. 1, PP. 3199–3207 (1963)

Donor–Acceptor Interaction in Cationic Polymerization. V. Influence of Some Alcohols on the Molecular Weight of Polyisobutylene in Polymerization Catalyzed by Aluminum Trichloride*

Z. ZLÁMAL and A. KAZDA, *Research Institute of Macromolecular Chemistry, Brno, Czechoslovakia*

Synopsis

$AlCl_3$ in ethyl chloride at −78.5°C. forms with lower aliphatic alcohols (MeOH, EtOH, *i*-PrOH, *tert*-BuOH) complexes of the type $4ROH \cdot AlCl_3$, $2ROH \cdot AlCl_3$, $ROH \cdot AlCl_3$ and $ROH \cdot AlCl_6$. The existence of these complexes was established from the conductivity–composition graphs of corresponding ROH-$AlCl_3$ systems. These complexes are ionized to different degrees and their ability to catalyze the polymerization of isobutylene is proportional to the acidity of the alcohol forming the complex. Phenol differs somewhat in its behavior. The conductivity–composition plot reveals the existence of complexes of the type $3C_6H_5OH \cdot AlCl_3$, $2C_6H_5OH \cdot AlCl_3$, and $C_6H_5OH \cdot AlCl_3$. The catalytic activity of complexes containing phenol and $AlCl_3$ is considerably higher than that of complexes involving aliphatic alcohols. The dependence of the molecular weight of polyisobutylene on the composition of the active complex is a mirror image of the conductivity graph. The rate of termination reactions changes with both concentration and quality of anions present. The termination activity of anions derived from phenol and containing —O—C_6H_5 group is considerably higher than the termination activity of anions derived from aliphatic alcohols.

INTRODUCTION

In previous work we have shown[1–5] that there is a close connection between the degree of polymerization of polymer formed and the electrical conductivity of the system in cationic $AlCl_3$-catalyzed polymerization of isobutylene.

A study of the electrical conductivity of such system has revealed that a basic cocatalyst usually forms with the catalyst ($AlCl_3$) several types of complexes of different molar content of basic and acidic components.[2] These complexes usually ionize to different degrees so that their formation is apparent from the specific conductivity versus composition curve. It has been found that a maximum molecular weight of polyisobutylene is reached in media such that the specific conductivity goes through a minimum.

* Much of this work was reported at the Macromolecular Symposium, Wiesbaden, Germany, 1959.

In the present investigation we studied the influence of several alcohols which are usually found in trace quantities in common chemicals even after a thorough purification and which we used in practice as cocatalysts.[6]

EXPERIMENTAL

Material Used

Ethyl chloride used as solvent was purified by distillation at ordinary pressure, the vapor being led through three absorbing towers packed with silica gel and wetted with sulfuric acid.[7] Contents of polar impurities reacting with aluminum trichloride ranged from 0.5 to 1.0 $\times$ 10^{-3} mole/l.

Isobutylene was prepared and purified as described previously.[3] Its purity was checked by means of melting point and chromatographic analysis. The melting point of -140.333 ± 0.002°C. corresponded to a content of isobutylene of $99.83 \pm 0.02\%$ which was in agreement with a chromatographic data. The water content was 30 ppm.

Anhydrous aluminum trichloride was obtained by twice subliming a pure commercial product.

All alcohols used were dehydrated by calcined CaO or BaO and subsequent distillation.[8]

Experimental Technique

Polymerization, conductivity measurement, and molecular weight determination were carried out as described earlier.[1-4] All experiments were run at the same monomer concentration.

Conductivity measurements were made in ethyl chloride solution at a concentration of 25 $\times$ 10^{-3} mole/l. ($AlCl_3$ or ROH) at the start of titration and at a temperature of -78.5°C. Results were plotted as conductivity–composition graphs and as molecular weight–composition graphs.

RESULTS AND DISCUSSION

Specific conductivity–composition relationships were obtained as above for the systems MeOH–$AlCl_3$, EtOH–$AlCl_3$, *i*-PrOH–$AlCl_3$ and *tert*-BuOH–$AlCl_3$. Results are shown in Figures 1 and 2. The plot representing the system MeOH–$AlCl_3$ is slightly deformed since under experimental conditions used the complexes formed in excess $AlCl_3$ were poorly soluble and a white crystalline precipitate settled out of solution. All other alcohols studied yielded soluble complexes under similar conditions.

The conductivity plot of the systems MeOH–$AlCl_3$ indicates the presence of the complexes $4ROH \cdot 2AlCl_3$, $2ROH \cdot AlCl_3$, $ROH \cdot AlCl_3$, and $ROH \cdot 2AlCl_3$ and the same was found to hold for the systems EtOH–$AlCl_3$ and *i*-PrOH–$AlCl_3$ as well.

In all three systems there was a minimum conductivity at the 1:1 molar ratio and a maximum conductivity at the composition $2\ ROH \cdot AlCl_3$. A difference between primary and secondary alcohols was not observed.

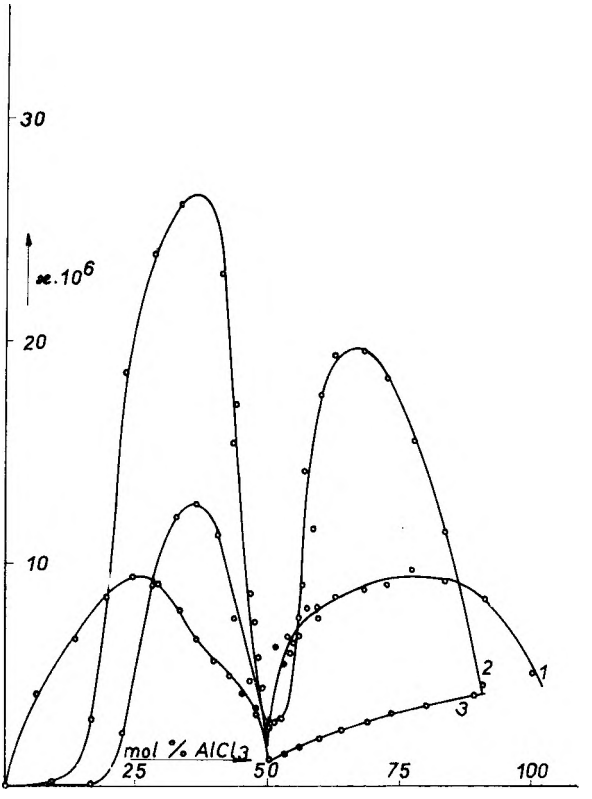

Fig. 1. Dependence of the specific conductivity $\varkappa$ of solutions of alcohols and aluminum trichloride in ethyl chloride on the molar ratio of dissolved components: (*1*) methanol; (*2*) isopropanol; (*3*) phenol. The initial concentration of alcohol was 25×10^{-3} mole/l. Titrated at -78.5°C.

A somewhat blunt transition in the case of *i*-PrOH in the region of the equivalence point was ascribed to incomplete removal of moisture from the alcohol, because a similar blunt transition was found in the case of incompletely dehydrated ethanol.

Marked deviations were observed, however, in the system *tert*-BuOH–$AlCl_3$ (Fig. 2). The maximum conductivity was found to correspond to the complex $4ROH \cdot AlCl_3$ unlike all other alcohols studied. The conductivity of this complex is almost four times stronger than that of the most conductive complex of MeOH. The $2ROH \cdot AlCl_3$ complex makes only an inflection on the conductivity curve, and the minimum conductivity was at the 1:1 molar ratio, as in the case of other alcohols studied.

The conductivity of complexes of the MeOH and EtOH series was independent of time, which implies that the reaction between the alcohols and $AlCl_3$ is a fast one and that the complexes formed are stable. In the case of isopropanol a certain change of conductivity with time was already noticeable and in the case of *tert*-butyl alcohol the time dependence was quite pronounced.

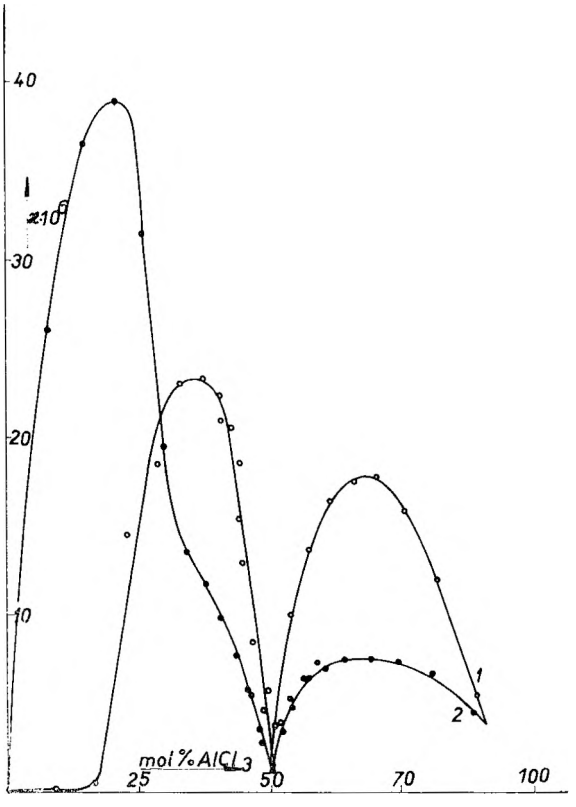

Fig. 2. Dependence of the specific conductivity $\varkappa$ of solutions of alcohol and aluminum trichloride in ethyl chloride on the molar ratio of dissolved components: (*1*) ethanol (*2*) *tert*-butanol. The initial concentration of alcohol was 25×10^{-3} mole/l. Titrated at -78.5°C.

We may therefore assume that lower aliphatic alcohols form four types of complexes with aluminum trichloride which appear on the conductivity-composition curve and that these four types will influence the molecular weight of polyisobutylene formed in polymerization. Conductivity changes with time indicate that all of these complexes are more stable than analogous complexes of ethers with aluminum trichloride; complexes with *tert*-butyl alcohol are relatively less stable.

Since hydrolysis and—even more so—the alcoholysis of aluminum halides proceed slowly and incompletely[9] even at elevated temperatures, it appears to us correct to derive the structure of the complexes observed from a gradual solvation of the protone by alcohol rather than from a replacement of the covalently bound halide by the alcohol.

We therefore assume the following reaction schemes:

Type 1:2 $\quad ROH + 2AlCl_3 \rightleftharpoons H^{\oplus}\,[Al_2Cl_6OR]^{\ominus}$

Type 1:1 $\quad ROH + AlCl_3 \rightleftharpoons H^{\oplus}\,[AlCl_3OR]^{\ominus}$

Type 2:1 $$ROH + H^{\oplus}[AlCl_3OR]^{\ominus} \rightleftharpoons [ROH_2]^{\oplus}[AlCl_3OR]^{\ominus}$$

Type 4:1

$$2ROH + [ROH_2]^{\oplus}[AlCl_3OR]^{\ominus} \rightleftharpoons [2ROH \cdot ROH_2]^{\oplus}[AlCl_3OR]^{\ominus}$$

Electrolysis which might prove these assumed structures has not been carried out so far. However, many of the complexes observed by us have been described by other workers.[10,11]

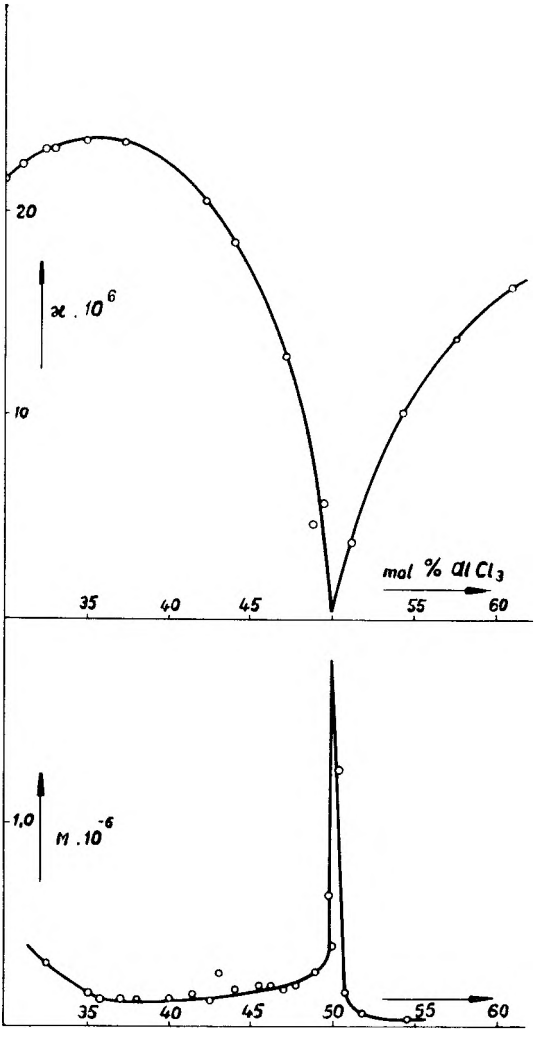

Fig. 3. Relation between the specific conductivity $\varkappa$ and the molecular weight of polyisobutylene formed: (top) a section of the conductivity graph of the system ethanol–$AlCl_3$; (bottom) dependence of the molecular weight of the polymer on the ethanol: $AlCl_3$ ratio. Polymerized in ethyl chloride solutions at −78.5°C.; the initial concentration of ethanol was 25×10^{-3} mole/l.

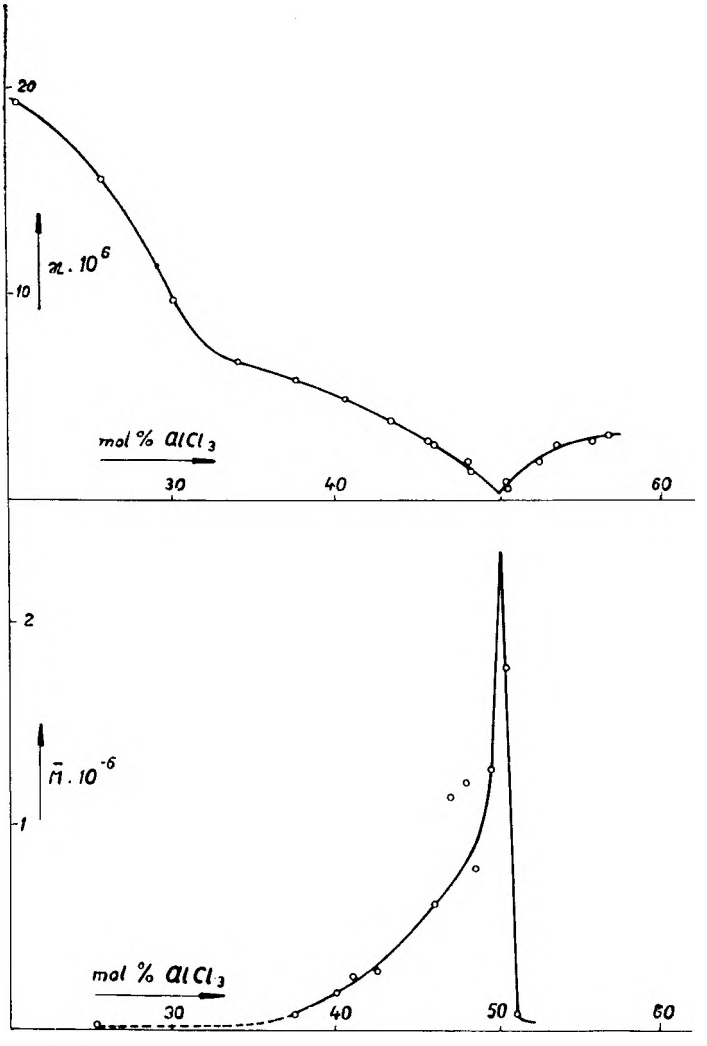

Fig. 4. Relation between the specific conductivity $\varkappa$ and the molecular weight of polyisobutylene formed: (top) a section of the conductivity graph of the system *tert*-butanol–$AlCl_3$; (bottom) dependence of the molecular weight of the polymer on *tert*-butanol–$AlCl_3$ ratio. Polymerized in ethyl chloride solutions at -78.5°C.; the initial concentration of *tert*-butanol was 25×10^{-3} mole/l.

Increasing volume of cations leads to increasing distance between positive and negative center of charge of ion- pairs and enhanced ionization. The conductivity of the system therefore increases unless the influence of ionization on conductivity is cancelled by decreased mobility of ions. Gradual solvation decreases the efficiency of cations in the process of initiation since the energetic balance of the transition to the carbonium salt of the monomer is poorer by the energy necessary to break oxonium formations.

The rate of polymerization of polyisobutylene (observed qualitatively) gradually decreases with increasing excess of alcohol over the 1:1 ratio with respect to $AlCl_3$ and the molecular weight of polymer decreases. This is due to the fact that the reactivity of anions in the process of termination does not change appreciably because their composition remains the same (with the exception of the 1:2 type) and with increasing dissociation their concentration increases.

However, even in an excess of alcohol at least part of cations or ion-pairs preserve their ability to catalyze polymerization as is shown by our polymerization experiments.

Figures 3 and 4 show results of polymerization tests carried out in the presence of ethanol and *tert*-butyl alcohol. We chose these alcohols because their conductivity–composition courses were not distorted by secondary effects. In the upper part of both figures are corresponding conductivity scales and in the lower part data on the molecular weight of polyisobutylene obtained by polymerization in solutions with changing ROH:-$AlCl_3$ ratio. The concentration of the alcohol at the beginning was in all cases 25×10^{-3} mole/l. (conductivity runs included).

It can be seen from these figures that the positions of maxima and minima in the conductivity curve are a mirror image of the molecular weight, even in the case of *tert*-butanol, which generally behaves differently from other alcohols studied.

The increased molecular weight in the region of excess *tert*-butanol could no longer be studied, since a turning-point in the conductivity behavior and hence also in molecular weight data lies at a fourfold excess of base, while for other alcohols this point lies at a twofold excess. At a fourfold excess of *tert*-butanol rates of polymerization and conversions obtained no longer could be studied by the methods in the present study.

In the case of ethanol, however, this turning-point is readily observed (see Fig. 3). In the region of excess base (alcohol in this case) the reaction rates and conversions are low and increase with increasing $AlCl_3$ content. In the region of excess $AlCl_3$ reactions are very fast, and at a content of 55–60 mole-% of $AlCl_3$ they are nonisothermal and sometimes explosive, with conversions reaching 100%.

A 100% conversion is observed also in the region of excess base, at compositions depending on the acidity of the base. In the system diethyl ether–$AlCl_3$ a 100% conversion is found at a content of 50 mole-% $AlCl_3$; in the system ethanol–$AlCl_3$ this occurs at 47 mole-% $AlCl_3$, and finally in the system *tert*-butanol–$AlCl_3$, at a content of 42 mole-% $AlCl_3$.

In experiments involving the phenol–$AlCl_3$ system the acidity of the phenol was so marked that at content of 33 mole-% $AlCl_3$ the reaction proceeded explosively, nonisothermally, and to 100% conversion. For these reasons a complete molecular weight–composition plot could not be constructed. Conductivity versus composition data are shown in Figure 1. The specific conductivity of the system differs considerably from that of aliphatic alcohols.

Figure 1 discloses the existence of complexes of the type $3C_6H_5OH \cdot AlCl_3$, $2C_6H_5OH \cdot AlCl_3$ (inflection), and $C_6H_5OH \cdot AlCl_3$ (minimum). A complex having the composition $C_6H_5OH \cdot Al_2Cl_6$ is either not formed or was not revealed by conductivity data.

The circumstance that in the presence of phenol the polymer produced is one of low molecular weight despite low specific conductivity of the system seems to imply that the termination efficiency of anions containing the $-O-C_6H_5$ group is considerably higher than that of anions derived from aliphatic alcohols and containing the $-O-R$ group. The low specific conductivity of this system is not due to decreased mobility of ions since considerably higher specific conductivity was found in the system diphenyl ether–$AlCl_3$ (it formed just the same anions as phenol) at the same molar concentrations.[12] Results reported in this work as well as in previous communications of this series[1-4] show that for a quantitative evaluation of relationship between the conductivity of the system and the molecular weight of polymer produced, it is essential to maintain a constant molar composition of the active complex, i.e., constant catalyst:cocatalyst ratio, since changes in its composition affect the mechanism and kinetics of polymerization much more than do changes in its summary concentration.

References

1. Zlámal, Z., L. Ambrož, and K. Veseleý, *J. Polymer Sci.*, **24**, 285 (1957).
2. Zlámal, Z., and L. Ambrož, *J. Polymer Sci.*, **29**, 595 (1958).
3. Ambrož, L., and Z. Zlámal, *J. Polymer Sci.*, **30**, 381 (1958).
4. Zlámal, Z., and A. Kazda, *J. Polymer Sci.*, **53**, 203 (1961).
5. Veseleý, K., *J. Polymer Sci.*, **30**, 375 (1958).
6. Zlámal, Z., and A. Kazda, Czech. Pat. 101733 (1961).
7. Zlámal Z., and A. Kazda, Czech. Pat. 89822 (1957).
8. Weissberger, A., and E. S. Proskauer, *Organic Solvents*, Interscience, New York, 1955.
9. Fairbrother F., and W. C. Frith, *J. Chem. Soc.*, **1953**, 2975.
10. Wilke, J., Dissentation, Humboldt Univ., Berlin, 1956.
11. Gorenbeĭn, E. J. and V. N. Davidova, *Obsch. Khim.*, **27**, 858 (1957).
12. Zlámal, Z., Dissertation, Institute of Physical Chemistry, ČSAV, Prague, 1959.

Résumé

$AlCl_3$ dans le chlorure d'éthyle à $-78.5°C$ forme avec les alcools aliphatiques de faible poids moléculaire (MeOH, EtOH, *iso*-PrOH, *tert*-Bu–OH) des complexes du type $4ROH \cdot AlCl_3$, $2ROH \cdot AlCl_3$, $ROH \cdot AlCl_3$ et $ROH \cdot Al_2Cl_6$. L'existence des ces complexes a été établie à partir des diagrammes conductivité–composition des sysmèmes ROH–$AlCl_3$. Ces complexes présentent différents degrés d'ionisation et leur aptitude à catalyser el polymérisation de l'isobutylène est proportionnelle à l'acidité de l'alcoool formant la complexe. Le phénol diffère quelque peu dans son comportement. Le diagramme conductivité composition montre l'existence des complexes du type $3C_6H_5OH \cdot AlCl_3$, $2C_6H_5$-OH-$ALCl_3$ et C_6H_5OH-$AlCl_3$. L'activité catalytique des complexes contenant du phénol et $AlCl_3$ est considéarble mentplus élevée que celle des complexes contenant des alcools aliphatiques. La dépendance du poids moléculaire du polyisobutylène avec la composition du complexe actif est une image du diagramme de conductivité. La vitesse des réactions de terminaison change avec la concentration et la qualité des anions

présents.[5] L'activité de terminaison des anions dérivés du phénol et contenent le groupe —O—C_6H est considérablement plus élevée que l'activité de terminaison des anions dérivés des alcools aliphatiques.

Zusammenfassung

$AlCl_3$ bildet in Äthylchlorid bei −78,5°C mit niedrigeren aliphatischen Alkoholen (MeOH, EtOH, *iso*-PrOH, *tert*-BuOH) Komplexe vom Typ $4ROH \cdot AlCl_3$, $2ROH \cdot AlCl_3$, $ROH \cdot AlCl_3$ und $ROH \cdot Al_2Cl_6$. Die Existenz dieser Komplexe wurde aus dem Leitfähigkeits-Zusammensetzungsdiagramm der betreffenden ROH–$AlCl_3$-Systeme abgeleitet. Die Komplexe sind zu verschiedenem Grad ionisiert und ihre Fähigkeit, die Polymerisation von Isobutylen zu katalysieren, ist der Acidität des den Komplex bildenden Alkohols proportional. Phenol zeigt ein etwas andersartiges Verhalten. Das Leitfähigkeits-Zusammensetzungdiagramm lässt die Existenz von Komplexen vom Typ $3C_6H_5OH \cdot AlCl_3$, $2C_6H_5OH \cdot AlCl_3$ und $C_6H_5OH \cdot AlCl_3$ erkennen. Die katalytische Aktivität der Phenol-$AlCl_3$-Komplexe ist bedeutend grösser als diejenige der Komplexe mit aliphatischen Alkoholen. Die Abhängigkeit des Molekulargewichts des Polyisobutylens von der Zusammensetzung des aktiven Komplexes bildet ein Spiegelbild des Leitfähigkeitsdiagramms. Die Geschwindigkeit der Abbruchsreaktion hängt von Konzentration und Art der anwesenden Anionen ab. Die Abbruchswirksamkeit der vom Phenol abgeleiteten Anionen mit —O—C_6H_5-Gruppen ist beträchlitch höher als die der von aliphatischen Alkoholen abgeleiteten.

Received April 26, 1962
Revised August 15, 1962

JOURNAL OF POLYMER SCIENCE: PART A VOL. 1, PP. 3209–3216 (1963)

Primary Radical Termination in Methyl Methacrylate Polymerization*

M. G. BALDWIN, *Rohm & Haas Company, Redstone Arsenal Research Division, Huntsville, Alabama*

Synopsis

The kinetics of polymerization of methyl methacrylate in benzene solution at 60°C., initiated by 2,2′-azobisisobutyronitrile (AIBN), were studied for monomer concentrations of 0.03–1*M*. The observed deviations in polymerization rate from the rates predicted by simple theory are discussed in terms of the occurrence of primary radical termination reactions. The fraction of primary radicals terminating chains was obtained for various monomer and initiator concentrations, and the ratio of rate constants for chain initiation and chain termination by a primary radical was determined.

I. INTRODUCTION

In the kinetic analysis of the polymerization of vinyl compounds by free radical mechanisms, termination reactions directly involving initiator radicals, hereafter referred to as primary radicals, are usually ignored. This is justified in most systems, namely those in which the monomer and primary radical concentrations are such that essentially every primary radical reacts with monomer shortly after its formation. However, if the monomer and primary radical concentrations are at levels which allow an appreciable lifetime for the primary radicals, primary radical terminations must be considered. It is the purpose of this report to describe an investigation of the rate of polymerization of methyl methacrylate (MMA) in benzene solution initiated by 2,2′-azobisisobutylronitrile (AIBN) at concentrations of MMA and AIBN such that primary radical termination reactions are important.

In recent years, several workers have reported on the importance of primary radical termination in various polymerization systems.[1–7] Most of the experimental work involved monomer concentration ranging upward from about 1*M*. Since the effect of primary radical termination should become more pronounced as the monomer concentration is decreased, the studies here reported involved the monomer concentration range of 0.03–1*M*. Initiator concentrations ranged from 1×10^{-4} to 5×10^{-3} *M*. The results have been interpreted in terms of a simple

* This work was performed under the sponsorship of the U. S. Army under Contract No. DA-01-021-ORD-11878.

kinetic model discussed by Bamford, Jenkins, and Johnston[2] which includes the termination reaction

$$R\cdot + M_n\cdot \rightarrow \text{Polymer}$$

where R· is a primary radical and M_n· is a polymer chain radical.

II. EXPERIMENTAL

Materials

Commercial methyl methacrylate (Rohm and Haas Company) was washed three times with 5% sodium hydroxide, once with water, twice with saturated aqueous sodium thiosulfate solution, then twice with water. It was dried over Drierite and fractionally distilled under reduced pressure. The middle cut, boiling at 41–42°C. (85 mm.) was retained and stored in the dark at −20°C. until used.

Commercial AIBN was recrystallized three times from absolute methanol (m.p. 102–103°C. with decomposition) and stored over Drierite at −20°C. in the dark until used.

Reagent-grade benzene was fractionally distilled from P_2O_5 through a 45 plate column.

Triply distilled mercury supplied by the Bethlehem Apparatus Company was used in all experiments. It was taken from freshly opened containers and used without further purification.

Dilatometric Procedure

The dilatometer consisted of a Pyrex bulb and a section of calibrated 1 mm. diameter capillary tubing, which constituted the two arms of a U. The bulb was attached to the capillary through a ground glass joint. Above the capillary was a reservoir for holding and degassing mercury, and a ground glass joint through which the entire dilatometer could be attached, through a removable stopcock, to a high vacuum source.

The procedure used in making a polymerization rate determination involved the following steps. The sample bulb containing weighed amounts of monomer, stock solutions of initiator in benzene, and solvent was attached to the inverted dilatometer and held in place by means of metal springs. The contents of the bulb were then degassed at 10^{-5} mm. by three alternate freeze–thaw cycles. After degassing, the sample was frozen and the dilatometer inverted while still under high vacuum, causing mercury to flow from the reservoir, filling the capillary and trapping the frozen sample in the bulb. The dilatometer was removed from the vacuum line and placed in a constant temperature bath. After thermal equilibration had occurred, excess mercury was removed from the capillary and periodic readings of the height of the mercury level in the capillary were made with a cathetometer accurate to ±0.03 mm. The bath temperature was controlled to ±0.005°C. The rate of polymerization was calculated from shrinkage data by assuming that the fraction of total polymerization shrinkage was equivalent to the fraction of polymerization which had

occurred at a given time. A total shrinkage of 25.1% at 60°C. was used. This value was estimated from the data of Fox and Loshaek[8] for the density of PMMA in monomer at 60°C.

The conclusions expressed in this paper are based on kinetic measurements made at high monomer dilution. It is thus important that the method used for measuring the polymerization rate be critically examined, and the possibility must be considered that the results obtained are due to adventitious impurities or extraneous reactions of some kind. In particular, it must be shown that the mercury used as the confining fluid in the dilatometers did not influence the observed result. The following observations bear on the reliability of the dilatometric data.

(*1*) The total shrinkage and capillary diameter were such that for the lowest monomer concentration studied (0.03*M*) the fraction of total shrinkage at a given time could be determined to within less than 1%. Errors due to fluctuations in bath temperature were found to be negligible.

(*2*) There was no appreciable induction period for even the lowest initiator concentrations studied: beginning of shrinkage was essentially coincident with thermal equilibration. Each run was carried to about 10% completion, and gave a linear first order plot.

(*3*) The possibility that the mercury surface affected the kinetics was investigated by using sample bulbs of different shapes and sizes such that the ratio V/A [volume of solution (cm.^{3})/mercury surface (cm.)^2] was varied from about 1 to 50 with no detectable effect on the rate.

III. KINETIC ANALYSIS INCLUDING PRIMARY TERMINATION

The usual kinetic analysis of free radical polymerization processes is based on the following reaction scheme (excluding transfer reactions).

Initiator decomposition:

$$\mathrm{I} \xrightarrow{k_d} 2\mathrm{R}\cdot \tag{1a}$$

Chain initiation:

$$\mathrm{R}\cdot + \mathrm{M} \xrightarrow{k_i} \mathrm{M}\cdot \tag{1b}$$

Chain propagation:

$$\mathrm{M}_n\cdot + \mathrm{M} \xrightarrow{k_p} \mathrm{M}_{n+1}\cdot \tag{1c}$$

Chain termination:

$$\mathrm{M}_n\cdot + \mathrm{M}_n\cdot \xrightarrow{k_t} \text{Polymer} \tag{1d}$$

Reaction (1b) is considered to be insignificant for long-chain polymer and is neglected. By applying the steady-state assumption, the familiar expression

$$R_p \equiv -d[\mathrm{M}]/d_t = k_p(fk_d[\mathrm{I}])^{1/2}[\mathrm{M}]/k_t^{1/2} \tag{2}$$

is obtained, where the initiator efficiency f represents the fraction of radicals produced in reaction (1a) which escape the "solvent cage" and initiate

chains by reaction (1b). Thus the quantity $R_p/[M][I]^{1/2}$ is predicted to be constant for a system described by reactions (1a)–(1d).

This treatment can be expanded to include the primary radical termination reactions:

$$R\cdot + M_n\cdot \xrightarrow{k'_t} \text{polymer} \tag{1e}$$

$$R\cdot + R\cdot \xrightarrow{k_t} \text{inactive product} \tag{1f}$$

Reaction (1f) refers to primary radical recombination involving radicals from different initiator molecules, i.e., primary recombinations other than those which occur in the solvent cage. In the present work, only reaction (1e) was considered, since it was felt that unless $k''_t \gg k'_t$, reaction (1f) would be of importance only in systems having vanishingly small monomer concentrations. Results described below are consistent with this assumption.

A relationship between R_p, [M], and [I] can readily be obtained for the expanded kinetic scheme involving reactions (1a)–(1e), as was shown by Bamford, Jenkins, and Johnston.[2] Making the usual steady-state assumptions with respect to the concentrations of both R· and M·, one obtains eq. (3):

$$\frac{R_p\delta}{[M]^2}\left(\frac{1 + \dfrac{R_p^2\delta^2}{[M]^2R_i}}{1 - \dfrac{R_p^2\delta^2}{[M]^2R_i}}\right) = k_t^{1/2}\frac{k_i}{k'_t} = \Lambda \tag{3}$$

where R_p is the polymerization rate, $-d[M]/dt$, $\delta = k_t^{1/2}/k_p$, and $R_i = 2fk_d[I]$ is the rate of production of radicals which have escaped from the solvent cage. The quantity Λ, or more precisely the ratio k_t/k'_t gives a measure of the importance of primary radical termination in a given system. If k_t is known for the monomer being considered, the value of k_t/k'_t can be calculated.

A knowledge of Λ for a particular system allows the calculation of the fraction ϕ of primary radicals which terminate polymer chains. According to the kinetic scheme represented by reaction (1a)–(1e), primary radicals R· are removed from the system in only two ways,

$$R\cdot + M \xrightarrow{k_i} M\cdot \tag{1b}$$

and

$$R\cdot + M_n\cdot \xrightarrow{k'_t} \text{polymer} \tag{1e}$$

The fraction of R· terminating chains is thus given by

$$\phi = \frac{k'_t[R\cdot][M_n\cdot]}{k'_t[R\cdot][M_n\cdot] + k_i[R\cdot][M]} \tag{4}$$

The rate of polymerization is given by

$$R_p = k_p[M_n\cdot][M] \tag{5}$$

from which one obtains

$$[M_n\cdot] = \frac{R_p}{k_p[M]} \tag{6}$$

Substitution for $[M_n\cdot]$ in eq. (3) and rearrangement leads to the expression

$$\phi = \frac{1}{1 + (k_i/k'_i)(k_p[M]^2/R_p)} \tag{7}$$

Substitution of

$$\Lambda = k_t^{1/2}(k_i/k'_i)$$

and

$$\delta = k_t^{1/2}/k_p$$

gives finally

$$\phi = \frac{1}{1 + (\Lambda[M]^2/\delta R_p)} \tag{8}$$

IV. RESULTS

Table I shows the polymerization rate data obtained at 60°C. for methyl methacrylate in benzene solution. The quantities Λ and ϕ have been calculated for the low monomer concentrations and are included in the table. The significance of each quantity is discussed below. The values of δ and

TABLE I

Experiment No.	[M], moles/l.	[I] × 10^3, moles/l.	$\frac{R_p}{[M][I]^{1/2}} \times 10^4$	$\Lambda \times 10^3$ [a]	ϕ
1	0.0298	5.84	0.98	1.86	0.62
2	0.0784	5.81	1.52	1.22	0.49
3	0.0844	5.03	1.79	1.34	0.50
4	0.0905	0.799	2.57	0.94	0.35
5	0.107	0.0825	3.23	0.44	0.15
6	0.108	2.89	2.32	1.22	0.43
7	0.116	1.05	2.47	0.77	0.31
8	0.117	1.86	2.37	0.94	0.37
9	0.117	0.802	2.65	0.77	0.30
10	0.118	4.89	2.08	1.19	0.45
11	0.119	2.99	2.23	1.05	0.40
12	0.120	0.569	2.68	0.65	0.26
13	0.131	4.89	2.17	1.16	0.43
14	0.236	5.02	2.63	0.94	0.34
15	0.462	4.98	3.07	0.69	0.24
16	0.955	5.04	3.45	—	—
17	1.66	3.85	3.56	—	—
18	3.66	4.34	3.58	—	—

[a] $\Lambda_{mean} = 1.05 \times 10^{-3}$. In the calculation of Λ_{mean} values from experiments 1 and 5 were excluded. These represent the lowest monomer and initiator concentrations that were used, and probably reflect high experimental error.

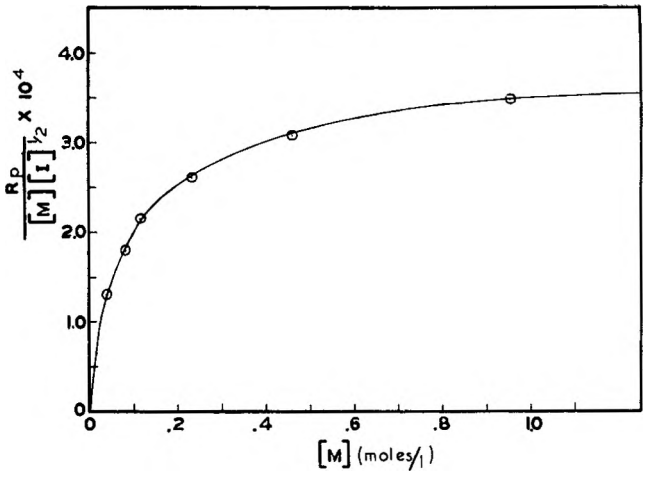

Fig. 1. The quantity $R_p/([M][I]^{1/2})$ obtained from polymerization of methyl methacrylate in benzene at 60°C. plotted against methyl methacrylate concentration for a constant AIBN concentration of $5 \times 10^{-3}M$.

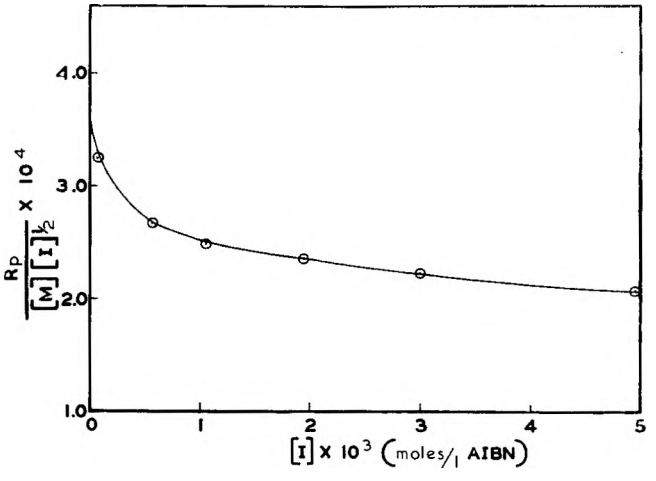

Fig. 2. The quantity $R_p/([M][I]^{1/2})$ obtained from polymerization of methyl methacrylate in benzene at 60°C. plotted against AIBN concentration for a constant methyl methacrylate concentration of $0.11M$.

R_i that were used in the calculations were: $\delta = 6.95$[9] and $R_i = 2fk_d[I] = 1.26 \times 10^{-5}[I]$. The expression for R_i was obtained from the value for (fk_d) calculated from the equation:

$$R_p/[M][I]^{1/2} = (fk_d)^{1/2}/\delta$$

which holds for high monomer concentration. The experimental limiting value for $R_p/[M][I]^{1/2}$ of 3.6×10^{-4} and the above δ value were used in calculating (fk_d). The R_i expression compares well with that obtained

from literature values of $f(0.6)$- and k_d (1.00×10^{-5}),[10,11] which give $R_i = 1.20 \times 10^{-5}[\mathrm{I}]$.

The variation of $R_p/[\mathrm{M}][\mathrm{I}]^{1/2}$ with monomer and initiator concentrations in the region of low monomer concentration is shown in Figures 1 and 2. The observed deviation of $R_p/[\mathrm{M}][\mathrm{I}]^{1/2}$ from the value of about 3.6×10^{-4} found for usual monomer concentrations (above $1M$ for practical initiator concentrations) is postulated to be due to the occurrence of primary radical termination reactions.* It is seen that in both figures the deviation of $R_p/[\mathrm{M}][\mathrm{I}]^{1/2}$ from the expected value (3.6×10^{-4}) increases as the ratio $[\mathrm{M}]/[\mathrm{I}]$ decreases, but approaches zero as $[\mathrm{M}]/[\mathrm{I}]$ increases. The effect of primary radical termination on the polymerization rate, and hence on $R_p/[\mathrm{M}][\mathrm{I}]^{1/2}$, is twofold. First, a radical that enters into a primary termination reaction according to reaction (1e) would otherwise have initiated a chain. Thus the effective initiation rate is lowered. And, second, each primary radical entering into a termination reaction, in addition to not starting a chain, stops a chain. It thus functions as an added inhibitor, decreasing the rate of polymerization.

The results shown in Figure 1 are similar to those obtained by Burnett and Loan,[7] whose explanation was in terms of termination reactions involving radicals formed by transfer with solvent, a situation which is kinetically similar to primary radical termination.

For a system accurately described by reactions (1a)–(1e), Λ is a characteristic constant which can be determined without knowledge of the absolute values of k_p and k_t for the monomer. If k_t is known for the monomer being studied, the ratio k_i/k'_t can be obtained from eq. (3). Bamford, Jenkins, and Johnston[2] obtained $\Lambda = 2.05 \times 10^{-3}$ for styrene initiated with AIBN in dimethylformamide solution at 60°C. Since k_t is known for MMA and styrene at 60°C., the values of k_i/k'_t can be calculated for both systems. For k_t(styrene) $= 3.6 \times 10^7$ (ref. 13) and k_t(MMA) $= 1.23 \times 10^7$ (ref. 9) at 60°C. one obtains

$$k_i/k'_t \text{ (Styrene)} = 3.4 \times 10^{-7}$$

$$k_i/k'_t \text{ (MMA)} = 3.0 \times 10^{-7}$$

From the Λ value for MMA, the fraction ϕ of primary radicals entering into termination reactions was calculated by means of eq. (8). It is seen from Table I that for very low monomer concentrations ϕ approaches, and actually exceeds in the extreme case, the theoretical upper limit of 0.5 predicted by the kinetic scheme 1a–1e. ϕ cannot be greater than 0.5 if only reactions (1a)–(1e) are included, since at least half of the available radicals must initiate chains. The value of ϕ exceeding 0.5 is perhaps an indication that reaction (1f) is significant at the lowest monomer concentrations, or

* Burnett and Loan[7] present graphical data for the system studied here from which a value of $R_p/[\mathrm{M}][\mathrm{I}]^{1/2}$ of 3.6–3.7 $\times 10^{-4}$ can be estimated. From the results of Baysal and Tobolsky[12] an average value of 3.4×10^{-4} for $R_p/[\mathrm{M}][\mathrm{I}]^{1/2}$ can be obtained for the AIBN-initiated bulk polymerization of methyl methacrylate at 60°C.

may merely reflect high experimental error at very low monomer concentrations.

By means of a technique involving endgroup analysis, Bevington and Allen[4] determined ϕ for the polymerization of styrene initiated by benzoyl peroxide in benzene solution at 60°C. Several monomer concentrations and rates of initiation were studied. The values of ϕ for the styrene system fall in the same range as those here reported for MMA.

References

1. Chapiro, A., M. Magat, J. Sebban, and P. Wahl, *Ric. Sci.*, **25A**, 73 (1955).
2. Bamford, C. H., A. D. Jenkins, and R. Johnston, *Trans. Faraday Soc.*, **55**, 1451 (1959).
3. Henrici-Olive, G., and S. Olivé, *Makromol. Chem.*, **37**, 71 (1960).
4. Bevington, J. C., and J. K. Allen, *Trans. Faraday Soc.*, **56**, 1762 (1960).
5. Hayden, P., and H. Melville, *J. Polymer Sci.*, **43**, 201 (1960).
6. Allen, P. E. M., and C. R. Patrick, *Makromol. Chem.*, **48**, 89 (1961).
7. Burnett, G. M., and L. D. Loan, *Trans. Faraday Soc.*, **51**, 219 (1955).
8. Fox, T. G, and S. Loshaek, *J. Polymer Sci.*, **15**, 371 (1955).
9. Schulz, G. V., G. Henrici-Olivé, and S. Olivé, *Z. Physik. Chem. (Frankfurt)*, **27**, 1 (1961).
10. Hammond, G. S., J. N. Sen, and C. E. Boozer, *J. Am. Chem. Soc.*, **77**, 3244 (1955).
11. van Hook, J. P., and A. V. Tobolsky, *J. Am. Chem. Soc.*, **80**, 779 (1958).
12. Baysal, B., and A. V. Tobolsky, *J. Polymer Sci.*, **8**, 529 (1952).
13. Matheson, M. S., E. E. Auer, E. B. Bevilacqua, and E. J. Hart, *J. Am. Chem. Soc.*, **73**, 1700 (1951).

Résumé

On a étudié les cinétiques de polymérisation du méthacrylate de méthyle en solution dans le benzène à 60°C, avec le 2,2′-azisobutyronitrile (AIBN) comme initiateur et pour des concentrations en monomères de 0.03—1 molaire. Les déviations observées dans la vitesse de polymérisation par rapport aux vitesses précises par la théorie sont discutées sur la base des réactions de terminaison par les radicaux primaries. La fraction de radicaux primaires participant à la terminaison de chaine a été obtenu pour différents monomères et à différentes concentrations en initiateur, et on a déterminé le rapport des constantes de vitesse pour l'initiation et la terminaison de chaîne pour un radical primaire.

Zusammenfassung

Die Kinetik der durch 2,2′-Azisobutyronitril (AIBN) gestarteten Polymerisation von Methylmethacrylat in Benzollösung wurde bei Monomerkonzentrationen von 0,03 bis 1 molar untersucht. Die beobachteten Abweichungen der Polymerisationsgeschwindigkeit von den nach der einfachen Theorie zu erwartenden Geschwindigkeiten werden als eine Folge des Auftretens eines Kettenabbruchs durch Primärradikale betrachtet. Der Bruchteil der am Kettenabbruch beteiligten Primärradikale wurde bei verschiedenen Monomer- und Starterkonzentrationen berechnet und das Verhältnis der Geschwindigkeitskonstanten für Kettenstart und Kettenabbruch durch ein Primärradikal bestimmt.

Received March 29, 1962
Revised August 10, 1962

JOURNAL OF POLYMER SCIENCE: PART A VOL. 1, PP. 3217–3229 (1963)

Phase Equilibria of Polymer–Solvent Systems at High Pressures Near Their Critical Loci: Polyethylene with *n*-Alkanes*

PAUL EHRLICH and JOHN J. KURPEN, *Monsanto Chemical Company, Plastics Division, Research Department, Springfield, Massachusetts*

Synopsis

Above the crystallization temperature slightly branched polyethylene and propane are miscible in all proportions above a critical pressure, defined as upper critical solution pressure (UCSP). This pressure decreases only very slightly from 110 to 150°C. At 110°C. the UCSP varies from 450 atm. for a polymer fraction of molecular weight 17,000, to 580 atm. for one of molecular weight 250,000. The critical polymer concentrations are low as in conventional polymer–solvent systems and shift with molecular weight in a similar manner. The pressures required to achieve solubility of the polymer in the gas at polymer concentrations less than critical (dew-point pressures) are nearly as high as the UCSP down to very low polymer concentrations. The data determine part of the critical locus in (P, T, composition) space. Experiments with other polyethylene–*n*-alkane systems (ethane, butane, and pentane) show that the critical locus changes gradually from a liquid–liquid to a gas–liquid boundary and might be termed a fluid-liquid locus. If crystallization of polymer does not intervene, this locus intersects the saturated vapor pressure curve at a lower critical end point (LCEP) which is the lower critical solution temperature (LCST) found only recently by Freeman and Rowlinson in many hydrocarbon polymers with hydrocarbon solvents. Incomplete miscibility extends over greater regions of temperature and pressure as the solvent molecule becomes smaller, but the critical locus would probably be closed along the pressure axis for a hypothetical amorphous polymethylene with ethane.

INTRODUCTION

We reported recently[1] that the phase equilibria of liquid high pressure polyethylene with compressed gases showed at least one of the usual characteristics of conventional polymer–solvent systems: a critical condition occurred at very low polymer concentration. This was associated with a change from negligible solubility of the polymer in the solvent to complete mutual miscibility over a small change in pressure. Polymers can therefore be completely miscible with compressed gases above a definite pressure[1,2] and the binary systems possess a gas–liquid critical locus in (P, T, composition) space.

Freeman and Rowlinson[3] found that hydrocarbon polymers heated

* Presented in part at the 145th Meeting of the American Chemical Society, September, 1963.

with hydrocarbon solvents under their own vapor pressure show liquid-liquid immiscibility above a lower critical solution temperature (LCST) which can be well below the critical point of the solvent. Such a LCST lies at the intersection of the vapor pressure surface with the critical locus and has been termed a lower critical end point (LCEP). A LCST generally increases with pressure near this point, i.e., the critical locus has a positive slope.[4] The solution of polymers in gases at high pressures is a possible consequence.

The work to be reported explores this connection further and provides data on the conditions of solubility of polyethylene in *n*-alkane solvents above and below their critical temperatures. The data will be seen to establish the general trends in the critical loci of binary alkane systems as the components assume extreme size differences.[5]

EXPERIMENTAL

Equipment

Figure 1 describes the experimental arrangement. The optical bomb A was supported inside a brass ring linked by a worm gear to a synchronous d.c. motor. It could be rocked automatically around the horizontal position in a plane perpendicular to the axis through either set of windows, and could be positioned at any desired angle. The bomb was connected via an arm of $^1/_4 \times {}^1/_{16}$ in. tubing (B) and a coil (D) made of $^1/_8 \times 0.020$ in. tubing, with its plane parallel to the plane of rotation of the bomb, to the

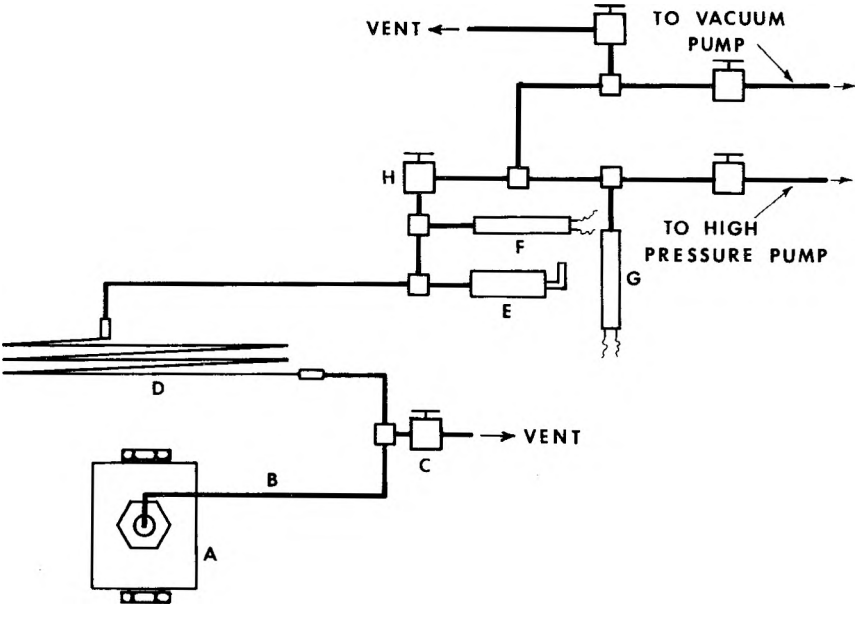

Fig. 1. Experimental arrangement.

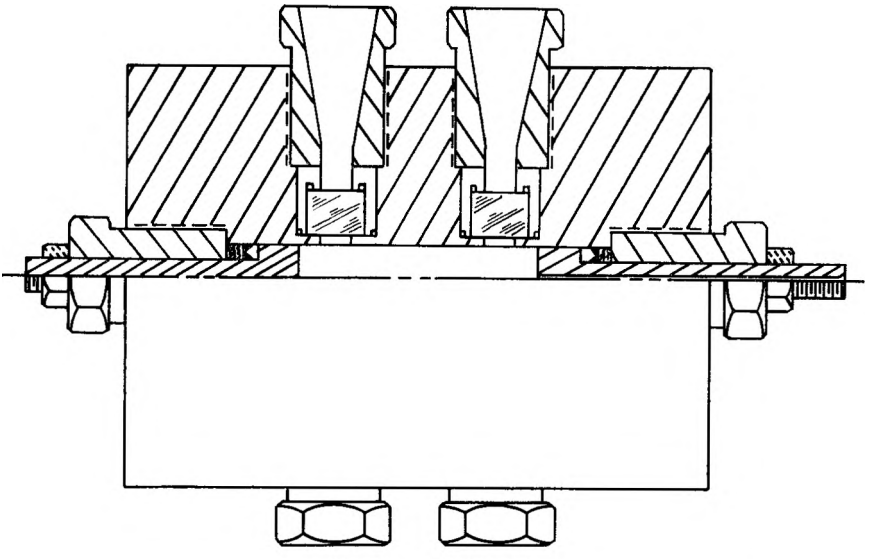

Fig. 2. Optical bomb.

filling system with connections to pressure transducers (F) and (G), vacuum line, and high pressure pump. (C) is a valve for venting.

The optical bomb (Fig. 2) was designed and built by the McCartney Mfg. Company (Baxter Springs, Kan.). It was made from 4340 double vacuum melt-forged steel and had two pairs of windows at 180° for viewing of the chamber by transmitted light. Windows (1 in. dia. × 3/4 in.) made from Pyrex, Feurex, or plate glass were sealed by two sets of Neoprene O-rings, and the two end closures were of the Bridgman type. The main dimensions of the bomb cavity were 4 × 1 in., and the volume was 62 cc.

Pressure transducer (F) was of the SR-4 type (Baldwin, Lima, Hamilton) and read on a Dynalog (Foxboro Co.) Recorder. It measured the pressure in the optical bomb. Transducer G (Microsen Type 145: Manning, Maxwell and Moore) measured the pressure on the pump side of the system and transmitted it to an indicating voltmeter. E is a rupture disk assembly (American Instrument Company). The high pressure pump was an air operated piston pump (Type 4444-J: McFarland Mfg. Corp.). A Bourdon gauge (not shown) measured the pressure in the experiments with pentane.

The bomb (but not the coil D) could be brought to the desired temperature by immersion in an oil bath raised by an air piston. The bath temperature was sensed by a thermocouple and recorded. A steady pressure in the bomb indicated thermal equilibrium.

Materials

Six polyethylene fractions were obtained by solvent–non-solvent fractionation from a high pressure polyethylene with 1.7% methyl content,

and the data to be reported were obtained with the four center fractions. The heterogeneity of the fractions was not determined. Molecular weights were measured osmometrically for the two high fractions and obtained from intrinsic viscosities[6] for the two low fractions. Ethane, *n*-propane, and *n*-butane were obtained from the Matheson Company, ethane at 99%, and *n*-propane and *n*-butane at 99.5% purity. *n*-Pentane was obtained from the Phillips Petroleum Company at 98.5% purity.

Procedure

A known weight of polymer and a steel ball, $^5/_8$ in. in diameter, were placed in the bomb which was then evacuated. Solvent was then compressed into the bomb (the pump chamber had to be cooled when ethane was used) such that, upon bringing it to the desired temperature, the system was at a pressure slightly greater than the anticipated dew-point or bubble-point pressure. When the desired temperature had been approached, the bomb was rocked. After the system had reached equilibrium in the one-phase region, it was vented slowly through valve C. Upon approaching the phase boundary, the transmitted light intensity diminished sharply, and a phase boundary became visible. The pressure interval over which these phenomena took place varied from barely resolvable (2 atm.) to as much as 30 atm. with the lowest molecular weight fraction at low polymer concentrations. Where the interval was relatively broad, the pressure at which the sharpest intensity change took place was taken as the dew-point or bubble-point pressure. Prior to phase separation the solution sometimes showed a dark orange color by transmitted light, indicating the occurrence of critical scattering. This generally happened at concentrations where the solution, upon lowering the pressure, separated such that the lower phase occupied 30–50% of the volume. The phase volume at a pressure as close as possible to that at which the phases separated was determined by means of a prior calibration of bomb angle versus phase volumes. During a run valve H was closed and, strictly speaking, the experimental system extended to that point. However, there was very little diffusion of polymer out of the bomb, and none into the coil. The volume between the bomb and the valve C was only about 1 cc., and the concentration change due to venting was always small. Concentration changes due to diffusion and venting were therefore ignored in the calculation.

The amount of solvent charged into the bomb was not measured. It was calculated for propane from the data of Reamer, Sage, and Lacey,[7] assuming no volume change of mixing. Since a negative volume change of mixing is, in fact, likely, this introduces an error into the calculation of weight per cent polymer. The isotherms, however, are reported at low polymer concentrations only, and judging from other experiments carried out in this laboratory, the error is not believed to exceed 10% at the highest polymer concentrations reported, and should be considerably less at the critical concentration. The critical conditions are also reported as volume fraction polymer, defined here as volume of pure polymer at the

temperature and pressure of the experiment[8] divided by the volume of the vessel. This description lacks physical reality in systems with volume changes of mixing, but will be made use of, since the critical conditions in lattice theories are described in terms of volume fractions. With solvents other than propane where only the critical loci, and not the isotherms, were determined, there was no need for accurate determinations of the weight or volume fractions.

RESULTS

Phase Behavior of Polyethylene–*n*-Propane

Perhaps the most characteristic feature of the system polyethylene–*n*-propane at 110°C. is the existence of a pressure, above which a single phase exists, and which is an only slowly varying function of composition at low polymer concentrations. This pressure is a dew-point or bubble-point pressure and may be represented by means of an isotherm, i.e., by a (pressure–composition) section of the three-dimensional model (Fig. 3).

The maximum pressure on the isotherm which also corresponds to incipient separation of two phases of equal composition is an upper critical solution pressure (UCSP). Since the curve is nearly flat near the UCSP, this pressure is easily determined, whereas the corresponding critical poly-

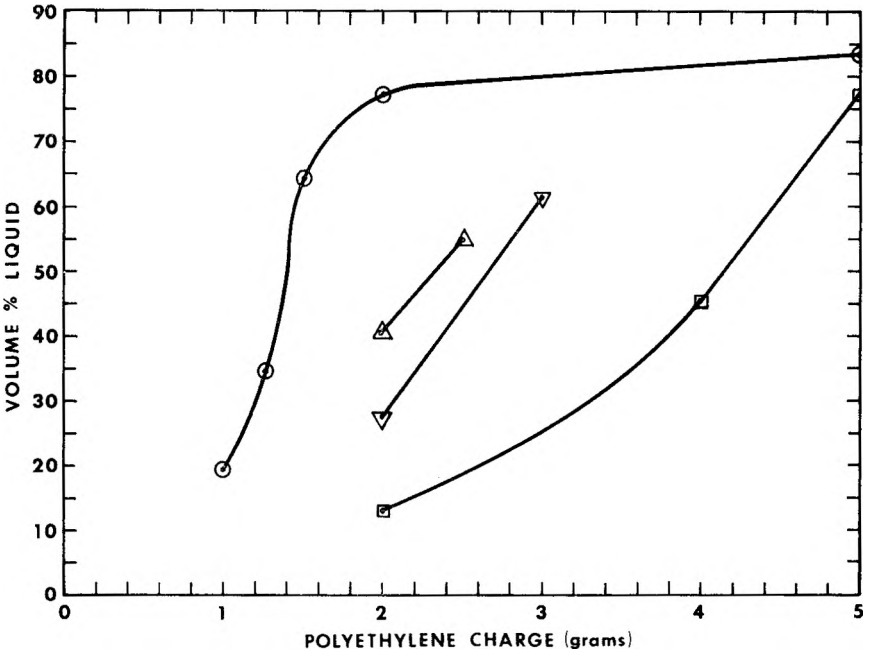

Fig. 3. Phase volumes at phase separation as a function of polymer charge for polyethylene-*n*-propane at 110°C.: (○) fraction 2; (△) fraction 3; (▽) fraction 4; (□) fraction 5.

mer concentration is not. The experimental error in the dew-point and bubble-point pressures is such that the maximum cannot be located along the composition axis by inspection. Instead, the weight fraction W_c' or volume fraction ϕ'_c of polymer at which the system breaks up into two phases of equal volumes can be located approximately from a plot of phase volume just below the isotherm as a function of composition (Fig. 3). For convenience, this is termed the apparent critical composition. The true critical concentration cannot be very far from the apparent critical concentration for two reasons: relative phase volumes change rapidly with composition (Fig. 3) and only extreme dissymmetry in the pressure-composition diagram close to the critical point could lead to a wide divergence between the two points. Also, although no attempt was made to define exactly the concentration range in which critical scattering occurred, the solutions which were darkest in color by transmitted light generally occurred at concentrations such that the lower phase occupied 30–50% of the volume. It seems legitimate to conclude that whereas W_c might possibly be as much as 30% lower than W'_c, it cannot greatly exceed the values of W'_c listed because of the noticeable drop in pressure on the isotherm (pressure–composition section) at concentrations greater than W'_c.

Table I presents the critical pressures and apparent critical compositions for four fractions of molecular weight 17,000–250,000 at 110°C. The critical points are seen to occur at low polymer concentrations, a situation typical for polymer–solvent systems. The critical pressures converge for the high fractions, suggesting the existence of a limiting value for polymer of infinite molecular weight. According to the Flory-Huggins theory,[9] the critical concentrations are given approximately by $x^{-1/2}$, where x is the ratio of molecular volumes of polymer and solvent. The apparent critical concentrations are seen to exceed $x^{-1/2}$, but the dependence is approximately of the form required.

The existence of a second, and higher, critical pressure at which the system again breaks up into two phases is conceivable. This, according to standard terminology, would be a lower critical solution pressure. No such phenomenon was encountered with the highest molecular weight fraction at pressures up to 2,000 atm. at 130–150°C.

TABLE I

Upper Critical Solution Pressures and Critical Polymer Concentrations for Fractions of Polyethylene in Propane at 110°C.

Designation of fraction	Molecular weight of fraction	Critical pressure, atm.	Apparent critical concentration of polymer		$x^{-1/2}$
			Wt. fraction	Vol. fraction	
2	246,000	582	0.042	0.027	0.017
3	89,000	561	0.072	0.045	0.028
4	37,000	531	0.082	0.054	0.044
5	17,000	449	0.129	0.090	0.066

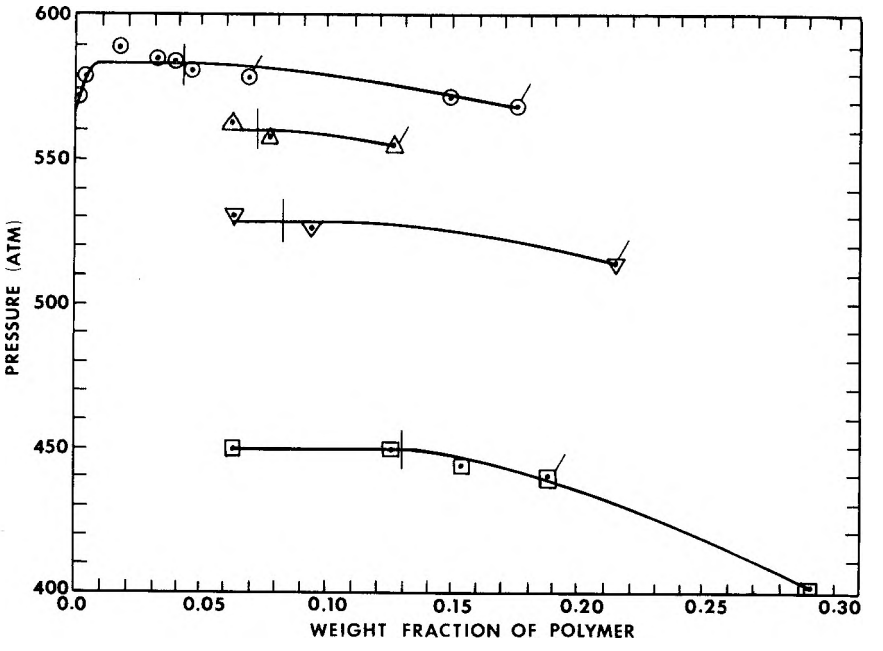

Fig. 4. Pressure-composition section for polyethylene-*n*-propane at 110°C.: (⊙) fraction 2; (△) fraction 3; (▽) fraction 4; (□) fraction 5. Bubble-point and dew-point pressures by direct observation (unprimed symbols); by calculation from phase volumes in two-phase region primed symbols. Vertical lines indicate apparent critical composition.

The effect of temperature on the UCSP is small. Several of the fractions were investigated up to 150°C., and although UCSP's at that temperature appeared to be lower, the effect was only slightly greater than the experimental error. In none of the systems studied was the UCSP lowered by more than 15 atm. in going from 110 to 150°C. In going to the higher temperature, the critical point appeared to shift only very slightly toward higher polymer concentrations.

At polymer concentrations less than critical the pressure on the phase boundary (dew-point pressure) was found to be very close to the critical pressure down to extremely low polymer concentrations. Thus, for fraction 2, dew-point pressures within experimental error of the UCSP were found for polymer concentrations down to 0.3, and possibly 0.15 wt.-% (0.2 and 0.1 vol.-%). On the low concentration side, the phase boundary runs along the pressure axis up to pressures closely approaching the UCSP. This makes it possible to estimate the phase diagram at pressures below the UCSP by determining the location of the meniscus and by assuming the critical composition to occur with the meniscus at 50 vol.-% bomb contents. The pressure–composition diagrams are shown in Figure 4. Points obtained by the less reliable method just described fall on the same plots as those obtained by the direct measurement of dew-point and bubble-point pressures.

Critical Loci of Polyethylene–*n*-Alkane Systems

The bubble- or dew-point pressures were also determined for the highest molecular weight fraction with ethane, butane, and pentane at several temperatures (Table II). These runs were carried out at about 5 wt.-% polymer, although not exactly at the critical polymer concentration. Because of the flatness of the dew-point–bubble-point curve near the UCSP and because of the slow shift in critical concentration with temperature, the pressures on the phase boundary are within experimental error of the UCSP and are listed as such. It is now clear that the data of Table I and Table II define sections of the critical locus for all systems investigated. These critical loci, i.e., the P, T projections of the (P, T, composition) space models, are shown in Figure 5.

With all solvents except pentane, solid precipitates at about 90–110°C., where the vapor pressure curve of the partly amorphous and partly crystalline polymer intersects the critical locus. The point of intersection, not

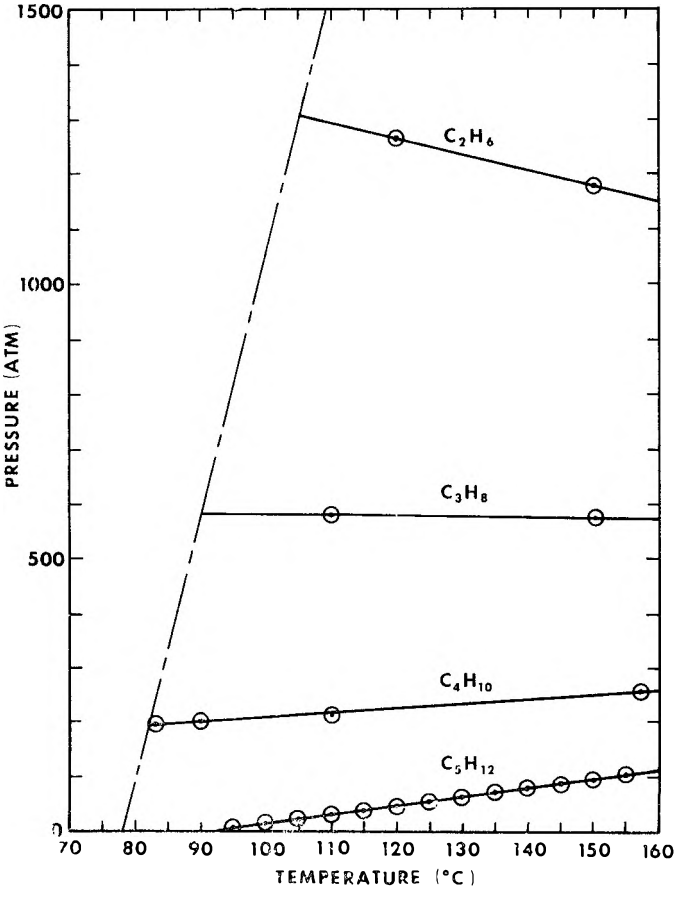

Fig. 5. Critical loci for polyethylene–*n*-alkane systems. The broken line indicates approximate crystallization boundary.

TABLE II
Some Thermodynamic Parameters of Some *n*-Alkanes at the UCSP with a Polyethylene Fraction of Molecular Weight 246,000

n-Alkane	Critical temperature of solvent, °C.	Reduced density	UCSP, atm.	T, °C.	Solubility parameter δ_1, $(cal./cc.)^{1/2}$
Ethane	32	2.32	1,270	120	6.18
		2.15	1,180	150	5.73
Propane	97	2.275	582	110	6.30
		2.15	575	150	5.72
Butane	152	2.32	204	110	6.12
		2.15	255	157	5.60
Pentane	197	2.35	34.3	110	5.91
		2.25	50	120	5.73
		2.175	89.5	150	5.51

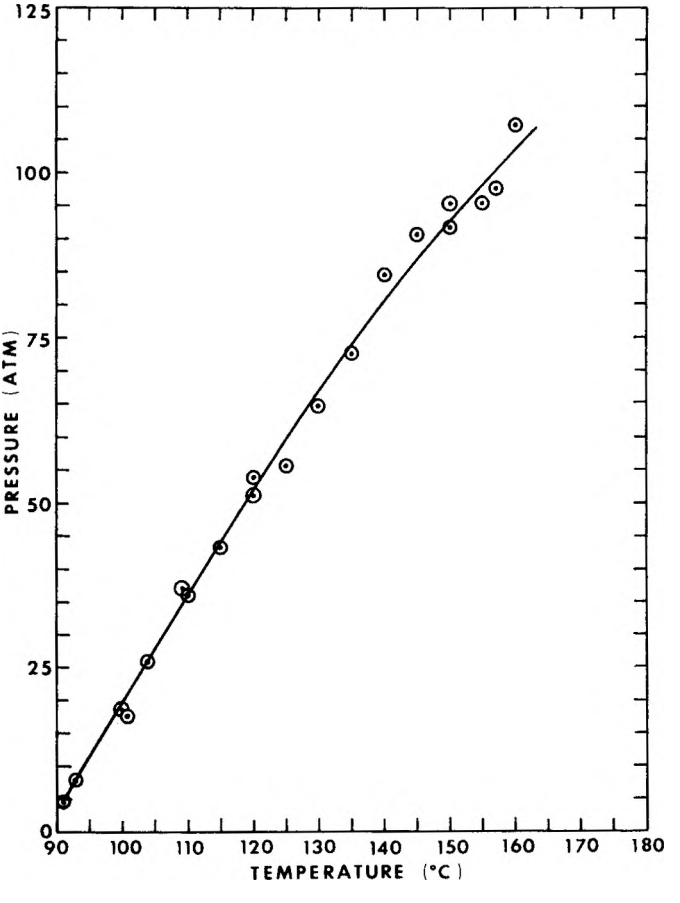

Fig. 6. Critical locus for polyethylene–*n*-pentane.

investigated in detail, should be given by the change in melting point of polyethylene with pressure[8] and with dilution.[10]

With pentane (Fig. 6), the critical locus can be followed down to the lower critical end point (LCEP), or the lower critical solution temperature (LCST) on the vapor pressure curve, where two liquid phases and a gas phase coexist.[3] This point lies at 91 °C. at a pressure indistinguishable from the vapor pressure of the pure solvent by the present method of measurement. Freeman and Rowlinson[3] did not attain complete miscibility in the system polyethylene–*n*-pentane, probably because they operated with linear polyethylene where the crystallization boundary was shifted to higher temperatures, intersecting the critical locus above the LCEP.

It is clear that a LCEP of high molecular weight polyethylene exists only for *n*-alkanes with five carbons and greater because of an increase in the LCEP with size of the solvent molecule and because of the increase in melting point of the polymer with pressure.

DISCUSSION

All systems reported are characterized by a large free volume and by large density differences between the components. There also should be a negative volume change of mixing ΔV along a critical locus of the type described. Every point on this locus, denoted by subscript c, may be considered as LCST with $(dP/dT)_c > 0$ or as UCST with $(dP/dT)_c < 0$. Certain inequalities involving the second derivatives with respect to composition of the thermodynamic mixing functions must be satisfied along the locus and, if there are no points of inflection, one has at an LCST $\Delta H < 0$, $\Delta S < 0$ and at an UCST $\Delta H > 0$, $\Delta S > 0$.[4] These latter conditions have been verified near an LCST in several cases.[11,12] In addition, $(dP/dT)_c$ is given by

$$\frac{\partial^2 \Delta S}{\partial x_2^2} \Big/ \frac{\partial^2 \Delta V}{\partial x_2^2}$$

where x_2 refers to the mole fraction of solute.

Clearly, all lattice treatments of polymer solutions seem here less satisfying physically than under ordinary conditions and violate one or more of the inequalities which must be met along the critical locus, particularly where $(dP/dT)_c > 0$. One objection to the use of the results obtained from lattice treatments is removed, when it is realized that expressions for the free energy of mixing formally identical to that of the Flory-Huggins equation have been obtained by considerations not requiring the lattice assumption.[13,14] In order to allow for negative, as well as positive, heats of mixing the Flory-Huggins interaction parameter χ must be considered as a free energy,[11] as indeed required by the more general lattice treatments[15] and by the theory of Longuet-Huggins.[13] Patterson[11] has suggested further that χ, although no longer a heat term, may still be identified with Hildebrand's solubility parameter term, which then becomes

a free energy, too. It seems therefore not unreasonable to discuss critical mixing in terms of the critcal conditions derived from the Flory-Huggins theory ($\chi_c = 0.5$ for polymer of infinite molecular weight), and to expect χ_c to be given approximately by the solubility parameter term.

Assuming the volume of change of mixing not to be excessive, the solubility parameter for a gas can be calculated by substituting its energy of compression, ΔE_1, for the energy of vaporization[1] of the standard treatment. The solubility parameter for the solvent, δ_1, is then taken to be the square root of the cohesive energy density, $\Delta E_1/V_1$, where V_1 is the molar volume of the solvent. Table II lists the solubility parameters at the UCSP, calculated by means of a reduced variable correlation.[16] δ_1 is seen to vary with temperature, but to be nearly constant at a given temperature for all alkanes studied, although a slight drop with the size of the solvent molecule seems indicated. If one uses the value of Allen et al.[17] for an amorphous linear polyethylene (δ_2 is 8.37 cal.$^{1/2}$ cc.$^{-1/2}$ at a density of 0.855 g. cc.$^{-1}$), and allows δ_2 to vary as $a^{1/2}/V_2^{-1}$ (van der Waals fluid behavior), one obtains values of χ in the range of 0.4–0.8. Positive deviations from 0.5 increase with the size of the solvent molecule and with temperature. The data are, therefore, not quantitatively consistent with the approach outlined. A very rough estimate of the UCSP from the thermodynamic properties of the components is, however, possible. In the *n*-alkane–polyethylene systems investigated, furthermore, the UCSP for a given solvent at a given temperature is evidently calculable with reasonable accuracy from that of another by assuming critical mixing to occur at a fixed value of δ_1. Note, however, that at least equally successful a calculation could be made in terms of reduced densities (Table II).

The critical locus of binary alkane systems whose components differ only moderately in size is a continuous unbroken line joining the critical points of the pure components. Katz and Rzasa[5] in a detailed optical study of methane with an oil fraction containing mostly C_{20} paraffin, have shown that, as the size difference between the components increases, the maximum pressure on the critical locus rises and is shifted toward the component of low molecular weight. Freeman and Rowlinson,[3] however, found that solutions of hydrocarbon polymers in hydrocarbon solvents, upon heating under their own vapor pressures, break up into two liquid phases at a LCST which can be well below the critical point of the solvent. This LCST must also be the lower critical end point (LCEP) of the critical locus which, if closed along the pressure axis, must change gradually from a liquid–liquid to a gas–liquid boundary.[4] This lack of sharp distinction between liquid and gaseous solvents is demonstrated in this study which shows sections of the critical locus of polyethylene with solvents which are above, below, and close to their critical temperatures. The slope of the critical locus at a given temperature differs in sign and magnitude (Table II, Fig. 5); it is close to zero, but slightly negative, with propane just above its own critical point of 97°C. This suggests that the critical

locus has its maximum pressure near the critical temperature of the solvent and, barring crystallization of polymer, is closed at the top (along the pressure axis). The size of the dome of immiscibility evidently increases as the size of the solvent molecule is reduced. The pressure maximum for ethane with a hypothetical amorphous polymethylene of infinite molecular weight would be presumably in the neighborhood of 1500 atm. Whereas all points on the critical locus may be referred to as lower and upper critical solution temperatures, the term upper critical solution pressure is perhaps more descriptive, since the critical locus extends over a great temperature range at a pressure which varies only slowly. This locus is best described as a fluid–liquid locus. It must be distinguished, of course, from the very short gas–liquid locus which extends presumably over a range of several degrees centigrade at most between the critical point of the pure solvent and the upper critical end point (UCEP).[3] Every point on the fluid–liquid locus for polymer of infinite molecular weight satisfies Flory's definition of a Θ-point.

Physically, the critical phenomena and shapes of the critical loci described here may be attributed to the high coefficients of thermal expansion and isothermal compressibility of the solvents near or above their critical points. In the more familiar case where an UCST is not the result of these conditions, such as with polystyrene–cyclohexane near room temperature, the slope of the critical locus, $(dP/dT)_c$, can be by one or two orders of magnitude greater and opposite in sign.[18]

We are indebted for discussions to Dr. D. C. Chappelear and to Professor J. S. Rowlinson who also pointed out the relevance of his work on the LCST to the solubility of polymers in gases. We are also grateful to Messrs. R. A. Isaksen and C. Crofoot for preparing the polyethylene fractions.

References

1. Ehrlich, P., and E. B. Graham, *J. Polymer Sci.*, **45**, 246 (1960).
2. Symcox, R. O., and P. Ehrlich, *J. Am. Chem. Soc.*, **84**, 531 (1962).
3. Freeman, P. I., and J. S. Rowlinson, *Polymer*, **1**, 20 (1960).
4. Rowlinson, J. S., *Liquids and Liquid Mixtures*, Academic Press, New York, and Butterworths, London, 1959, Chaps. 5 and 6.
5. Rzasa, M. J., and D. L. Katz, *Petroleum Transactions, AIME*, **189**, 119 (1950).
6. Trementozzi, Q. A., *J. Polymer Sci.*, **23**, 887 (1957).
7. Reamer, H. H., B. H. Sage, and N. W. Lacey, *Ind. Eng. Chem.*, **41**, 482 (1949).
8. Parks, W., and R. B. Richards, *Trans. Faraday Soc.*, **45**, 203 (1949).
9. Flory, P. J., *Principles of Polymer Chemistry*, Cornell Univ. Press, Ithaca, N. Y., 1953, chaps. 12 and 13.
10. Richards, R. B., *Trans. Faraday Soc.*, **42**, 10 (1946).
11. Delmas, G., D. Patterson, and T. Somcynsky, *J. Polymer Sci.*, **57**, 79 (1962).
12. Baker, C. H., W. B. Brown, G. Gee, J. S. Rowlinson, D. Stubley, and R. E. Yeadon, *Polymer*, **3**, 215 (1962).
13. Longuet-Higgins, H. C., *Discussions Faraday Soc.*, **15**, 73 (1953).
14. Hildebrand, J. H., and R. L. Scott, *The Solubility of Nonelectrolytes*, Reinhold, New York, 1950, p. 107.
15. Guggenheim, E. A., *Mixtures*, Clarendon Press, Oxford, 1952, p. 78.

16. Lyderson, A. L., R. A. Greenkorn, and O. A. Hougen, *Generalized Thermodynamic Properties of Pure Fluids*, Univ. of Wisconsin, Engineering Experiment Station, Report No. 4.

17. Allen, G., G. Gee, D. Mangaraj, D. Sims, and G. J. Wilson, *Polymer*, **1**, 456 (1960).

18. Ham, J. S., M. C. Bolen, and J. K. Hughes, *J. Polymer Sci.*, **57**, 25 (1962).

Résumé

Au-dessus de la température de cristallisation le polyéthylène légèrement ramifié et le propane sont miscibles en toutes proportions au-dessus d'une pression critique définie comme la pression critique supérieure de solution (UCSP). Cette pression décroît seulement très faiblement de 110° à 150°C. A 110°C l'UCSP varie de 450 atmosphères pour une fraction de polymère de poids molèculaire 17.000 à 580 atm. pour une fraction de poids moléculaire 250.000. Les concentrations critiques en polymères sont basses comme dans des systèmes conventionnels polymère–solvant et changent de même façon avec le poids moléculaire. Les pressions requises pour solubiliser le polymère dans le gaz à des concentrations critiques (pressions du point de rosée) sont presqu'aussi élevées que le UCSP jusqu'à des concentrations très basses en polymère. Les résultats déterminent une partie du lieu critique dans l'espace (composition P, T). D'autres expériences avec d'autres systèmes polyéthylène–*n*-alcane (éthane, butane et pentane) montrent que le lieu critique change graduellement d'une séparation liquide–liquide vers une séparation gaz–liquide et peut être appelé un lieu fluide–liquide. S'il n'intervient pas de cristallisation du polymère, ce lieu intersepte la courbe de la tension de vapeur saturée à un point critique terminal inférieur (LCEP) qui est la température critique inférieure de solution (LCST) trouvée tout récemment par Freeman et Rowlinson dans beaucoup de polymères hydrocarbonés avec des solvants hydrocarbonés. La miscibilité incomplète s'etend sur des plus grandes régions de température et de pression lorsque la molécule de solvant devient plus petite, mais le lieu critique serait probablement fermé au long de l'axe des pressions pour un unpolyméthylène amorphe hypothétique avec l'éthane.

Zusammenfassung

Oberhalb der Kristallisationstemperatur sind schwach verzweigtes Polyäthylen und Propan oberhalb eines kritischen, als oberer, kritischer Lösungsdruck (UCSP) definierten Druckes in allen Verhältnissen mischbar. Dieser Druck nimmt im Bereich von 110° bis 150°C nur sehr wenig ab. Bei 110°C steigt der UCSP von 450 Atmosphären für eine Polymerfraktion vom Molekulargewicht 17000 auf 580 Atmosphären für eine solche vom Molekulargewicht 250000 an. Die kritische Polymerkonzentration ist, ähnlich wie in konventionellen Polymer–Lösungsmittelsystemen, niedrig und vom Molekulargewicht abhängig. Die für eine Löslichkeit des Polymeren in der Gasphase bei Polymerkonzentrationen kleiner als der kritischen erforderlichen Drucke (Taupunktsdrucke) sind bis zu sehr kleinen Polymerkonzentrationen fast so hoch wie die UCSP. Die Daten bestimmen einen Teil des kritischen Ortes im (P, T, Zusammensetzungs)-Raum. Versuche mit anderen Polyäthylen–*n*-Alkansystemen (Äthan, Butan, Pentan) zeigen, dass das kritische Gebiet allmählich von einer Flüssig–Flüssig- zu einer Gas–Flüssiggrenze übergeht und als Fluid-flüssig-Ort bezeichnet werden kann. Falls keine Kristallisation des Polymeren auftritt, schneidet dieses Gebiet die Sättigungsdruckkurve bei einem unteren kritischen Endpunkt (LCEP), welcher mit der erst vor kurzem von Freeman und Rowlinson bei vielen Kohlenwasserstoffpolymeren mit Kohlenwasserstofflösungsmitteln gefundenen unteren kritischen Lösungstemperatur (LCST) identisch ist. Mit abnehmender Grösse der Lösungsmittelmoleküle erstreckt sich die begrenzte Mischbarkeit über grössere Temperatur- und Druckbereiche; bei einem hypothetischen amorphen Polyäthylen würde aber wahrscheinlich mit Athan der kritische Ort der Druckachse entlang geschlossen sein.

Received August 28, 1962

JOURNAL OF POLYMER SCIENCE: PART A VOL. 1, PP. 3231–3260 (1963)

Colligative Properties of Polyelectrolyte Solutions in Excess of Salt

Z. ALEXANDROWICZ and A. KATCHALSKY, *Weizmann Institute of Science, Rehovot, Israel*

Synopsis

This work treats the equilibrium properties of polyelectrolyte solutions containing an excess of low molecular salt. In this case the simple rule of additivity, dealt with previously, fails to describe the experimental results. A detailed treatment, based on an approximate solution of the Poisson-Boltzmann equation, was therefore undertaken. The calculation is based on a subdivision of the electrostatic potential into two parts corresponding to two regions: (*1*) an inner region in the close neighborhood of the polyion, free of coions and described by the Poisson-Boltzmann equation in the salt-free case, and (*2*) an outer region screened off from the central macroion and adequately treated by a Debyean approximation. An analytical solution for the electrostatic potential was obtained and used for the theoretical description of potentiometric behavior, Donnan distribution of salt, and Donnan osmotic pressure. The predicted values compare favorably with the measured results in a wide range of experimental conditions.

I. Introduction

The remarkable fact that osmotic properties of polyelectrolyte solutions obey a simple rule of additivity was dealt with theoretically in several previous communications.[1–3] This rule permits the calculation with fair accuracy of the activity of the polyelectrolyte, of the added salt, and of the solvent in a mixed system of any composition. It was found, however, that the requirement of additivity is not exact enough for the description of polyelectrolyte solutions for which very precise measurements are available. A case in point is the question of activities in polyelectrolyte solutions containing salt in a large excess. Hence, despite the usefulness of the simpler rules in describing the colligative properties of the solutions in a general way, a more detailed analysis becomes necessary if a better approximation is required.

The fundamental treatment of polyelectrolyte solutions is based on the evaluation of the electrostatic potential and the distribution of the small ions around the charged polymeric molecules. Since no exact solution of the Poisson-Boltzmann equations is available for polyelectrolyte–salt mixtures, we shall proceed here along the lines proposed by one of us[2] earlier. The method is based on the division of the electrostatic potential into two parts: the potential ψ^{inner} in the solution region close to the poly-

ions where the central electrostatic field is relatively strong, and the potential ψ^{outer} in a region relatively far removed from the charged macromolecules. The coions are strongly repelled from the proximity of the polyion, and it is therefore assumed that the inner region contains counterions only. The value of the potential in solutions of rigid macromolecules surrounded by counterions was obtained in a rigorous manner by Lifson and Katchalsky,[4] and this solution, with suitably chosen boundary conditions, is used here for the evaluation of ψ^{inner}. On the other hand, the influence of the largely screened polyion on the behavior in the outer region is relatively small, so that $\epsilon\psi/kT \ll 1$ and the Debyean approximation $e^{\epsilon\psi/kT} = 1 + \epsilon\psi/kT$ can be used. This approximation leads to an analytical expression for ψ^{outer}. The two solutions for the potential, ψ^{inner} and ψ^{outer} are then allowed to meet at a suitably chosen junction point b, and the integration constants which determine the run of the potential are thereby fixed.

The results obtained by this procedure lead to a set of theoretical values for the colligative properties of polyelectrolyte solutions containing mono-monovalent salt. The calculations predict an additivity of osmotic pressures and of activity coefficients as a good approximation in a wide range of salt and polymer concentrations. The calculations also show that when very precise experimental results are considered the additivity rules are no longer sufficient, and more involved calculations are required. Although the potentials ψ^{inner} and ψ^{outer} can be expressed in an analytical form, the evaluation of the parameters requires the use of repetitive numerical approximations. These numerical computations become particularly unwieldy when the ratio of salt to polymer concentration becomes large. It is shown below, however, that in the latter case, called here the case of excess salt, a completely analytical solution can be obtained. Our aim here is to present this analytical solution and to compare it with results obtained by several independent methods.

At first the electrostatic potential calculated for the surface of the polyion is compared with the results of potentiometric titration. The formulae obtained have a wider validity and may be used for the evaluation of potentiometric titration in salt-free as well as in mixed salt–polyelectrolyte solutions of any composition.

The distribution of small ions in the potential field of the polyions is next considered. The result is used for the evaluation of the Donnan distribution and of the osmotic pressure established between the polyelectrolyte solution and an external salt solution and compared with experimental results.

II. Preliminary Discussion of the System

1. In this section we shall introduce briefly the characteristic parameters of the system and discuss some of their properties. The solution under consideration contains n_p polymer molecules and n_s mono-monovalent salt

molecules per milliliter or, alternatively, it contains m_p moles polymer per milliliter and m_s moles salt per milliter. It is assumed that the polymeric salt and low molecular salt have one ion in common known as the counterion. Let us assume that the polyion carries ν negative charges and is accompanied by ν positive monovalent counterions. The concentration of the counterions is $m_+ = \nu m_p + m_s$ while that of the coions is simply $m_- = m_s$. The degree of polymerization of the polymer is called Z, and if each monomeric unit carries an ionizable group, the degree of ionization is $\alpha = \nu/Z$. It is often convenient to use the monomolar concentration of the polymer $m_m = Zm_p$. The macromolecules in the present model are endowed with a cylindrical symmetry, the effective total length of each molecular cylinder being h and its radius a. We shall return later to the problem of the real symmetry properties of the macromolecules and their relation to the parameters of the cylindrical model which is used here for the sake of mathematical simplicity.

Following the model adopted in previous studies,[4] we shall regard the solution as an array of parallel rodlike cylinders at an average distance $2R$ between the molecular axes. The influence of deviations from this equidistant arrangement is discussed below in Section VI. Each macromolecule serves as the center of an average subvolume V given by the expression

$$V = 1/n_p = \pi R^2 h \tag{1}$$

Since the self-volume of each macromolecule is $\pi a^2 h$, the volume fraction of the polyelectrolyte in solution is

$$\pi a^2 h/\pi R^2 h = a^2/R^2 = V_p \tag{2}$$

Strictly speaking, a is the radius of closest approach of the counterion to the center of the polyion, and a^2/R^2 is consequently larger than V_p by a suitable correction factor.

2. A cylindrically symmetrical electrostatic potential ψ is established around the macromolecules. For symmetry reasons it is clear that the absolute magnitude of ψ will be maximal on the polymolecule and will pass through a minimum on the boundary surface between neighboring subvolumes. In other words, $(\nabla\psi)_R = 0$, or no electrical forces act on the ions in the surface region. For this reason the solution in the region between two neighboring subvolumes may be regarded as ideal, at least as regards the interaction of the small ions with the charged macromolecules.

If the concentration of the positive counterions in the boundary surface be denoted by m_+^R and the concentration of the negative coions is denoted by m_-^R, it is readily seen that the consideration of the behavior at the surface leads to the following important equations. For the Donnan equilibrium of the polyelectrolyte solution with an external salt solution of concentration m'_s (which is assumed to be equal to its activity) we obtain

$$m_+^R m_-^R = m'^2_s \tag{3}$$

and for the equilibrium osmotic pressure π of the polyelectrolyte–salt mixture with the external solution

$$\pi + 2m'_sRT = (m_+^R + m_-^R + m_p)RT \tag{4}$$

Equation (3) may be obtained in the following way: since the small ions are subjected to the action of the central field of a polyion, their concentration can be represented by Boltzmann's distribution law or

$$m_+^{(\vec{r})} = m_+^0 e^{-\epsilon\psi(\vec{r})/kT}$$

and

$$m_-^{(\vec{r})} = m_-^0 e^{\epsilon\psi(\vec{r})/kT} \tag{5}$$

where m_+^0 and m_-^0 are the concentrations at an arbitrary reference point. From eq. (5) it follows that the product $m_+^{(\vec{r})}m_-^{(\vec{r})} = m_+^R m_-^R$ is independent of the position vector $\vec{r}$. The local chemical potential of the low molecular salt at point $\vec{r}$ is

$$\mu_s = \mu_s^0 + kT \ln m_+^{\vec{r}} m_-^{\vec{r}} = \mu_s^0 + kT \ln m_+^R m_-^R \tag{6}$$

and is also independent of $\vec{r}$. The potential μ_s may therefore be identified with the macroscopic thermodynamic potential of the salt. At Donnan equilibrium it should be equal to the potential of the salt in the external solution which is

$$\mu'_s = \mu_s^0 + kT \ln m'^2_s \tag{7}$$

and by equating eqs. (6) and (7) we obtain eq. (3).

Equation (4) results directly from the assumption that the field of the macromolecule at the surface of the subvolume equals zero, so that the colligative contributions of the ions on both sides of the semipermeable membrane differ only in the hydrostatic pressure π. The possible effect of higher order virial coefficients due to non electrostatic phenomena is neglected here for the sake of simplicity. Equation (4) was derived for a planar model by Langmuir[5] and by Verwey and Overbeek[6] and generalized to any system of charged colloidal particles by Marcus.[7]

Since many solution properties may be represented in terms of the concentration at the surface of the subvolumes, it is convenient to identify the latter with the arbitrary reference concentrations m_+^0 and m_-^0 which appear in eqs. (5); or, fixing the arbitrary reference point at these surfaces we write

$$\begin{aligned} \psi_R &= 0 \\ m_+^R &= m_+^0 \\ m_-^R &= m_-^0 \end{aligned} \tag{8}$$

and in the following the convention of eqs. (8) will be used throughout. The reference concentrations are related to the overall macroscopic concentrations by the following self explanatory normalization conditions:

[Total mole number of counterions in V]

$$= (\nu m_p + m_s)V = m_+^0 \int_V e^{-\epsilon\psi/kT} dV \quad (9)$$

[Total mole number of coions in V]

$$= m_s V = m_-^0 \int_V e^{\epsilon\psi/kT} dV \quad (10)$$

3. Without going into a detailed calculation of m_+^R and m_-^R, which will be carried out in the following paragraphs, we can make some general remarks on their magnitude and their relation to the external salt concentration m'_s. Let us consider the potential difference E (see the schematic Fig. 1) which will exist between the subvolume surface layer and the external salt solution. Putting $-\epsilon E/kT = q$, and making use of Boltzmann distribution, we write

$$m_+^R = m'_s e^q = m'_s(1 + q + q^2/2 + \ldots) \quad (11)$$

$$m_-^R = m'_s e^{-q} = m'_s(1 - q + q^2/2 - \ldots) \quad (12)$$

Throughout the polymer solution the concentration of the counterions exceeds that of the coions; the difference decreases towards the surface of the subvolume but retains its positive value everywhere.* For a negative polyelectrolyte considered here q is therefore positive and $m_+^R > m'_s > m_-^R$. Equations (11) and (12) evidently satisfy the Donnan equilibrium of eq. (3). Subtracting eq. (12) from eq. (11) gives the quantity $m_+^R - m_-^R$, which will be shown below to characterize the form of the potential ψ^{outer}

$$m_+^R - m_-^R = 2m'_s q + m'_s q^3/3 + \ldots \quad (13)$$

while introduction of eqs. (11) and (12) into eq. (4) leads to an expression which correlates q with the Donnan osmotic pressure:

* This may be proved as follows. At the surface of a positively charged macroion, $\nabla\psi$ is negative (Gauss theorem). The bulk of the polyelectrolyte solution outside the polyions contains, on the average, an excess of negative ions. The latter are attracted preferentially from the bulk of the solution to the vicinity of the polyion, so that an excess negative charge accumulates at the surface of the polyion and $\nabla^2\psi$ is positive (Poisson's equation). On the other hand, for symmetry reasons, $\nabla\psi$ at R is zero. Under these boundary conditions the potential and the absolute value of the negative $\nabla\psi$ must decrease monotonically from a to R in the manner depicted in Figure 1, since any intermediate extremum would divide the potential curve into two asymmetric parts. Such an asymmetric curve however would allow for isopotential points, which must have equal charge density (Boltzmann), to have differently valued $\nabla^2\psi$—in contradiction to Poisson's equation. If the potential and $|\nabla\psi|$ decrease toward a minimum monotonically, $\nabla^2\psi$ is positive everywhere and, by Poisson's equation again, the number of the (negative) counterions is everywhere larger than the number of the coions.

$$\pi/RT = m_p + m_+^R + m_-^R - 2m'_s$$
$$= m_p + m'_s q^2 + m'_s q^4/12 + \ldots \quad (14)$$

As is well known, when the ratio of polymer to salt concentration decreases, the difference between m_+^R and m_-^R grows smaller, and the Donnan osmotic pressure becomes equal to the osmotic pressure of undissociated polymer molecules (m_p). This result is also obtained from the detailed calculation of the preceding communication.[2] In the present work we shall therefore limit ourselves to cases when q is small enough so that terms

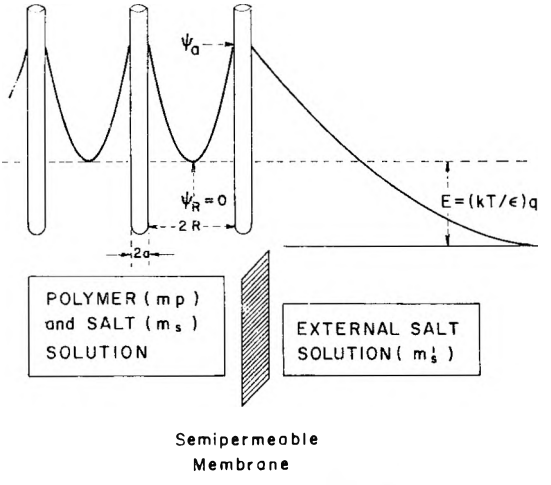

Fig. 1. A schematic representation of the potential ψ inside the polymer solution and of the potential difference E between the surface layers of the subvolumes on one hand, and an external salt solution on the other.

of power higher than q^2 may be neglected. It should be stressed, however, that the difference between the concentrations m_+^R and m_-^R becomes zero only when the polymer concentration itself equals zero; under all other conditions $q \neq 0$, and there is a nonvanishing contribution of the counterions to the Donnan osmotic pressure. This point is often overlooked in treatments which solve the Poisson-Boltzmann equation for polyelectrolytes with the tacit assumption that $m_+^R = m_-^R = m'_s$ and use the results to discuss the properties of solutions in which the ratio of polymer to salt is by no means small enough to justify this approximation. For example, the validity of the aforementioned rule of additivity cannot be proved on this basis.[3] Furthermore, since q turns out to depend mainly on the ratio of polymer to salt concentration, the approximation should be judged in terms of the relative composition of the solution and not—as is again often done—in terms of the absolute value of the ionic strength. Anticipating the results obtained below it may be stated that q for the typical polyelectrolyte systems considered is found to be of the order of 0.1 m_m/m'_s;

the range of validity of the present approximation for any given system may be estimated accordingly.

III. The Electrostatic Potential

1. The electrostatic potential established by a polyelectrolyte in solution can be obtained by solving the Poisson equation

$$\nabla^2\psi = -4\pi\rho/D \tag{15}$$

where the local charge density ρ is given by the Boltzmann expression

$$\rho = m_+^0\epsilon e^{-\epsilon\psi/kT} - m_-^0\epsilon e^{\epsilon\psi/kT} \tag{16}$$

No general solution of eq. (15) has been found for macromolecules of any symmetry in the mixed salt-polyelectrolyte system. Hence in the following the approximate method[2] outlined in the introduction will be pursued, and an attempt will be made to combine in a plausible way two solutions for the potential: one solution for the potential in the "inner" region extending from the surface of the macromolecules at a to the meeting place b and the second for the potential in the "outer" region which extends from b to the surface of the subvolume at R.

In the inner region $\epsilon\psi$ is on the whole larger that kT and it may be safely assumed that the coions are so effectively repelled that the region $a \leqslant r \leqslant b$ is practically free of their presence. Thus the potential in the inner region may be given by the solution for a polyelectrolyte surrounded by counterions only:

$$\phi^{\text{inner}} = \ln\,[2\pi\epsilon^2 m_+^R\gamma^2/DkT\beta^2\sinh^2(\beta\ln A'r)] \tag{17}$$

where the notation $\phi = \epsilon\psi/kT$ is used. The form of eq. (17) is identical with that given previously for salt-free solutions.[4,8,9] It should be, however, borne in mind that the integration constants β and A' of eq. (17) differ from those of the salt-free case. They have to be evaluated from new boundary conditions based on the requirement that at point b the potential function of the inner region has to merge satisfactorily with that of the outer region. Furthermore, in salt-free solutions the total number ν of the counterions in subvolume is known, whereas in the present case the $(\nu + m_sV)$ counterions are divided between the two regions of the subvolume in a way which has yet to be determined.

The outer region $b \leqslant r \leqslant R$ is characterized by a low potential so that $\epsilon\psi \ll kT$. In this region we may use the Debye-Hückel approximation and solve eqs. (15)–(16) for the case of cylindrical symmetry[2] to obtain

$$\begin{aligned}\phi^{\text{outer}} &= AI_0(\kappa r) + BK_0(\kappa r) + \frac{m_+^R - m_-^R}{m_+^R + m_-^R} \\ &\simeq AI_0(\kappa r) + BK_0(\kappa r) + q\end{aligned} \tag{18}$$

where I_0 and K_0 are modified Bessel functions of zero'th order, A and B are integration constants, while κ is defined by

$$\kappa^2 = (4\pi\epsilon^2/DkT)(m_+{}^R + m_-{}^R) = (8\pi\epsilon^2/DkT)m'_s(1 + q^2/2) \quad (19)$$

2. The two boundary conditions for ϕ^{outer}, on the surface of the subvolume, are

$$\phi_R{}^{\text{outer}} = AI_0(\kappa R) + BK_0(\kappa R) + q = 0 \quad (20)$$

and

$$(\nabla\phi^{\text{outer}})_R = \kappa[AI_1(\kappa R) - BK_1(\kappa R)] = 0$$

or

$$A = BK_1(\kappa R)/I_1(\kappa R) \quad (21)$$

Combination of eqs. (20) and (21) with the use of a transformation of the Bessel functions[10] gives

$$q = -B/\kappa RI_1(\kappa R) \quad (22)$$

The boundary condition for the inner potential at the surface of the polyion follows from Gauss' theorem

$$(d\psi^{\text{inner}}/dr)_a = -4\pi\sigma/D \quad (23)$$

The value of σ is evidently $\sigma = -\nu\epsilon/2\pi ah$, while $d\psi/dr$ is readily derived from eq. (17). Hence we get from eq. (23)

$$1 + \beta \operatorname{cotgh}(\beta \ln A'a) = \nu\epsilon^2/DhkT = \lambda \quad (24)$$

The dimensionless parameter λ appearing in eq. (24) has been called[4] the charge density and was found to be a fundamental parameter for the description of the electrostatic properties of the polyion. In eq. (24), ν is known, and the dielectric constant D is assumed to be equal to that of the solvent. The effective cylindrical length h of the polyion will be discussed in more detail below.

In choosing the arbitrary junction between the outer and the inner regions, we shall try to minimize the error introduced by our approximate expressions for the local charge density in the two regions [c.f. eq. (16)].

In the inner region we neglect the coion concentration so that the error in the local charge density is equal to

$$\begin{aligned}[\text{True density}] - [\text{approximate density}] &= [m_+{}^R e^{-\phi} - m_-{}^R e^{\phi}] - [m_+{}^R e^{-\phi}] \\ &\simeq m'_s(1 - q)e^{\phi}\end{aligned}$$

In the outer region we linearize the exponentials or neglect a term equal to

$$\begin{aligned}[\text{True density}] - [\text{approximate density}] &= [m_+{}^R e^{-\phi} - m_-{}^R e^{\phi} \\ &\quad - (m_+{}^R - m_-{}^R) - (m_+{}^R + m_-{}^R)\phi] \\ &\simeq -m'_s\phi^2(\phi/3 - q)\end{aligned}$$

Since both errors are found to increase towards b, the junction point is preferably placed in such a way that the absolute values of the errors on both sides of b become equal. The exact choice of the junction point does not affect the result materially.

The equation which guides our choice of $\phi(b)$ has therefore the following form

$$(1 - q)e^{\phi(b)} \simeq \phi^2(b)[-\phi(b)/3 + q] \tag{25}$$

Equation (25) determines the value of $\phi(b)$ as function of q only (for example when $q = 0$, $\phi(b) \simeq -1$). The error thus introduced in the calculated value of the charge density seems to be not unduly large, and, even in the "worst" case, when the polymer to salt (and hence q) is equal to zero, the error still does not exceed 16%. Indeed, in the latter case the value of ϕ has also been calculated by a numerical intergration,[3] and the result is practically identical to our approximate analytical solution, as shown in Figure 2.

Having decided on the principle for the choice of the junction point, we shall consider the restrictions which this boundary will set upon the inner and outer potentials. First we require that

$$\phi^{\text{outer}}(b) = \phi^{\text{inner}}(b) = \phi(b) \tag{26}$$

Secondly we require that the division into two regions will leave the potential normalized correctly in the sense of eqs. (9) and (10); or, subtracting eq. (10) from eq. (9), and recalling eq. (16), we obtain

$$\nu = \int_V m_+^P e^{-\phi}\, dV - \int_V m_-^R e^{\phi}\, dV = (1/\epsilon)\int_V \rho\, dV \tag{27}$$

Equation (27) states that the number of charges per macroion is equal to the total net charge in the subvolume. Utilizing a well known substitution[11] based on eq. (15) we may write

$$\begin{aligned}\nu &= (-D/4\pi\epsilon)\int_V \nabla^2\psi dV = (-DkTh/2\epsilon^2)\int_a^R [d/dr](rd\phi/dr)]dr \\ &= (\nu a/2\lambda)(d\phi^{\text{inner}}/dr)_a - (\nu b/2\lambda)[(d\phi^{\text{inner}}/dr)_b - (d\phi^{\text{outer}}/dr)_b] \\ &\qquad - (\nu R/2\lambda)(d\phi^{\text{outer}}/dr)_R\end{aligned} \tag{28}$$

From eqs. (23) and (24) we obtain

$$(d\phi^{\text{inner}}/dr)_a = 2\lambda/a$$

while by eq. (20)

$$(d\phi^{\text{outer}}/dr)_R = 0$$

hence, eq. (27) reduces to the simple continuity condition

$$(d\phi^{\text{inner}}/dr)_b = (d\phi^{\text{outer}}/dr)_b \tag{29}$$

The first continuity condition, eq. (26), written for the outer potential with eqs. (18), (21), and (22), gives for the boundary at b:

$$\begin{aligned}\phi(b) &= BK_0(\kappa b) + AI_0(\kappa b) + q \\ &= B[K_0(\kappa b) + I_0(\kappa b)K_1(\kappa R)/I_1(\kappa R) - 1/\kappa R I_1(\kappa R)]\end{aligned} \tag{30}$$

Equation (26) may be written also for the inner potential, by using eqs. (17), (11), and (19):

$$\begin{aligned}e^{\phi(b)} &= 2\pi\epsilon^2 m_s'(1 + q + q^2/2)b^2 \sinh^2(\beta \ln A'b)/DkT\beta^2 \\ &= (\kappa b/2)^2(1 + q)/[\beta^2 \coth^2(\beta \ln A'b) - \beta^2]\end{aligned}$$

or

$$\beta^2 \coth^2 (\beta \ln A'b) = (\kappa b/2)^2(1 + q)e^{-\phi(b)} + \beta^2 \tag{31}$$

while the second continuity condition, eq. (29), may be used with the explicit expressions for $\nabla\phi^{\text{inner}}$ and for $\nabla\phi^{\text{outer}}$ to give

$$\beta \coth (\beta \ln A'b) = -1 - \{(\kappa b/2B)\ [K_1(\kappa b) - I_1(\kappa b)K_1(\kappa R)/I_1(\kappa R)]\} \tag{32}$$

Combining eqs. (31) and (32) we get the final expression for β:

$$\beta^2 = \{1 + (\kappa b/2)B[K_1(\kappa b) - I_1(\kappa b)K_1(\kappa R)/I_1(\kappa R)]\}^2 - (\kappa b/2)^2(1 + q)e^{-\phi(b)} \tag{33}$$

In this expression β is a function of κb and κR only, since the parameters q, B, and $\phi(b)$ are also determined by κb and κR through eqs. (22), (25), and (30). The last step to be taken is to combine eqs. (24) and (32), for coth ($\beta \ln A'a$) and coth ($\beta \ln A'b$) respectively, to give an expression which determines the charge parameter in terms of the parameters κb, κR, and κa:

$$\lambda = \{1 + (\kappa b/2)B[K_1(\kappa b) - I_1(\kappa b)K_1(\kappa R)/I_1(\kappa R)] - \beta^2 - (\kappa b/2)B \times [K_1(\kappa b) - I(\kappa b)K_1(\kappa R)/I_1(\kappa R)]\beta \coth (\beta \ln b/a)\}/ \{1 + (\kappa b/2)B[K_1(\kappa b) - I_1(\kappa b)K_1(\kappa R)/I_1(\kappa R)] + \beta \coth (\beta \ln b/a)\} \tag{34}$$

3. We would like to conclude this section by outlining the mode of calculation with the aid of the equations presented above. A given polyelectrolyte solution is characterized by the concentrations m'_s and m_p and by the radius a and charge per unit length ν/h of the macroion. It would be therefore advantageous to base the calculation of the potential on a corresponding set of parameters namely on $\kappa = \kappa(m'_s{}^{1/2})$, $R = R(m_p{}^{-1/2})$; a and $\lambda = \lambda(\nu/h)$. This approach, however, is barred by the transcendental nature of some of the equations and the following indirect procedure has been adopted instead. We start with a given set of values of κR, κa, and κb and proceed to solve eqs. (30) and (22) to obtain $B/\phi(b)$ and $q/\phi(b)$. A calibration curve of $\phi(b)$ versus $q/\phi(b)$, which is simply obtained from eq. (25), guides our choice of the appropriate value of the potential at the junction point. With $\phi(b)$ thus chosen, B and q become separately available, and eqs. (33) and (34) are solved for β^2 and λ, respectively.

It is found that in all cases of excess of salt which fulfill our criterion of small q values (interpreted here as $q \leq 1/2$), the results of the calculation are practically independent of κR. The range of relative concentrations to which this finding applies may be expressed in terms of $\kappa R = \kappa R(m_s{}^{1/2}/m_p{}^{1/2})$ and for typical polyelectrolytes is found to correspond to κR values larger than about 2–3. A considerable simplification becomes thus available, since the parameters B, β, and λ may be calculated for all systems which contain an excess of salt (of arbitrary κR value exceeding 2–3) on the basis of the equations which describe the limiting case $\kappa R = \infty$. As follows from eqs. (25) and (22), in the latter case $\phi(b) \simeq -1$ and $q = 0$, while eqs. (30), (33), and (34) reduce to

$$-1 = BK_0(\kappa b) \tag{30'}$$

$$\beta^2 = [1 + (\kappa b/2)BK_1(\kappa b)]^2 - e(\kappa b/2) \tag{33'}$$

$$\lambda = \frac{[1 + (\kappa b/2)BK_1(\kappa b) - \beta^2 - (\kappa b/2)BK_1(\kappa b)\beta \coth (\beta \ln b/a)]}{[1 + (\kappa b/2)BK_1(\kappa b) + \beta \coth (\beta \ln b/a)]} \tag{34'}$$

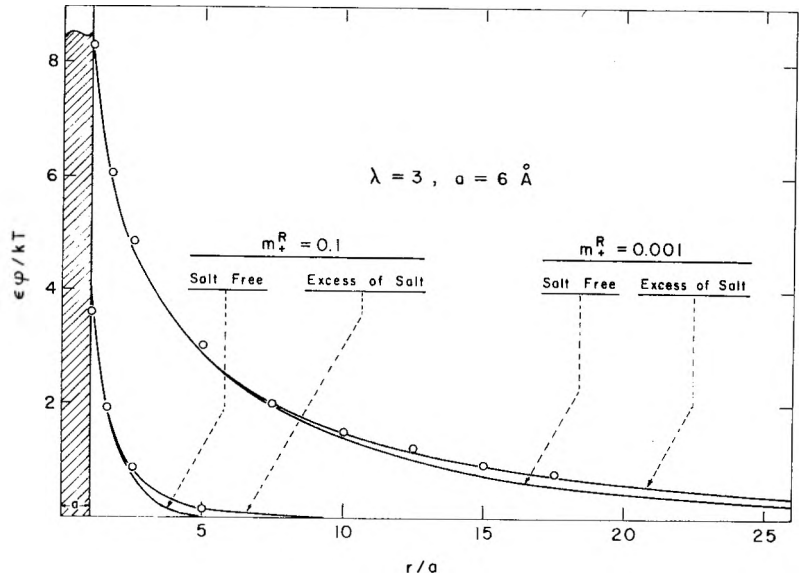

Fig. 2. The dependence of the electrostatic potential ψ on the distance r from the center of the macroion (relative units (r/a) are used, where a is the radius of the macroion): (——) calculated for $\lambda = 3$, $a = 6$ A. in excess of salt or in salt-free solutions of equivalent counterion activities m_+^R; (O) values interpolated from the numerical calculation of Kotin and Nagasawa.[3]

Having evaluated the parameters B, β^2, and λ for given κa and κb, we may proceed and replot the results in order to provide a description which is related in a more natural way to the known parameters of the polyelectrolyte solution, viz., give B, β^2, and κb as a function of κa and λ. Since the additional parameters, namely A, q, and A' are readily obtained from eqs. (21), (22), and (24), the set B, β^2, and κb is sufficient for the evaluation of the potentials ψ^{inner} and ψ^{outer} and for finding the junction point b. A typical example of the potential thus calculated is given in Figure 2. In Figures 3, 4, and 5 we have plotted B, β^2, and κb, respectively, for the values of λ encountered in practice and for κa values which in typical polyelectrolytes correspond to salt concentrations of $10^{-3} - 1N$.

IV. Potentiometric Titration

1. The results of the potentiometric titration are related in a direct way to the potential of the polyelectrolyte. As is well known, the pH of a weak polyacid with negligible nearest-neighbor interactions is given by the equation

$$\text{pH} = \text{p}K_0 + \log [\alpha/(1 - \alpha)] - 0.434\epsilon\Delta\psi/kT \qquad (35)$$

$\text{p}K_0$ is the intrinsic dissociation constant and $\Delta\psi$ is the difference in potential between the surface of the polyion (where the dissociating group is situated) and a point at which the polyelectrolyte field becomes zero. The term $-0.434\epsilon\Delta\psi/kT$ is also denoted by $\Delta\text{p}K$, which implies that it is the contribution of the polyelectrolyte field to the standard free energy of ionization of a single group, in addition to the free energy of ionization in surroundings in which no such field is acting ($\text{p}K_0$). According to our con-

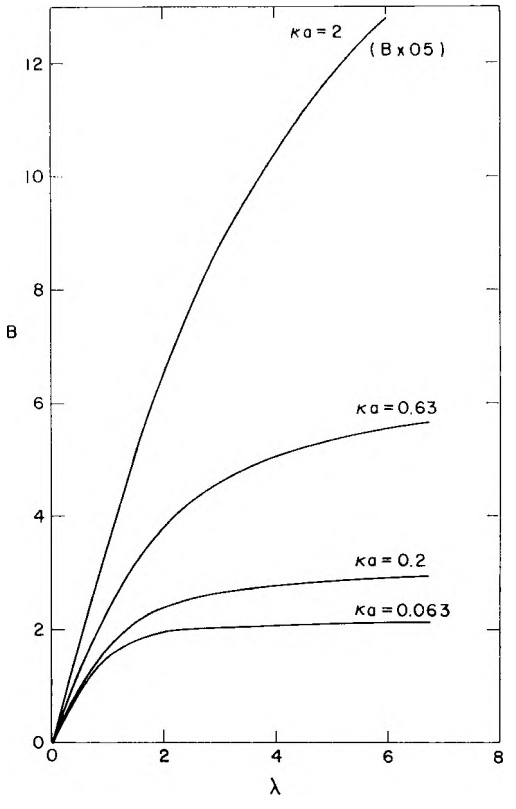

Fig. 3. The dependence of B (the parameter of ψ^{outer}) on the charge density λ at given κa and for $\kappa R = \infty$ (infinite excess of salt). κ (c.f. eq. (19)) in excess of salt is identical with Debye's κ, a is the radius of the macroion, and R the radius of the solution volume per macroion. The values of B at $\kappa a = 2$ have been reduced by half.

vention, the polyelectrolyte field density and potential are both zero at the same point R, so that

$$\Delta pK = -0.434\epsilon\Delta\psi/kT = -0.434\epsilon\psi_a^{\text{inner}}/kT \tag{36}$$

where ψ_a^{inner} is described by eq. (17), while its value at a is determined by the boundary condition in eq. (24). Thus

$$\Delta pK = -\log (2\pi\epsilon^2 m_+^R a^2/DkT) + \log [(\lambda - 1)^2 - \beta^2]$$
$$= -2 \log (\kappa a/2) + \log [(\lambda - 1)^2 - \beta^2] \tag{37}$$

which may be written in yet another form

$$\Delta pK = \log [(\nu/\pi a^2 h)/m_+^R] + \log \{[(\lambda - 1)^2 - \beta^2]/2\lambda\} \tag{38}$$

In dilute solutions and at high charge densities the second term on the right-hand side is generally much smaller than the first, so that to a rough approximation

$$\Delta pK = \log [(\nu/\pi a^2 h)/m_+^R] \tag{39}$$

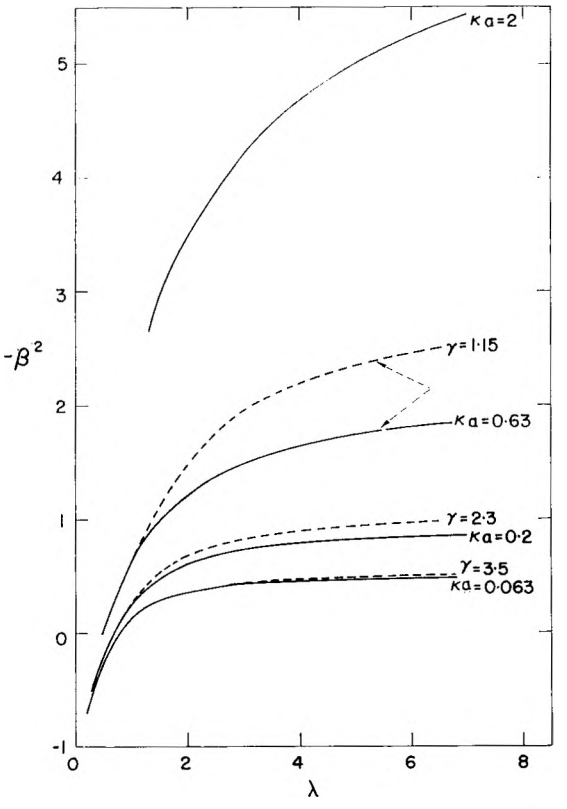

Fig. 4. The dependence of (——) β^2 (the parameter of ψ^{inner}) on the charge density λ at given κa and for $\kappa R = \infty$ (infinite excess of salt); (- -) values of β^2 in salt-free solutions of corresponding ionic activities ($m_{\pm}^{R}$) [c.f. eq. (41)] and below. The parameter γ of Lifson and Katchalsky is $\gamma = \ln R/a$.

This expression has a rather interesting physical interpretation: $\nu/\pi a^2 h$ is evidently the concentration of the counterion in the self volume of the polyion, while m_+^R, according to eqs. (3) and (4), represents the counterion activity throughout the subvolume V. If we consider a hypothetical two-phase microsystem which consists of the polyion and of the subvolume, then the logarithmic term of eq. (39) represents the Donnan potential between the phases.[12,13] This rough approximation breaks down, however, at lower values of charge density and at higher κa values and will not be further followed up here.

2. Since ΔpK depends only on ψ^{inner} and the latter, except for different boundary conditions, is identical with the potential developed for salt-free solutions, it is to be expected that a simple formula can describe the titration behavior of salt-containing and of salt-free solutions alike. We note that the only terms in eq. (38) which depend on the composition of the solutions are m_+^R, the counterion concentration in the surface of the subvolume, and the integration constant β. m_+^R is a complicated function of the composi-

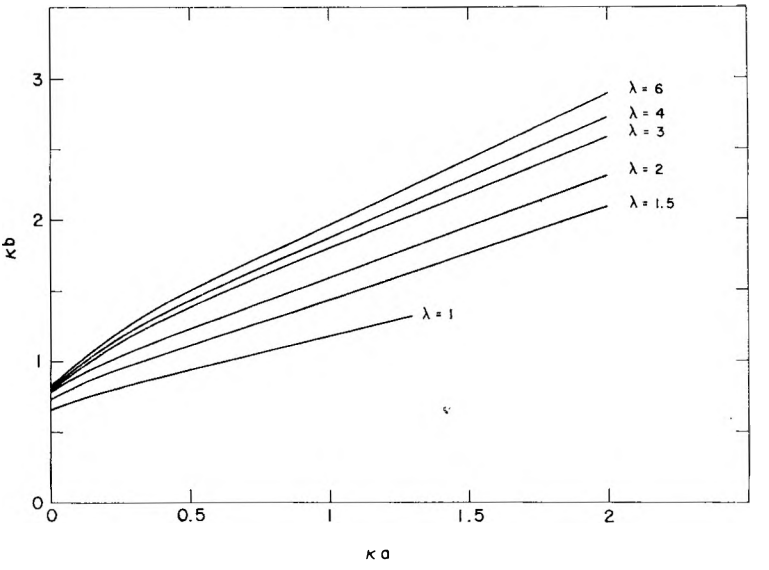

Fig. 5. κb (the parameter of the meeting point between ψ^{outer} and ψ^{inner}) as a function of κa at given λ and for $\kappa R = \infty$ (infinite excess of salt).

tion of the solution, and its exact evaluation constitutes in fact one of the aims of this report. However, for the purpose of the logarithmic term of eq. (38), the aforementioned approximate rule of additivity is accurate enough. According to this rule,[1,2] m_+^R in a mixed solution of any composition is given by

$$m_+^R \simeq \alpha\varphi_p m_m + m_s \tag{40}$$

where φ_p, the osmotic coefficient of the salt-free polyelectrolyte solution, is independent of m_s and is determined by and large by the degree of polyion ionization. Furthermore, it is noted that (except for very high ionic strength) when the values of the constant β are calculated for a given λ and m_+^R, the results in the case of salt-free solutions turn out to be practically identical to those obtained in the present case of excess of salt (c.f. Fig. 4). We may therefore rewrite eq. (38) in a generalized form which gives ΔpK in polyelectrolyte solutions of any composition

$$\Delta pK = \log [(\nu/\pi a^2 h)/(\varphi_p \alpha m_m + m_s)] + \log \{[(\lambda - 1)^2 - \beta^2]/2\lambda\} \tag{41}$$

With the understanding that the values of the constant β, for a given charge density λ and counterion activity m_+^R, are to be taken from the present work when $\alpha\varphi_p m_m < m_s$ and from Lifson and Katchalsky's work[4] when $\alpha\varphi_p m_m > m_s$. More explicitly, in salt-free solutions $\beta = \beta(\lambda, a/R)$ and a/R is related to m_+^R by

$$a^2/R^2 = m_m M_m/1000\rho = m_+^R M_m/\alpha\varphi_p 1000\rho$$

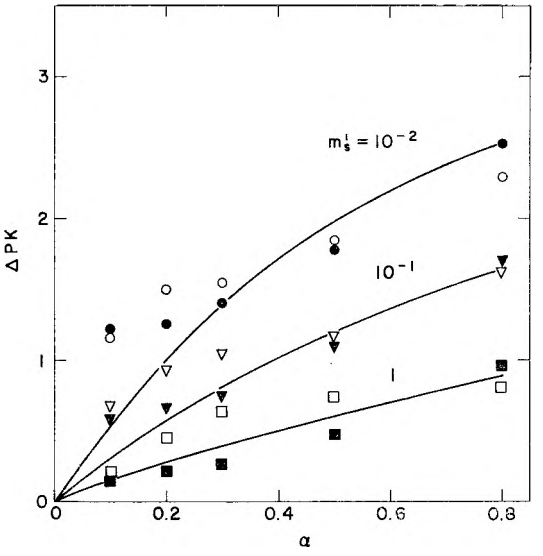

Fig. 6. ΔpK of potentiometric titration in excess of salt, as a function of the degree of neutralization α: (——) calculated for $\lambda_{stretched}/\alpha = 3$; $a = 5$ A.; experimental results of Samelson[13] at salt concentrations m'_s of (●) 10^{-2}, (▼) 10^{-1}, and (■) 1 mole/l.; experimental results of Arnold and Overbeek[16] at salt concentrations of (○) 10^{-2}, (▽) 10^{-1}, and (□) 1 mole/l.

where M_m is the monomer molecular weight and ρ the density of polymer; in excess of salt $\beta = \beta(\lambda, \kappa a)$ and $(\kappa a)^2 = 0.108\, m_+^R a^2$.] The similar run of the potential at a given λ and m_+^R, in case of excess of salt and salt-free solutions, is demonstrated in Figure 2.

The outstanding feature of the potentiometric eq. (41) is, that in the presence of excess of salt, ΔpK decreases with log m_s and does not depend on the polymer concentration. On the other hand, in solutions which contain an excess of polymer, the opposite rule becomes valid; ΔpK decreases with log m_m and does not depend on whatever small amount of salt is added. These rules have been formulated by Samelson[13] on the basis of an extensive experimental study and can be also deduced from other results[14-18] (see Figs. 6 and 7). In the intermediate range, when $\varphi_p \alpha m_m$ and m_s are of the same order of magnitude, ΔpK is determined by the total effective concentration of the counterions, eq. (40), resembling similar rules postulated in several previous publications.[19,20]

The dependence of ΔpK on the charge density λ, or on (what amounts to the same) the degree of ionization α, may be likewise given a simple qualitative description: at λ values higher than about 1.5 the increase of ΔpK with the ionization becomes relatively small and is caused only by the relatively slowly growing term log $[(\lambda - 1)^2 - \beta^2]$. At low λ, however, the changes grow more pronounced, and ultimately ΔpK becomes a linear function of the degree of ionization, in close analogy to expressions based on the Debye-Hückel approximation; a typical example being the

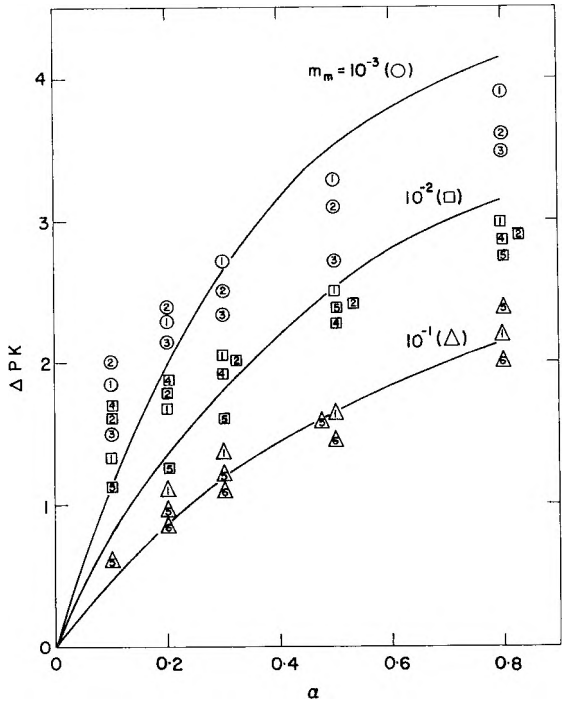

Fig. 7. ΔpK of potentiometric titration in salt-free solutions, as a function of the degree of neutralization α: (——) calculated for $\lambda_{stretched}/\alpha = 3$, $a = 5$ A.; experimental results at polymer concentrations of (○) 10^{-3}, (□) 10^{-2}, and (△) 10^{-1} monomole/l.; as given in the literature by (*1*) Samelson,[13] (*2*) Gregor and Frederick,[14] (*3*) Oth and Doty,[15] (*4*) Arnold and Overbeek,[16] (*5*) Kern,[17] and (*6*) Katchalsky and Spitnik.[18]

formula used by Tanford[21] to describe titration of proteins. This asymptotic approach to the linear form may be readily deduced from the potential in excess salt, as follows. When $|\phi_a| \leqslant 1$ (or when $\Delta pK \leqslant 0.43$) the function ϕ^{outer} extends from R right to the surface of the polyion, since the requirement $\phi^{outer} \leqslant 1$ is fulfilled everywhere. Utilizing the boundary eqs. (23) and (32) for $\Delta\phi^{outer}$ we obtain

$$\lambda = (\kappa a/2)BK_1(\kappa a) \tag{42}$$

and

$$\Delta pK = 0.434\ \phi_a^{outer} = 0.434\ \lambda\ (\kappa a/2)^{-1}K_0(\kappa a)/K_1(\kappa a) \tag{43}$$

which makes ΔpK depend on $\alpha m_s^{-1/2}$. At higher λ, however, this linear dependence breaks down, as has been observed even in the case of the moderately charged protein polyions.[22]

In order to compare eq. (41) to experimental results obtained for flexible polyions we have yet to decide what is the length h of the equivalent cylinder, which determines the charge parameter λ. As shown in Figure 2, the main increase in the potential occurs very close to the surface of the polyion; it seems therefore reasonable to assume that $(\phi_a - \phi_R)$ or ΔpK, is

determined by and large by the contour length of the polyion $h = Zl$, where l is the contribution of the monomer unit to the fully extended chain. This choice has been adopted in calculating the theoretical ΔpK's, so that for polyvinyl polymers, for example, $\lambda = 7.4$ A. $^{-1}/l = 3$.

In Fig. 6 we have plotted results for ΔpK in polymethacrylic and polyacrylic acids measured in solutions which contained an excess of salt, for a hundredfold change of salt concentrations; the theory appears to predict reasonably well the experimental behavior. In Figure 7 we have plotted results obtained in solutions which contained relatively little or no added salt and again the theory appears to give a reasonable description of the behavior observed for a hundredfold change in concentration. At low degrees of ionization, below $\alpha = 0.2$, the agreement with the experimental results becomes increasingly poor, and the latter in fact do not exhibit the expected tendency to decrease linearly toward zero. This behavior may be probably attributed to the strong coiling of the polyion which makes untenable the fully extended cylindrical model.

V. Donnan Equilibria in Excess of Salt

1. The results of the Donnan distribution of a low molecular salt are often characterized by the ratio

$$\Gamma = (m'_s - m_s)/\nu m_p \tag{44}$$

where Γ is the salt excluded per unit macromolecular charge. When the ratio of the polymer to salt decreases to zero, the salt exclusion effect becomes a single-molecule phenomenon and as such is expected to reach a constant value independent of m_p. In other words, when $\nu m_p/m'_s \to 0$, Γ should approach a limiting value determined solely by the properties of the *single* polyelectrolyte molecules and by the nature and the ionic strength of the salt solution. The limiting value of Γ is easily calculated for the ideal case, when the activities of the ions are equal to their concentrations. In view of our representation of activities by the surface concentration [cf. eq. (4)] in the ideal case we have

$$\begin{aligned} m_+^R &= \nu m_p + m_s \\ m_-^R &= m_s \end{aligned} \tag{45}$$

On the other hand, taking into account the Donnan equilibrium of eq. (3), Γ may be also written as

$$\Gamma = [(m_+^R m_-^R)^{1/2} - m_s)]/\nu m_p \tag{46}$$

Combination of eqs. (45) and (46), with the neglect of terms higher than $\nu m_p/m_s$, leads immediately to the well known result

$$\lim_{\nu m_p/m_s \to 0} \Gamma = [(\nu m_p + m_s)^{1/2} m_s^{1/2} - m_s]/\nu m_p = 1/2 \quad \text{(ideal case)} \tag{47}$$

An identical calculation may be carried out for systems described by the aforementioned rule of additivity according to which

$$\begin{aligned} m_+^R &= \varphi_p \nu m_p + m_s \\ m_-^R &= m_s \end{aligned} \tag{48}$$

which gives

$$\lim_{\nu m_p/m_s \to 0} \Gamma = \varphi_p/2 \text{ (rule of additivity)} \tag{49}$$

At higher $\nu m_p/m_s$ or $\alpha m_m/m_s$ ratios Γ is no longer expected to remain contant and is found to decrease from its limiting value to zero.[2] In the present treatment, however, we shall restrict ourselves to low m_m/m_s ratios, which is the case studied in the majority of the experimental reports. As has often been observed, eq. (47) is generally not satisfactory for the description of the actually measured limiting values of Γ. Equation (49) provides a better description, yet it is not precise enough for a quantitative description. Its weakness becomes more evident at high ionic strengths when Γ is found to increase strongly,[2,23] whereas $\varphi_p/2$ is a constant quantity, which by definition [see eq. (40)] does not depend on the salt concentration. It is therefore of interest to calculate Γ in a more systematic manner on the basis of the theoretical treatment presented here.

2. The theoretical evaluation of Γ requires the calculation of m_s only, since the external salt concentration m'_s and the equivalent charge density of the ionized groups νm_p are specified in the experiment. On the basis of the normalization eq. (10) and in view of the discussion presented in section III-1, we may write for m_s

$$\begin{aligned} m_s &= (m_-^R/V) \int_a^R e^{\phi}\, dV \\ &= m'_s\,[(1 - q + q^2/2)/V] \int_b^R (1 + \phi^{\text{outer}})\, dV \\ &= m'_s[(1 - q + q^2/2)/V] \{(V - \pi b^2 h)(1 + q) \\ &\qquad + 2\pi\, hB \int_b^R [K_0(\kappa r) + I_0(\kappa r)\, K_1(\kappa R)/I_1(\kappa R)]\, r dr\} \end{aligned} \tag{50}$$

Using the appropriate integration formulae[10] and taking note of eq. (20), and of the correlations $V = m_p^{-1}$ and $\kappa^2 \nu = 8\pi h \lambda m'_s\,(1 + q^2/2)$ we obtain as a result eq. (51):

$$\begin{aligned} m_s = m'_s\{1 - q^2/2 - (\kappa b)^2 \nu m_p/8\lambda m'_s + (\kappa b \nu m_p/4\lambda m'_s) \\ \times B[K_1(\kappa b) - I_1(\kappa b) K_1(\kappa R)/I_1(\kappa R)]\} \end{aligned} \tag{51}$$

In deriving eq. (51) we omit $b^2 q^2/R^2$ which is proportional to $(m_m/m_s)^3$. If the limiting case of low m_m/m_s ratios is considered, the terms of the argument (κR) go to zero while B becomes equal to $-1/K_0(\kappa b)$ as has been shown before. The simplified result for m_s may be now introduced into the definition eq. (44) to give the required expression for Γ

$$\lim_{m_m/m_s \to 0} \Gamma = (1/4\lambda)[\kappa b K_1(\kappa b)/K_0(\kappa b) + (\kappa b)^2/2] \tag{52}$$

At higher m_m/m_s ratios a more complicated but analogous expression holds, while for very high ratios, when the salt is no longer present in excess, higher order terms than $q^2/2$ have to be included, and the present approach is no longer feasible. In practice, however, detailed calculations show that the limiting value of eq. (52) provides a reasonable approximation up to about $m_m/m_s \leq 1$. In what follows we shall refer only to this limiting value of Γ.

3. Equation (52) may be given the following simple physical interpretation. If the salt (or coion) concentration inside (m_s) were to equal the external concentration (m'_s), then the exclusion factor Γ would equal zero. The two factors which make for a smaller m_s (and hence positive Γ) are the total exclusion of the coions from the inner volume (viz., the term-πb^2h in eq. (50)) and the partial repulsion of coions from the outer volume (viz., the integral of ϕ^{outer} over the outer volume) which are represented by the second and first terms, respectively, on the right-hand side of eq. (52). The magnitude of these effects may be also expressed in a simple way. The calculation shows that, at very low ionic strengths and for all charge densities of actual interest, κb varies only between the limits of about 0.6–0.8. This makes the first and second term of the order of $1/4\ \lambda$ and of $0.3/4\ \lambda$. On the other hand, we know also that the limiting value (calculated from Lifson and Katchalsky's work[4]) of $\varphi_p/2$ at low polymer concentration is $1/4\ \lambda$ with an increase of some 50% at higher concentrations. This leads to the qualitative similarity between eq. (49) derived from the rule of additivity and our theoretical eq. (52). At higher ionic strengths however, the calculated κb increase strongly and so do both terms of our equation, leading to Γ values much higher than $\varphi_p/2$.

Equation (52) may be also compared to another description put forward by Strauss and Ander.[23] The latter have assumed that an electroneutral central core, which roughly corresponds to our "inner volume" πb^2h, is totally excluded to the coions, while in the remaining outer volume the salt is uniformly distributed. This should lead to the effect given by our second term of eq. (52) and indeed, when Strauss and Ander's eq. (7) is transcribed to the present notation, it reads

$$\Gamma = m'_s \pi b^2 h/\nu = (\kappa b)^2/8\lambda$$

An interesting situation arises when the polyelectrolyte potential is sufficiently suppressed either by high ionic strength or by low charge density so that the linearized potential ϕ^{outer} may be used up to the surface of the polyion, or when $b = a$. Using eq. (42) developed for this case and eq. (30′) we obtain for Γ

$$\Gamma = {}^1/_2 + (\pi a^2 h/\nu) m'_s \tag{53}$$

which means that, except for the effect of the excluded volume of the polyion itself, Γ obeys the ideal law of eq. (47). This seems puzzling, since we have not postulated that the electrostatic potential ϕ vanishes and required only that e^{ϕ} may be linearized everywhere. The same result may be also

obtained in a different way, which throws light on the meaning of this "pseudo-ideal" behavior. Using the alternative eq. (46) for Γ and combining it with the linearized normalization integrals of eqs. (9) and (10) we obtain

$$\Gamma = (1/\nu m_p)\{[(\nu m_p + m_s)/\int_{V^{outer}}(1 - \phi^{outer})dV]^{1/2}[m_s / \int_{V^{outer}}(1 + \phi^{outer})dV]^{1/2} - m_s\} \simeq 1/2 + (\pi a^2 h/\nu)m_s \qquad (53')$$

This alternative derivation shows that although both m_+^R and m_-^R differ from uniform distribution as indicated by the presence of the ϕ terms, the latter cancel out mutually in the final expression for Γ. In other words, in the linear case the counterions are attracted towards the polyion in the same degree as the coions are repelled, so that the activity of the salt ($a_s = m_+^R \cdot m_-^R$) remains unaffected. This rather unexpected behavior according to which in certain cases the salt behaves ideally, or even in a sense more than ideally ($\Gamma > 1/2$) because of the presence of the excluded volume term, has been observed experimentally as shown below in Figure 9. We have assumed here that the polyion is wholly impermeable to the small ions; if it were not and a completely permeable behavior were exhibited, the maximum value of Γ would be $1/2$. (In this case b in the equations should be replaced by $b - a$.) The different real polyions might be well expected to exhibit various intermediate modes of behavior.

4. The theoretical evaluation of Γ for polyions which are not fully stretched rigid cylinders requires a further assumption regarding the value of λ. This implies some information on the effective length of the macromolecules. Since no convincing theory on the relation between viscosity and molecular dimensions exists for polyelectrolyte solutions and since the viscometric radius need not necessarily be the factor which determines the electrostatic interaction, we prefer to derive λ from a colligative property related to Donnan equilibria. As shown by Lifson and Katchalsky,[4] the osmotic coefficient of salt-free polyelectrolyte solutions φ_p is given by

$$\varphi_p = (1 - \beta^2)/2\lambda \qquad (54)$$

and since $\beta = \beta(m_p\lambda)$ therefore at a given polymer concentration φ_p is determined by λ or vice versa.

The concept of φ_p osmotically active counterions also retains its validity in the presence of salt as shown in previous reports.[1-3] The effective value of λ derived from eq. (54) on the basis of experimental values of φ_p, may therefore be regarded as an adequate charging parameter for the calculations. The semiempirical aspect of this procedure may be made more palatable by the observation that in many cases of different flexible macroions, such as the vinylic polyelectrolytes at sufficiently high degrees of ionization, $\lambda_{effective}$ is invariably found to be about twice the magnitude calculated for the wholly stretched chain. We recall that the latter is defined by

$$\lambda_{stretched} = \alpha\epsilon^2/DkTl \simeq 7.4 \text{ A.}^{-1}/l$$

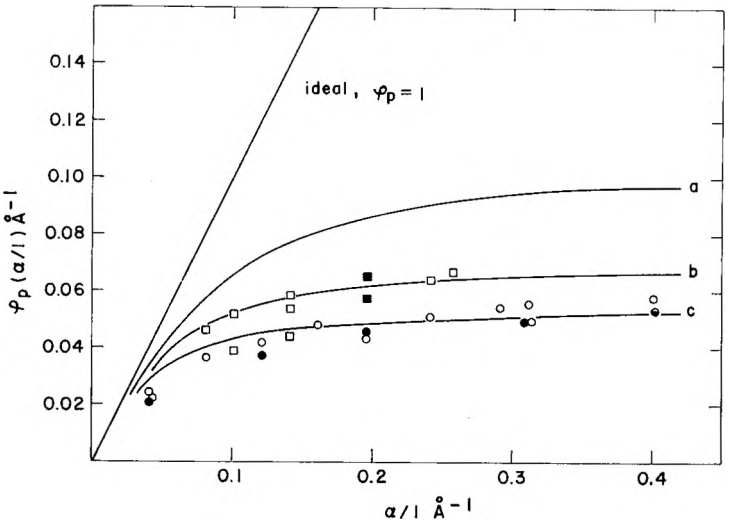

Fig. 8. $\varphi_p(\alpha/l)$, (the number of osmotically active ions per unit length of macroion, as a function of the total (stoichiometric) number of such ions (α/l): (——) values calculated from Lifson and Katchalsky's[4] equation for φ_p in salt-free solutions at $\gamma = 3$ for (*a*) $\lambda_{effective} = \lambda_{stretched}$, (*b*) $\lambda_{effective} = 1.5\ \lambda_{stretched}$, (*c*) $\lambda_{effective} = 2\lambda_{strecthed}$; experimental results for (O) polyacrylates,[2,17,29] (●) polymethacrylates,[24,29] (◒) polyphosphates, (□) carboxymethyl cellulose,[29,30] and (■) alginates.[31]

l being the length per monomer of the fully stretched chain. On the other hand, it was found that stiffer molecules, such as the substituted cellulose derivatives, or polyelectrolyte salts of extremely bulky counterions, obey a different relationship, with $\lambda_{effective} = 1.3\ \lambda_{stretched}$. This general behavior is illustrated in Figure 8, in which we have collected the currently available data on φ_p. Since our procedure substitutes the actual potential of flexible macroions—which is not cylindrical—by a hypothetical cylindrical potential and corrects for the approximation by the use of $\lambda_{effective}$, the latter will clearly depend on the physical property considered, since different properties depend in a different way on potential. The colligative properties of the small ions are determined by the volume integrals of the type $\int e^{\pm\phi}\, dV$, and all of them are expected to give the same value of $\lambda_{effective}$. The outstanding feature of these volume integrals is that the outer layers, in which $\epsilon\psi/kT$ is very small, still play an important role in the integral since the total volume of these layers (which increases with r) is relatively large. Consequently, the effective cylinder length which determines $\lambda_{effective}$ of the osmotic properties, will lie somewhere between the contour length and the actual end to end distance. In contrast the potentiometric potential—which (as has been pointed out above) is closely related to the immediate surrounding of the polyion—is determined mainly by the contour length of the polyion and described by $\lambda_{stretched}$.

In conclusion we would like to emphasize that whatever be the choice of $\lambda_{effective}$ for a particular polyion, this value was found to describe the colliga-

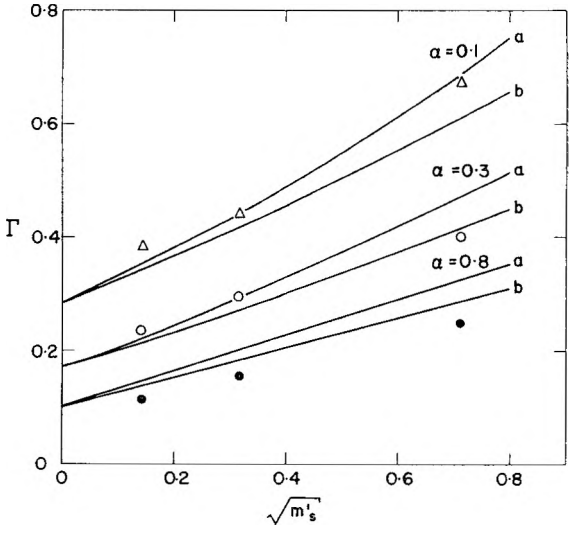

Fig. 9. The dependence of the salt exclusion per polymer Γ on the salt concentration m'_s (in moles/l.): (——) calculated for $\lambda_{effective} = 4$; 2.4 and 1.25, respectively, and with a polyion radius a of (a) 6 A. and (b) 5 A.; experimental results obtained with PAA at degrees of ionization α of (Δ) 0.8,(O) 0.3, and (●) 0.1. (Note that $\lambda_{effective}$ re-evaluated from experimental results are slightly different from those found previously.[2])

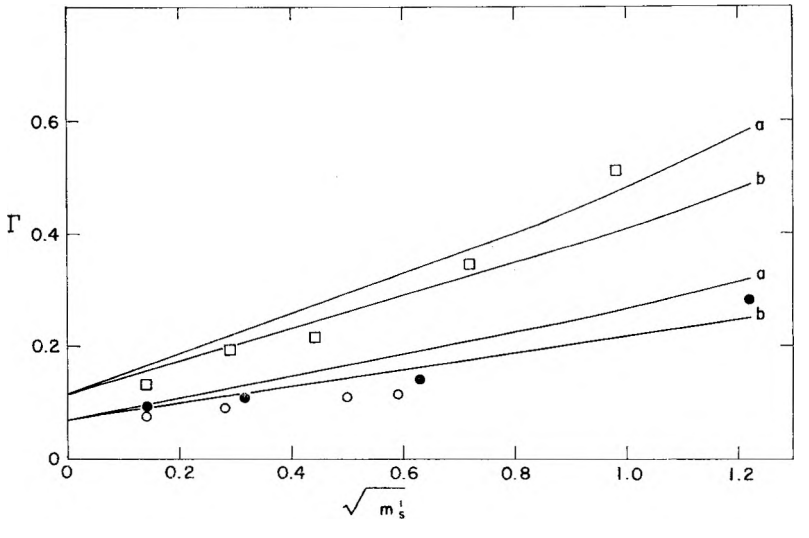

Fig. 10. The dependence of the salt exclusion per polymer Γ on the salt concentration m'_s (in moles/l.: (——) calculated for $\lambda_{effective} = 6$ with ionic radii a of (a) 5 A. and (b) 4 A. and for $\lambda_{effective} = 3.5$ with ionic radii a of (a) 6 A. and (b) 5 A.; experimental results of Strauss and Ander[23] for (O) Na polyphosphate, (●) Li polyphosphate, and (□) tetramethylammonium polyphosphate.

tive properties at *all* ionic strengths of the polymer and of the salt (otherwise of course the concept of $\lambda_{effective}$ would become valueless). The changes in the end to end distance which presumably occur upon variation of the ionic strength, do not therefore influence markedly the effective cylinder length. This indicates that fairly long segments of the polyion retain their conformation at different ionic strengths.

In Figures 9 and 10 we have drawn theoretical values of Γ, based on $\lambda_{effective}$ which are calculated from eq. (54), on the basis of the experimentally determined φ_p. The φ_p values of the polyphosphates were specially measured for the purpose of this work. The results at $m_m = 0.02$ were $\varphi_p = 0.13$ for Li and Na polyphosphate and, at $m_m = 0.014$, $\varphi_p = 0.22$ for TMA polyphosphate. The values $\lambda_{effective} = 6.6$ and 3.5 were adopted accordingly. The theoretical Γ are compared in Figure 10 to the experimental results obtained by Strauss and Ander[23] with three different polyphosphate salts. In Figure 9 the Γ are compared to results obtained by us with sodium polyacrylate at three degrees of ionization. The experimental technique and the results for φ_p, from which $\lambda_{effective}$ were estimated are described elsewhere.[2,24] Considering the fact that no freely adjustable parameter is used here, we consider that the agreement between the calculated and measured Γ values is satisfactory.

VI. Donnan Osmotic Pressure

1. The hydrostatic pressure required to maintain equilibrium of a polyelectrolyte solution with an external solution through a membrane permeable to both salt and water, is called the Donnan osmotic pressure. The Donnan osmotic pressure of an elementary volume $V = 1/n_p$, comprising a single macromolecule and numerous small ions and at equilibrium with external salt solution of concentration m'_s, is obtained by combining eqs. (14) and (22)

$$\pi_{calc}\, V/kT = 1 + \nu B^2/8\lambda I_1^2(\kappa R) \tag{55}$$

where B is the integration constant plotted in Figure 3 and κR is determined by the relative concentrations m'_s and m_p. For polyions of given charge density and at constant external salt concentration κR is simply proportional to V

$$\kappa R = (8\lambda m'_s/\nu m_p)^{1/2} = u\nu^{1/2} \tag{56}$$

where

$$u = (8\lambda m'_s/V)^{1/2}$$

Under those conditions the second term on the right-hand side of eq. (55) depends on V only and is denoted as $\varphi(V)$

$$\varphi(V) = \nu B^2/8\lambda I_1^2(\kappa R) \tag{57}$$

For many purposes it may be assumed that no fluctuations occur and that the volume elements are all equal to the average value $\bar{V}$. In this case the

product of the macroscopic pressure (π_0) and a unit volume v, may be obtained by summing over the n_p elements of the volume

$$\pi_0 v/kT = \sum_{n_p} \pi_{calc}\bar{V}/kT = \sum_{n_p} [1 + \varphi(\bar{V})] = n_p \pi_{calc}\bar{V}/kT$$

since

$$n_p \bar{V} = v = 1$$

$$\pi_0 = \pi_{calc} \tag{58}$$

or the macroscopic pressure in the absence of fluctuations is equal to that calculated for a single volume element. Since the Donnan osmotic pressure depends strongly on the absolute magnitude of V, the approximation of equally sized cells is not precise enough. We have therefore to consider explicitly the fluctuation of the volume per macromolecule V. (The fluctuations are negligible in salt-free solutions when the electrostatic repulsion keeps the macroions in relatively fixed position; they become important, however, when the macroions are largely screened by the presence of excess salt.[25]) Let us denote the fluctuating volume of the ith element by V_i, with the condition $\sum_{n_p} V_i = 1$. The activity of the relatively numerous salt ions is assumed to be constant and equal for all the fluctuating volumes, so that the osmotic pressure in the element (π_i) is related to V_i by the theoretical eq. (55), or

$$\pi_i V_i/kT = 1 + \varphi(V_i) \tag{59}$$

Let the real macroscopic pressure be π; then the work of a single fluctuation is given by $(\pi - \pi_i)V_i$. The total work of fluctuation of the n_p elements at equilibrium is zero, so that

$$\sum_{n_p} (\pi - \pi_i)V_i = \pi \sum_{n_p} V_i - \sum_{n_p} \pi_i V_i = 0$$

or

$$\pi = \sum_{n_p} \pi_i V_i \tag{60}$$

together with eq. (59) we obtain

$$\pi/kT = n_p + \sum_{n_p} \varphi(V_i) \tag{61}$$

$\varphi(V_i)$ may be developed in Taylor series, up to the second term, around the average value $\bar{V}$

$$\varphi(V_i) = \varphi(\bar{V}) + \delta_i\varphi'(\bar{V}) + \delta_i^2\varphi''(\bar{V})/2$$

where δ_i is the derivation from the mean value $\delta_i = V_i - \bar{V}$. Summation of $\varphi(V_i)$ over all the elements then gives

$$\sum_{n_p} \varphi(V_i) = n_p\varphi(\bar{V}) + \varphi'(\bar{V}) \sum_{n_p} \delta_i + \varphi''(\bar{V})/2 \sum_{n_p} \delta_i^2 \tag{62}$$

The sum of the linear fluctuations δ_i at equilibrium is zero, while δ_i^2, according to a well known result of fluctuation theory, is

$$\sum_{n_p} \delta_i^2 = n_p\overline{(V_i - \bar{V})^2}$$
$$= n_p kT/(\partial^2 G/\partial V^2)_{\bar{V}}$$
$$= n_p kT/-(\partial\pi/\partial V)_{\bar{V}}$$

With these results eq. (61) becomes

$$\pi/kT = n_p + n_p\varphi(\bar{V}) + [n_p\varphi''(\bar{V})kT/-2(\partial\pi/\partial V)_{\bar{V}}] \tag{63}$$

Comparing eq. (63) to eqs. (58) and (55) we observe that the real pressure π exceeds π_0 (or π_{calc}) by the last term on the right-hand side of eq. (63). To calculate $\varphi''(V)$ we use the asymptotic formula for large values of κR:[10]

$$I_1^2(\kappa R) \simeq e^2\kappa R/2\pi^{\kappa R} = e^{2uV^{1/2}}/2\pi u V^{1/2}$$

so that

$$\varphi(V) \simeq (\nu B^2 2\pi u/8\lambda)V^{1/2}e^{-2uV^{1/2}} \tag{64}$$

and with this approximation obtain

$$\varphi'(V) = -[u\varphi(V)/V^{1/2}][1 - (1/2uV^{1/2})]$$
$$\simeq -\kappa R\varphi(V)/V \tag{65}$$

and

$$\varphi''(V) = [u^2\varphi(V)/2V][1 - (1/2uV^{1/2}) - (1/4u^2V)] \tag{66}$$
$$\simeq (\kappa R)^2\varphi(V)/2V^2$$

while eqs. (65) and (59) give an estimate for $(\partial\pi/\partial V)$

$$-\partial(\pi/RT)/\partial V = 1/V^2 + \varphi(V)/V^2 - \varphi'(V)/V$$
$$= [1 + (1 + \kappa R)\varphi(V)]/V^2 \tag{67}$$

Introducing eqs. (66) and (67) into eq. (63) leads to the required expression for the macroscopic osmotic pressure:

$$\pi/kT = n_p + n_p\varphi(\bar{V}) + n_p(\kappa R)^2\varphi(\bar{V})/2[1 + (1 + \kappa R)\varphi(\bar{V})] \tag{68}$$

The Donnan osmotic pressure is usually plotted as the reduced pressure (π/c) versus the polymer concentration. For the monomolar scale of concentration, where

$$m_m = m_p Z = Z/VN$$

N being the Avogadro number, eq. (68) becomes

$$(\pi/RT)/m_m\text{moles/l.} = 1/Z + \{1 + (\kappa R)^2/2[1 + (1 + \kappa R)\varphi(V)]\}\varphi(V)/Z \tag{68'}$$

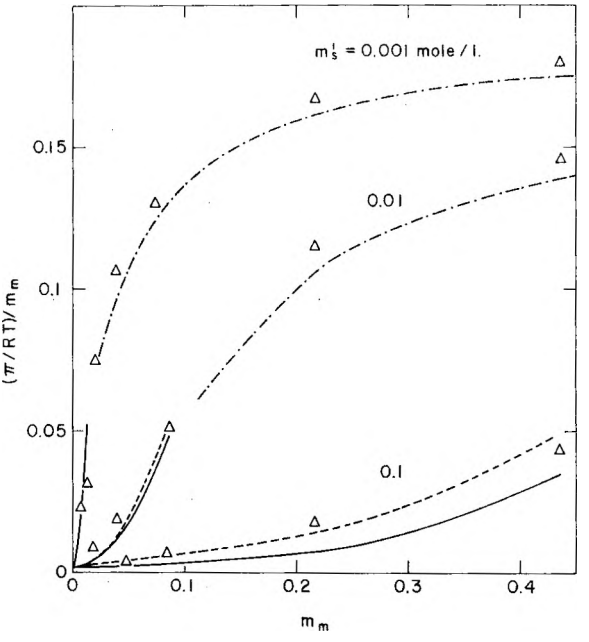

Fig. 11. The dependence of the reduced Donnan osmotic pressure $(\pi/RT)/m_m$, on the polymer concentration m_m in monomoles/l.: (——) calculated for $\lambda_{effective} = 4$ and $a = 5$ A.; (- -) calculated as above, but corrected for $A_2 m_m = 0.03\ m_m$; (—·—·—) calculated from the additivity rule;[2] (Δ) experimental results obtained[2] for polyacrylic acid of $\alpha = 0.8$ at salt concentrations $m'_s = 0.001$, 0.01, and 0.1 mole/l.

Except for a relatively minor variation of the constant B with m'_s the function $\varphi(V)$, as defined by eq. (57), is determined by κR. The second term on the right-hand side of eq. (68′) (which expresses the electrostatic contribution to π) is seen therefore to be a function of κR or of the ratio of salt and polymer concentrations. Since $\varphi(V)$ is proportional to ν, $\varphi(V)/Z$ does not depend on the molecular weight.

With the commonly used polymer concentration c_p (in grams/100 ml.) and the pressure π expressed in grams/cm.^{2}, the eq. (68′) becomes

$$\pi/c_p = (2.4 \times 10^5/M_m)\ 1/Z + (2.4 \times 10^5/M_m) \{1 + (\kappa R)^2/2[1 + (1 + \kappa R)\varphi(V)]\}\varphi(V)/Z \quad (68'')$$

where M_m is the molecular weight of the monomer and

$$\kappa R = (8\lambda M_m/10\alpha)^{1/2}(m'_s/c_p)^{1/2}$$

Following the reasoning of the preceding section the effective values of λ (which are determined from experimental φ_p values on the basis of eq. (54)) are to be used in calculating the osmotic pressure.

2. Using eqs. (68′) and (68″) we have calculated the reduced osmotic pressure for polyacrylic acid (PAA) of $\alpha = 0.8$ and for a fully neutralized ($\alpha = 1$) carboxymethylcellulose (CMC) of a degree of substitution D.S. =

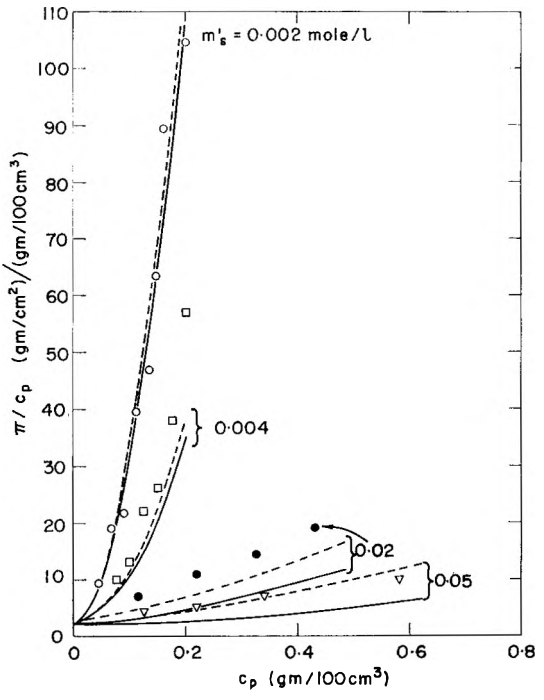

Fig. 12. The dependence of the reduced Donnan osmotic pressure (π/c_p), on the polymer concentration c_p in g./100 cm.^{3}: (——) calculated for $\lambda_{effective} = 0.8$ and $a =$ 6 A.; (- -) as above, but corrected for $A_2c_p = 20\ c_p$. Experimental results obtained by Inagaki and Hirami[26] with methyl cellulose of D.S. = 0.45 at salt concentrations of (O) 0.002, (□) 0.004, (●) 0.02, and (▽) 0.05 mole/l.

0.45 and $M_m = 435$. The effective charge parameter for CMC is $\lambda_{effective} \simeq 1.3\ \lambda_{stretched} \simeq 0.8$ (Fig. 8 and other results[29]) while for PAA, at $\alpha = 0.8$, $\lambda_{effective} \simeq 1.8\ \lambda_{stretched} \simeq 4$ (as in section V-4). In Figures 11 and 12 these values are compared to the experimental results, which have been reported by one of us[2] and by Inagaki and Hirami.[26] The overall agreement between theory and experiment is moderately satisfactory. The theory predicts that at low c_p/m'_s ratios the virial term will decrease towards zero so that a nonlinear plot of π/c_p versus c_p will result. The experimental results indicate that the decrease in π/c_p is smaller than that predicted theoretically, but they do provide a clear enough confirmation of the nonlinear behavior at low ionic strengths. It should be realized that this deviation from linear behavior is of basic importance in relation to the linear extrapolation of π/c_p results to zero concentration for the evaluation of molecular weight.

In our treatment we have neglected the nonelectrolytic second virial coefficient which is always present in polymer solutions, except at the θ temperature.[27] This coefficient, commonly denoted as A_2, should be added to eqs. (68′) and (68″). In order to estimate its magnitude we shall utilize the fact that the theoretically evaluated electrostatic virial term depends strongly on the ionic strength, being roughly proportional to m_s^{-1}. On the

other hand, the coefficient A_2 does not depend markedly on the composition of the solution and is determined by and large by the excluded volume of the polyion. The latter is affected strongly by the degree of ionization but not strongly, if at all, by the ionic strength, as indicated by the validity of the present model according to which a nearly fully stretched cylinder of constant length is seen to represent the macroion at all ionic strengths. The intercept at $m_s^{-1} = 0$, of the plot of some average values of the experimental slopes $d(\pi/c_p)/dc_p$ versus m_s^{-1} should therefore give an estimate of the magnitude of A_2. Having thus determined A_2 we have added the terms $A_2 m_m$ or $A_2 c_p$ to eqs. (68′) or (68″), respectively; the result is described by the broken line in Figures 11 and 12 and is seen to bring the calculated curves closer to the experimental results.

3. In conclusion, some remarks may be made regarding the description of the osmotic pressure in the total range of polymer concentrations which includes solutions of high polymer-to-salt ratios, when the salt is no longer in excess. In the latter case the parameter B which determines $\varphi(\kappa R)$ can be no longer evaluated from the simplified eq. (30′), which was found to hold up to κR values of 2–3. This puts the limit of the treatment at m_m/m_s ratios smaller than 5–10 or 2–4 for polyacrylics and carboxymethyl celluloses, respectively. Above this level the more exact eq. (30) could be used, but in this range the theory ceases to be valid due to the neglect of $q^4/12$ and higher terms in the basic expression for π [eq. (14)]. At high m_m/m_s ratios the π/m_m lines become concave down and eventually reach the limiting value for salt-free solutions $(\pi/RT)/m_m = \varphi_p$. The theoretical description in this region is given by the more complete (and much more complicated) calculation in which no assumption of excess salt is made; but, as the result of this calculation has shown,[2] an equivalent and much simpler description of the osmotic pressure in this region is provided when the additivity rule [eq. (48)] is used in conjunction with eq. (14). The result at low m_m/m_s ratios is

$$(\pi/RT)/m_m = 1/Z + \alpha^2 \varphi_p^2 m_m/4m'_s \qquad (69)$$

At higher m_m/m'_s ratios the required concave down curve is obtained, and the limiting value of φ_p is ultimately reached.[2] The portion of the curve which obeys eq. (69) is linear only in so far as φ_p is truly constant. Since, however, φ_p decreases to a certain degree with the polymer concentration,[2,4] a somewhat concave up curve is obtained at low m_m/m'_s ratios. The π/m_m curve in the total range of polymer concentrations $0 \leqslant m_m/m_s \leqslant \infty$ is therefore S-shaped. The experimental results are usually measured in the middle and lower portion of the S and this fact probably explains the often reported linear behavior, which contradicts the findings obtained from the present theory on the one hand, from the additivity rule on the other, and confirmed experimentally by several workers.[2,26,28] The theoretical treatment predicts however that the electrostatic contribution to the second and higher virial coefficients vanishes when $m_m/m_s \to 0$, whereas according to the additivity rule the contribution reaches a finite value since $\varphi_p \to 1/2\lambda$

when $m_m \to 0$. The experimental data available at present do not permit a decision to be reached on this point.

In fact in the whole range of m_m/m_s ratios the description provided by the simple additivity rule fits the experimentally determined osmotic pressures as satisfactorily as do the more complicated theoretical calculations; the latter, however, constitute part of a more comprehensive framework which derives all equilibrium properties from the electrostatic potential of the polyions.

References

1. Katchalsky, A., and Z. Alexandrowicz, *J. Polymer Sci.*, **A1**, 2093 (1963).
2. Alexandrowicz, Z., *J. Polymer Sci.*, **56**, 97, 115 (1962).
3. Kotin, L., and M. Nagasawa, *J. Chem. Phys.*, **36**, 873 (1962).
4. Lifson, S., and A. Katchalsky, *J. Polymer Sci.*, **13**, 43 (1953).
5. Langmuir, I., *J. Chem. Phys.*, **6**, 893 (1938).
6. Verwey, E. J. W., and J. Th. G. Overbeek, *Theory of the Stability of Lyophobic Colloids*, Elsevier, New York, 1948, p. 92.
7. Marcus, R. A., *J. Chem. Phys.*, **23**, 1057 (1955).
8. Alfrey, T., P. W. Berg, and H. Morawetz, *J. Polymer Sci.*, **7**, 543 (1951).
9. Fuoss, R. M., A. Katchalsky, and S. Lifson, *Proc. Natl. Acad. Sci. (U. S.)*, **37**, 579 (1951).
10. McLachlan, N. W., *Bessel Functions for Engineers*, Oxford Univ. Press, London. 2nd Ed., 1955, pp. 201, 204, 220, 221.
11. Rutgers, A. J., *Physical Chemistry*, Interscience, New York, 1954, p. 437.
12. Cox, R. A., and A. R. Peacocke, *J. Chem. Soc.*, **1956**, 2499.
13. Samelson, H., Dissertation, Columbia University, 1952.
14. Gregor, H. P., and M. Frederick, *J. Polymer Sci.*, **23**, 451 (1957).
15. Oth, A., and P. Doty, *J. Phys. Chem.*, **56**, 43 (1952).
16. Arnold, A., and J. Th. G. Overbeek, *Rec. Trav. Chim.*, **69**, 2 (1950).
17. Kern, W., *Z. Physik. Chem.*, **A184**, 197 (1937).
18. Katchalsky, A., and P. Spitnik, *J. Polymer Sci.*, **4**, 432 (1947).
19. Kagawa, I., and H. P. Gregor, *J. Polymer Sci.*, **23**, 477 (1957).
20. Katchalsky, A., N. Shavit, and H. Eisenberg, *J. Polymer Sci.*, **13**, 69 (1954).
21. Tanford, C., S. A. Swanson, and W. S. Shore, *J. Am. Chem. Soc.*, **77**, 6414 (1955).
22. Foster, J. F., in *The Plasma Proteins*, F. W. Putnam, Ed., Academic Press, New York, 1960, Vol. I, p. 188.
23. Strauss, U. P., and P. Ander, *J. Am. Chem. Soc.*, **80**, 6494 (1958).
24. Alexandrowicz, Z., *J. Polymer Sci.*, **43**, 337 (1960).
25. This has been suggested to us, by Prof. U. P. Strauss.
26. Inagaki, H., and M. Hirami, *Z. Elektrochem.*, **63**, 419 (1959).
27. Eisenberg, H., and D. Woodside, *J. Chem. Phys.*, **36**, 1844 (1962).
28. Orofino, T. A., *Rec. Trav. Chim.*, **78**, 434 (1959).
29. Alexandrowicz, Z., unpublished results.
30. Kagawa, I., H. Yamada, and I. Imai, *J. Chem. Soc. Japan Ind. Chem. Sect.*, **53**, 120 (1950).
31. Katchalsky, A., R. E. Cooper, J. Upadhyay, and A. Wasserman, *J. Chem. Soc.*, **1961**, 5198.

Résumé

Ce travail traite des propriétés d'équilibre de solution de polyélectrolyte renfermant un excès de sel de faible poids moléculaire. Dans ce cas, la loi simple d'additivité utilisée antérieurement, tombe en défaut pour décrire les résultats expérimentaux. On a dès

lors entrepris un traitement détaillé basé sur une solution approximative de l'équation de Poisson-Boltzmann. Le calcul est basé sur une subdivision du potentiel électrostatique en deux parties correspondant à deux régions: (*1*) une région interne dans le voisinage immédiat du polyion, libre de co-ions et décrite par l'equation de Poisson-Boltzmann en absence de sel libre, et (*2*) une région externe, séparée du macro-ion central et traitée de façon adéquate par une approximation suivant Debye. On a obtenu une solution analytique pour le potentiel électrostatique et on a utilisé pour la description théorique du comportement potentiométrique, la distribution de sel et la pression osmotique de Donnan. Les valeurs prédites se comparent favorablement avec les résultats mesurés dans un large domaine de conditions expérimentales.

Zusammenfassung

In der vorliegenden Arbeit werden die Gleichgewichtseigenschaften von Polyelektrolytlösungen mit einem Überschuss an niedermolekularem Salz behandelt. In diesem Fall versagt das früher mitgeteilte einfache Additivitätsgesetz bei der Beschreibung der Versuchsergebnisse. Es wurde daher eine auf einer Näherungslösung der Poisson-Boltzmann-Gleichung beruhende eingehende modellmässige Behandlung durchgeführt. Die Berechnung beruht auf einer Unterteilung des elektrostatischen Potentials in zwei, zwei Bereichen entsprechenden Teile: (*1*) Ein innerer Bereich in der unmittelbaren Nachbarschaft des Polyions, frei von Coionen und im salz-freien Fall durch die Poisson-Boltzmann-Gleichung beschrieben und (*2*) ein äusserer Bereich, von Zentralmakroion abgeschirmt und durch eine Debye-Näherung zu behandeln. Für das elektrostatische Potential wurde eine analytische Lösung erhalten und zur theoretischen Beschreibung des potentiometrischen Verhaltens, der Donnan-Verteilung des Salzes und des Donnanschen osmotischen Druckes angewendet. Die berechneten Werte stimmen über einen grossen Bereich der Versuchsbedingungen mit den Messergebnissen gut überein.

Received September 19, 1962

JOURNAL OF POLYMER SCIENCE: PART A VOL. 1, PP. 3261–3264 (1963)

Polydiacrylylmethane*

W. DEWINTER, C. S. MARVEL, and AZIZ ABDUL-KARIM,
Department of Chemistry, University of Arizona, Tucson, Arizona

Synopsis

Pure diacrylylmethane does not polymerize smoothly on free radical initiation. It gives a higher yield of the polymer as a sodium salt when initiated by sodium methoxide. The molecular weight is obviously low. The polymer formed from its sodium salt is insoluble. Attempts to prepare the dioxime yielded an intractable monooxime.

The polydiacrylylmethane (I) prepared by Jones[1] by the action of sodium methoxide on methyl vinyl ketone and methyl acrylate seems to be a copolymer of this monomer and methyl vinyl ketone.[2] Since pure diacrylylmethane (II) is now available,[3] study of its polymerization has been undertaken.

When diacrylylmethane is allowed to stand it polymerizes slowly at room temperature to yield a hard insoluble slightly yellow polymer which is intractable. Anionic initiation with sodium methoxide at −75°C. gives a 90% yield of a bright yellow polymer which is soluble in water, dimethylsulfoxide, dimethylacetamide and dimethylformamide. This polymer is a sodium salt of polydiacrylylmethane.

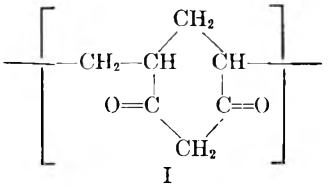

I

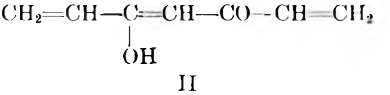

II

The ultraviolet spectrum of the polymer, in dimethylsulfoxide solvent, shows strong absorption bands at $\lambda = 258$ mμ ($\epsilon = 0.6 \times 10^3$), and at $\lambda = 376$ mμ ($\epsilon = 0.4 \times 10^4$), with an absorption shoulder at 385–390 mμ ($\epsilon = 0.35 \times 10^4$). This absorption corresponds very well with that of the copper chelate of diacrylylmethane,[3] with, however, a shift to higher values, due probably to the solvent and the polymer structure. The infrared spectrum does not show any absorption bands characteristic of vinyl or methyl structures; but it indicates two shifted carbonyl functions at 1580 and 1650 cm.$^{-1}$ The polymer turns brown and shrinks above 250°C., but it does

* The work discussed herein was supported by contract AF 33(616)7908 with the Materials Laboratory, Wright Air Development Division, Wright-Patterson Air Force Base, Ohio.

not melt below 350°C. Viscosity measurements on dimethylsulfoxide solutions of the polymer give a value for the intrinsic viscosity of $[\eta] = 0.16$, indicating a low molecular weight.

When this sodium-salt of the polydiacrylylmethane is treated with methanol or acetic acid, a white, insoluble precipitate is formed. The product seems to be the acid form of the polydiacrylylmethane and is insoluble in all the solvents tested. The infrared spectrum, in potassium bromide pellets, shows the typical β-diketone conjugate chelation absorption bands at 1620 and 1705 cm.$^{-1}$,[4,5] and also an absorption band at 1260 cm.$^{-1}$, indicating an ether bond, which may explain the insolubility of the polymer through crosslinkage.

Other polymerization attempts, in order to obtain higher molecular polydiacrylylmethane, were made by working in emulsion, the results however were negative; also a large number of experiments on the free radical initiated polymerization of diacrylylmethane were performed. Temperatures of 50–78°C., times of preparation of 5–70 hrs., and dilution of the monomer with benzene over a tenfold range were tried, but the polymer was only obtained in very low yield and once it was isolated and dried it could not be redissolved (Table I).

An attempt to prepare a dioxime[6] from the soluble sodium salt of polydiacrylylmethane in water gave an insoluble product which appears to be a monooxime on the basis of its nitrogen content. It shows infrared absorption at 3500–3400 cm.$^{-1}$ (OH bands), 1720 cm.$^{-1}$ (carbonyl band), 1650 cm.$^{-1}$ (C=N—), and 1260 cm.$^{-1}$ (ether group). Only about 10% of this polymer will dissolve in dimethylsulfoxide. It is possible that some isoxazole structure may be found or there may be some crosslinking by loss of water.

Since some δ-diketones react with ammonia to yield dihydropyridine structures, an attempt was made to convert this diacrylylmethane to a dihydropyridine structure by reaction with ammonia, but no reaction was achieved.

TABLE I
Free Radical Polymerization of Diacrylylmethane

Monomer, mg.	Benzene, ml.	Initiator (AIBN), % monomer	Reaction time, hr.	Reaction temp., °C.	Polymer yield, mg.
500	10	0.8	36	40–62	10
600	10	0.1	24	50–65	15
600	12	0.15	15	65–70	—[a]
1200	12	0.5	5	60	—[a]
700	12	0.5	70	70–78	150
700	12	0.5	48	65–70	73
600	60	0.5	48	65–75	43
500	50	0.1	21	60–65	15

[a] The solution was slightly turbid at the end of the reaction, but the amount of polymer was too small to be isolated.